Investigating the systemic pathological mechanisms of FUS and TDP-43



Zeinab Ali

Corpus Christi College

Department of Physiology, Anatomy and Genetics

Medical Sciences Division

University of Oxford

A thesis submitted for the degree of *Doctor of Philosophy*

Word count: ~ 31,000

Trinity 2022

I, Zeinab Ali confirm that the work presented in this thesis is my own. Where information has been derived from other sources, I confirm that it has been clearly indicated in the thesis.

Abstract

Amyotrophic lateral sclerosis (ALS) and frontotemporal dementia (FTD) are fatal neurodegenerative disorders (NDDs), with no cures. These conditions sit on a spectrum and have overlapping clinical symptoms, genetics and pathology. In particular, FUS and TDP-43 inclusions have been observed in familial and sporadic cases of both conditions. FUS and TDP-43 are highly conserved and involved in several cellular processes, mainly RNA metabolism. These proteins are expressed in most tissues, however, their pathological effects have been mainly studied in neuronal tissues. ALS and FTD are considered multi-system disorders therefore peripheral alterations could be contributing to disease aetiology. For example, metabolic alterations have been shown to have disease-modifying effects in both conditions.

This project investigated the systemic pathological mechanisms of FUS and TDP-43 using physiological knock-in mouse models carrying disease-relevant mutations. Unlike transgenic models, physiological models express the target endogenous levels, at the right place and time, ensuring that only mutation-specific effects are investigated. The *Tardbp*^{M323K} mouse and the partially humanised *Fus*$^{\Delta 14}$ mouse underwent an extensive phenotyping pipeline which revealed cognitive, motor and metabolic phenotypes in homozygous mice.

Systemic transcriptomic analysis of the *Fus*$^{\Delta 14}$ homozygous mouse revealed tissue-specific mutation effects. In response to systemic glucose alterations, metabolic reprogramming occurred in the muscles and this preceded neuromuscular changes. Early brain morphological changes and innate behaviour deficits in these mice point to the developmental effects of the *Fus*$^{\Delta 14}$ mutation.

Previous characterisation of the *Tardbp*^{M323K} mutation revealed late neuromuscular changes and motor phenotypes in homozygous mice. This project identified additional cognitive deficits, coupled with early brain structural changes. Metabolic phenotypes included increased body weights, increased fat mass and hypermetabolism. These phenotypes reintroduce the *Tardbp*^{M323K} homozygous mouse as a novel ALS-FTD model.

Both mutations on the C57BL/6J background caused embryonic lethality in homozygosity. This lethality was rescued on a F1 hybrid genetic background (C57BL/6J x DBA/2J). The *Fus*$^{\Delta 14}$ mutation in heterozygosity produced different body composition effects between mouse strains. This demonstrates that genetic backgrounds can interact with mutation effects.

Metabolic alterations have been documented across the ALS-FTD spectrum. Observational studies have shown that metabolic disturbances have contrasting effects on motor and cognitive functioning, suggesting that metabolic status can modify phenotypes within the spectrum. This hypothesis was investigated by modifying metabolic parameters using different diets in the *Tardbp*^{M323K} homozygous mouse. A high fat diet (HFD) and a matching control low fat diet (LFD) were used. The LFD modified metabolic parameters in homozygous mice to modulate mutation-driven motor phenotypes, in a sex-dependent manner. This data opens the door for patients to potentially modify their disease progression and phenotypes using diet as a therapeutic tool.

Acknowledgements

I am hugely grateful to my principal supervisors Dr Silvia Corrochano and Dr Thomas Cunningham for the opportunity to work on such an engaging and interdisciplinary project. I appreciate their enthusiasm, guidance and support. I am lucky to have so many additional supervisors who did not hesitate to take me under their wings: Dr Peter Oliver, Professor Ana Domingos Jansen and Professor Elizabeth Fisher. This project has been a collaborative effort with the Corrochano group in Madrid, mainly Juan Miguel Godoy-Corchuelo. Dr Pietro Fratta and Dr Abraham Acevedo-Arozena laid the foundations for this project and I am grateful for their continued support and contributions.

Many people have been involved in my doctoral training. I owe all my metabolism knowledge to the Cox group and Dr Lee Moir. I cannot thank Dr Debbie Williams enough for her genetics expertise and for letting me take over her lab. Dr Michelle Stewart and Dr Heather Cater provided all my *in vivo* behavioural training. Thank you Dr Mhoriam Ahmed for spending your precious weekends teaching me muscle physiology. I am grateful to all the members of the MMoN group (past and present) for their help and support, especially Remya. A massive thank you to Gemma, Jackie, Anju and Ward 5 for looking after my mice and dealing with my chaotic phenotyping pipelines. Most importantly, thank you to all the mice sacrificed for this project. Their contributions have been invaluable and have put us closer to understanding FUS and TDP-43 pathomechanisms.

I cannot thank my college, Corpus Christi, enough for their pastoral care. Rachel Clifford has always been a supportive hand in everything I do. Paul Dellar, Krzysztof Lewandowski and the rest of the Corpus staff have been so welcoming

and kind. Thank you Helen Moore for giving me the freedom to pursue the things important to me. I am immensely proud of the changes we have implemented to make the college a more inclusive environment, e.g., the alumni mentoring scheme.

This thesis also marks the end of my time at Oxford. It has been a period of independence, growth and happiness. I have met so many wonderful people during this journey. A special mention goes to Ebs for providing a safe space to cry, rant and laugh. Words cannot describe how much your friendship means to me. My support bubble would not be complete without Rainn, Dom and Layla. So many fond memories of living in the Rectory house during the pandemic. Thank you Rand for being the sister I never had, I love you. Thank you Hugo, aka Bubba, for the healing purrs and snuggles. Thank you Javier for all the fun adventures and for being my happy place.

This thesis would not have been possible without the unwavering love and support from my family, especially my Hooyo and Baba. Their belief and encouragement in my studies have pushed me to achieve things I did not think were possible. Whenever things get hard, I can always hear them saying "*naag nool iska dhig"*. I hope I can continue to make them proud. I dedicate this thesis to them.

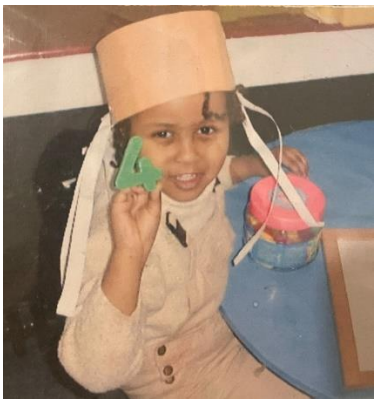


Table of Contents

Abstract 2
Acknowledgements 4
List of figures 10
List of tables 12
Appendices 13
List of abbreviations 14
1 Introduction 18
1.1 Amyotrophic lateral sclerosis (ALS) 18
1.2 Frontotemporal dementia (FTD) 20
1.3 ALS-FTD spectrum 21
1.3.1 Cognitive and motor symptoms 23
1.3.2 Metabolic symptoms 23
1.3.3 Genetics 26
1.3.4 Pathological inclusions 30
1.4 TDP-43 and FUS 32
1.4.1 Structure 32
1.4.2 Physiological function 33
1.4.3 Pathological roles 36
1.5 Models in ALS/FTD research 40
1.6 Selecting a mouse model 43
1.6.1 Transgenic versus physiological models 43
1.6.2 Strains and genetic backgrounds 54
1.6.3 Models used in this project 56
1.7 Aims 57
2 Materials and Methods 60
2.1 Animals 60
2.1.1 Housing conditions and Licensing 60
2.1.2 Generation of *Fus*$^{\Delta 14}$mice 60
2.1.3 Generation of *Tardbp*^{M323K} mice 61
2.1.4 Genotyping 61
2.2 *In vivo* phenotyping tests 63
2.2.1 Body weight 63
2.2.2 EchoMRI 63

2.2.3 Indirect calorimetry 63
2.2.4 Grip strength test 63
2.2.5 Gait analysis 64
2.2.6 Muscle physiology 64
2.2.7 Nesting 65
2.2.8 Marble burying 65
2.2.9 Light-dark box 66
2.2.10 Y-maze (forced alteration) 66
2.2.11 3-chamber test 66
2.2.12 Fear conditioning test 67
2.2.13 Food intake 68
2.2.14 Lipolysis 68
2.2.15 Intraperitoneal glucose tolerance test (IPGTT) 68
2.2.16 Plasma clinical chemistry 68
2.3 Molecular techniques 70
2.3.1 Tissue preparation 70
2.3.2 RNA-sequencing 70
2.3.3 Quantitative real-time PCR (qRT-PCR) 72
2.3.4 Adipose precursor isolation, culture and differentiation 73
2.3.5 Oil Red O staining 74
2.3.6 Motor neuron counts 75
2.3.7 Structural MRI scans 76
2.4 Statistical analysis and graphical representations 76
3 Investigating the systemic effects of the *Fus*$^{\Delta 14}$ mutation in homozygosity 80
3.1 Introduction 80
3.2 Results 83
3.2.1 Generation and viability of *Fus*$^{\Delta 14/\Delta 14}$ mice 83
3.2.2 *Fus*$^{\Delta 14/\Delta 14}$ mice are proportionately smaller than control littermates 84
3.2.3 Widespread transcriptomic dysregulation in *Fus*$^{\Delta 14/\Delta 14}$ mice 88
3.2.4 Structural brain alterations and behavioural deficits in *Fus*$^{\Delta 14/\Delta 14}$ mice 96
3.2.5 Muscle composition changes in *Fus*$^{\Delta 14/\Delta 14}$ mice 99
3.2.6 Systemic metabolic alterations in *Fus*$^{\Delta 14/\Delta 14}$ mice 101
3.2.7 Genetic backgrounds effects on metabolic phenotypes 112

3.3 Discussion 115
3.3.1 *Fus*$^{\Delta 14}$ mutation causes widespread effects 115
3.3.2 Genetic background effects 122
3.3.3 Conclusion 125
4 Investigating the systemic effects of the *Tardbp*^{M323K} mutation in homozygosity 129
4.1 Introduction 129
4.2 Results 132
4.2.1 Metabolic alterations in *Tardbp*$^{M323K/M323K}$ mice 132
4.2.2 Motor phenotypes in *Tardbp*$^{M323K/M323K}$ mice 138
4.2.3 Neuromuscular analysis in *Tardbp*$^{M323K/M323K}$ mice 141
4.2.4 Behavioural and cognitive impairments in *Tardbp*$^{M323K/M323K}$ mice 143
4.2.5 Early structural brain alterations in *Tardbp*$^{M323K/M323K}$ mice 151
4.3 Discussion 155
4.3.1 Earlier motor phenotypes 156
4.3.2 Novel behavioural and cognitive deficits 157
4.3.3 Metabolic alterations 160
4.3.4 Model considerations 161
4.3.5 Comparison to the *Tardbp*^{Q331K} mouse 164
4.3.6 Conclusion 166
5 Shifting ALS-FTD spectrum phenotypes using diet 169
5.1 Introduction 169
5.2 Results 172
5.2.1 Diet effects on mutation-driven metabolic phenotypes 172
5.2.2 Diet effects on mutation-driven cognitive phenotypes 191
5.2.3 Diet effects on mutation-driven motor phenotypes 198
5.3 Discussion 204
5.3.1 Summary 204
5.3.2 Can diet shift phenotypes in the ALS-FTD spectrum? 210
5.3.3 Future experiments 213
6 Final discussion 215
6.1 Main findings and contributions to the field 215
6.1.1 Widespread systemic effects of *Fus* and *Tardbp* mutations 215
6.1.2 Protein aggregates are not necessary in early disease mechanisms 219

6.1.3 Sex-differences in *Fus* and *Tardbp* mutations 220
6.1.4 Genetic background effects 221
6.1.5 Diet can modulate mutation phenotypes 222
6.2 Future experiments 223
6.3 Concluding remarks 226
7 References 229
8 Appendices 259

List of figures

Figure 1.1. The pattern of motor neuron involvement in different ALS sub-groups..... 19
Figure 1.2. Clinical, genetic and pathological overlap of ALS and FTD. 22
Figure 1.3. Pathological protein inclusions in ALS and FTLD..... 31
Figure 1.4. Structural and functional domains of TDP-43 (A) and FUS (B). .. 33
Figure 1.5. Physiological roles of TDP-43 and FUS in RNA processing..... 35
Figure 3.1. Generation of viable *Fus*$^{\Delta 14/1\Delta 14}$ mice on a hybrid background. .. 84
Figure 3.2. Weights and sizes of *Fus*$^{\Delta 14}$ mice. 85
Figure 3.3. Number of DEGs across *Fus*$^{\Delta 14/\Delta 14}$ tissues..... 89
Figure 3.4. Volcano plots. 90
Figure 3.5. Venn diagram comparing DEGs across the tissues..... 92
Figure 3.6. Gene ontology (GO) pathways. 95
Figure 3.7. Brain morphological analysis of *Fus*$^{\Delta 14}$ mice..... 97
Figure 3.8. Nesting test in *Fus*$^{\Delta 14}$ mice. 98
Figure 3.9. Muscle fibre gene screen in *Fus*$^{\Delta 14}$ mice..... 100
Figure 3.10. Liver lipid droplet (LD) staining in *Fus*$^{\Delta 14}$ mice..... 102
Figure 3.11. Body composition of *Fus*$^{\Delta 14}$ mice. 104
Figure 3.12. Plasma lipid profile of *Fus*$^{\Delta 14}$ mice. 105
Figure 3.13. *In vivo* lipolysis measurements in *Fus*$^{\Delta 14}$ mice..... 107
Figure 3.14. *In vitro* adipogenesis measurements in *Fus*$^{\Delta 14}$ mice. 108
Figure 3.15. Intraperitoneal glucose tolerance test (IPGTT) in *Fus*$^{\Delta 14}$ mice.109
Figure 3.16. Indirect calorimetry analysis of *Fus*$^{\Delta 14}$ mice. 111
Figure 3.17. Body composition of *Fus*$^{\Delta 14}$ mice on different genetic backgrounds. 113
Figure 3.18. Indirect calorimetry analysis of *Fus*$^{\Delta 14}$ mice on different genetic backgrounds. 114
Figure 3.19. *FUS*$^{\Delta 14}$ mutation caused systemic effects in homozygosity.... 127
Figure 4.1. Phenotyping pipeline to characterise the *Tardbp*^{M323K} mouse. . 131
Figure 4.2. Body weights of female *Tardbp*^{M323K} mice..... 132
Figure 4.3. Body composition of female *Tardbp*^{M323K} mice..... 134
Figure 4.4. Indirect calorimetry analysis on female *Tardbp*^{M323K} mice. 136
Figure 4.5. Food intake analysis of *Tardbp*^{M323K} mice. 137

Figure 4.6. Fore and hind limb grip strength analysis of female *Tardbp*^{M323K} mice..... 139
Figure 4.7. Gait analysis of female *Tardbp*^{M323K} mice..... 140
Figure 4.8. Neuromuscular analysis of female *Tardbp*^{M323K} mice. 142
Figure 4.9. Innate rodent behaviour analysis of female *Tardbp*^{M323K} mice.. 143
Figure 4.10. Light-dark box test in female *Tardbp*^{M323K} mice. 145
Figure 4.11. Y-maze (forced alteration) test in female *Tardbp*^{M323K} mice..... 146
Figure 4.12. 3-chamber test in female *Tardbp*^{M323K} mice..... 147
Figure 4.13. Fear conditioning test in female *Tardbp*^{M323K} mice..... 149
Figure 4.14. Brain volumes of female *Tardbp*^{M323K} mice. 151
Figure 4.15. Structural MRI scans of female *Tardbp*$^{M323K/M323K}$ mice (absolute changes). 153
Figure 4.16. Structural MRI scans of female *Tardbp*$^{M323K/M323K}$ mice (relative changes). 154
Figure 4.17. The knock-in *Tardbp*^{M323K} mouse is a novel ALS-FTD model.. 167
Figure 5.1. Diet study pipeline..... 170
Figure 5.2. Body weights of male *Tardbp*^{M323K} mice in diet study..... 174
Figure 5.3. Body weights of female *Tardbp*^{M323K} mice in diet study. 177
Figure 5.4. Body composition of male *Tardbp*^{M323K} mice in diet study..... 182
Figure 5.5. Body composition of female *Tardbp*^{M323K} mice in diet study..... 183
Figure 5.6. Indirect calorimetry analysis of male *Tardbp*^{M323K} mice in diet study. 186
Figure 5.7. Indirect calorimetry analysis of female *Tardbp*^{M323K} mice in diet study. 189
Figure 5.8. Light-dark box test in male *Tardbp*^{M323K} mice in diet study. 193
Figure 5.9. Light-dark box test in female *Tardbp*^{M323K} mice in diet study. ... 194
Figure 5.10. Fear conditioning test in male *Tardbp*^{M323K} mice in the diet study. 196
Figure 5.11. Fear conditioning test in female *Tardbp*^{M323K} mice in the diet study. 197
Figure 5.12. Gait analysis of male *Tardbp*^{M323K} mice in the diet study..... 201
Figure 5.13. Gait analysis of female *Tardbp*^{M323K} mice in the diet study. 203

List of tables

Table 1.1. Causative mutations in both ALS and FTD. 29
Table 1.2. TDP-43 and FUS brain RNA-binding properties. 36
Table 1.3. *Tardbp* mouse models detailing mean disease onset, survival, phenotype and pathology. 51
Table 1.4. *Fus* mouse models detailing mean disease onset, survival, phenotype and pathology. 53
Table 2.1. Sequences used to genotype *Fus*$^{\Delta 14}$ mutants 62
Table 2.2. Sequences used to genotype *Tardbp*^{M323K} mutants 62
Table 2.3. Primer sequences 72
Table 2.4. Taqman assays 73
Table 2.5. Cell culture reagents 74
Table 3.1. Mean body weights of male *Fus*$^{\Delta 14}$ mice and statistical analysis. 86
Table 3.2. Mean body weights of female *Fus*$^{\Delta 14}$ mice and statistical analysis. 87
Table 3.3. Summary of male *Fus*$^{\Delta 14/\Delta 14}$ phenotypes on the hybrid background. 116
Table 4.1. Mean body weights of female *Tardbp*^{M323K} mice and statistical analysis. 133
Table 4.2. Summary of *Tardbp*$^{M323K/M323K}$ phenotypes. 155
Table 5.1. Mean body weights of male *Tardbp*^{M323K} mice in diet study and statistical analysis. 176
Table 5.2. Mean body weights of female Tardbp^{M323K} mice in diet study and statistical analysis. 179
Table 5.3. Summary of phenotypes in the diet study. 204
Table 5.4. Summary of gait parameters from the diet study. 209

Appendices

Appendix A. RNA-seq tables of significantly differentiated genes (DEGs) in each tissue of the *Fus*$^{\Delta 14}$ homozygous mouse (A1-5), *Fus* gene expression in *Fus*$^{\Delta 14}$ tissues (A6) and quality of RNA samples used for transcriptomic analysis (A7).

Appendix B. Additional metabolic data from the *Fus*$^{\Delta 14}$ mouse.

Appendix C. Significantly altered brain structural volumes in *Tardbp*$^{M323K/M323K}$ mice.

Appendix D. Mouse cohort information.

List of abbreviations

AD	Alzheimer’s disease
ALS	Amyotrophic lateral sclerosis
ALSbi	ALS behavioural
ALSci	ALS cognitive
BAC	Bacterial artificial chromosome
BAT	Brown adipose tissue
BDNF	Brain-derived neurotrophic factor
BMI	Body mass index
CARTS	Cerebral age-related TDP-43 with sclerosis
cDNA	Complementary DNA
CRISPR	Clustered regularly interspaced shot palindromic repeats
Cas9	CRISPR-associated endonuclease
DEGs	Differentially expressed genes
EDL	Extensor digitorum longus
EE	Energy expenditure
ENU	N-ethyl-N-nitrosourea
ES	Embryonic stem
fALS	Familial ALS
FFAs	Free fatty acids
FTD	Frontotemporal dementia
FTLD	Frontotemporal lobular degeneration?

FUS	Fused-in-sarcoma
Fus	The mouse gene encoding FUS
FUS	The human gene encoding FUS
GO	Gene ontology
GOF	Gain-of-function
GOI	Gene of interest
HDL	High-density lipoprotein
HFD	High fat diet
hnRNP	Heterogeneous nuclear ribonucleoprotein
IPGGT	Intraperitoneal glucose tolerance test
iPSCs	Human-induced pluripotent stem cells
iWAT	Inguinal white adipose tissue
jALS	Juvenile ALS
KI	Knock-in
KO	Knock-out
LATE	Limbic-predominant age-related TDP-43 encephalopathy
LDL	Low-density lipoprotein
LFD	Low fat diet
MND	Motor neuron disease
MNs	Motor neurons
MUNE	Motor unit number estimate
NDDs	Neurodegenerative disorders

NHEJ	Non-homologous end joining
NMJs	Neuromuscular junction
PD	Parkinson’s disease
PFNA	Progressive non-fluent aphasia
RER	Respiratory exchange ratio
sALS	Sporadic ALS
SD	Semantic dementia
T2DM	Type 2 Diabetes Mellitus
TA	Tibialis anterior
TDP-43	Transactive response DNA binding protein of 43 kDa
TARDBP	The human gene encoding TDP-43
Tardbp	The mouse gene encoding TDP-43
UPS	Ubiquitin proteasome system

Introduction

1 Introduction

1.1 Amyotrophic lateral sclerosis (ALS)

ALS is a fatal motor neuron disease that is characterised by the progressive loss of the upper and lower motor neurons (MNs) at the spinal or bulbar level (Brooks et al., 2000; Zarei et al., 2015). ALS pathological changes were first described in a patient by Lockhart Clarke and Charles Bland Radcliffe in 1862 (Radcliffe & Clarke, 1862). These findings were built upon and further validated by the French neurologist Jean-Martin Charcot, who proposed the term “amyotrophic lateral sclerosis” in 1874 (Charcot, 1965; JM, 1874). This disease became widely known when the baseball player Lou Gehrig was diagnosed with the disease in 1939 (Ma & Li, 2019).

The involvement of upper and lower MNs is variable and yields a spectrum of phenotypes, making ALS a highly heterogeneous disease (**Figure 1.1**). UMNs in the primary motor cortex and LMNs in the bulbospinal region are preferentially affected in ALS. Degeneration of the UMNs usually leads to Babinski sign, hyperreflexia, spasticity and exaggerated jaw or gag reflex, while degeneration of the LMNs leads to muscle atrophy and weakness. (Swinnen & Robberecht, 2014). However, ALS is now being recognised as a multi-system disorder rather than a disease limited to MNs. Involvement of neurons in the frontotemporal cortex causes cognitive and behavioural impairments in ~50% of patients. Extrapyramidal involvement has been observed in ~5-10% of ALS patients in the form of mild parkinsonism, postural instability and backward falls (Desai & Swash, 1999). Cerebellar ataxia, sensory symptoms, autonomic nervous system alterations and deafness are rarer symptoms and are usually detected in

advanced disease (Baltadzhieva et al., 2005; Green et al., 2010; Isaacs et al., 2007; Lindquist et al., 2013).

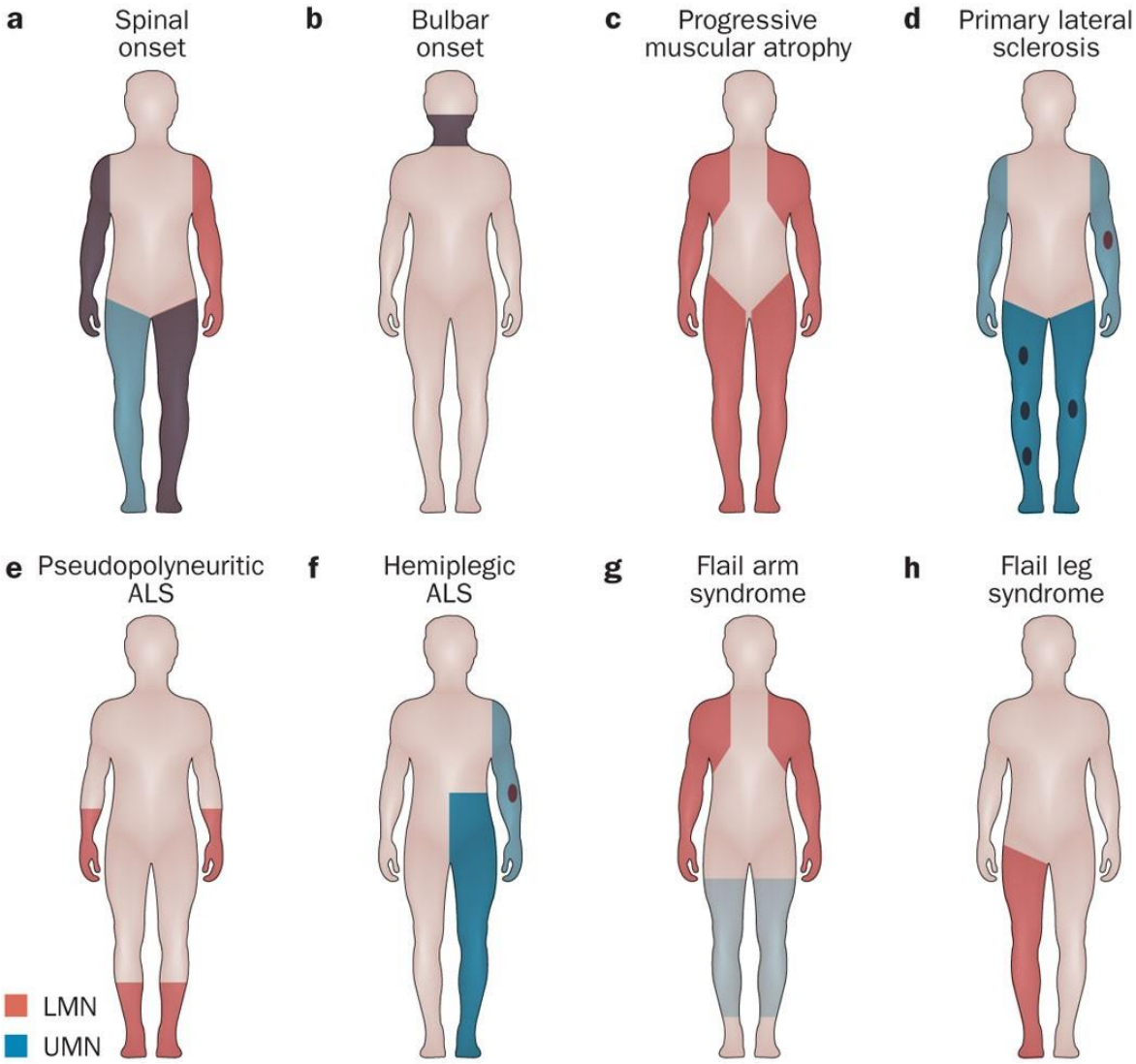


Figure 1.1. The pattern of motor neuron involvement in different ALS sub-groups. (Swinnen & Robberecht, 2014).

The majority of ALS cases are sporadic (90%) with no clear genetic linkage (Chen et al., 2013). The global prevalence and incidence is 4.42 per 100,000 population and 1.59 per 100,000 person-years, respectively (Xu et al., 2020). ALS is rare before the age of 40 years, with a mean age onset age of 58-63 years in sporadic ALS (sALS) and 40-60 years in familial ALS (fALS) (Ingre et al., 2015). However,

there are juvenile forms of ALS (jALS) that have a disease onset before the age of 25 years (Lehky & Grunseich, 2021). Men have a higher risk of developing ALS than women (male-to-female ratio of 1.2-1.5), although this changes with age (Manjaly et al., 2010). A higher incidence rate is observed in Europe and the United States (Xu et al., 2020).

ALS usually has a rapid fatal prognosis with a median survival time of 24-48 months (Chiò et al., 2013). To date, there is no cure for ALS and current pharmacological treatments have limited efficacy. Riluzole is the only drug licensed to treat ALS in Europe. It acts as a glutamate antagonist in neurons to reduce excitotoxicity, however, the exact mechanism of action remains unknown. Riluzole prolongs survival by a few months (Bensimon et al., 1994). Edaravone is licensed in Japan and the United States however its efficacy is debated as the symptomatic benefit was only seen in a subpopulation of a wider clinical trial (Abe et al., 2017; Witzel et al., 2022). Sodium phenylbutyrate-taurursodiol was recently approved in the United States and Canada after clinical trials showed that it slowed ALS functional decline (Paganoni et al., 2021; Paganoni et al., 2020). Marketing approval for this drug is currently under review in Europe.

1.2 Frontotemporal dementia (FTD)

Following its initial characterisation in 1892 by Arnold Pick, FTD (behavioural variant FTD, bvFTD) is now recognised as one of the three major clinical syndromes of Frontotemporal Lobar Degeneration (FTLD), the others being semantic dementia (SD) and progressive non-fluent aphasia (PFNA) (Mohandas & Rajmohan, 2009; Pearce, 2003). FTLD is characterised by progressive degeneration in the prefrontal and anterior temporal lobes, however, other

subcortical areas are affected as the disease progresses. Differences in affected sub-regions correlate to different clinical syndromes. Atrophy in the frontal and temporal lobes in FTD causes behavioural/social changes and executive deficits. Asymmetrical atrophy of the left hemisphere in PFNA causes deficits in language and word retrieval. Bilateral atrophy of the middle and inferior temporal neocortex in SD causes a loss of semantic knowledge of objects, faces and languages (Neary et al., 2005).

There is a strong genetic linkage in FTD as ~40% of patients have a family history (Rohrer et al., 2009). Prevalence and incidence are 15-22 per 100,000 population and 2.7-4.1 per 100,000 person-years, respectively. Population studies show equal sex distribution (Onyike & Diehl-Schmid, 2013). The mean age of onset is 45-65 years, and the mean survival time of 6-8 years (Neary et al., 2005). There is currently no cure for FTLD syndromes. Selective serotonin reuptake inhibitors (SSRIs) are used for the symptomatic management of behavioural symptoms in FTD and SD patients (Vossel & Miller, 2008).

1.3 ALS-FTD spectrum

Overwhelming evidence shows that ALS and FTD represent a continuum of a broad NDD with each presenting as extremes of a spectrum of overlapping clinical symptoms, genetics and pathology (Ling et al., 2013) (**Figure 1.2**).

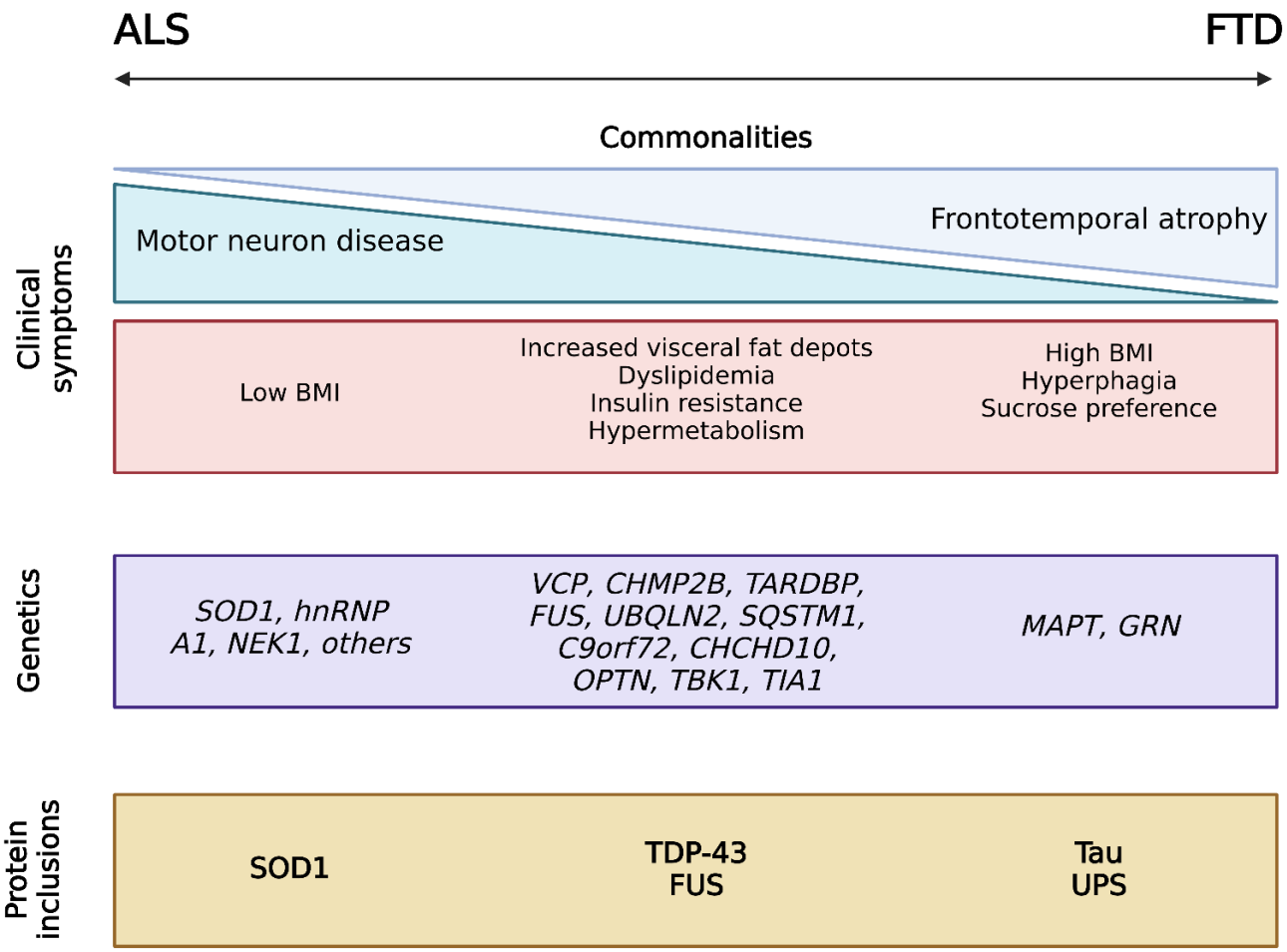


Figure 1.2. Clinical, genetic and pathological overlap of ALS and FTD. Data was taken from (Ahmed, Irish, Piguet, et al., 2016; Gao et al., 2017; J. M. Godoy-Corchuelo et al., 2022; Van Langenhove et al., 2012). Figure created using BioRender.com.

1.3.1 Cognitive and motor symptoms

Some degree of frontotemporal dysfunction is observed in ~50% of ALS patients in the form of cognitive or behavioural impairments (ALSci and ALSbi, ALS-plus), whilst ~15% of ALS patients develop FTD (ALS-FTD) (Saxon et al., 2017). The pattern of cognitive/behavioural changes in ALS-FTD usually closely resembles FTD, while the motor neuron disease pattern is similar to classic ALS (spinal/bulbar onset) (Van Langenhove et al., 2012). FTD symptoms usually precede those of ALS in these patients (Hu et al., 2009). Similarly, up to 30% of FTD patients develop motor dysfunction (Burrell et al., 2011).

1.3.2 Metabolic symptoms

Another clinical overlap in the ALS-FTD spectrum is metabolic alterations, which have been shown to have disease-modifying effects. Patients with ALS typically have a normal or low BMI and lose weight/body fat as the disease progresses, which in turn negatively affects the disease prognosis (Desport et al., 1999). A low BMI is a risk factor for ALS, while a high BMI at diagnosis is associated with a slower disease progression and delayed mortality (Jawaid et al., 2018). Clinical studies have found that BMI differs across the spectrum. ALS-plus, ALS-FTD and FTD patients are usually overweight and obese (Ahmed et al., 2014), linking a high BMI to cognitive deficits. Increased body weights in FTD are believed to be associated with altered eating patterns, e.g., hyperphagia and sucrose preference (Ahmed, Irish, Henning, et al., 2016). Despite opposing body weight profiles, increased visceral fat depots have been reported in both ALS and FTD patients (Ahmed et al., 2019; Lindauer et al., 2013).

Hypermetabolism has been extensively reported in ALS patients, despite muscle denervation and atrophy (Desport et al., 2005). Mitochondrial dysfunction and

increased muscle energy demand are believed to underline the increased energy expenditure (EE) (Ahmed, Irish, Piguet, et al., 2016). Hypermetabolism has also been reported in FTD patients (Ahmed, 2021) but its origin is undefined.

Dyslipidaemia has been observed in the ALS-FTD spectrum. In a cohort of 369 ALS patients, increased low-density lipoprotein (LDL) cholesterol and/or decreased high-density lipoprotein (HDL) concentrations were observed in 67% of patients, this was accompanied by increased apolipoprotein E levels in 38% of patients (Dupuis et al., 2008). Hyperlipidaemia has been suggested to be protective in ALS as increased triglyceride and total cholesterol concentrations were associated with longer survival times (Dorst et al., 2011). Increased cholesterol levels were also associated with reduced functional decline but this was only present in women, contributing to the sex differences seen in this disease (Ikeda et al., 2012; McCombe & Henderson, 2010). In contrast to ALS, blood LDL levels were not altered in FTD patients but decreased HDL concentrations were reported (Ahmed et al., 2018). However, another study reported increased blood levels of all cholesterol species in FTD, indicating other factors that could be contributing to population differences (Wang et al., 2020). Increased triglycerides, diglycerides and very long-chain fatty acid levels were reported in the blood of ALS and FTD patients. Commonalities and differences in neuronal tissue lipids have been reported in the ALS-FTD spectrum (Juan Miguel Godoy-Corchuelo et al., 2022), suggesting that altered lipid metabolism may underlie neuronal dysfunction in these conditions.

Increased prevalence of insulin resistance and Type 2 Diabetes Mellitus (T2DM) have been reported in both ALS and FTD (Golimstok et al., 2014; Mariosa et al., 2015). In ALS, these metabolic conditions have been shown to have a protective

effect, either by reducing the risk or delaying the onset of the disease (D'Ovidio et al., 2018; Jawaid et al., 2010). Limited studies have been conducted to explore the disease-modifying effects of these metabolic conditions in FTD.

The disease-modifying effects of metabolic perturbations have led to several clinical trials investigating diet-based treatments for ALS. Diet is a modifiable factor that can compensate for the increased energy demand and lower BMIs observed in ALS, therefore influencing disease progression. Several high calorie and high-fat and/or low carbohydrate (ketogenic) diets have been shown to improve survival in animal models and patients (Pape & Grose, 2020). Energetic imbalance observed in transgenic SOD1^{G93A} mice (reduced adipose tissue stores and hypermetabolism) was corrected through the administrated of a high caloric fatty diet (HCFD), extending survival by 20% (Dupuis et al., 2004). In the clinic, HCFD improved survival in fast-progressing ALS patients (Ludolph et al., 2020). Another study confirmed the survival benefits of HCFD and also showed that it was well tolerated, with no reported adverse effects (Wills et al., 2014).

1.3.2.1 Gaps in the field

Despite the extensive characterisation of these metabolic alterations and evidence of their modulating effect in ALS-FTD spectrum disorders, their exact pathological mechanisms remains unsolved.

While there are numerous metabolic overlaps between ALS and FTD, there are also differences within these parameters, e.g., body weight, BMI and lipid species. This provides a novel way to delineate ALS-FTD spectrum disorders and a mechanism to stratify patients for treatment options and clinical trials. However, these differences have broader clinical implications. It appears that metabolic disturbances have contrasting effects on motor and cognitive functioning. Pre-

morbid T2DM delayed the onset of ALS motor symptoms but impaired frontotemporal cognitive functioning (Jawaid et al., 2010). Additionally, it has been shown that a higher body weight/BMI is linked to cognitive deficits (ALS-FTD and FTD) (Ahmed et al., 2014). These differences suggest that metabolic status could directly influence ALS-FTD symptoms. This has been partly demonstrated through the use of diet. Literature has shown that a HFD can negatively impact cognitive functioning. A HFD caused rapid deficits in episodic memory in the C57BL/6J mouse, which was reversed by a LFD (McLean et al., 2018). A HFD accelerated hippocampus-dependent learning deficits in a transgenic mouse model of orexin neurodegeneration (Duffy et al., 2019). There are several postulated biological mechanisms underlying HFD's effects on cognition; neuroinflammation, oxidative stress, reduced BDNF levels, dendritic deficits in the hippocampus and insulin resistance (Freeman et al., 2014). Despite causing significant dysfunction in brain structure and function, a HFD appeared to improve the motor symptoms in ALS patients (see previous section). Following this line of evidence, a LFD can improve cognitive functioning but negatively impact motor functioning. Diet may modulate these phenotypes by modifying metabolic states. Confirming this hypothesis will provide invaluable knowledge to the ALS/FTD field. Patients will have the autonomy to directly modify their disease phenotypes and progression. Dietary changes do not need a prescription and can be practised by anyone.

1.3.3 Genetics

FTD is a highly heritable disorder. Autosomal dominant mutations in *MAPT* and *GRN* account for ~10-20% of all clinical cases (Cruts et al., 2006; Rohrer et al., 2009). Conversely, ALS is largely sporadic but *SOD1* mutations account for 20% of familial cases and 3% of sporadic cases (Andersen, 2006; Rosen et al., 1993).

However, there is considerable genetic overlap between ALS and FTD (**Figure 1.2**, **Table 1.1**). *C9orf72*, *TARDBP*, *SQSTM1*, *VCP*, *FUS*, *TBK1* and *CHCHD10* are considered critical genetic players in both ALS and FTD (Abramzon et al., 2020). These genes are implicated in pathways that are dysregulated in ALS and FTD, e.g., RNA-processing, autophagy, protein homeostasis, mitochondrial function and vesicle trafficking (Weishaupt et al., 2016).

Gene	Locus	Protein Function	Heredity	Onset	Frequency (%)			Other diseases	Pathology	References
					fALS	sALS	FTLD			
C9orf72	9p21.2	Autophagy and inflammation	AD	Adult	25	5	10	PD, AD, HD	TDP-43 DPRs	(Beck et al., 2013; DeJesus-Hernandez et al., 2011; Freibaum & Taylor, 2017; Renton et al., 2011; Smeyers et al., 2021)
FUS	16p11.2	RNA processing	AD, AR	Adult, juvenile	5	<1	<1		FUS	(Kwiatkowski et al., 2009; Vance et al., 2009)
TARDBP	1p36.22	RNA processing	AD	Adult	5	<1	<1	MND, SNGP, chorea	TDP-43	(Abramzon et al., 2020; Kabashi et al., 2008; Sreedharan et al., 2008)
SQSTM1	5p35	Protein degradation	AD	Adult	1		3	PDB	p62	(Fecto et al., 2011; Teyssou et al., 2013)
VCP	9p13.3	Protein quality control	AD	Adult	9		<1	IDMPDB, PD, AD	TDP-43	(Abramzon et al., 2020; Al-Obeidi et al., 2018; Johnson et al., 2010)
TBK1	12p14.1	Autophagy, mitophagy, innate immune signalling	AD	Adult	1		1.8		TDP-43, p62	(Lamb et al., 2019; Ticozzi et al., 2011; Van Mossevelde et al., 2016; Weidberg & Elazar, 2011)

CHCHD10	22p11.23	Multifunctional	AD	Adult	U	U	U	Mitochondrial myopathy		(Abramzon et al., 2020; Bannwarth et al., 2014; Zhou et al., 2017)
CHMP2B	3p11.2	Vesicle tracking	AD	Adult	<1	U	<1		p62	(Parkinson et al., 2006; Skibinski et al., 2005)
UBQLN2	Xp11.21	Protein degradation	XD	Adult	<1	U	<1		TDP-43, FUS	(Deng et al., 2011)
OPTN	10p13	Multifunctional	AD, AR	Adult	4	<1	U	POAG, PDB	TDP-43	(Maruyama et al., 2010)
ANXA11	10q22.3	Bind Ca2+, RNA, other proteins, and lipid membranes	AD	Adult	U	U	U		Profuse annexin A11-positive aggregates	(Wang et al., 2022)

Table 1.1. Causative mutations in both ALS and FTD. AD: autosomal dominant. AR: autosomal recessive. XD: X-lined dominant. U: undetermined. PD: Parkinson's disease. AD: Alzheimer's disease. HD: Huntington's disease. MND: Motor neurone disease. SNGP: Supranuclear gaze palsy. PDB: Paget's disease of the bone. IDMPDB: Inclusion body myopathy with Paget's disease and FTD. POAG: Primary open angle glaucoma. DPR: dipeptide repeats. p62: phosphotyrosine-independent ligand of the SH2 domain of p56lck. Diagram adapted from (Abramzon et al., 2020; Ling et al., 2013).

1.3.4 Pathological inclusions

Dysregulation in RNA metabolism as a communal pathomechanism in ALS and FTD was demonstrated by mutations in *TARDBP* and *FUS* (**Figure 1.2**). Although these mutations are rare, TDP-43 and FUS protein inclusions are seen in sporadic ALS and FTD patients (**Figure 1.3**).

Ubiquitinated TDP-43 protein inclusions are seen in both sporadic ALS patients and a large subset of FTD patients (Neumann et al., 2006). In ALS, inclusions are found in glia and neurons in the primary motor cortex, brainstem motor nuclei, spinal cord and associated white matter tracts (Mackenzie et al., 2007). ALS patients with FTD display TDP-43 accumulation in the extramotor cortex and hippocampus (Geser et al., 2009). FTLD-TDP is characterised by TDP-43-positive cytoplasmic inclusions in the frontotemporal neocortex and dentate granule cells of the hippocampus (Davidson et al., 2007). According to the morphology and neuroanatomical distribution of TDP-43 inclusions, FTLD-TDP can be further classified into types A to E (Mackenzie, Neumann, et al., 2011). However, TDP-43 pathology can be present in a wide range of subcortical brain regions, especially as the disease progresses (Josephs et al., 2009). Interestingly, amyloid fibres from the brains of FTLD-TDP types A to D are primarily composed of TMEM106B, not TDP-43 (Jiang et al., 2022); a characteristic shared with other NDDs like progressive supranuclear palsy and dementia with Lewy bodies (Chang et al., 2022)

Subsequent identification of FUS inclusions in FTD, without TDP-43 inclusions, led to the reclassification of FTLD based on the main protein component accumulated (I. R. Mackenzie et al., 2010). In FTLD-FUS, FUS-positive inclusions are usually seen in the frontotemporal neocortex and hippocampus, but they are also present

in the thalamus, striatum and brainstem. Most FTLD-FUS patients also have FUS inclusions in lower motor neurons, without motor neurone disease (Neumann, Rademakers, et al., 2009). FUS inclusions are usually seen in the lower motor neurons of ALS patients with *FUS* mutations, although FUS mislocalisation has been reported in sporadic clinical cases (Tyzack et al., 2019).

Shared TDP-43 and FUS protein inclusions indicate that problems in RNA processing are central to ALS and FTD pathogenesis. Understanding the pathomechanisms of these RNA-binding proteins may uncover key therapeutic targets.

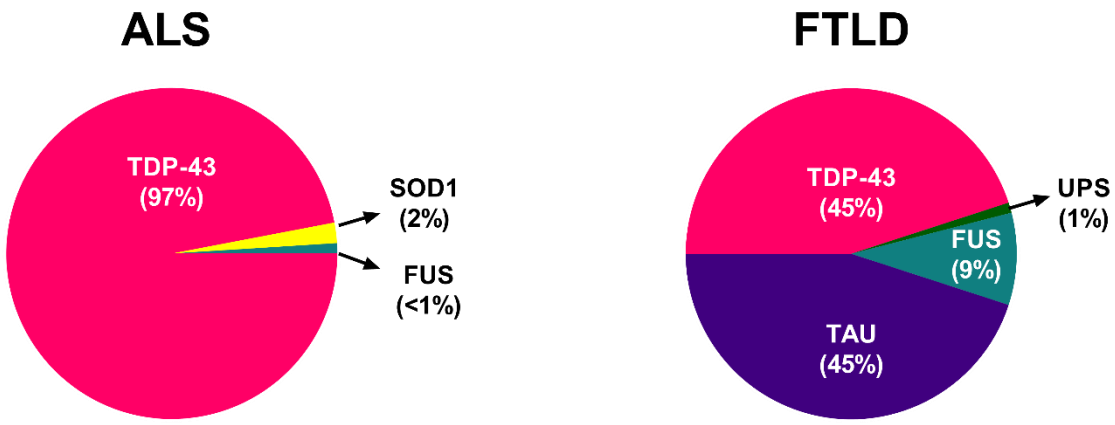


Figure 1.3. Pathological protein inclusions in ALS and FTLD. In the clinic, FTD cases are grouped based on their pathological protein: FTLD-tau, FTLD-TDP, FTLD-FUS and FTLD-UPS. Correct classification can help identify common disease mechanisms, biomarkers and possible treatments. (Mackenzie, Munoz, et al., 2011). Figure adapted from (Ling et al., 2013).

1.4 TDP-43 and FUS

1.4.1 Structure

TDP-43 protein contains 414 amino acids and is encoded by the *transactive response DNA binding protein 43 (TARDBP)* gene located on chromosome 1. It is classed under the heterogeneous nuclear ribonucleoprotein (hnRNP) family. (**Figure 1.4A**). The majority of ALS-linked mutations are found in the C-terminal domain. These mutations have been found to enhance the protein's intrinsic aggregation propensity and promote cytotoxicity *in vitro* (Johnson et al., 2009). Splicing activity is also mediated in this domain, as well as interactions with other members of the hnRNP family (Buratti et al., 2005; Buratti et al., 2001).

FUS is encoded by the *fused-in-sarcoma* (*FUS*) gene. The human protein consists of 526 amino acid residues, containing several highly conserved functional domains (**Figure 1.4B**). FUS belongs to the FET/TET family of DNA/RNA binding proteins. The N-terminus is a predicted prion-like region, which is involved in protein interactions and liquid-liquid phase separations. The C-terminal region is involved in RNA binding. RMM and Znf bind to RNA in a sequence-specific manner (RRM at the step loop and Znf to GGU), contributing to splicing functions. At the same time, RGG binds to RNA in a sequence-independent manner to increase mRNA binding and destabilise the RNA structure (Loughlin et al., 2019). The majority of ALS-linked mutations are found in the C-terminal NLS domain in exon 15. The NLS domain is necessary for the import of FUS into the nucleus; disruptions in this region can lead to the mislocalisation of the protein (Efimova et al., 2017).

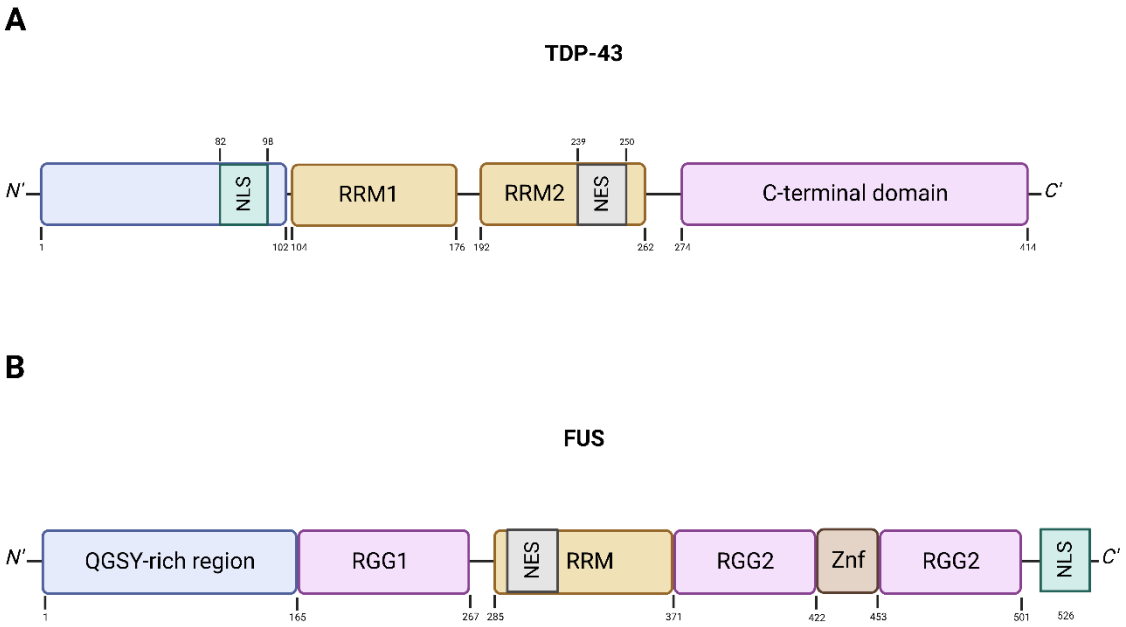


Figure 1.4. Structural and functional domains of TDP-43 (A) and FUS (B). The TDP-43 protein contains two RNA recognition motifs (RRM) and a glycine-rich C-terminal region which binds to single-stranded DNA, RNA and proteins. The nuclear localisation signal (NLS) is located in the N-terminal domain, while the nuclear export signal (NES) is located in the second RRM (Prasad et al., 2019). The FUS protein consists of an N-terminal Glutamine-Glycine-Serine-Tyrosine-rich domain, NES, three arginine-glycine-glycine regions, conserved RRM, zinc finger motif (Znf) and NLS at the C-terminus (Nolan et al., 2016). Figure created using BioRender.com.

1.4.2 Physiological function

TDP-43 and FUS are RNA/DNA binding proteins (Bertolotti et al., 1996; Buratti et al., 2001) that are expressed in most tissues, at varying levels. They are primarily localised in the nucleus but are regularly shuttled to the cytoplasm, a process regulated by their NLS and NES domains (Ayala et al., 2008; Zinszner et al., 1997). Through their binding to single- and double-stranded DNA, as well as RNA, these proteins are involved in a wide range of cellular processes. TDP-43 is involved in apoptosis and cell division (Fiesel et al., 2010), while FUS has been implicated in genome stability and DNA repair (Law et al., 2006). However, both

proteins are significantly involved in various aspects of RNA processing (**Figure 1.5**). In the nucleus, they are involved in transcription regulation, splicing, stabilisation of long introns and miRNA biogenesis. In the cytoplasm, they are involved in transporting mRNA for local translation. RNA transport is a key process in maintaining neuronal plasticity and dendritic integrity. FUS and TDP-43 transport RNA granules to dendritic spines for local translation (Fujii et al., 2005; Fujii & Takumi, 2005; Kiebler & Bassell, 2006). Under neuronal activation, TDP-43 and FUS are localised in dendrites (Wang et al., 2008). TDP-43 and FUS are also components of cytoplasmic stress granules (Li et al., 2013). Stress granules temporarily repress general translation and store mRNAs during stress, and disassemble in the absence of stress (Anderson & Kedersha, 2009).

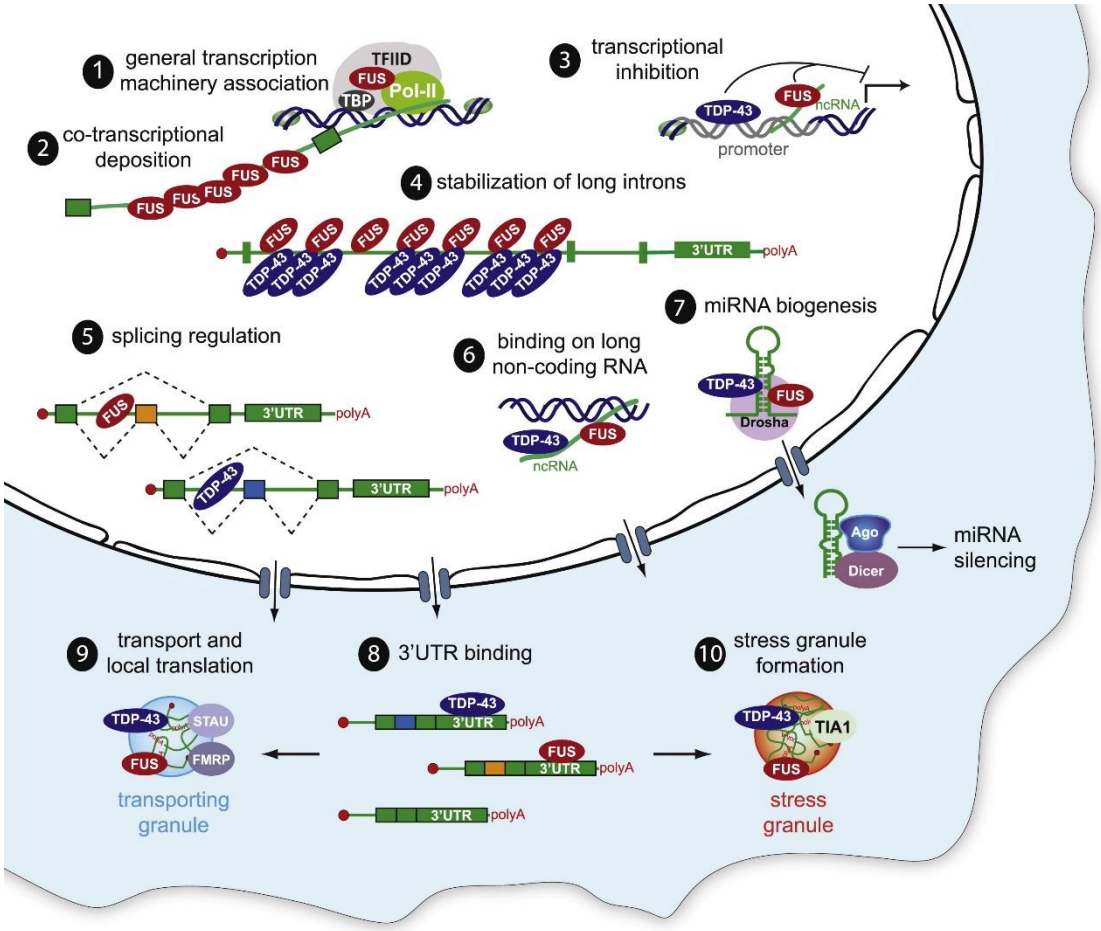


Figure 1.5. Physiological roles of TDP-43 and FUS in RNA processing. Figure reprinted from "Converging Mechanisms in ALS and FTD: Disrupted RNA and Protein Homeostasis" (Ling et al., 2013), Copyright (2013), with permission from Elsevier.

Genome-wide approaches have identified *in vivo* RNA-binding properties of TDP-43 and RNA in mouse and human brains (**Table 1.2**). Despite the shared RNA-related functions, TDP-43 and FUS affected expression levels and processing of largely distinct sets of RNAs; they only had 86 gene regulation events and 78 splicing events in common (Lagier-Tourenne et al., 2012). Only 45 transcripts were downregulated upon TDP-43 or FUS depletion. These transcripts contained exceptionally long introns and encoded for proteins essential for neuronal function. A subset of these mRNAs were downregulated in TDP-43 aggregate-containing

motor neurons isolated from a sALS patient, suggesting a common loss-of-function pathway underlying neuronal cell death in TDP-43 and FUS pathology.

Binding properties		TDP-43	FUS
Brain RNA targets		>6,000	>5,500
RNA binding sites		>40.000	>44,000
Binding sequence		UG repeats	GUGGU repeats
Knockdown	Splicing changes	>950	>370
	RNAs changes	>600	>600

Table 1.2. TDP-43 and FUS brain RNA-binding properties. Figure adapted from (Ling et al., 2013). Data collected from (Colombrita et al., 2012; Hoell et al., 2011; Ishigaki et al., 2012; Lagier-Tourenne et al., 2012; Nakaya et al., 2013; Polymenidou et al., 2011; Rogelj et al., 2012; Sephton et al., 2011; Tollervey et al., 2011).

1.4.3 Pathological roles

TDP-43 proteinopathies are defined by the presence of inclusions composed of abnormal TDP-43 (Keating et al., 2022), often accompanied by the loss of normal nuclear TDP-43. Pathological TDP-43 exists as truncated N-terminals and C-terminal fragments that are hyperphosphorylated and ubiquitinated (Neumann et al., 2006). The lack of the NLS can cause mislocalisation from the nucleus and cytoplasmic accumulation. Once in the cytoplasm, TDP-43 is prone to aggregation. Some *TARDBP* mutations are associated with a greater aggregation propensity and increased formation of neurotoxic, insoluble TDP-43 species (Benson et al., 2021). TDP-43 pathology has been observed in other NDDs, like PD, AD and HD (de Boer et al., 2021). It is also the primary proteinopathy in a

newly classified form of dementia, limbic-predominant age-related TDP-43 encephalopathy (LATE) (Nelson et al., 2019).

FUS proteinopathies are also defined by the presence of FUS-positive inclusions. Mislocalisation of FUS from the nucleus to the cytoplasm happens to a lesser degree than TDP-43 pathology, as some nuclear FUS staining is preserved in neurons with inclusions (Rademakers et al., 2010). Many mutations cause FUS redistribution to the cytoplasm (Kwiatkowski et al., 2009; Vance et al., 2009). FUS does not undergo the same post-translation modifications as TDP-43; it is neither ubiquitinated nor hyperphosphorylated as FUS is full length with no signs of cleavage products (Lanson & Pandey, 2012). Non-mutated FUS inclusions have been found in other NDDs like FUS-FTLD and neuronal intermediate filament inclusion disease (NIFID) (Neumann, Roeber, et al., 2009)

These key histological hallmarks suggest two non-mutually exclusive disease mechanisms underlying ALS-FTD spectrum disorders; nuclear loss-of-function (LOF) and cytoplasmic gain-of-function (GOF).

Nuclear LOF includes alterations in RNA-metabolism processes (**Figure 1.5**). This is evidenced by the dysregulation of brain RNA targets and splicing patterns after TDP-43 and FUS knock-down (**Table 1.2**). When TDP-43 is depleted, pre-mRNA with exceptionally long introns are predominately affected. Expression of these abnormal transcripts are enriched in the brain and they encode for proteins involved in synaptic function and other neurological diseases, e.g., *PARK2*, *NRXN1*, *NRXN2* and *NLGN1* (Polymenidou et al., 2011; Sephton et al., 2011). FUS regulates the processing of long intron-containing transcripts involved in neurogenesis and its RNA targets encode for proteins involved in DNA damage

response and repair pathways (Zhou et al., 2014). Dysregulation of these RNA processes in disease will reduce protein levels, leading to neuronal dysfunction. Alterations in splicing patterns can occur. Loss of TDP-43 from the nucleus can cause the abnormal inclusion of cryptic exons in mRNA and thus reduced protein expression. This mechanism has been linked to reduced UNC13A and STMN2 protein levels following TDP-43 knockdown and mislocalisation in cell lines, as well as in iPSCs motor neurons and post-mortem neuronal tissues (Klim et al., 2019; Ma et al., 2022). Variants of their genes have been linked to ALS and/or FTD, e.g., a *STMN2* variant linked to sALS (Theunissen et al., 2021). Two common intronic *UNC13A* polymorphisms associated with ALS and FTD were found to promote cryptic splicing, making cells more sensitive to partial TDP-43 loss seen in early disease stages (Brown et al., 2022; Brown et al., 2021). Mutations targeting alternative splicing can affect the autoregulation of TDP-43 and FUS, causing increased increase nuclear and cytoplasmic protein levels (Ayala et al., 2011; Humphrey et al., 2020; Y. Zhou et al., 2013)

Cytoplasmic GOF refers to the toxic effects caused by mutant proteins/cytoplasmic accumulation and their associated aggregates/inclusions. This is purported to cause cellular stress, mitochondrial dysfunction, aberrant stress granule formation, reduced autophagy and deficits in proteasomal processes (Carey & Guo, 2022; Chung et al., 2018; de Boer et al., 2021). Prion-like templating is another purported cytoplasmic GOF mechanism implicated in ALS-FTD pathology (Polymenidou & Cleveland, 2011). Prion-like domains have been identified in both TDP-43 and FUS. Insoluble TDP-43, isolated from the brains of ALS and FTLD-TDP patients, triggered prion-like seeding and aggregation in cells (Nonaka et al., 2013).

1.4.3.1 Gaps in the field

Despite the extensive research in this field, very little is known about early-stage ALS/FTD pathomechanisms. It remains unclear if FUS/TDP-43 mediated toxicity is driven by GOF, LOF or both. This is further complicated by the fact that not all clinical aspects of TDP-43 or FUS pathology are found in animal models and patients, e.g., the absence of aggregates in the *Fus*$^{\Delta 14}$ mouse despite displaying neuromuscular and motor phenotypes (Devoy et al., 2017), and lack of TDP-43 cytoplasmic mislocalisation in the ALS-causing *Tardbp*^{Q331K} mutation. This indicates that protein aggregates may not be important in early disease pathomechanisms and these models may shed light on initial disease processes.

Pathological characterisation of TDP-43 and FUS is usually restricted to neuronal tissues. However, both proteins are expressed throughout the body and their associated disorders, ALS and FTD, are clinically considered multi-system. Peripheral pathomechanisms may be playing a significant role in key clinical symptoms, e.g., metabolic perturbations. FUS and TDP-43 RNA-processing functions in non-neuronal tissues are unknown, so it is difficult to determine if similar or different pathways are affected across tissues/systems. Therefore, it is important to understand the systemic pathological mechanisms of these RNA-binding proteins.

1.5 Models in ALS/FTD research

ALS-FTD spectrum disorders are highly complex and heterogeneous, involving multiple systems. To add to the complexity, a continuously increasing number of genes have been found to be causative or modifiers of these devastating conditions. While our ALS and FTD knowledge has progressively increased over the years, the precise pathomechanisms underlying these conditions remain to be elucidated. Despite these conditions being characterised over 130 years ago, there are still no cures.

As patient tissues are usually only available post-mortem, *in vitro* and *in vivo* models are widely used to understand early pathological mechanisms. The goal is to translate discoveries from a less complex model to human patients. It is impossible for models to recapitulate every clinical feature. Each model has its advantages and limitations which should be considered when weighing their contributions to the field and selecting a model for a particular study (Lutz, 2018; Morrice et al., 2018). Models need to be evaluated in three ways; disease-relevant mechanisms (construct validity), phenotypes modelling clinical symptoms (face validity) and the translatability of the data they generate (predictive validity) (Tadenev & Burgess, 2019).

In vitro models are used in research for several reasons; cheap, infinite lifespan (to an extent) and shorter experimental duration (Slanzi et al., 2020). In ALS-FTD research, cell lines expressing disease-linked genes have greatly helped in the understanding of cellular and molecular pathomechanisms, like aberrant aggregation and protein misfolding (Boeynaems et al., 2018). For example, FUS and TDP-43 roles in liquid-liquid phase separation and stress granule formation

were discovered using human cell-lines with mutations in the LCD domains of these proteins (Han et al., 2012; Molliex et al., 2015). The budding yeast *Saccharomyces cerevisiae* has been used to model cytotoxicity induced by ALS-linked proteins and the screening of modifier genes (Elden et al., 2010; Jovičić et al., 2015; Kim et al., 2014). Human-induced pluripotent stem cells (iPSCs) are generated directly from individual patients with endogenous familial or sporadic mutations (Chang et al., 2020). Although iPSC technology removes the species-specificity problem associated with animal models, it is still a “closed” *in vitro* system with numerous limitations (Karagiannis & Inoue, 2020). Cells are unable to recapitulate the complex *in vivo* environment of tissues and the cell-cell interactions which are needed in the study of human diseases. Additionally, NDDs are multi-system disorders and cells cannot reproduce the systemic interactions that occur in disease.

The mouse (*Mus musculus*) is the most commonly used *in vivo* model in modern biomedical research. Mice and humans share >90% of genes (Monaco et al., 2015), allowing comparative mechanistic studies. There are practical advantages of using mice in research; small, easy to transport and can be maintained in a laboratory setting. Mice have short gestation times and produce large litters. They also have a rapid development to adulthood and relatively short lifespans (Bryda, 2013).

Genetic linkage mapping, genome sequencing and sophisticated strategies for genetic manipulation have accelerated the application of mice in ALS/FTD research (Masopust et al., 2017). To date, there are >100 different ALS mouse models, covering almost all known causative genes for ALS and FTD. This has

significantly contributed to the understanding of pathological mechanisms and phenotypic outcomes of ALS/FTD mutations (Ahmed et al., 2017; Lutz, 2018).

1.6 Selecting a mouse model

This project will be using mouse models to investigate the systemic pathological effects of TDP-43 and FUS. There are various *Tardbp* and *Fus* mouse models available (**Table 1.3** and **1.4**), each modelling different aspects of the disease. Selecting the most appropriate model for a particular study is vital as it can affect reproducibility and clinical translatability. Various factors that influence the selection process.

1.6.1 Transgenic versus physiological models

1.6.1.1 Transgenic models

Traditionally, the majority of mouse models used in ALS/FTD research are transgenic animals, overexpressing the mutant or wild-type human protein of interest. The transgene DNA is injected into embryos and randomly inserted into the host mouse genome, under the control of exogenous promoters (e.g., Thy 1.2, CAMKII and CAG) or endogenous promoters of the transgene. Exogenous promoters ensure high levels of protein expression in the tissues of interest. Issues can arise with the choice of the promoter as the sequence may not be present in all tissues, affecting the spatial and temporal expression of the transgene and thus phenotypes (Haruyama et al., 2009). Due to constraints on DNA insert size in the plasmid vectors used to subclone constructs, often the coding complementary DNA (cDNA) sequence of the transgene is used to create transgenic animals. Bacterial artificial chromosome (BAC) vectors avoids these problems by inserting the non-coding and regulatory sequences of the gene of interest (GOI), inserts of up to ~200 Kb. This is particularly important in *C9orf72*-ALS modelling as the mutation is intronic. This process results in low copy

numbers, limiting the effects of overexpression of the GOI (De Giorgio et al., 2019).

Before clustered regularly interspaced short palindromic repeats (CRISPR) and CRISPR-associated endonuclease (Cas9) (CRISPR/Cas9)-based technologies, transgenics were the fastest way to produce new mouse strains. The dominant nature of the transgene and high protein levels means that phenotypes usually manifest earlier and models have a fast disease progression. The *SOD1*^{G93A} mouse was the first ALS transgenic line (Gurney et al., 1994), and has since been the standard for testing new therapeutics for ALS. However, the overreliance on this model has contributed to the lack of pre-clinical translatability in ALS research. *SOD1* mutations account for a small percentage of all ALS cases (sporadic and familial), therefore this model is not reflective of the wider clinical population. As a result, there is a need to study a range of models that represent different genetics and pathologies.

Transgenic animals have many limitations. A study found that at least 75% of commonly used transgenic mice had altered DNA sequences around the insertion site, including large deletions and structural changes that disrupted coding genes (Goodwin et al., 2019). This may cause phenotypes unrelated to the transgene sequence. The exogenous DNA usually inserts multiple copies which affects the transgene protein levels. The success of the *SOD*^{G93A} mouse is due to this characteristic as high protein levels mediate the fast onset of phenotypes, enabling researchers to study disease trajectory within ~5 months. However, multiple copies can cause instability within the transgene arrays and stochastic changes in copy numbers which can significantly alter phenotypes (Acevedo-Arozena et al., 2011; Alexander et al., 2004; Devoy et al., 2021).

These consideration are crucial when studying the biological function of RNA-binding proteins. TDP-43 and FUS are extremely dosage sensitive and a slight change from physiological levels can cause severe phenotypes, even if the protein product is wild-type. The transgenic hTDP-43^{WT} mouse expresses wild-type protein levels 3.8-5.1x more than endogenous levels, and this caused a 25% motor neuron loss and TDP-43-containing cytoplasmic inclusions (**Table 1.3**) (Wils et al., 2010). Overexpression of the human wild-type FUS (h*FUS*^{WT}) resulted in severe motor phenotypes; a 60% loss of motor neurons and FUS aggregates (**Table 1.4**) (Mitchell et al., 2013). The mouse protein may also interfere with the human protein's toxicity. Additionally, RNA-binding proteins tightly autoregulate the expression of their transcripts. When expression levels of wild-type or mutant proteins rise above a threshold, autoregulation mechanisms reduce endogenous transcript expression levels which can contribute towards toxicity (De Giorgio et al., 2019). Therefore, phenotypes observed in transgenic models may not be representative of the underlying disease mechanisms (de Boer et al., 2021).

1.6.1.2 Physiological models

Due to advancing genetic manipulation methods, there are multiple methods to generate mutant mouse models that express the relevant protein at physiological levels, at the right place and time. These include random mutagenesis, gene targeting and editing, and genomic humanisation by homologous recombination (HR).

i. Random mutagenesis

Random mutagenesis is the method of introducing random mutations in the genome. This is commonly done by injecting the powerful mutagen N-ethyl-N-nitrosourea (ENU) into adult male mice, inducing point mutations in the

spermatogonial stem cells. These mice mate with wild-type females and the progeny are screened for phenotypes. The DNA and sperm from male progeny are stored for later genotype screens, in which scientists assess the DNA for point mutations in their gene of interest. The sperm sample containing the 'hit' point mutation is then used for *in vitro* fertilisation to rederive the mouse line (Acevedo-Arozena et al., 2008; Stottmann & Beier, 2014). This method was used to generate the *Tardbp*^{M323K} mouse (**Table 1.3**). A mutation identified in the genotype screen does not guarantee a disease-relevant phenotype, which can be time and cost consuming, e.g., the *Tardbp*^{Q101X} mouse (**Table 1.3**) (Ricketts et al., 2014). However, recent biochemistry and structural knowledge of protein domains can help predict which mutations will cause phenotypes (e.g., NLS region of FUS).

ii. Gene targeting and editing

Gene targeting involves the targeting and modification of an endogenous locus of interest. In KO models, the sequences critical for the expression of a functional gene product are removed. KO models are useful to understand the biological function of the gene. For example, TDP-43 KO mice are not viable, indicating a developmental role of this protein. KO models can also determine if there is a LOF component in disease pathomechanisms, e.g., conditional TDP-43 KO mice develop motor neuron degeneration (Kraemer et al., 2010).

Gene targeting can also insert specific mutations into the endogenous mouse gene, resulting in the physiological expression of the mutant protein. Previously, homologous recombination (HR) in embryonic stem (ES) cells was used for gene targeting. A construct containing the mutation of interest (flanked by two regions homologous to the target region) and a selection cassette is electroporated into

mouse ES cells. Once the cassette is incorporated, the selection cassette can be used to identify the correctly targeted clone via antibiotic resistance (Leavitt & Hamlett, 2011). Gene targeting is now achieved using CRISPR/Cas9, to introduce point mutations into the genome (Doudna & Charpentier, 2014). This method is more efficient, quicker and cheaper than HR in ES cells; it was used to generate the *Tardbp*^{Q331K} mouse (**Table 1.3**) (White et al., 2018).

iii. Humanised knock-in (KI) models

Gene targeting techniques can be used to knock-in human genomic loci, generating humanised mouse models. These models are clinically relevant when modelling human conditions. For example, the human SOD1 protein has distinct biochemical properties associated with specific residues that are not present in the endogenous mouse protein but are important in proteinopathies (Crown et al., 2020; Nagano et al., 2015). The *Fus*$^{\Delta 14}$ mouse was the first genomically humanised knock-in model, but this was partial humanisation (**Table 1.4**) (Devoy et al., 2017). Recently, fully genomically humanised knock-in models of *hSOD1*, *hTARDBP* and *hFUS* were produced by HR. All genes functionally replaced their mouse orthologs, leading to the expression of the human protein at endogenous levels in homozygous mice. Phenotypic and molecular characterisation revealed that *hFUS* mice were normal throughout their entire lifespan, indicating that humanisation is not toxic and can be used to introduce fully mutated human genes in the future (Devoy et al., 2021).

Model	Method	Strain	Protein levels*	Phenotype							Pathology							References
				Onset	Survival	Weakness	Paralysis	Motor	Weight loss	Cognitive	MN damage	TDP-43 inclusions		Protein nuclear loss	Gliosis	Brain changes	Other	
												N	C					
hTDP-43^{WT}	Transgenic (mPrP)	C57BL/6	2.5x	2-w	4.5-8.5w	n.s.	✓	✓	✓	n.s.	✓	✓	✓	✓	✓	✓		(Xu et al., 2010)
hTDP-43^{WT}	Transgenic (mPrP)	CD1 or mixed	3-4x		N	✓	✓	✓	✓	n.s.	x	x	x	x	✓	n.s.	Ubiquitin staining in neurons	(Stallings et al., 2010)
hTDP-43^{WT}	Transgenic (mThy1.2)	C57BL/6	2.3-4.6x	M: 2-2.5w, F: 12w	N	✓	n.s.	✓		n.s.	✓	✓	x	n.s.	✓	n.s.	TDP-43 negative cytoplasmic accumulations of mitochondria, abnormal NMJ morphology	(Shan et al., 2010)
hTDP-43^{WT}	Transgenic (mThy1.2)	C57BL/6	3.8-5.1x	2-8.5w (PTE)	4-29w (PTE)	n.s.	✓	✓	n.s.	n.s.	✓	✓	✓	✓	✓	✓		(Wils et al., 2010)
hTDP-43^{WT}	Transgenic (mCaMKII TRE)	C57BL/6J x C3HeJ	8-9x	8-49w	n.s.	n.s.	n.s.	✓	✓	✓	✓	x	✓	✓	✓	✓		(Igaz et al., 2011)

mTDP-43^{WT}	Transgenic (mCaMKII)	FVB	2x	8w	71w	✓	n.s.	✓	n.s.	✓	n.s.	x	✓	✓	✓	✓		(Tsai et al., 2010)
hTDP-43^{G348C}	BAC transgenic (mTardbp)	C3H x C57BL/6	3x	30w	N	n.s.	n.s.	✓	n.s.	✓	✓	x	✓	x	✓	n.s.	Peripherin aggregates, neurofilaments	(Swarup et al., 2011)
hTDP-43^{A315T}	BAC transgenic (mTardbp)	C3H x C57BL/6	x	30w	N	n.s.	n.s.	✓	n.s.	✓	✓	x	✓	x	✓	n.s.	Peripherin aggregates, increase in small motor axons	(Swarup et al., 2011)
hTDP-43^{M337V}	Transgenic (mPrP)	CD1 or mixed	>10x	?	16-42d	✓	n.s.	✓	✓	n.s.	✓	x	✓	x	✓	n.s.	Neuronal morphological abnormalities	(Stallings et al., 2010)
hTDP-43^{A315T}	Transgenic (mPrP)	CD1 or mixed	4x	4w	10.7-37.5 w	✓	✓	✓	✓	n.s.	✓	x	✓	x	✓	n.s.	Ubiquitinated cytoplasmic inclusions	(Stallings et al., 2010)
hTDP-43^{M337V}	Transgenic (mPrP)	C57BL/6	1-2.7x	3w	4w	✓	n.s.	✓	✓	n.s.	✓	✓	✓	x	✓	✓	Hyperphosphorylated tau	(Xu et al., 2011)
hTDP-43^{M337V}	Transgenic (mPrP) myc-tagged	C57BL/6	Similar	40w	N	n.s.	x	✓	n.s.	n.s.	✓	x	x	x	n.s.	n.s.		(Arnold et al., 2013)

hTDP-43^{M337V}	Transgenic (mThy1.2)	C57BL/6J	1.7x	11d	17-18d	✓	✓	✓	✓	n.s.	n.s.	x	✓	✓	✓	✓		(Janssens et al., 2013)
hTDP-43^{Q331K}	Transgenic (mPrP) myc-tagged	C57BL/6	3x	3m	N	✓	x	✓	n.s.	n.s.	✓	n.s.	n.s.	x	✓	n.s.	Vacuolisation and myelin defects in motor axons, reduced NMJ endplates	(Arnold et al., 2013)
hTDP-43$^{Q331K\text{-}low}$	Transgenic (mPrP) myc-tagged	C57BL/6	n.s.	n.s.	n.s.	n.s.	x	✓	n.s.	n.s.	✓	x	x	x	n.s.	n.s.		(Arnold et al., 2013)
hTDP-43$^{WT/Q331K}$	Transgenic (mPrP) myc-tagged	C57BL/6	3.3x	3w	60-68d	✓	✓	✓	✓	n.s.	✓	x	✓	✓	✓	✓		(Mitchell et al., 2015)
TDP-43$^{\Delta NLS}$	Transgenic (mCaMKII TRE)	C57BL/6J x C3HeJ	1.7x	7d PI	n.s.	n.s.	✓	✓	n.s.	✓	✓	x	✓	✓	✓	✓		(Igaz et al., 2011)
TDP-43$^{\Delta NLS}$	Transgenic (NEFH) doxycycline (DOX)-suppressive	C57BL/6J x C3HeJ	<10x	2w OD	10.3 w OD	✓	n.s.	✓	✓	n.s.	✓	x	✓	✓	✓	✓		(Walker et al., 2015)
***Tardbp*^{Q331K}**	Gene-targeted knock-in (mTardbp)	C57BL/6J	Similar	4m	N	x	x	x	↑	✓	x	x	x	x	?	✓	Brain splicing differences, altered TDP-43 autoregulation	(Lin et al., 2021; White et al., 2018)

***Tardbp*^{Q101X}**	ENU	C57BL/6J	Similar	32w	N	x	x	✓	x	x	x	n.s.	n.s.	n.s.	n.s.	n.s.		(Ricketts et al., 2014)
***Tardbp*^{F2101} (RRM2mut)**	ENU	C57BL/6J	Similar		N	x	x	x		x	x	x	x	x	x	?	TDP-43 LOF (exon inclusion leading to cryptic exons), reduced RNA binding, HOMS embryonic lethal	(Fratta et al., 2018; Oliveira, 2014)
***Tardbp*^{M323K}**	ENU	C57BL/6J x DBA/2J	Similar	7m	N	x	x	✓	?	?	✓	x	x	x	?	?	TDP-43 GOF (increased exon exclusion leading to skiptic exons), increased Tardbp intron 7 retention	(Fratta et al., 2018; Oliveira, 2014)

Table 1.3. *Tardbp* mouse models detailing mean disease onset, survival, phenotype and pathology. Proportional to expression (PTE). Post induction (PI). Off DOX (OD). *compared to endogenous protein levels. Onset and survival: days (d), weeks (w), months (m) and normal (N). TDP-43 inclusions: nuclear (N) or cytoplasmic (C). Not significant (n.s.). Present (✓). Absent (x). Unknown (?).

Model	Method	Strain	Protein levels*	Phenotype							Pathology								References
				Onset	Survival	Weakness	Paralysis	Motor	Weight loss	Cognitive	MN loss	FUS inclusions		Protein nuclear loss	Gliosis	Brain changes	Other		
												N	C						
***FUS* KO**	n.s.	C56BL/6	n.s.	EL	16h	n.s.	n.s.	n.s.	n.s.	n.s.	n.s.	n.s.	n.s.	n.s.	n.s.	n.s.	Failed to suckle, reduced thymus volume		(Hicks et al., 2000)
***FUS* KO**	n.s.	C57BL/6 J x ICR	<20%	n.s.	n.s.	n.s.	n.s.	n.s.	✓	✓	x	n.s.	n.s.	n.s.	n.s.	✓			(Kino et al., 2015)
h*FUS*^{WT}	Transgenic (CAG)	C57BL/6 x Meox2	Similar	10d	<30d	✓	n.s.	✓	✓	x	x	x	x	n.s.	✓	n.s.	NMJ loss		(Sephton et al., 2014)
h*FUS*^{R521G}	Transgenic (CAG)	C57BL/6 x Meox2	Similar	10d	<30d - N	x	n.s.	✓	✓	x	x	x	x	n.s.	✓	n.s.	NMJ loss, dendritic defects		(Sephton et al., 2014)
h*FUS*^{WT}	Transgenic (mPrP)	C57BL/6	1.7x	4w	12w	n.s.	✓	✓	✓	x	✓	✓	✓	x	✓	x	NMJ loss, muscular atrophy		(Mitchell et al., 2013)

Partial *FUS*$^{\Delta NLS}$ KO	Transgenic (Thy 1.2)	n.s.	12w	n.s.	✓	n.s.	✓	x	x	x	✓	x	✓	x	✓	x	UMN loss, cytoplasmic FUS, p62	(Shiihashi et al., 2016)
***Fus*$^{\Delta 14}$**	Gene targeted and partial humanisation	C57BL/6 J	Similar	N	n.s.	x	x	✓	x	x	✓	x	x	✓	n.s.	x	HOM embryonic lethal, progressive motor deficits, altered gene expression	(Devoy et al., 2017)

Table 1.4. *Fus* mouse models detailing mean disease onset, survival, phenotype and pathology. *compared to endogenous protein levels. Onset and survival: days (d), weeks (w), months (m) and normal (N). FUS inclusions: nuclear (N) or cytoplasmic (C). Not significant (n.s.). Present (✓). Absent (x). Unknown (?).

*Tables 1.3 and 1.4 do not provide a comprehensive list of all the *Tardbp* and *Fus* mouse models in literature. The purpose of these tables is to give examples of the different technologies used to develop mouse models.

1.6.2 Strains and genetic backgrounds

Inbred mouse strains are commonly used in research because these mice display lower within-strain phenotypic variability. This is important when determining the relative contribution of genetic and environmental factors on phenotypic readouts. Ruling out genetic variance means that researchers can modify parameters of interest and measure their effect, allowing for the discovery of causal factors and ensuring experimental reproducibility (Chebib et al., 2021). Inbred lines are created through generations of backcross breeding; mice are expected to be >99.8% homogenous after 20 generations of full-sibling mating (Green, 1981; Lyon & Searle, 1989). Minimal genetic variance is assumed within inbred strains but spontaneous mutations can occur in each generation causing mutation accumulation and genetic drift (Uchimura et al., 2015). However, there are breeding schemes designed to maintain the genetic stability of inbred lines, such as backcrossing (Flurkey et al., 2009).

Generations of interbreeding mean that animals are essentially homozygous at all loci. While this is desirable for investigating mutation/gene function, it can have some detrimental effects. Some mutations on inbred strains cause embryonic/perinatal lethality in homozygosity, e.g., the *Tardbp*^{M323K} and *Fus*$^{\Delta 14}$ mutations on the C57BL/6J background. However, this lethality can be rescued when the mutation is placed on congenic hybrid mouse strains (C57BL/6J x DBA/2J) (Fratta et al., 2018). Hybrid mice are generated by crossing mice of two inbred strains. The resulting F1 hybrids are genetically identical and carry alleles from each inbred parent. It is unclear how hybrid backgrounds can rescue homozygous lethality but it is thought that heterozygosity at all loci may play a role (Sprott & Ramirez, 1997).

Genetic drifts between inbred strains mean that there are differences in the genetic backgrounds, leading to inbred strain characteristics. Understanding the endogenous traits of inbred strains can be useful in the selection process. BALB/c and C3H mice are useful in mutagenesis programmes because they are particularly sensitive to mutagenesis by ENU (Beck et al., 2000). FVB mice are the preferred strain in producing transgenics due to their large pronuclei (Taketo et al., 1991). In neuroscience, genetic background selection is particularly important due to the distinct behavioural phenotypes of inbred strains (Crawley et al., 1997). FVS/NJ, SJL, A/J and Bub/BNJ mice are visually impaired and therefore not recommended for most behavioural tests. C57BL/6J mice are known to perform well in complex learning tasks (Morris water task, contextual fear conditioning and eight-way radical arm maze), while DBA/2 and BALB mice perform poorly. C57BL/6J and Swiss Webster mice show the strongest response to anxiolytic drugs and are used in the screening of new drugs. C57BL/6 mice are routinely used for substance research studies due to their preference for drugs and alcohol (Peirce et al., 1998). Despite the C57BL/6J strain displaying a high behavioural score, it does not necessarily mean that it is the best strain for all studies. A strain should be selected for its predicted sensitivity to the 'null' mutation effect. Therefore, a low-scoring strain may be ideal to detect mutations expected to increase a behavioural phenotype.

The genetic backgrounds of inbred strains can interact with mutations causing phenotypic differences. For example, differences in disease presentation and progression were reported between C57BL/6J and B6SJL mice carrying the *Sod1*^{G93A} mutation (Mancuso et al., 2012). Each strain may have different modifier

genes interacting with the target mutation, causing phenotypic variability (Montagutelli, 2000).

1.6.3 Models used in this project

After careful consideration of the literature and the particular aims of this project, physiological mouse models were the preferred choice. Homozygous mice carrying the *Fus*$^{\Delta 14}$ and *Tardbp*^{M323K} mutations were used to investigate the systemic pathological mechanisms of FUS and TDP-43. In addition to expressing proteins at endogenous levels, these models have been previously studied by collaborators (Devoy et al., 2017; Fratta et al., 2018). More information on each mouse line is available in the relevant results chapter.

Strain selection was very important in this project as both mutations caused embryonic lethality in homozygosity on the C57BL/6J background. Viable *Tardbp*^{M323K} homozygotes were produced on a F1 hybrid background (C57BL/6J x DBA/2J) and were subsequently published. However, the *Fus*$^{\Delta 14}$ mutation was only characterised in heterozygosity (C57BL/6J) background. F1 hybrid background progeny are known to survive better under stress, live longer and are more viable than their parental strains (hybrid vigour/heterosis) (Selman & Swindell, 2018). As a result, this project placed the mutation on a constant F1 hybrid background to generate viable homozygous mice. The *Fus*$^{\Delta 14}$ mutation was backcrossed onto congenic C57BL/6J and DBA/2J strains for at least ten generations, before intercrossing to produce F1 C57BL/6J x DBA/2J progeny. Despite the majority of clinical ALS and FTD cases being autosomal dominant, previous characterisation of these models revealed minimal phenotypes in heterozygous mice. As a result, this project investigated these mutations in homozygous mice.

1.7 Aims

Dysregulation in RNA processing is central in ALS and FTD pathogenesis, with TDP-43 and FUS being the main players. However, research into the pathological properties of these proteins has been restricted to neuronal tissues. Both proteins are expressed in most tissues and their related disorders, ALS and FTD, have multi-system effects. This project aims to understand the systemic pathological mechanisms of FUS and TDP-43 by characterising physiological mouse models containing *Tardbp* and *Fus* mutations. The mutations used in this project, *Tardbp*^{M323K} and *Fus*$^{\Delta 14}$, have already been documented in the literature (Devoy et al., 2017; Fratta et al., 2018) so this project will build on existing knowledge through the following aims.

1. The effects of the *Fus*$^{\Delta 14}$ mutation in homozygosity are unknown due to embryonic lethality on the C56BL/6J background. This project will:
    a) Produce viable homozygotes using a hybrid genetic background
    b) Generate comparative gene expression profiles from multiple tissues (neuronal and non-neuronal)
    c) Conduct follow-up behavioural (motor, cognitive and metabolic) and molecular (gene expression and staining) characterisation studies
    d) Determine genetic background interactions with the *Fus*$^{\Delta 14}$ mutation
2. Currently, the characterisation of the *Tardbp*^{M323K} mutation in homozygosity is incomplete (Fratta et al., 2018; Oliveira, 2014). By conducting a longitudinal phenotyping pipeline, this project will:
    a) Determine the motor, cognitive and metabolic effects of the *Tardbp*^{M323K} mutation
    b) Identify any early and/or progressive phenotypes

c) Determine the validity of the *Tardbp*^{M323K} mouse as a model to study characteristics of ALS-FTD spectrum disorders

The *Tardbp*^{M323K} homozygous mouse will be used to investigate if metabolic status can determine ALS-FTD spectrum phenotypes. Diet will be used to modify metabolic parameters.

3. Using the validated *Tardbp*^{M323K} mouse, this project will conduct a longitudinal diet study, comparing mutation phenotypic effects of a HFD and control LFD. This project will:
    a) Determine the diet modulation of mutation-driven motor and cognitive phenotypes
    b) Understanding the molecular mechanisms underpinning diet modulation

Materials and Methods

2 Materials and Methods

2.1 Animals

2.1.1 Housing conditions and Licensing

All mice were maintained and studied according to the UK Home Office legislation at the Medical Research Council (MRC) Harwell (project license 20/0005), with local ethical approval (MRC Harwell AWERB committee). Mice were group housed (same sex and mixed genotypes) in individually ventilated cages. Each cage contained aspen chip bedding, shredded paper and a cardboard tunnel for enrichment. Food and water were available *ad libitum*. Mice were kept under regular 12:12 hour light and dark conditions.

Mice in the diet study switched from the standard chow diet to either a 45 kcal% fat diet (HFD, Research Diets, D12451i) or a control 10 kcal% fat diet (LFD, Research Diets, D12450H) from 6 weeks of age. Diets had the same sugar content (17% sucrose) and were available *ad libitum*.

2.1.2 Generation of *Fus*$^{\Delta 14}$mice

The *Fus*$^{\Delta 14}$ mutation (g.13845A>G) at the splice acceptor site of intron 13 results in the skipping of exon 14, out-of-frame translation of exon 15, and C-terminal truncation of the FUS protein (FUS p.G466VfsX14). The *Fus* gene was genetically modified in C57BL6/N mouse ES cells (Devoy et al., 2017). Heterozygous mice carrying the point mutation were backcrossed for at least ten generations to place the *Fus*$^{\Delta 14}$ mutation on congenic C57BL/6J and DBA/2J backgrounds and eliminate other potential mutations. Subsequently, the two congenic lines were crossed to produce viable F1 C57BL/6J x DBA/2J homozygotes.

2.1.3 Generation of *Tardbp*^{M323K} mice

This line was identified after screening DNA archives from large-scale chemical mutagenesis projects (Acevedo-Arozena et al., 2008; Gondo et al., 2010). A missense mutation (p.M323K), within the C-terminal low complexity domain (LCD) of the endogenous mouse *Tardbp* gene, was selected. This mutation was placed on congenic C57BL/6J and DBA/2J backgrounds to eliminate other potential mutations. Subsequently, the two congenic lines were crossed to produce viable F1 C57BL/6J x DBA/2J homozygotes (Fratta et al., 2018).

2.1.4 Genotyping

At weaning, animals were earmarked using ear punch biopsy. This served as a tool to identify individual animals in a cage. The tissue from the biopsy was used for standard DNA extraction and genotyping.

Fus$^{\Delta 14}$ mice were genotyped using a qPCR copy count Taqman assay, in which the progress of the reaction was measured using a Taqman probe. Both wild-type (WT) and mutant (Mut) assays were run with an internal control, *Dot1l*. Primer and probe sequences can be found in **Table 2.1**.

The Allelic Discrimination assay was used to genotype *Tardbp*^{M323K} mutants. It is a multiplexed assay (two primer/probe pairs) with data collected at the end of the PCR process. Two Taqman probes were used in this assay, one detecting WT and the other detecting Mut. Primer and probe sequences can be found in **Table 2.2**.

Assay	Primers	Probe
FUSDelta14-TM1-WT1 (FAM labelled)	TGTTGGGTAGCAGAGACTTGA	TGTCTGTGCTCGCCC
	GAACTTCAGGAGCCAGGCTAATAT	
FUSDelta14-TM1-Mut1 (FAM labelled)	TGTTGGGTAGCAGAGACTTGA	CCTGTCTGTCGACACCC
	CTTCAGGAGCCAGGCTAATTAATAC	
Dot1l internal control	GCCCCAGCACGACCATT	CCAGCTCTCAAGTCG
	TAGTTGGCATCCTTATGCTTCATC	

Table 2.1. Sequences used to genotype *Fus*$^{\Delta 14}$ mutants

Primer	Allele 1 WT probe (FAM labelled)	Allele 1 Mut probe (TET labelled)
TCTGCAACGCTGCCTGAG	CCGCAGCCATCATCG	CGCAGCCTTCATCG
AGCTGGCTTGGGAAATAACCA		

Table 2.2. Sequences used to genotype *Tardbp*^{M323K} mutants

2.2 *In vivo* phenotyping tests

2.2.1 Body weight

Without being anesthetised, mice were weighed inside a beaker. To correct for animal movements, weight measurements were taken after five seconds. Body weights were collected weekly and before certain phenotyping tests, e.g., EchoMRI and indirect calorimetry.

2.2.2 EchoMRI

The non-anesthetised mouse was placed in a transparent plastic tube, which was then placed inside the EchoMRI^{TM}-100H machine. Using quantitative magnetic resonance technology, fat and lean mass measurements were obtained. Each measurement was corrected for the individual animal's body weight to give a % value.

2.2.3 Indirect calorimetry

Mice were placed in individual metabolic cages overnight. Each cage was connected to the PhenoMaster Indirect Gas Calorimetry module (TSE systems). The system was connected to the Siemens High-Speed Sensor Unit, which contained oxygen and carbon dioxide sensors. The amount of oxygen used and carbon dioxide released by the body was measured to determine EE and the respiratory exchange ratio (RER). EE values were corrected for the average genotype lean mass using 2-way ANCOVA (SPSS). Adjusted EE values were used for statistical analysis.

2.2.4 Grip strength test

Mice were placed on the grip meter (Bioseb) with all four paws on the grid. Once on the apparatus, traction was applied via the tail. The resistance the mouse

applied on the grid was recorded. Each mouse had three runs. The median value was corrected for the individual animal's body weight.

2.2.5 Gait analysis

Mice were placed in the Mousewalker apparatus as previously described (Mendes et al, 2015) and videos of them running along the walkway were recorded using a camera mounted on a tripod. Video recordings were exported using StreamPix6 software (NorPix, Montreal, Canada) and subsequently cropped. Gait analysis was conducted by Dr Rasneer Sonia Bains (Mary Lyon Centre). An unpublished Python script and deeplabcut deep learning platform (http://www.mackenziemathislab.org/deeplabcut) was used to extract the location of key mouse points, on a frame-by-frame basis, from the videos. The Python code used the outputs of the Deeplabcut model to extract different gait parameters (Mendes et al., 2015). For each animal, parameters are from the mean gait cycle. A gait (stride) cycle refers to the completion of a stance and swing phase in one limb. The stance phase is when the limb is on the ground. The swing phase is when the limb is in the air. Therefore, stride calculations require two sequential footprints. Stride length is the distance between two sequential footprints created by the same limb. Stride width is the distance between the left and right front limbs or hind limbs (Au - Wertman et al., 2019). Step length is the distance covered in one step.

2.2.6 Muscle physiology

Muscle force and motor unit numbers were examined following a published protocol (Joyce et al, 2016). In summary, the distal tendons of the tibialis anterior (TA) and extensor digitorum longus (EDL) muscles in the hind limbs of anesthetised mice were attached to isometric force transducers (Dynamometer

UFI Devices, Welwyn Garden City, UK), and the sciatic nerve was exposed. Squarewave pulses of 0.02 ms duration at supra-maximal intensity were used to stimulate the nerve to elicit TA or EDL isometric contractions. Trains of stimuli at frequencies of 40, 80 and 100 Hz were used and measured using the Scope software. Stimuli of increasing intensities were used to determine motor unit numbers innervating the EDL; this resulted in incremental increases in twitch tension due to successive recruitment of motor axons. The number of increments was counted giving an estimated number of functional motor units present in the EDL muscle (Fratta et al., 2018). These experiments were conducted at UCL, under the supervision of Dr Mhoriam Ahmed.

2.2.7 Nesting

Mice were placed in individual cages with aspen bedding and a single square nestlet (3g weight), with no tunnel enrichment. Nests were assessed the next day using the 'Deacon' score (R. M. Deacon, 2006): (1) nestlet not touched (90% intact), (2) nestlet partially torn (50-90% remaining intact), (3) nestlet mostly shredded but no identifiable nest site (4) an identifiable nest site but flat (more than 90% of the nestle torn) and (5) a near perfect nest with walls higher than mouse body height.

2.2.8 Marble burying

Nine glass marbles were evenly spaced in rows of three, in a cage containing approximately 4cm depth of aspen bedding. Mice were placed in the cage for 30 minutes. The number of marbles more than two-thirds buried were recorded (R. M. J. Deacon, 2006).

2.2.9 Light-dark box

A high sided Perspex box split into two zones, dark and light, was used in this test. The dark zone had black walls and a black lid. The light zone had clear walls, a white floor and no lid. The dark wall separating the zones had a small opening, allowing unrestricted movement between the zones. Light levels in the testing room (and light zone) were set at 100 lux. At the start of the experiment, the mouse was placed in the light zone and video tracking was initiated. The mouse was removed from the box after 5 minutes. The time spent in each zone and frequency of entries were calculated from the videos using the Ethovision software (Noldus, Netherlands).

2.2.10 Y-maze (forced alteration)

Mice were placed in a y-maze (40x 8 cm per arm, height 15cm) with one arm blocked off (novel arm) for 10 minutes (habituation period). Mice were allowed to explore the start arm and the familiar arm. At the end of this period, mice were returned to their home cage for ~2 minutes. The maze was cleaned with Distel disinfectant to remove odour cues. Mice were returned to the maze and allowed to explore all three arms, including the novel arm, for 5 minutes (test period). Time spent in each arm and the frequency of entries were recorded using the Ethovision software (Noldus, Netherlands).

2.2.11 3-chamber test

An arena with three chambers was used in this test. On days 1 and 2, mice underwent the habituation period. The mouse was placed in the empty arena for 10 minutes. All chambers were empty and open so the mouse was able to freely explore the entire arena. On day 3, mice underwent the test period. In the left chamber, there was a bar cage containing a novel mouse. In the right chamber,

there was an empty bar cage (novel object). The test mouse was placed in the arena for 5 minutes. Doors to both chambers were open so the test mouse could freely explore the entire arena. The time spent in each chamber and the frequency of entries were recorded using the Ethovision software (Noldus, Netherlands).

2.2.12 Fear conditioning test

On day 1, mice were placed individually into square arenas (17x17 cm, height 25cm) with metal grid floors (Ugo Basile, Italy). Light levels were set to ~26 lux in each arena. A conditioning protocol was initiated using the AnyMaze software (Version 4.5, Stoelting, USA) and consisted of 120s baseline recording, a 20s 90db tone (conditioned stimulus, CS), immediately followed by a 0.5s 0.4mA shock (unconditioned stimulus, UCS). The conditioning test lasted for 4 minutes and 20 seconds. Mice were then removed and placed in the home cage (Nobili et al, 2017). The arena was cleaned with Distel disinfectant and dried between each trial. The conditioning trial was carried out in the morning.

On day two, mice were placed back in the same arena to assess response to context. No tones or shocks were administered. This was carried out in the morning. Each trial lasted for 5 minutes. Four hours after the context trial, mice were placed in a new environment to assess response to a cue. Round arenas, with plastic floors and stripped walls, were used. The scent of vanillin was rubbed on the sides of the arena. Light levels were reduced to 15 lux. The trial consisted of a 120s baseline recording, followed immediately by a 20s 90db tone. The cue trial lasted for 3 minutes.

Mice were video tracked using AnyMaze software and freezing time was calculated using AnyMaze freezing detection parameters.

2.2.13 Food intake

Pairs of the same genotype were placed in a new cage to avoid stress from single housing. Food was weighed before and after a feeding period of ~24 hours. Food intake per cage was then divided by two.

2.2.14 Lipolysis

Mice were injected with 0.1mg/kg CL316243 (Cayman Chemical), a β3-adrenergic receptor agonist or phosphate-buffered saline as vehicle control. Blood was collected 1-hour post-injection via a terminal retro-orbital collection. Blood was centrifuged at 2000 rpm for 10 minutes to isolate plasma. To measure lipolysis, free fatty acids (FFAs) and glycerol levels were quantified using enzyme colorimetric assays on the Beckman Coulter AU680 clinical chemistry analyser.

2.2.15 Intraperitoneal glucose tolerance test (IPGTT)

Mice were fasted for 12 hours. Local anaesthetic cream (Lidocaine/Prilocaine cream, 25mg, Aspen Pharmacare) was applied to the tail of the mouse. An intraperitoneal (IP) injection of 20mg/kg glucose was administered. A small incision was made at the lateral vein of the tail to produce a drop of blood and baseline glucose levels (0 minutes) were recorded using the ACCU-CHECK Performa meter. Additional glucose measurements were taken at 15, 30, 60 and 120 minutes. These experiments were performed by Juan Miguel Godoy-Corchuelo (Corrochano group).

2.2.16 Plasma clinical chemistry

Mice were fasted for at least 4 hours. A non-recovery dose of sodium pentobarbital was administered (I.P). Once the mouse was unconscious (lack of corneal and pedal reflex but breathing), retro-orbital bleeds were conducted. A glass capillary was inserted in the posterior corner of the eye. Once the membrane

of the retro-orbital sinus is punctured, blood was collected in Lithium/Heparin collection tubes. Blood was centrifuged at 2000 rpm for 10 minutes to isolate plasma. Lipid levels (total cholesterol, triglycerides, LDL, HDL and FFAs) were quantified using enzyme colorimetric assays on the Beckman Coulter AU680 clinical chemistry analyser.

2.3 Molecular techniques

2.3.1 Tissue preparation

Mice were euthanized using appropriate Home Office Schedule 1 method.

Tissues used for staining: Terminal anaesthesia was administered to some animals before undergoing cardiac perfusion of fixative (4% in PBS, pH 7.4, ThermoFisher). Tissues were stored in PBS at 4ºC until required.

Tissues used for RNA: After dissections, tissues were snap-frozen in liquid nitrogen before being stored at -80ºC, until required.

Tissues were dissected from some animals and weighed. The weight, length and width of some brains were measured (without the cerebellum).

Livers from perfused animals were immersed in 30% sucrose for 2 days (cryoprotection). Tissues were dried and embedded in OCT using isopentane and dry ice. Using the cryostat, 12-µm sections were placed on charged slides and stored at -20°C. Before Oil Red O staining, slides were thawed at room temperature for ~30 minutes.

2.3.2 RNA-sequencing

RNA was extracted from snap-frozen tissues using the RNeasy Lipid Tissue Mini Kit (Qiagen). RNA quality and quantity were assessed using the RNA Nano 6000 Assay Kit of the Bioanalyzer 2100 system (Agilent Technologies, CA, USA). Individual tissue RIN values are available in **Appendix A7**. Samples were sent to Novogene Bioinformatics Technology Co., Ltd (Cambridge, UK) for library preparation, RNA sequencing and initial data analysis.

Sequencing libraries were generated using NEBNext® UltraTM RNA Library Prep Kit for Illumina® (NEB, USA) following the manufacturer’s recommendations and

index codes were added to attribute sequences to each sample. The clustering of the index-coded samples was performed on a cBot Cluster Generation System using PE Cluster Kit cBot-HS (Illumina) according to the manufacturer's instructions. After cluster generation, the library preparations were sequenced on an Illumina platform and paired-end reads were generated. The total number of reads was 30 million per sample.

Reference genome and gene model annotation files were downloaded from the genome website browser (NCBI/UCSC/Ensembl) directly. Indexes of the reference genome were built using STAR and paired-end clean reads were aligned to the reference genome using STAR (v2.5). HTSeq v0.6.1 was used to count the read numbers mapped of each gene. And then FPKM of each gene was calculated based on the length of the gene and reads count mapped to this gene. Differential expression analysis between genotypes was performed using the DESeq2 R package (2_1.6.3). The resulting P-values were adjusted using the Benjamini and Hochberg's approach for controlling the False Discovery Rate (FDR). Genes with an adjusted P-value <0.05 found by DESeq2 were assigned as differentially expressed.

Gene Ontology (GO) enrichment analysis of differentially expressed genes (DEGs) was performed using gprofiler. The gene ranking metric, determined by the inverse p-value, assigned a sign based on the direction of the log2 fold change. GO terms with corrected p-value<0.05 were considered significantly enriched by differentially expressed genes.

2.3.3 Quantitative real-time PCR (qRT-PCR)

RNA was extracted from snap-frozen tissues using the RNeasy Lipid Tissue Mini Kit (Qiagen). RNA extraction from cells (adipocytes) was performed using the Maxwell® RSC Instrument (Promega).

cDNA synthesis was performed using the High Capacity cDNA Reverse Transcriptase Kit (ThermoFisher Scientific) with 2µg of total RNA. cDNA for qPCR reactions was used at a final concentration of 20ng per well. Either Fast Sybr Green mastermix (ThermoFisher Scientific) or TaqMan™ PCR mastermix (ThermoFisher Scientific) was added, followed by the appropriate primer (**Table 2.3**) or Taqman assay (**Table 2.4**); final well volume of 20µl. All reactions were run in triplicates. Fold changes were calculated using the 2-ddct method using the 7500 Software v2.06 and normalised to appropriate reference genes (*s16* or *Canx*) relative to the wild-type genotype.

Gene	Primer Sequence (5'-3')		Supplier
Myosin heavy chain 1 (*Myh1*)	Forward	GCGAATCGAGGCTCAGAACAA	Integrated DNA Technologies
	Reverse	GTAGTTCCGCCTTCGGTCTTG	
Myosin heavy chain 2 (*Myh2*)	Forward	ACTTTGGCACTACGGGGAAAC	Integrated DNA Technologies
	Reverse	CAGCAGCATTTCGATCAGCTC	
Myosin heavy chain 4 (*Myh4*)	Forward	CTTTGCTTACGTCAGTCAAGGT	Integrated DNA Technologies
	Reverse	AGCGCCTGTGAGCTTGTAAA	
Myosin heavy chain 7 (*Myh7*)	Forward	ACTGTCAACACTAAGAGGGTCA	Integrated DNA Technologies
	Reverse	TTGGATGATTTGATCTTCCAGGG	
Sodium voltage-gated alpha subunit 4 (*Scn4a*)	Forward	TCTCCTCCTCCACCATCATC	Integrated DNA Technologies
	Reverse	CACCCTCCTCCATCTCAAAG	

Table 2.3. Primer sequences

Gene	Assay ID	Supplier
Adiponectin (*Adipoq*)	Mm00456425_m1	ThermoFisher Scientific
Peripilin 1 (*Plin1*)	Mm00558672_m1	ThermoFisher Scientific
Glucose Transporter 4 (*Glut4*)	Mm00436615_m1	ThermoFisher Scientific
Peroxisome proliferator activated receptor gamma (*Pparγ*)	Mm01184322_m1	ThermoFisher Scientific
Fatty acid synthase (*FASN*)	Mm00662319_m1	ThermoFisher Scientific
Lipase (*Lipe*)	Mm00495359_m1	ThermoFisher Scientific
Calnexin (*Canx*)	Mm00500330_m1	ThermoFisher Scientific

Table 2.4. Taqman assays

2.3.4 Adipose precursor isolation, culture and differentiation

Intestinal white adipose tissue (iWAT) was isolated from 8-week old mice and digested into individual wells of a 6-well plate containing 500µl digestion buffer. Tissues were manually minced on ice, and transferred into a 15ml tube and 4.5ml digestion buffer was added to ensure complete sample submersion. Samples were then incubated in a 37 ºC water bath for 60 minutes. Tubes containing the digested tissues were centrifuged for 3 minutes at 300g. The supernatant (floating adipocytes) was discarded to leave the pellet containing the supravascular fraction. This pellet was resuspended in 1ml growth media and the solution was filtered, through a 40um nylon cell strainer, into a 10cm dish. The cell strainer mesh was washed with an additional 9ml growth media. Media was changed the next day to remove dead cells.

Once cells were confluent, they were plated into a 6-well plate at approximately 240,000 cells/well. When cells were 2 days post-confluent, 2ml/well DIFF1

medium was added (day 0). On day 2, DIFF1 medium was refreshed. On day 4, DIFF1 medium was removed and replaced with DIFF2 medium. Media was changed every 2 days until adipocyte differentiation was complete on day 7.

Reagent details can be found in **Table 2.5**.

Reagents	Components
Digestion buffer	Sterile Hank's Balanced Salt solution (Sigma), 0.8 mg/ml collagenase type 2 (Worthington Biochemical Corporation), 3g per 100ml BSA with fatty acids
Growth Media	DMEM (ThermoFisher), GlutaMax (Gibco), 10% FBS (Life), 1% PS (Life)
DIFF1 Medium (per well)	2ml growth media, 2ul 0.5M IBMX (Sigma), 1ul 2mM Dexa (Sigma), 1ul 10mg/ml human insulin (Sigma)
DIFF2 Medium (per well)	2ml growth media, 1ul 10mg/ml human insulin (Sigma)

Table 2.5. Cell culture reagents

2.3.5 Oil Red O staining

Primary adipocytes grown on coverslips and liver sections were washed with PBS and fixed with 4% paraformaldehyde (PFA) (Sigma-Aldrich) for 30 minutes at room temperature. The fixative was removed, and samples were rinsed with deionised water. 1.5ml 60% isopropanol (Sigma-Aldrich) was added to each well and incubated at room temperature for 5 minutes. To make working Oil Red O, stock Oil Red O (300mg dissolved in 100ml 99% isopropanol) was diluted in deionised water (3:2). Isopropanol was removed from the samples and 1.5ml working Oil

Red O was added (30 minute incubation time for cells and 15 minutes for tissue sections). The stain was removed, and samples were washed with deionised water until the waste water was clear.

Liver sections were counterstained with haematoxylin gill 1 for 1-2 minutes. Sections were then washed with deionised water, dipped in 1% acid alcohol for 2-3 seconds and washed under running tape water until samples turned blue. Samples were covered with a coverslip using an aqueous mounting medium (Abcam). Liver sections were scanned using a Nanozoomer slide scanner (Hamamatsu) at 40x zoom.

Lipid accumulation in adipocytes was quantified using optical density (OD) absorbance measured at a wavelength of 500 nm, using a spectrophotometer (BioTek Epoch).

2.3.6 Motor neuron counts

Motor neuron counts were performed following a published protocol (Austin et al., 2022). Spinal cords were removed via hydraulic extrusion. A 1 cm section of the lumbar spinal cord bulge was dissected and embedded in OCT and frozen over isopentane on dry ice. Serial transverse sections (20μm) were cut from regions L1 to L6 of the lumbar spinal cord and collected onto glass slides. Every third section was analysed leaving a gap of 60μm between sections and ensuring the same motor neuron was not counted twice. Slides were stained for 20 minutes in Gallocyanin (0.3g gallyocyanin, 10g chrome alum, distilled water up to 100ml), rinsed with water, dehydrated and mounted using CV Ultra Mounting Media (Leica Biosystems). Sections were scanned using a Nanozoomer slide scanner (Hamamatsu) at 40x zoom and motor neurons counted. Motor neurons with the following criteria were counted: visible nucleolus, dense, a diameter of >15μm and

visible dendritic branching. About 35-40 sections were counted per animal and the level of the spinal cord standardised by morphological assessment, such that equivalent sections from L4-L5 were included for counting

2.3.7 Structural MRI scans

Mice were anesthetised with ketamine/xylazine and then intracardially perfused with PBS followed by 4% formalin, both containing a Godovist-constrat agent (Gd-CA, 2Mm, Bayer Vital GmbH, Germany). Brains were kept in the skulls and immersed overnight in 4% formalin/Gd-CA (2mM). They were then transferred to a PBS solution containing Gd-CA (2mM) and sodium azide (0.05%) and stored at 4°C until scanning.

Brains were shipped to the Mouse Imaging Centre (Toronto, Canada) for structural MRI scans. The scans were performed on a 7.0 tesla MRI scanner (Agilent Inc, California) using sixteen custom-built solenoid coils in parallel8. Images were registered using MBM.py10. Volumes were estimated from the Jacobian determinants and modelled as a function of genotype. Voxel-wise and structure-wise data was obtained. To obtain structure-wise data, volumes were compared to the DSURQE mouse atlas (Dorr et al., 2008). Local volume changes were used to calculate the absolute Jacobian determinant. Global scaling differences were used to calculate the relative Jacobian determinant. Analysis was conducted by Shoshana Spring (Mouse Imaging Centre, Canada).

2.4 Statistical analysis and graphical representations

Statistical analysis was conducted using GraphPad Prism and IBM SPSS Statistics.

At a single time point, two groups were compared using an unpaired t-test. Body weights between genotypes, across multiple time points, were compared using 2-way ANOVA repeated measures/mixed models and Bonferroni correction of multiple testing. The comparison of two independent variables (e.g., time and genotype), on a dependent variable, was conducted using 2-way ANOVA followed by the appropriate multiple comparisons test. Three or more groups were compared at a single time point using one-way ANOVA followed by the appropriate multiple comparisons test. Statistical analysis of qRT-PCR data was performed on ΔCT values. 2-way ANCOVA (SPSS) was used to correct EE data for genotype lean mass interaction. Statistical significance was defined as $p \leq 0.05$ for the analysis of phenotyping and molecular data. Refer to figure legends for n numbers (biological replicates), statistical tests and significance details. Where indicated, $*$=p≤0.05, $**$=p≤0.01, $***$=p≤0.001, $****$=p≤0.0001.

All graphs were generated using GraphPad Prism 9. Venn diagrams were created using Venny[2.1]. BioRender.com was used to create original diagrams/figures.

Results

Results I

Investigating the systemic effects of the *Fus*$^{\Delta 14}$ mutation in homozygosity

3 Investigating the systemic effects of the *Fus*$^{\Delta 14}$ mutation in homozygosity

3.1 Introduction

FUS has been implicated in several NDDs such as ALS, FTD and essential tremor (Deng et al., 2014). *FUS* mutations account for ~4% of fALS, the majority of which are found in the C-terminal NLS domain in exon 15 (Ticozzi et al., 2009; Vance et al., 2013). The NLS is necessary for the import of FUS into the nucleus, therefore disruption in this region can lead to the mislocalisation of the protein (Efimova et al., 2017; Nolan et al., 2016). However, FUS mislocalisation has been observed in ALS patients without *FUS* mutations (Tyzack et al., 2019), indicating a wider disease relevance and distinct mechanisms for pathological FUS development. Ubiquitinated, phosphorylated FUS cytoplasmic inclusions are seen in the motor neurons and glia of the motor cortex and spinal cord of ALS patients (Da Cruz & Cleveland, 2011). While *FUS* mutations are rare in FTD, cytoplasmic inclusions are seen in the frontal cortex, hippocampus and striatum of FTD patients (FTLD-FUS) (Mackenzie, Munoz, et al., 2011).

FUS pathology in NDDs means that research in this protein has been mainly focused in neuronal tissues (brain and spinal cord) (Deng et al., 2014). However, this protein is expressed in most tissues so FUS pathology (mislocalisation or cytoplasmic inclusions) might also be present in other cells and systems. This would mean that widespread FUS dysregulation, beyond cognitive and motor symptoms, is expected in these disorders. To investigate this hypothesis, the partially humanised *Fus*$^{\Delta 14}$ knock-in mouse was used. This mouse contains a point mutation (g.13845A>G) at the splice acceptor site of intron 13, causing the

skipping of exon 14, and a frameshifted exon 15 which has been partially humanised to mimic the human frameshifted C-terminus. This results in the abolition of the NLS and most of the third RGG-rich RNA-binding domain (Devoy et al., 2017). Unlike transgenic mice, where altered target protein levels can have toxic effects, this mutant FUS protein is expressed at physiological levels in this model.

Previous characterisation of *Fus*$^{\Delta 14}$ heterozygous mice on the C57BL/6J background revealed mild, late-onset neuromuscular and motor phenotypes (Devoy et al., 2017). No metabolic and cognitive/behavioural phenotypes were observed in these mice (data not published). These mild phenotypes were inconsistent with the aggressive nature of *FUS* mutations in humans, which can give rise to jALS cases with rapid lethal disease progression (Waibel et al., 2013). Studying this mutation in homozygosity may show more evident phenotypes and effects. Homozygous mice on the C57BL/6J background died at birth. Perinatal lethality of *Fus*$^{\Delta 14}$ homozygotes was rescued by producing this mutation on a congenic F1 hybrid genetic background (**Figure 3.1**). RNA-sequencing was performed on 6 different tissues to study the potential effects of the *Fus*$^{\Delta 14}$ mutation in and outside the neuronal system, and in relation to motor, cognitive and metabolic phenotypes. The transcriptomic data guided follow-up behavioural and molecular experiments, to relate altered genes/pathways to observed phenotypes.

The rescuing of perinatal lethality of homozygotes on a hybrid background suggests an interaction between the *Fus*$^{\Delta 14}$ mutation and genetic backgrounds. Each mouse strain has a unique background of alleles that may interact with and modify the mutant gene (Linder, 2001). It is important to determine how much of

the observed phenotypes are influenced by mutation and genetic background interactions. To determine the presence of these interactions, phenotypic differences between genetic backgrounds were investigated. Significant phenotypes observed in *FUS*$^{\Delta 14}$ heterozygous mice on the hybrid background (C57BL/6J x DBA/2J) were compared to heterozygous mice on the congenic C57BL/6J and DBA/2J backgrounds.

3.2 Results

3.2.1 Generation and viability of *Fus*$^{\Delta 14/\Delta 14}$ mice

Perinatal lethality of homozygous (*Fus*$^{\Delta 14/1\Delta 14}$) mice on the congenic C57BL/6J background meant that previous characterisation of this mutation was only conducted in heterozygous mice (*Fus*$^{\Delta 14/+}$) (Devoy et al., 2017). To overcome this, a hybrid background was used. Heterozygous mice carrying the point mutation were backcrossed and bred on two different congenic backgrounds, C57BL/6J and DBA.2J. These two congenic lines were crossed (C57BL/6J x DBA/2J) to produce viable *Fus*$^{\Delta 14/\Delta 14}$ mice on a F1 hybrid genetic background (**Figure 3.1**).

Fus$^{\Delta 14/\Delta 14}$ mice on this hybrid F1 background had reduced lifespans compared to their control *Fus*$^{+/+}$ littermates. Mortality was due to fatal seizures from 12 weeks of age. Therefore, this time-point was used as a humane end-point to avoid unnecessary suffering of the mice. Since male *Fus*$^{\Delta 14/\Delta 14}$ mice developed seizures slightly later, male mice were used for most studies. Significant phenotypes were verified in females when possible.

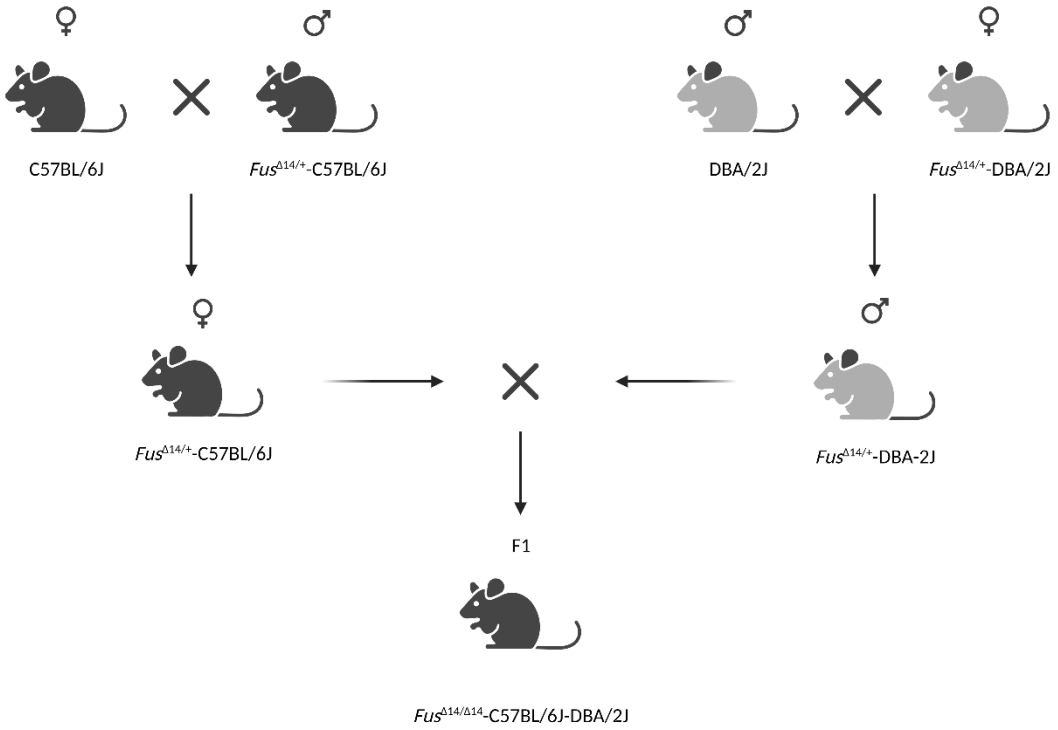


Figure 3.1. Generation of viable *Fus*$^{\Delta 14/1\Delta 14}$ mice on a hybrid background. The *Fus*$^{\Delta 14}$ mutation (g.13845A>G) at the splice acceptor site of intron 13 results in the skipping of exon 14, out-of-frame translation of exon 15, and C-terminal truncation of the FUS protein (FUS p.G466VfsX14). The *Fus* gene was genetically modified in C57BL6/N mouse embryonic stem cells (ESC). Heterozygous mice carrying the point mutation were backcrossed for at least ten generations to place the *Fus*$^{\Delta 14}$ mutation on congenic C57BL/6J and DBA/2J backgrounds and eliminate other potential mutations. Subsequently, the two congenic lines were crossed (C57BL/6J; DBA/2J) to produce viable *Fus*$^{\Delta 14/\Delta 14}$ mice on a constant F1 hybrid background. Diagram created using BioRender.com.

3.2.2 *Fus*$^{\Delta 14/\Delta 14}$ mice are proportionately smaller than control littermates

Mice were weighed weekly to monitor development and possible disease progression. Body weights were collected longitudinally and the data was analysed using 2-way ANOVA mixed effects and Bonferroni correction for multiple testing to evaluate genotype differences at each time-point.

From birth, *Fus*$^{\Delta 14/\Delta 14}$ mice were significantly smaller than control *Fus*$^{+/+}$ littermates (**Figure 3.2B**). *Fus*$^{\Delta 14/\Delta 14}$ mice weighed significantly less than *Fus*$^{\Delta 14/\Delta 14}$ mice

Fus$^{+/+}$ mice, and those differences remained throughout their lifespan in both sexes (**Figure 3.2A, Table 3.1** and **3.2**). No significant weight differences were seen between *Fus*$^{+/+}$ and *Fus*$^{\Delta 14/+}$ mice.

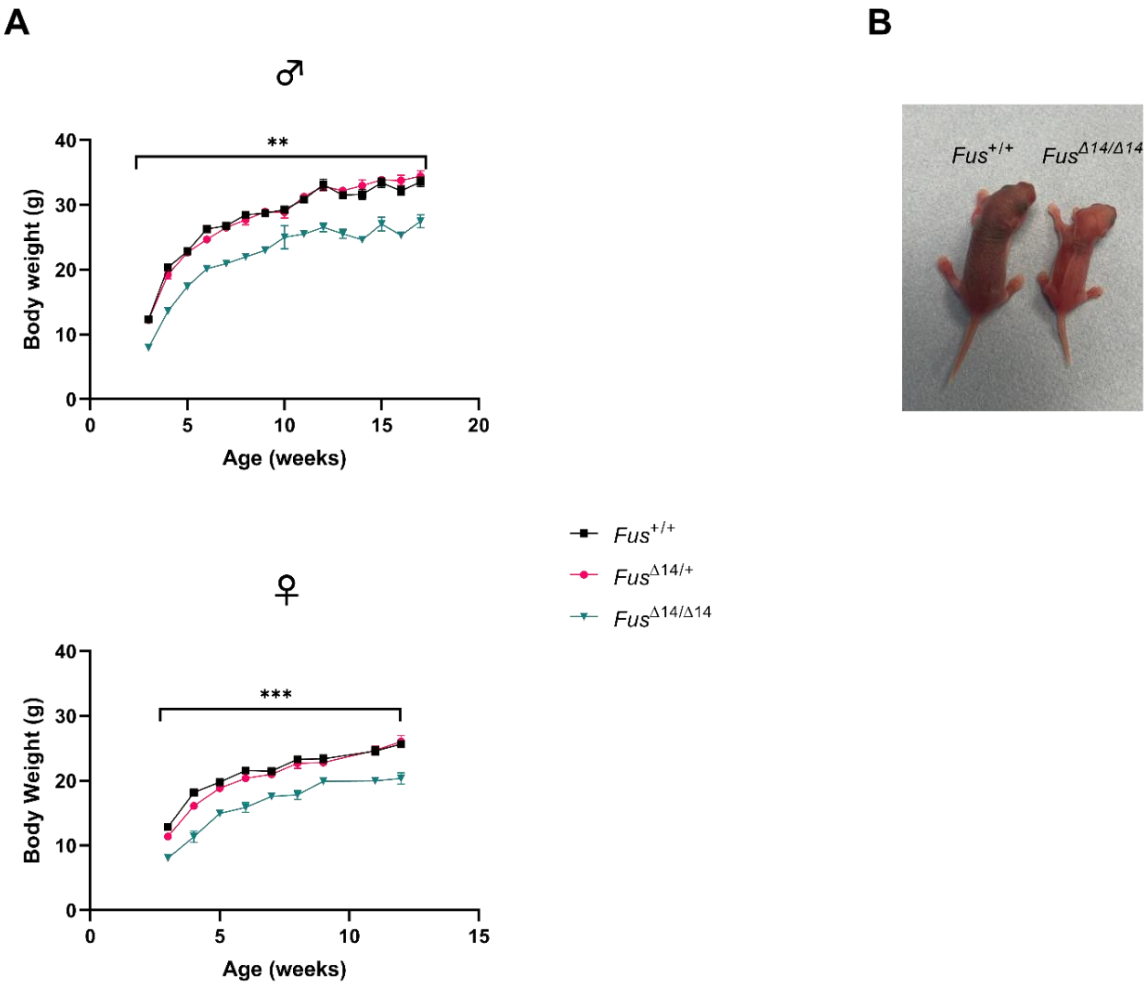


Figure 3.2. Weights and sizes of *Fus*$^{\Delta 14}$ mice. Figure shows weekly weights of male and female *Fus*$^{\Delta 14}$ mice (**A**) and a representative image comparing *Fus*$^{+/+}$ and *Fus*$^{\Delta 14/\Delta 14}$ mice at P0 (**B**). *Fus*$^{\Delta 14/\Delta 14}$ mice were smaller than their littermate controls from birth. Data shown as mean. Error bars denote SEM of data. Data analysed using 2-way mixed effects analysis and Bonferroni correction for multiple testing to evaluate genotype differences at each time-point. n numbers for each time-point can be found in **Table 3.1** and **3.2**. **p<0.01. ***p<0.001.

Age (weeks) ♂	Genotype									Adjusted p-value: *Fus*$^{+/+}$ vs *Fus*$^{\Delta 14/+}$	Adjusted p-value: *Fus*$^{+/+}$ vs *Fus*$^{\Delta 14/\Delta 14}$
	Fus$^{+/+}$			*Fus*$^{\Delta 14/+}$			*Fus*$^{\Delta 14/\Delta 14}$				
	Mean weight (grams)	SEM	n	Mean weight (grams)	SEM	*n*	Mean weight (grams)	SEM	*n*		
3	12.31	0.54	11	12.24	0.50	16	7.96	0.29	10	>0.9999	**<0.0001**
4	20.35	0.45	8	19.24	0.69	13	13.62	0.42	8	>0.9999	**<0.0001**
5	22.84	0.39	11	22.66	0.37	16	17.41	0.43	13	>0.9999	**<0.0001**
6	26.28	0.27	8	24.68	0.52	13	20.14	0.31	8	>0.9999	**<0.0001**
7	26.77	0.47	11	26.51	0.42	16	20.94	0.49	13	>0.9999	**<0.0001**
8	28.49	0.36	8	27.73	0.79	13	21.99	0.58	8	>0.9999	**<0.0001**
9	28.75	0.50	11	28.96	0.49	16	22.99	0.59	11	>0.9999	**<0.0001**
10	29.29	0.07	2	28.87	0.92	4	25.01	1.82	3	>0.9999	0.42700
11	30.85	0.56	11	31.28	0.44	16	25.51	0.49	13	>0.9999	**<0.0001**
12	33.15	0.84	7	32.87	0.67	13	26.54	0.69	8	>0.9999	**0.00020**
13	31.50	0.58	6	32.21	0.39	7	25.56	0.71	4	>0.9999	**0.00130**
14	31.66	0.78	2	32.99	0.92	4	24.62	0.00	1	>0.9999	
15	33.42	0.73	6	33.87	0.58	7	27.05	1.06	4	>0.9999	**0.00890**
16	32.17	0.71	2	33.77	0.81	4	25.32	0.00	1	0.67	
17	33.54	0.74	6	34.44	0.83	7	27.49	0.99	4	>0.9999	0.00770

Table 3.1. Mean body weights of male *Fus*$^{\Delta 14}$ mice and statistical analysis. Table showing mean weights, SEM, n numbers and adjusted p-values. Adjusted p-values in bold red indicate statistical significance.

Age (weeks) ♂	Genotype									Adjusted p-value: *Fus*$^{+/+}$ vs *Fus*$^{\Delta 14/+}$	Adjusted p-value: *Fus*$^{+/+}$ vs *Fus*$^{\Delta 14/\Delta 14}$
	Fus$^{+/+}$			*Fus*$^{\Delta 14/+}$			*Fus*$^{\Delta 14/\Delta 14}$				
	Mean weight (grams)	SEM	n	Mean weight (grams)	SEM	*n*	Mean weight (grams)	SEM	*n*		
3	12.83	0.42	16.00	11.37	0.41	17.00	8.06	0.45	10.00	>0.9999	**<0.0001**
4	18.18	0.26	11.00	16.13	0.50	10.00	11.34	0.88	9.00	>0.9999	**<0.0001**
5	19.80	0.33	16.00	18.86	0.26	17.00	14.96	0.37	13.00	>0.9999	**<0.0001**
6	21.60	0.24	11.00	20.39	0.40	10.00	15.88	0.77	9.00	>0.9999	**<0.0001**
7	21.49	0.47	16.00	20.98	0.43	17.00	17.59	0.43	13.00	>0.9999	**<0.0001**
8	23.32	0.34	11.00	22.68	0.78	10.00	17.83	0.71	9.00	>0.9999	**<0.0001**
9	23.37	0.62	16.00	22.83	0.52	17.00	19.92	0.52	13.00	>0.9999	**0.00080**
11	24.57	0.64	16.00	24.68	0.67	17.00	20.00	0.52	10.00	>0.9999	**<0.0001**
12	25.64	0.45	11.00	26.05	0.94	10.00	20.33	0.88	8.00	>0.9999	**0.00080**

Table 3.2. Mean body weights of female *Fus*$^{\Delta 14}$ mice and statistical analysis. Table showing mean weights, SEM, n numbers and adjusted p-values. Adjusted p-values in bold red indicate statistical significance.

3.2.3 Widespread transcriptomic dysregulation in *Fus*$^{\Delta 14/\Delta 14}$ mice

FUS is widely expressed. However, research into its pathological effects is mainly conducted in neuronal tissue. It remains unknown if, and how, *FUS* mutations affect other tissues and systems. This project aims to understand the wider role of FUS by conducting RNA-sequencing experiments in multiple tissues. A range of tissues were selected for analysis including the frontal brain, spinal cord, tibialis anterior (TA) muscle, liver, brown adipose tissue (BAT) and inguinal white adipose tissue (iWAT). Tissues related to metabolism (liver and adipose tissues) were selected since metabolic dysfunction has been observed in FUS-linked diseases, e.g., ALS and FTD (J. M. Godoy-Corchuelo et al., 2022). Tissues were collected from *Fus*$^{+/+}$ and *Fus*$^{\Delta 14/\Delta 14}$ male mice at 9 weeks of age (n=4 per genotype) and total RNA was extracted and quality checked. This time-point was selected to identify initial molecular or pathological changes in an early adult-stage mouse. The RNA quality and quantity from the iWAT were not sufficient to obtain reliable data. Regardless, some of the data from this tissue is presented below.

Bulk RNA-Sequencing was performed by Novogene Bioinformatics Technology Co., Ltd (Cambridge, UK), who generated a list of DEGs from each tissue. Genes at false discovery rate (FDR) <0.05 were considered statistically significant and differentially expressed in *Fus*$^{\Delta 14/\Delta 14}$ mice. Raw data can be found in **Appendix A1-5**. Gene ontology (GO) enrichment analysis was performed using gprofiler. GO terms with an adjusted p<0.05 were considered statistically enriched. The top 10-15 significant terms were selected in each tissue.

The numbers of DEGs varied across the tissues (**Figure 3.3**). The frontal brain and muscle were the most transcriptionally dysregulated tissues, while BAT and iWAT were the least dysregulated. The lack of DEGs in the iWAT was likely due to

technical problems related to difficulties extracting RNA from these tissues. All *Fus*$^{\Delta 14/\Delta 14}$ tissues showed an equal mix of upregulated and downregulated genes, relative to *Fus*$^{+/+}$ tissues (**Figure 3.4**).

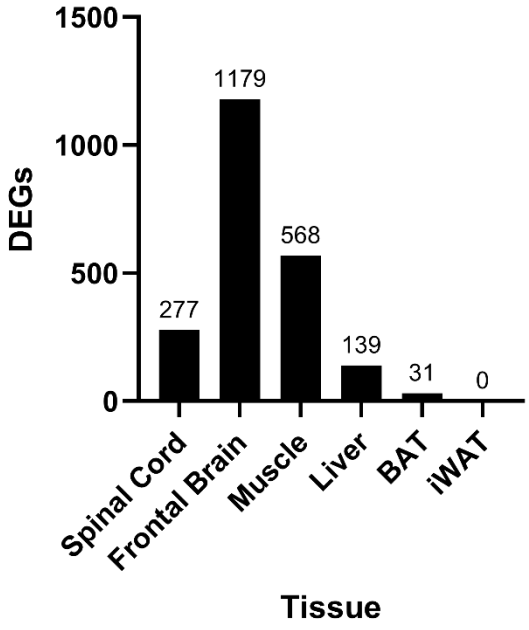


Figure 3.3. Number of DEGs across *Fus*$^{\Delta 14/\Delta 14}$ tissues. RNA-sequencing was performed on tissues collected from 9 week old male *Fus*$^{+/+}$ and *Fus*$^{\Delta 14/\Delta 14}$ mice. Genes with an adjusted p-value (FDR) <0.05 were considered statistically significant and differentially expressed in *Fus*$^{\Delta 14/\Delta 14}$ mice. n= 4 *Fus*$^{+/+}$ and n=4 *Fus*$^{\Delta 14/\Delta 14}$.

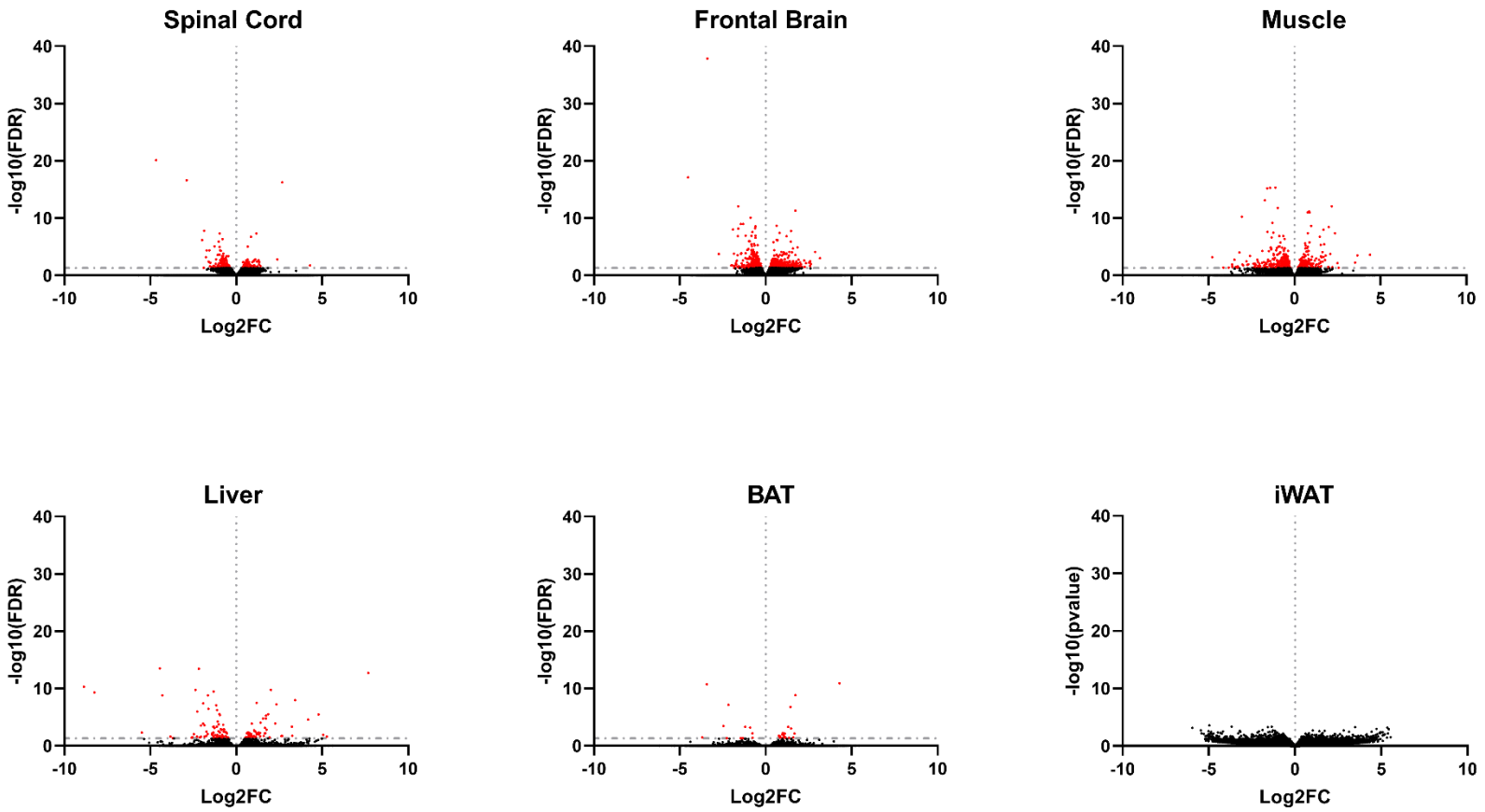


Figure 3.4. Volcano plots. Graphs show statistical significance (FDR) and magnitude of change compared to *Fus*$^{+/+}$ mice (Log2 fold change). Red points above the dashed horizontal line indicate statistically significant DEGs (FDR <0.05). Points to the right of the vertical dashed line indicate an increase in fold change compared to *Fus*$^{\Delta 14/\Delta 14}$ (upregulation), while points to the left indicate a decrease in fold change (downregulation).

When comparing DEGs across *Fus*$^{\Delta 14/\Delta 14}$ tissues, there were commonalities and differences (**Figure 3.5**). The spinal cord and frontal brain shared the most DEGs (104 genes). The majority of these genes were downregulated and involved in processes related to the extracellular region, membrane, mitochondria, metal-binding and development. The frontal brain and muscle shared 67 genes- related to the extracellular region oxidoreductase activity, lipid metabolism and actin cytoskeleton organisation. Only 3 genes were found to be commonly dysregulated in the spinal cord, brain, muscle and liver- *Fus*, *Hist1h1c* and *Rps15a-ps7*. These genes were downregulated. Despite these commonalities, more tissue-specific DEGs were observed; 51.6% in frontal brain, 8.2% in spinal cord, 24.8% in muscle and 6.2% in liver. It was difficult to group tissue-specific genes into pathways due to the small candidate lists.

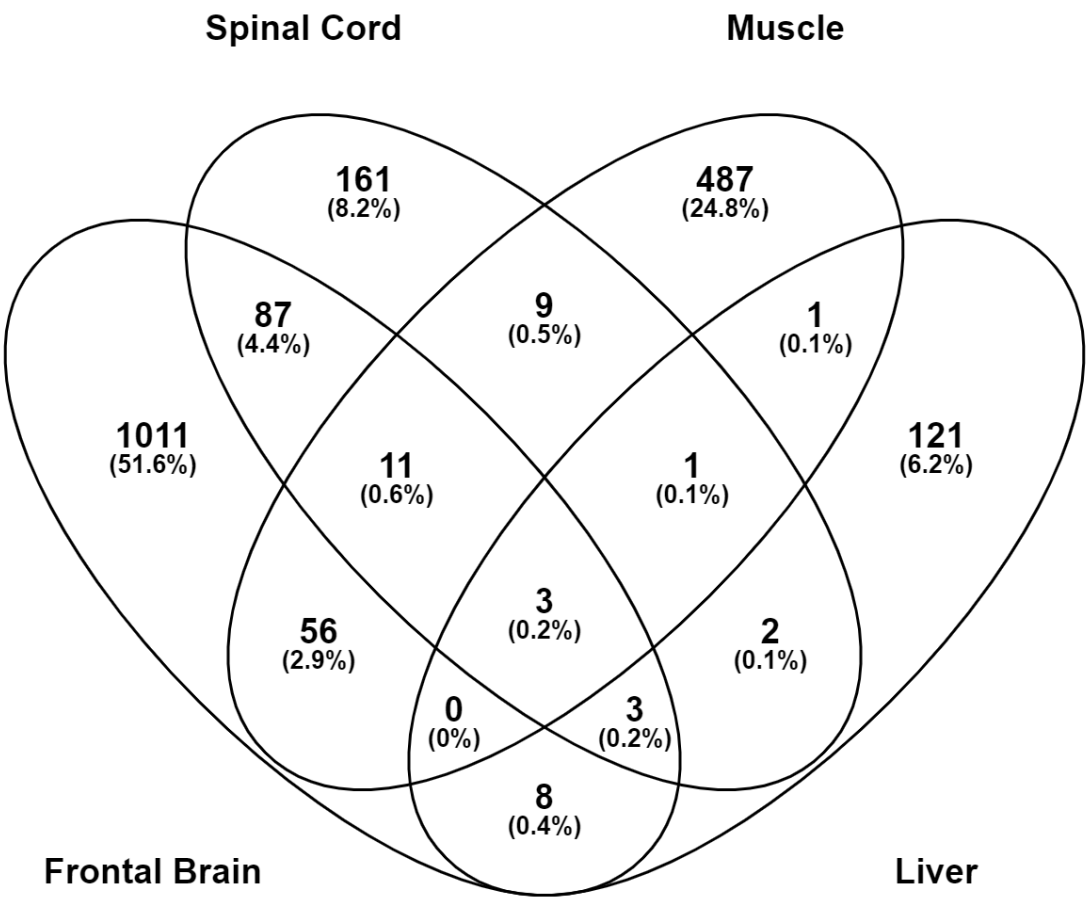


Figure 3.5. Venn diagram comparing DEGs across the tissues. Diagram produced using Venny[2.1].

GO analysis was conducted to identify general pathways and biological processes that were significantly altered in the analysed tissues (**Figure 3.6**). Synapse pruning, a developmental process, was the most significantly enriched biological process in neuronal tissues (frontal brain and spinal cord). Pathways related to mitochondria structure and function were significantly altered in the frontal brain, along with oxidant and detoxification processes. The spinal cord showed

significant enrichment of molecular functions related to the extracellular matrix. Dysregulation of cellular components related to neuronal bodies (and projections) was observed in the spinal cord, as well as collagen trimers.

The (TA) muscle shared several deregulated pathways with neuronal tissues, e.g., cellular components related to the extracellular matrix (shared with spinal cord) and mitochondria (shared with frontal brain). Biological processes related to cell-matrix adhesion and cell-junction assembly were significantly dysregulated in the muscles. Pathways related to laminin binding and actin filaments were also significantly enriched.

Hepatic detoxification pathways (P40 pathway, drug catabolic processes and monooxygenase activity) were significantly dysregulated in the liver, along with lipid metabolic processes. Brush border membrane pathways were also enriched. Similar to the frontal brain, cellular components related to the extracellular space were dysregulated in the liver.

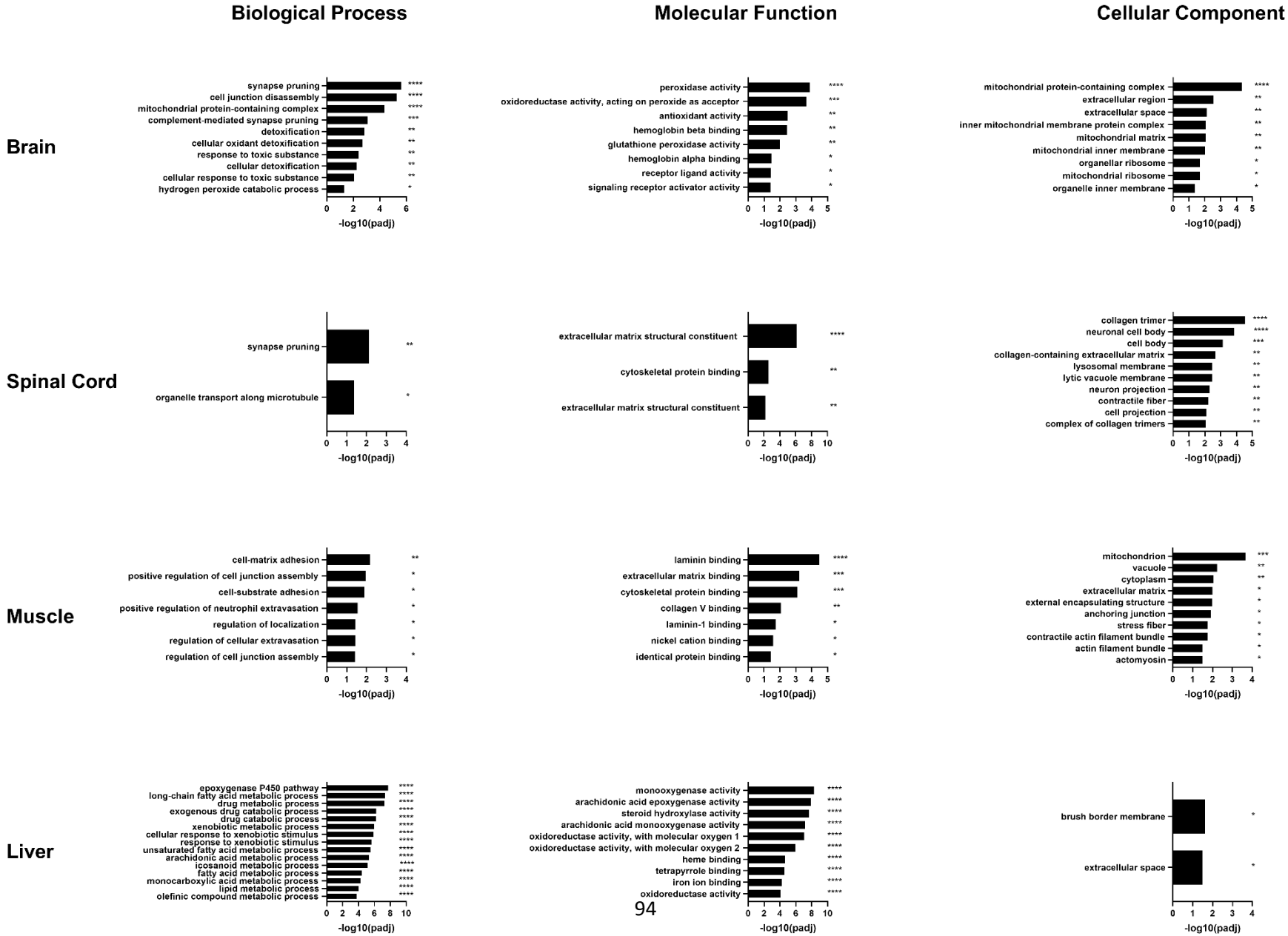

Biological Process
Molecular Function
Cellular Component
Brain
synapse pruning ****
cell junction disassembly ****
mitochondrial protein-containing complex ****
complement-mediated synapse pruning ***
detoxification **
cellular oxidant detoxification **
response to toxic substance **
cellular detoxification **
cellular response to toxic substance **
hydrogen peroxide catabolic process *
0 2 4 6
-log10(padj)
peroxidase activity ****
oxidoreductase activity, acting on peroxide as acceptor ***
antioxidant activity **
hemoglobin beta binding **
glutathione peroxidase activity **
hemoglobin alpha binding *
receptor ligand activity *
signaling receptor activator activity *
0 1 2 3 4 5
-log10(padj)
mitochondrial protein-containing complex ****
extracellular region **
extracellular space **
inner mitochondrial membrane protein complex **
mitochondrial matrix **
mitochondrial inner membrane **
organellar ribosome *
mitochondrial ribosome *
organelle inner membrane *
0 1 2 3 4 5
-log10(padj)
Spinal Cord
synapse pruning **
organelle transport along microtubule *
0 1 2 3 4
-log10(padj)
extracellular matrix structural constituent ****
cytoskeletal protein binding **
extracellular matrix structural constituent **
0 2 4 6 8 10
-log10(padj)
collagen trimer ****
neuronal cell body ****
cell body ***
collagen-containing extracellular matrix **
lysosomal membrane **
lytic vacuole membrane **
neuron projection **
contractile fiber **
cell projection **
complex of collagen trimers **
0 1 2 3 4 5
-log10(padj)
Muscle
cell-matrix adhesion **
positive regulation of cell junction assembly *
cell-substrate adhesion *
positive regulation of neutrophil extravasation *
regulation of localization *
regulation of cellular extravasation *
regulation of cell junction assembly *
0 1 2 3 4
-log10(padj)
laminin binding ****
extracellular matrix binding ***
cytoskeletal protein binding ***
collagen V binding **
laminin-1 binding *
nickel cation binding *
identical protein binding *
0 1 2 3 4 5
-log10(padj)
mitochondrion ***
vacuole **
cytoplasm **
extracellular matrix *
external encapsulating structure *
anchoring junction *
stress fiber *
contractile actin filament bundle *
actin filament bundle *
actomyosin *
0 1 2 3 4
-log10(padj)
Liver
epoxygenase P450 pathway ****
long-chain fatty acid metabolic process ****
drug metabolic process ****
exogenous drug catabolic process ****
drug catabolic process ****
xenobiotic metabolic process ****
cellular response to xenobiotic stimulus ****
response to xenobiotic stimulus ****
unsaturated fatty acid metabolic process ****
arachidonic acid metabolic process ****
icosanoid metabolic process ****
fatty acid metabolic process ****
monocarboxylic acid metabolic process ****
lipid metabolic process ****
olefinic compound metabolic process ****
0 2 4 6 8 10
-log10(padj)
monooxygenase activity ****
arachidonic acid epoxygenase activity ****
steroid hydroxylase activity ****
arachidonic acid monooxygenase activity ****
oxidoreductase activity, with molecular oxygen 1 ****
oxidoreductase activity, with molecular oxygen 2 ****
heme binding ****
tetrapyrrole binding ****
iron ion binding ****
oxidoreductase activity ****
0 2 4 6 8 10
-log10(padj)
brush border membrane *
extracellular space *
0 1 2 3 4
-log10(padj)

Figure 3.6. Gene ontology (GO) pathways.GO terms with an adjusted p<0.05 were considered statistically enriched. Top 10-15 significant terms were selected in each tissue. Analysis was conducted using gprofiler. *p<0.05. **p<0.01. ***p<0.001. ****p<0.0001.

3.2.4 Structural brain alterations and behavioural deficits in *Fus*$^{\Delta 14/\Delta 14}$ mice

The RNA-sequencing data revealed the brain to be the most transcriptionally altered tissue, with multiple neuronal functional processes significantly dysregulated. Therefore, altered brain structure and function were anticipated in this model. The neurodevelopmental delays seen in FUS-jALS patients further supported the need to investigate these phenotypes.

Dissected brains from perfused 10-week old female *Fus*$^{+/+}$ and *Fus*$^{\Delta 14/\Delta 14}$ mice were weighed, followed by width and length measurements. Data was analysed using one-way ANOVA followed by Sidak's multiple comparisons test to compare between genotypes. As previously mentioned, *Fus*$^{\Delta 14/\Delta 14}$ mice were proportionately smaller than *Fus*$^{+/+}$ and *Fus*$^{\Delta 14/+}$ littermates. *Fus*$^{\Delta 14/\Delta 14}$ brains also weighed significantly less than control *Fus*$^{+/+}$ and *Fus*$^{\Delta 14/+}$ brains ($p<0.001$, **Figure 3.7A**). The *Fus*$^{\Delta 14}$ mutation in homozygosity caused notable brain morphological alterations (**Figure 3.7B**) as these mice had narrower brains compared to littermate controls ($p<0.05$). No significant differences were seen between *Fus*$^{+/+}$ and *Fus*$^{\Delta 14/+}$ mice.

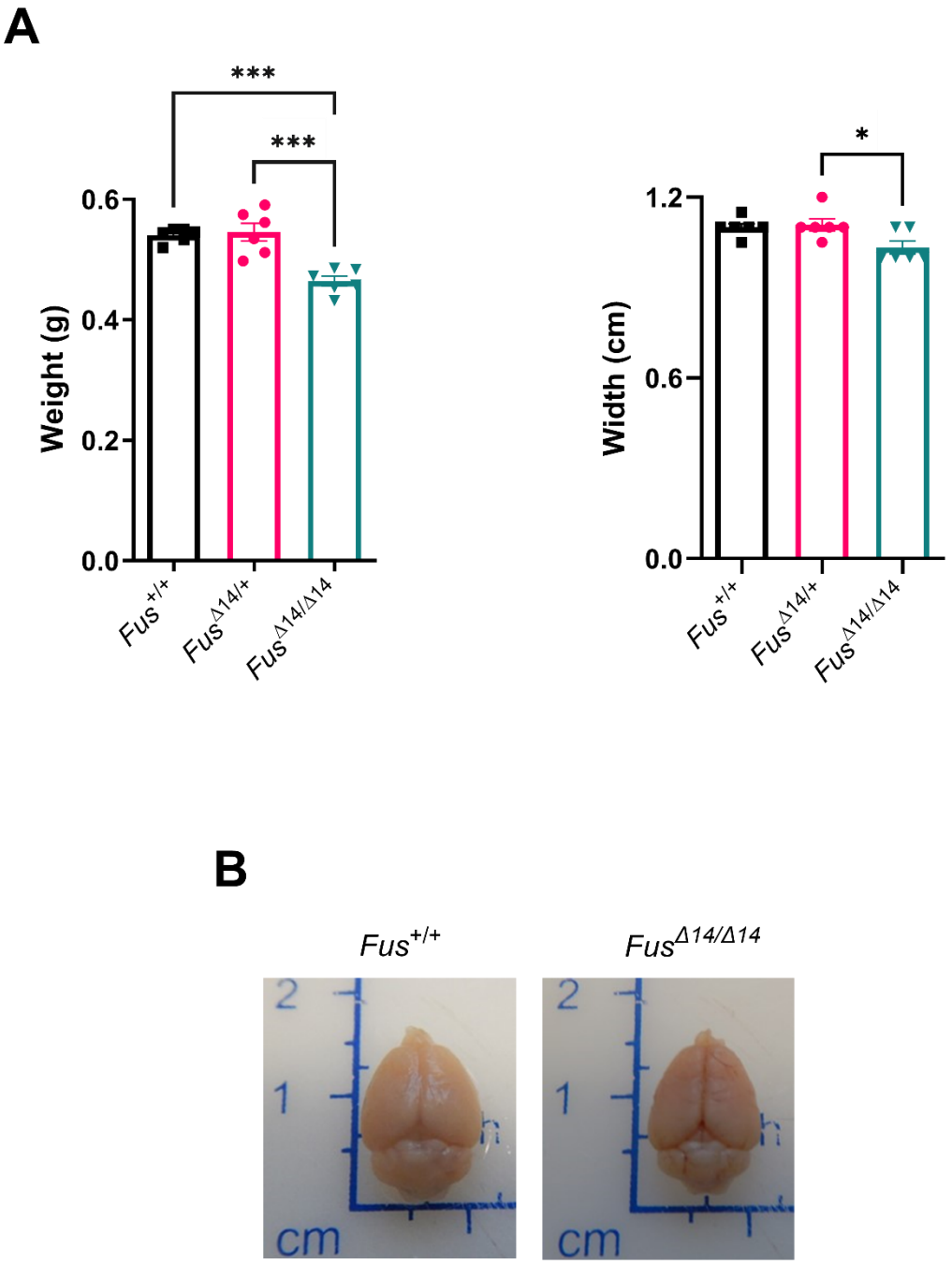


Figure 3.7. Brain morphological analysis of *Fus*$^{\Delta 14}$ mice. Figure shows brain measurements (**A**) and representative images (**B**) from 10-week old female mice. *Fus*$^{\Delta 14/\Delta 14}$ mice had altered brain morphology. Measurements from the frontal brain (cerebellum removed). Data shown as mean. Error bars denote SEM of data. Data analysed using one-way ANOVA followed by Sidak's multiple comparisons test to compare between genotypes. n=6 *Fus*$^{+/+}$, n=6 *Fus*$^{\Delta 14/+}$ and n=6 *Fus*$^{\Delta 14/\Delta 14}$. *p<0.05. ***p<0.001.

It was important to determine if the brain morphological changes correlated to alterations in cognition/behaviour. Due to the reduced lifespan of *Fus*$^{\Delta 14/\Delta 14}$ mice and their susceptibility to developing lethal seizures after handling, nesting was the only behavioural test conducted. This quick observational test measures innate rodent behaviour and it was used to determine the presence of general cognitive dysfunction. Data was analysed using Kruskal-Wallis test followed by the Dunn's multiple comparisons test to compare between genotypes. At 9 weeks of age, male *Fus*$^{\Delta 14/\Delta 14}$ mice displayed lower nesting scores compared to *Fus*$^{+/+}$ and *Fus*$^{\Delta 14/+}$ mice ($p<0.01$, **Figure 3.8**). No significant differences were seen between *Fus*$^{+/+}$ and *Fus*$^{\Delta 14/+}$ mice.

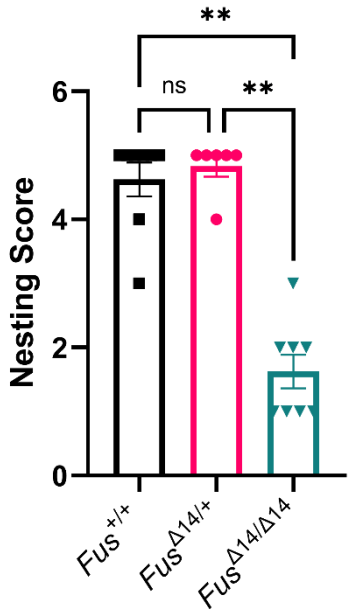


Figure 3.8. Nesting test in *Fus*$^{\Delta 14}$ mice. Graph shows nesting data from 9 week old male mice. *Fus*$^{\Delta 14/\Delta 14}$ mice had a lower nesting score compared to their control littermates. Data shown as mean. Error bars denote SEM of data. Data analysed using Kruskal-Wallis test followed by the Dunn's multiple comparisons test to compare between genotypes. ns= not significant. n=8 *Fus*$^{+/+}$, n=6 *Fus*$^{\Delta 14/+}$ and n=8 *Fus*$^{\Delta 14/\Delta 14}$. **p<0.01.

3.2.5 Muscle composition changes in *Fus*$^{\Delta 14/\Delta 14}$ mice

The muscle was the second most transcriptionally altered tissue. At 9 weeks of age, *Fus*$^{\Delta 14/\Delta 14}$ mice did not show alterations in the grip strength and grid test (Corrochano group). This was supported by the transcriptomic data as pathways relating to muscle atrophy and degeneration were not dysregulated in the muscles at this early time-point.

Processes related to muscle composition, such as actin filaments and actomyosin, were dysregulated in the transcriptomic data. Therefore, a muscle fibre gene screen was conducted to understand the molecular changes caused by the mutation. qRT-PCRs were conducted on the TA muscles of 9-week old male *Fus*$^{+/+}$ and *Fus*$^{\Delta 14/\Delta 14}$ mice (different mice to the ones used in the sequencing experiment). Gene levels of a pre-determined muscle fibre panel were assessed. Data was analysed using unpaired t-test to compare between genotypes.

Fus$^{\Delta 14/\Delta 14}$ muscles displayed significant upregulation of *Myh7* (4.11 fold change, $p<0.01$) and downregulation of *Myh2* (0.48 fold change, $p<0.001$) compared to control *Fus*$^{+/+}$ muscle (**Figure 3.9**). The *Myh2* gene encodes for the skeletal muscle myosin heavy chain isoform that is expressed in fast type 2A fibres (Tajsharghi et al., 2014), while *Myh7* encodes for the isoform found in slow type 1 fibres (Fiorillo et al., 2016) The transcriptomic data also showed significant upregulation of *Myh7* (3.65 fold change), however *Myh2* (and the other panel genes) did not reach the threshold DEG significance levels (FDR <0.05).

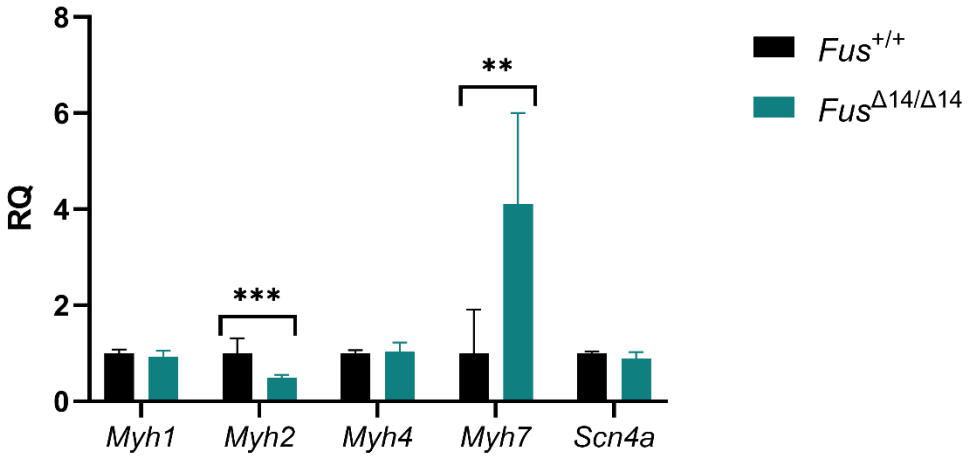


Figure 3.9. Muscle fibre gene screen in *Fus*$^{\Delta 14}$ mice. Graph shows qRT-PCR data from the TA muscles of 9-week old male *Fus*$^{+/+}$ and *Fus*$^{\Delta 14/\Delta 14}$ mice. *Fus*$^{\Delta 14/\Delta 14}$ muscles showed upregulation of *Myh7* and downregulation of *Myh2*. Panel consists of genes related to muscle composition. Data shown as mean relative quantification (RQ) - *Fus*$^{\Delta 14/\Delta 14}$ gene changes compared to *Fus*$^{+/+}$. Error bars denote upper and lower limits. Data analysed using unpaired t-test to compare between genotypes. *s16* was used as the reference gene. n=6 *Fus*$^{+/+}$ and n=6 *Fus*$^{\Delta 14/\Delta 14}$. **p<0.01. ***p<0.001.

3.2.6 Systemic metabolic alterations in *Fus*$^{\Delta 14/\Delta 14}$ mice

3.2.6.1 Hepatic lipid droplet (LD) accumulation

GO terms linked to lipid metabolic processes were significantly dysregulated in the *Fus*$^{\Delta 14/\Delta 14}$ liver. This is not surprising as the liver plays a key role in lipid metabolism (Nguyen et al., 2008). As a result, hepatic lipids were analysed in these mice by staining the liver for lipid droplets (LDs). Liver sections from 3-month old male mice were stained with Oil Red O to visualise LDs. LD numbers per cell were quantified using ImageJ and the data was analysed using unpaired t-test to compare between genotypes.

Fus$^{\Delta 14/\Delta 14}$ livers had significantly more LDs compared to control *Fus*$^{+/+}$ livers ($p<0.05$, **Figure 3.10**). There were more LDs around the blood vessels indicating that the liver accumulates lipids from the blood. This suggests the *Fus*$^{\Delta 14}$ mutation caused systemic metabolic alterations which required further investigation.

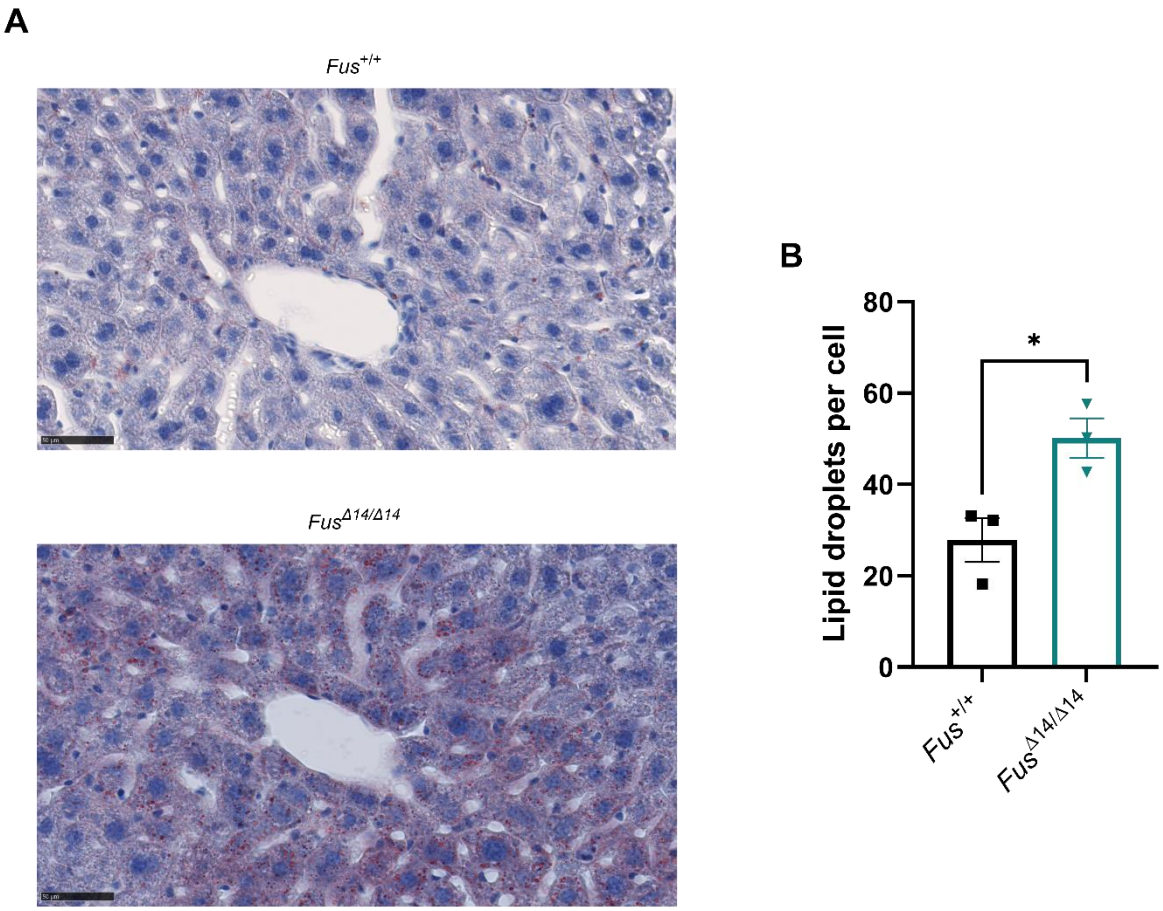


Figure 3.10. Liver lipid droplet (LD) staining in *Fus*$^{\Delta 14}$ mice. Figure shows representative histological images of LD stains (**A**) and quantification (**B**) in the livers of perfused 3-month old male mice. *Fus*$^{\Delta 14/\Delta 14}$ livers had more lipid droplets. Data shown as mean. Error bars denote SEM of data. Data analysed using unpaired t-test to compare between genotypes. n=3 *Fus*$^{+/+}$ and n=3 *Fus*$^{\Delta 14/\Delta 14}$. *p<0.05.

3.2.6.2 Altered body composition

Increased fat stores can elevate blood FFAs levels causing hepatic LD accumulation. As a result, body composition was assessed in 9-week old mice (males and females) using EchoMRI. Data was analysed using one-way ANOVA followed by Dunnett's multiple comparisons test to compare between genotypes.

Despite *Fus*$^{\Delta 14/\Delta 14}$ mice being proportionately smaller, they had increased fat mass compared to control *Fus*$^{+/+}$ mice (**Figure 3.11**). *Fus*$^{\Delta 14/+}$ mice also had increased fat mass compared to *Fus*$^{+/+}$ mice. These trends were seen in both sexes.

Increased fat stores in *Fus*$^{\Delta 14/\Delta 14}$ and *Fus*$^{\Delta 14/+}$ mice were accompanied by increased subcutaneous inguinal fat depots (**Appendix B1**). Increased fat stores were maintained in *Fus*$^{\Delta 14/+}$ mice at later time-points, indicating that these metabolic effects were not time-specific (**Appendix B2**). Male *Fus*$^{\Delta 14/\Delta 14}$ and *Fus*$^{\Delta 14/+}$ mice had reduced lean mass compared to controls ($p<0.01$). There were no significant genotype differences in female lean mass measurements.

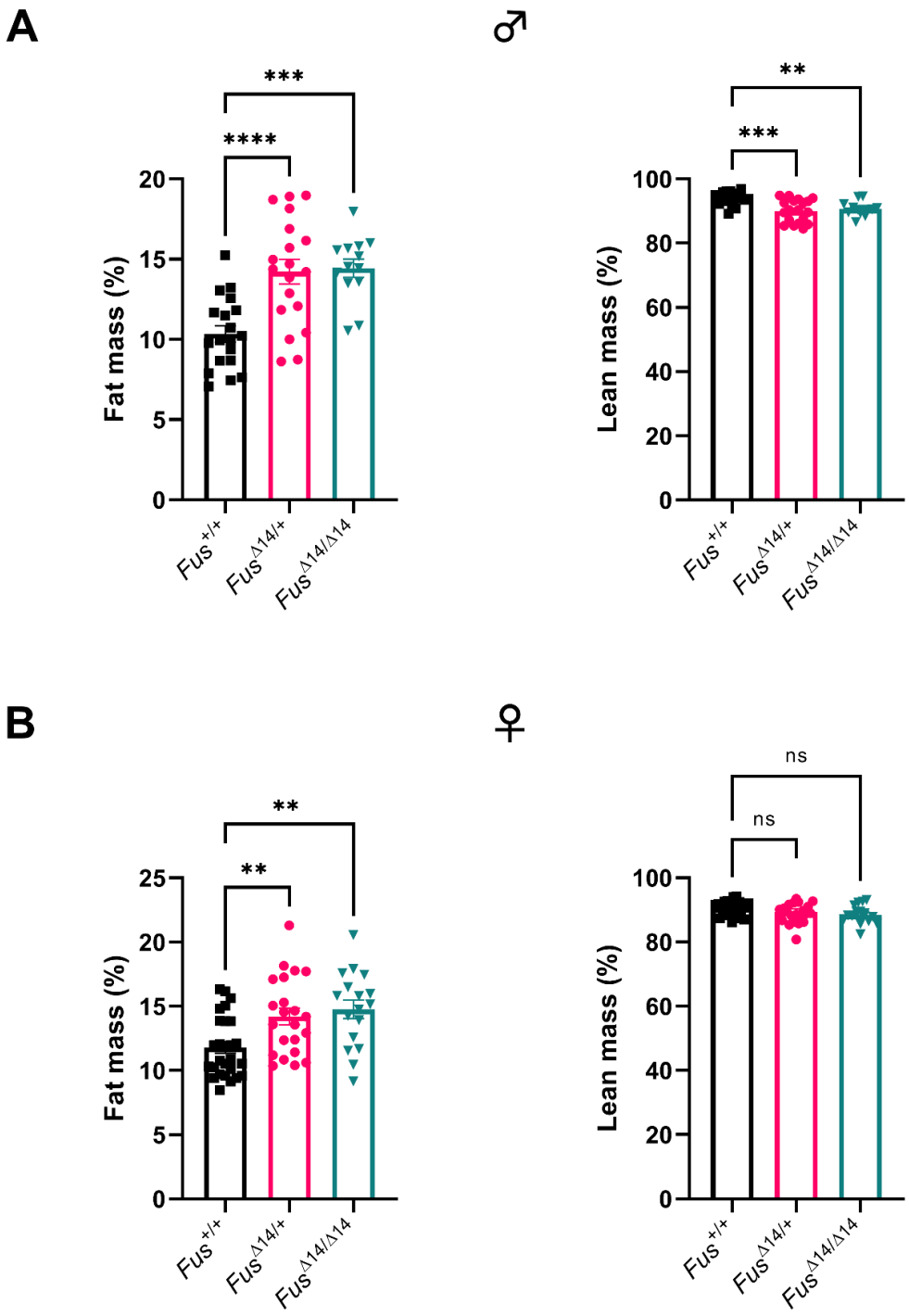


Figure 3.11. Body composition of *Fus*$^{\Delta 14}$ mice. Graphs show data from male (**A**) and female (**B**) mice at 9-weeks. All *Fus*$^{\Delta 14/\Delta 14}$ and *Fus*$^{\Delta 14/+}$ mice had increased fat mass compared to littermate controls. Male *Fus*$^{\Delta 14/\Delta 14}$ and *Fus*$^{\Delta 14/+}$ mice had reduced lean mass. Data shown as mean. Error bars denote SEM of data. Data analysed using one-way ANOVA followed by Dunnett's multiple comparisons test to compare between genotypes. Males: n=19 *Fus*$^{+/+}$, n=19 *Fus*$^{\Delta 14/+}$ and n=13 *Fus*$^{\Delta 14/\Delta 14}$. Females: n=27 *Fus*$^{+/+}$, n=22 *Fus*$^{\Delta 14/+}$ and n=17 *Fus*$^{\Delta 14/\Delta 14}$. ns= not significant. *p<0.05. **p<0.01. ***p<0.001. ***p<0.0001.

3.2.6.3 Unaltered plasma FFAs levels

Male mice were fasted for 4hours and blood was collected through retro-orbital bleeds. Plasma FFA levels, along with other lipids, were analysed. Data was analysed using 2-way ANOVA followed by Dunnett's multiple comparisons test to compare between genotypes. Despite the increased fat stores, there were no differences in FFA levels in the plasma of fasted *Fus*$^{\Delta 14/\Delta 14}$ and *Fus*$^{\Delta 14/+}$ mice, compared to *Fus*$^{+/+}$ mice (**Figure 3.12**). *Fus*$^{\Delta 14/\Delta 14}$ mice had significantly lower plasma LDL levels compared to control *Fus*$^{+/+}$ mice ($p<0.05$). No genotype differences were seen in the other plasma lipids levels.

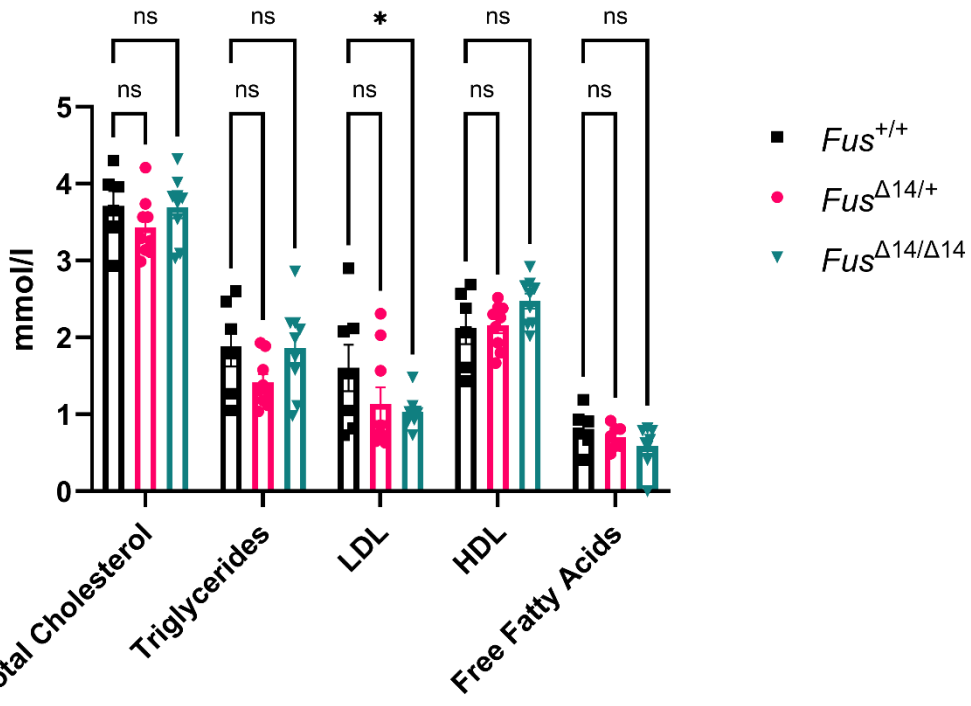


Figure 3.12. Plasma lipid profile of *Fus*$^{\Delta 14}$ mice. Graph shows plasma lipid levels from fasted, 9-week old male mice. *Fus*$^{\Delta 14/\Delta 14}$ mice had reduced plasma LDL levels. Data shown as mean. Error bars denote SEM of data. Data analysed using 2-way ANOVA followed by Dunnett's multiple comparisons test to compare between genotypes. n=7 *Fus*$^{+/+}$, n=11 *Fus*$^{\Delta 14/+}$ and n=9 *Fus*$^{\Delta 14/\Delta 14}$. ns= not significant. *p<0.05. LDL= low-density lipoprotein. HDL= high-density lipoprotein.

3.2.6.4 Increased adipogenesis but unaltered lipolysis

A comprehensive histological analysis of the iWAT tissue by the Corrochano group revealed that the *Fus*$^{\Delta 14}$ mutation increased fat depots through hyperplasia. The mutation caused larger adipocytes but the exact mechanism remains unsolved. The mutation could be impacting the breakdown of fat stores (lipolysis) or the formation of adipocytes (adipogenesis).

To investigate *in vivo* lipolysis, 9-week old male mice were injected with either a β3-adrenergic receptor agonist (lipolysis stimulant drug) or phosphate buffered saline (vehicle). Plasma was collected 1-hour post-injection. Lipolysis was measured by quantifying plasma FFAs and glycerol levels. Data analysed using 2-way ANOVA followed by Dunnett's multiple comparisons test to compare between genotypes. All mice injected with the lipolysis drug had more plasma FFAs and glycerol levels compared to vehicle-treated mice (**Figure 3.13**). However, there were no genotype differences in the drug-treated group, showing that the *Fus*$^{\Delta 14}$ mutation does not impact lipolysis. This data, coupled with unaffected plasma FFA levels, indicate that *Fus*$^{\Delta 14/\Delta 14}$ mice liberated lipids from their fat stores at a normal rate.

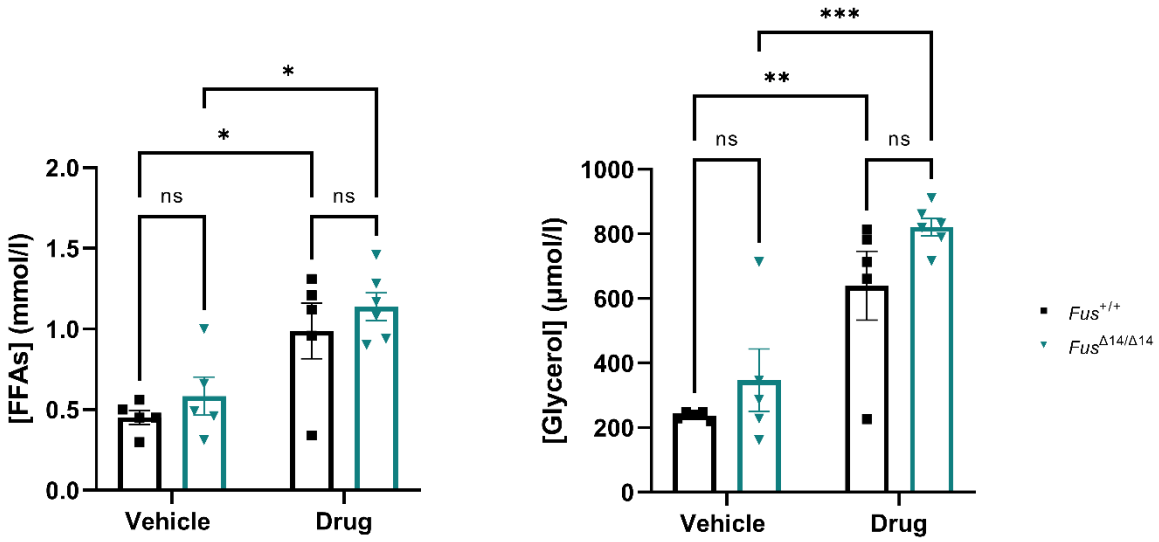


Figure 3.13. *In vivo* lipolysis measurements in *Fus*$^{\Delta 14}$ mice. Graphs showing FFAs and glycerol concentrations after vehicle (PBS) or drug (β3-adrenergic receptor agonist) were administered to 9-week old male mice. No genotype differences in the drug group. Data shown as mean. Error bars denote SEM of data. Data analysed using 2-way ANOVA followed by Dunnett's multiple comparisons test to compare between genotypes. n=5 *Fus*$^{+/+}$ and n=5 *Fus*$^{\Delta 14/\Delta 14}$. ns= not significant. *p<0.05. **p<0.01. ***p<0.001.

Adipogenesis was evaluated *in vitro* using primary adipocytes isolated from 8-week old male mice. Pre-adipocytes were isolated from iWAT depots, cultured and differentiated into mature adipocytes (adipogenesis). Once differentiated, adipocytes were stained with the dye Oil Red O to identify LDs. Data was analysed using one-way ANOVA followed by Dunnett's multiple comparisons test to compare between genotypes. RNA was collected from mature, unstained adipocytes. Levels of key adipogenesis genes were measured using qRT-PCR with Taqman assays and data was analysed using unpaired t-test.

There were no genotype differences in Oil Red O absorbance suggesting that there were no differences in LD/adipocyte numbers (**Figure 3.14A**). However, this could be due to technical issues. Preparation of the Oil Red O dye can affect cellular uptake (Kinkel et al., 2004). There are better, more specific dyes available

(e.g., AdipoRed) that can be used in future experiments. Despite this, there was significant upregulation of all adipogenesis genes in *Fus*$^{\Delta 14/\Delta 14}$ adipocytes (**Figure 3.14B**). No changes were seen between *Fus*$^{\Delta 14/+}$ and *Fus*$^{+/+}$ adipocytes despite *FUS*$^{\Delta 14/+}$ mice also showing increased fat depots. The *Fus*$^{\Delta 14}$ mutation increases adipogenesis in homozygosity, leading to increased fat stores in these mice.

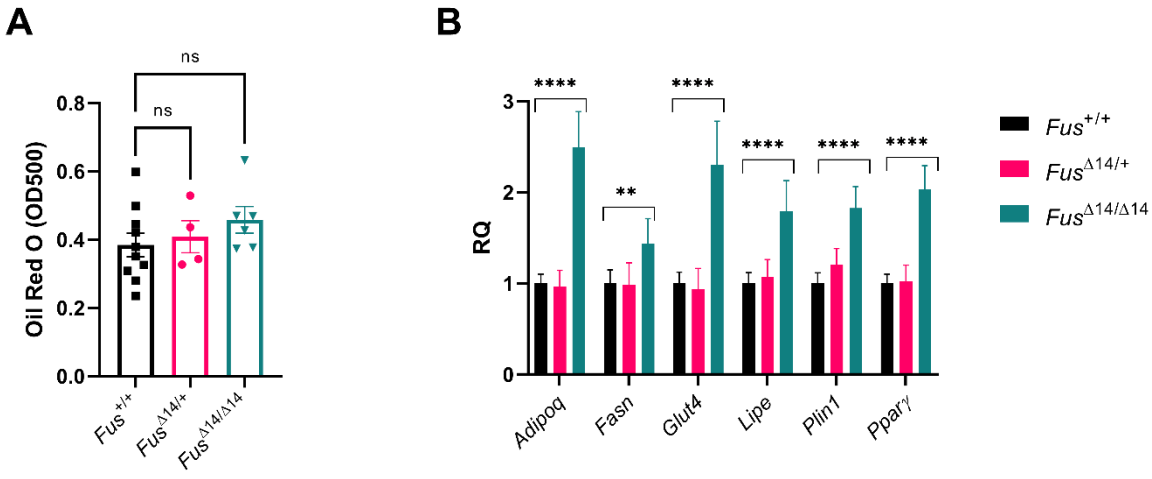


Figure 3.14. *In vitro* adipogenesis measurements in *Fus*$^{\Delta 14}$ mice. Figure showing quantification of Oil Red O (**A**) and adipogenesis gene panel (**B**) of primary adipocytes from 8-week old male mice. Upregulation of adipogenesis genes in *Fus*$^{\Delta 14/\Delta 14}$ adipocytes. A) Data shown as mean. Error bars denote SEM of data. Data analysed using one-way ANOVA followed by Dunnett's multiple comparisons test to compare between genotypes. B) Data shown as mean relative quantification (RQ) - *Fus*$^{\Delta 14/\Delta 14}$ gene changes compared to *Fus*$^{+/+}$. Error bars denote upper and lower limits. Data analysed using unpaired t-test to compare between genotypes. *Canx* was used as the reference gene. n=10 *Fus*$^{+/+}$, n=4 *Fus*$^{\Delta 14/+}$ and n=6 *Fus*$^{\Delta 14/\Delta 14}$. ns= not significant. **p<0.01. ****p<0.0001.

3.2.6.5 Impaired glucose uptake

A known consequence of increased subcutaneous iWAT stores is impaired glucose metabolism and insulin resistance (Patel & Abate, 2013). To determine if the large fat depots in *Fus*$^{\Delta 14/\Delta 14}$ mice affected systemic glucose responses, the IPGTT was conducted on fasted male mice at 9 weeks of age (Corrochano group). This test measures the clearance of injected glucose from the body.

At the time-points 15, 30 and 60 minutes, *Fus*$^{\Delta 14/\Delta 14}$ mice had significantly more glucose in their blood compared to *Fus*$^{+/+}$ and *Fus*$^{\Delta 14/+}$ mice (**Figure 3.15**),

indicating a slower glucose uptake rate. Interestingly, *Fus*$^{\Delta 14/+}$ mice did not show alterations in the IPGTT despite having increased fat depots. This shows that the *Fus*$^{\Delta 14}$ mutation causes glucose handling problems only in homozygosity.

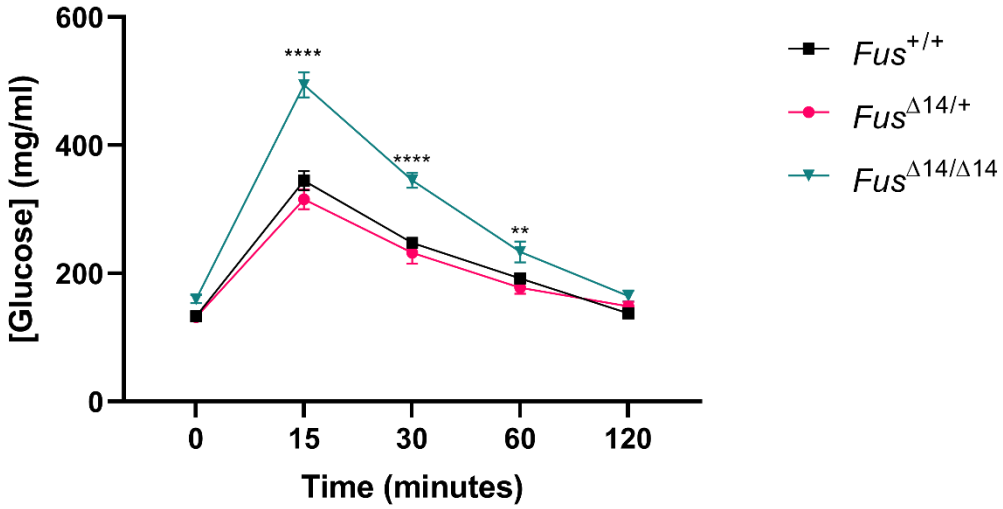


Figure 3.15. Intraperitoneal glucose tolerance test (IPGTT) in *Fus*$^{\Delta 14}$ mice. Graph shows blood glucose concentrations from 9-week old male mice, after the administration of glucose at 0 minutes. *Fus*$^{\Delta 14/\Delta 14}$ mice had elevated glucose levels at 15, 30 and 60 minutes. Data shown as mean. Error bars denote SEM of data. Data analysed using 2-way ANOVA followed by Tukey's multiple comparisons test to compare between genotypes. n=9 *Fus*$^{+/+}$, n=9 *Fus*$^{\Delta 14/+}$ and n=9 *Fus*$^{\Delta 14/\Delta 14}$. ns= not significant. *p<0.05. **p<0.01. ***p<0.001.

3.2.6.6 Altered metabolic rate and a fat fuel preference

Indirect calorimetry was performed to determine if the systemic metabolic alterations were due to changes in EE. EE is a measure of whole-body metabolism so changes in this parameter were expected. The RER is another metabolic readout from indirect calorimetry. The RER is used to determine the proportion of carbohydrates and fats utilised as fuel in tissues. A ratio of 0.7 indicates sole fat use, while a ratio of 1.0 indicates exclusive use of carbohydrates (Deuster & Heled, 2008). Mice were placed in a metabolic cage and the amount of oxygen used and carbon dioxide released by the body was measured to determine EE and RER values. EE measurements were corrected by genotype

lean mass using 2-way ANCOVA to give adjusted mean EE values. Data was analysed using 2-way ANOVA followed by Tukey's multiple comparisons test to compare between genotypes in each phase.

Male *Fus*$^{\Delta 14/\Delta 14}$ mice had reduced EE rates in the light and dark phase, compared to *Fus*$^{+/+}$ and *Fus*$^{\Delta 14/+}$ mice (**Figure 3.16A**), indicating hypometabolism. No differences were seen between *Fus*$^{+/+}$ and *Fus*$^{\Delta 14/+}$ mice. Male *Fus*$^{\Delta 14/\Delta 14}$ had a reduced RER in the light phase, compared to *Fus*$^{\Delta 14/+}$ mice ($p<0.05$). Female mice did not show genotype differences in any of the measured parameters (**Figure 3.16B**), indicating sex-specific effects of the mutation.

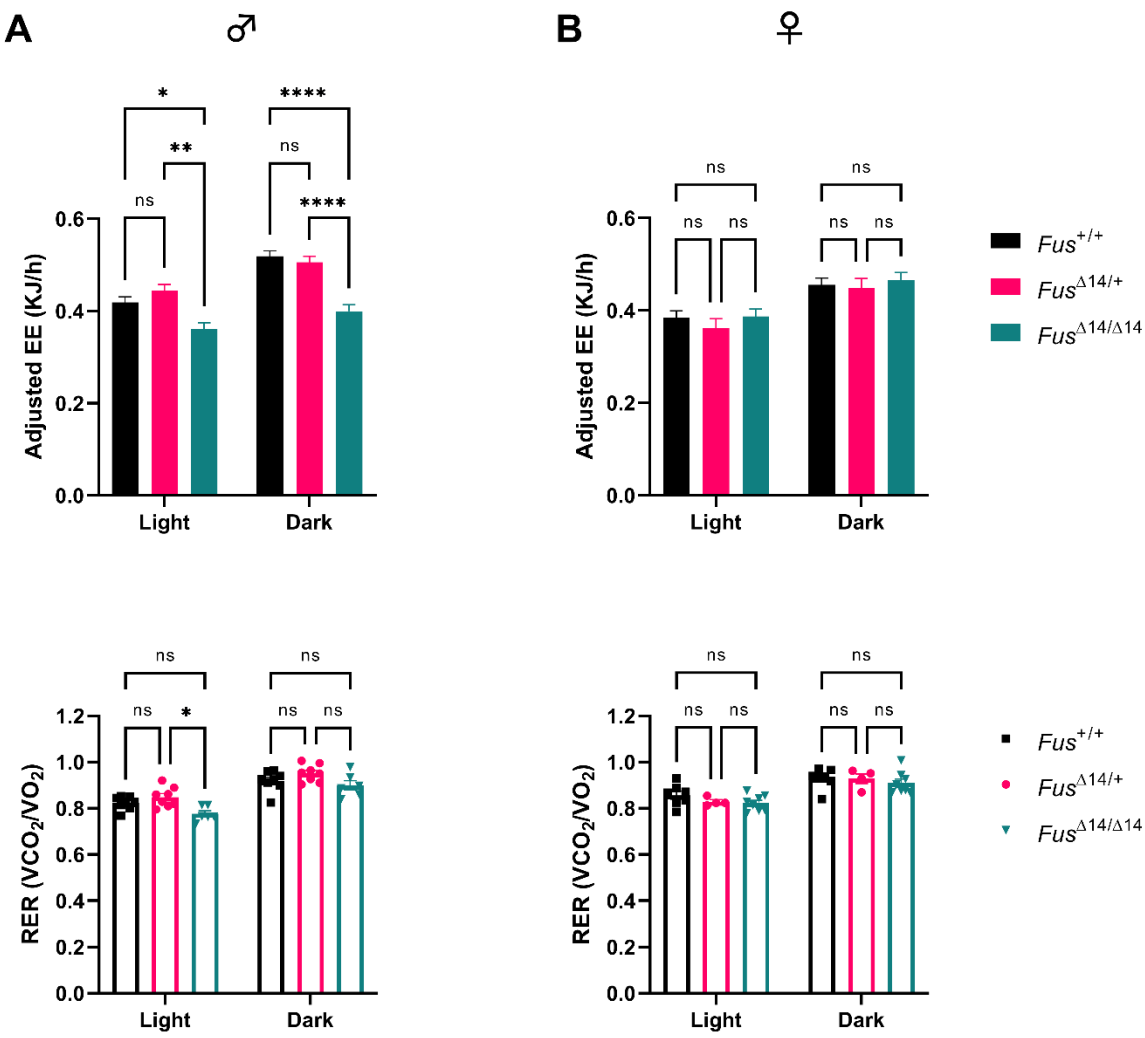


Figure 3.16. Indirect calorimetry analysis of *Fus*$^{\Delta 14}$ mice. Graphs show indirect calorimetry parameters from 9-week old male (**A**) and female (**B**) mice. Male *Fus*$^{\Delta 14/\Delta 14}$ mice had reduced EE rates compared to control littermates. These mice also had reduced RER in the light phase. EE corrected by lean mass using 2-way ANCOVA to give an adjusted EE mean value. Parameters are separated by time (light and dark). Light: 12- 5pm and 7- 10am. Dark: 6pm- 6am. Data shown as mean. Error bars denote SEM of data. Data was analysed using 2-way ANOVA followed by Tukey's multiple comparisons test to compare between genotypes in each phase. Males: n=8 *Fus*$^{+/+}$, n=8 *Fus*$^{\Delta 14/+}$ and n=6 *Fus*$^{\Delta 14/\Delta 14}$. Females: n=7 *Fus*$^{+/+}$, n=4 *Fus*$^{\Delta 14/+}$ and n=8 *Fus*$^{\Delta 14/\Delta 14}$ ns= not significant. *p<0.05. **p<0.01. ***p<0.0001.

3.2.7 Genetic backgrounds effects on metabolic phenotypes

To evaluate the *FUS*$^{\Delta 14}$ mutation in homozygosity, all mentioned experiments were conducted in mice on the F1 hybrid genetic background (C57BL6J x DBA/2J). It remains unknown if the same mutation phenotype effects are observed on the parental congenic inbred lines. To evaluate background differences, the following experiments were conducted in male mice on the following congenic backgrounds, C57BL/6J and DBA/2J. Due to the perinatal lethality of homozygotes on these congenic backgrounds, *Fus*$^{+/+}$ and *Fus*$^{\Delta 14/+}$ mice were used.

In both congenic backgrounds, there were no body weight differences between *Fus*$^{+/+}$ and *Fus*$^{\Delta 14/+}$ mice at 9 weeks of age (**Figure 3.17**). However, *Fus*$^{\Delta 14/+}$ mice on the DBA/2J background had increased fat mass and reduced lean mass compared to control littermates ($p<0.05$, **Figure 3.17B**), a similar body composition profile to the hybrid background. Unlike the hybrid genetic background, these body composition alterations were time-specific as they were not present at 6-months. No genotype differences were seen in the C56BL/6J background at 9-weeks. Neither backgrounds displayed genotype differences 6-months (**Appendix B3**). At 12-months, *Fus*$^{\Delta 14/+}$ mice on the C57BL/6J background appeared to have reduced fat mass compared to control littermates, however, this was not statistically significant (**Appendix B4**).

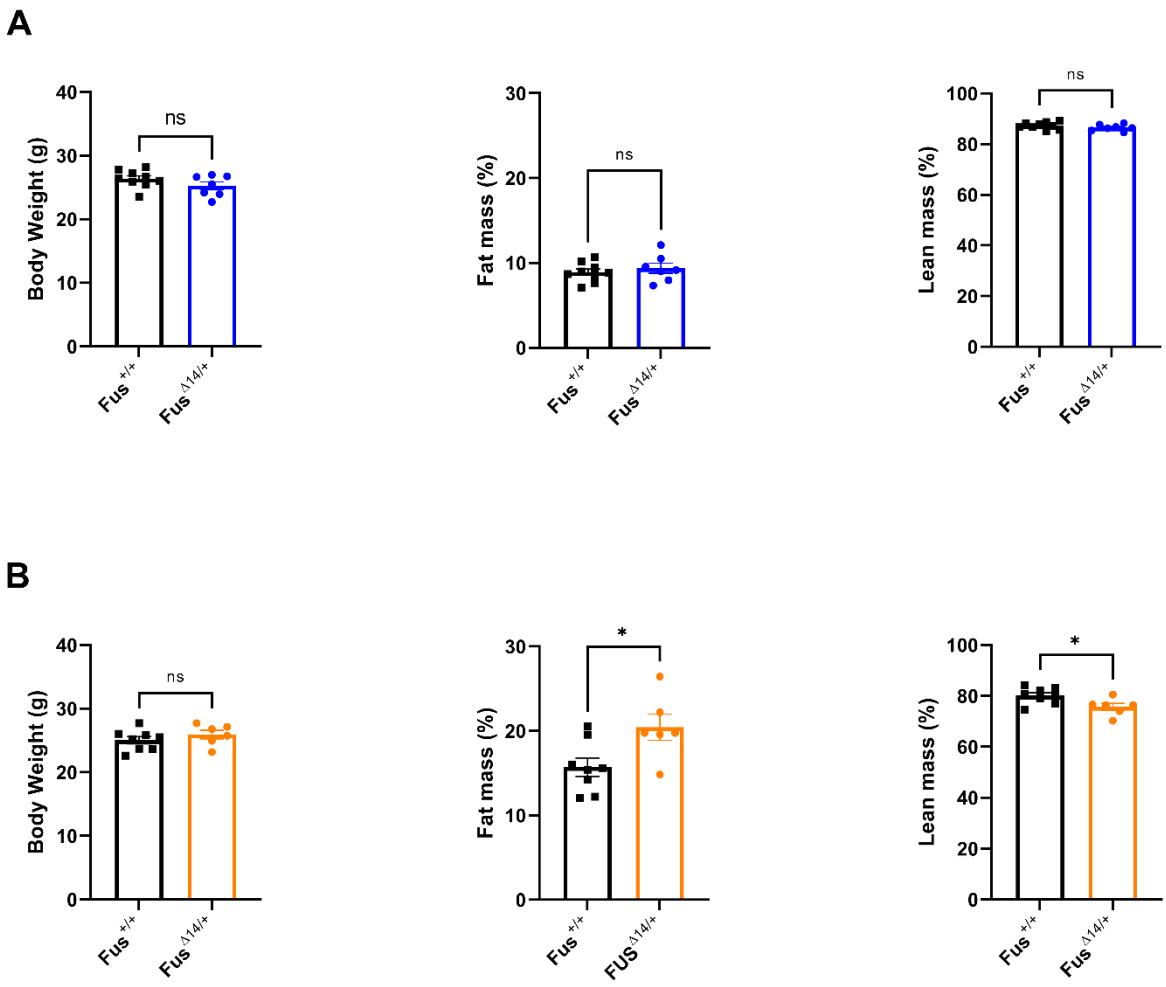


Figure 3.17. Body composition of *Fus*$^{\Delta 14}$ mice on different genetic backgrounds. Graphs show data from 9-week old male mice on the C57BL/6J (**A**) and DBA/2J (**B**) backgrounds. *Fus*$^{\Delta 14/+}$ mice on the DBA-2J background had increased fat mass and reduced lean mass compared to control littermates. Data shown as mean. Error bars denote SEM of data. Data analysed using unpaired t-test to compare between genotypes. C57BL/6J: n=9 *Fus*$^{+/+}$ and n=7 *Fus*$^{\Delta 14/+}$. DBA/2J: n=4 *Fus*$^{+/+}$ and n=7 *Fus*$^{\Delta 14/+}$. ns= not significant. *p<0.05.

Fus$^{\Delta 14/+}$ mice on the hybrid background did not show differences in indirect calorimetry parameters at 9 weeks of age. This experiment was repeated at 12-months because phenotypes may appear later. Comparisons were only made with mice on the C57BL/6J background because *Fus*$^{\Delta 14/+}$ mice on the DBA/2J were culled suddenly due to age-related eye problems. The DBA/2J strain is known to develop a progressive form of glaucoma, which can cause welfare issues (John et

al., 1998). In the hybrid and C57BL/6J background, no genotype differences were observed in any of the measured parameters (**Figure 3.18**).

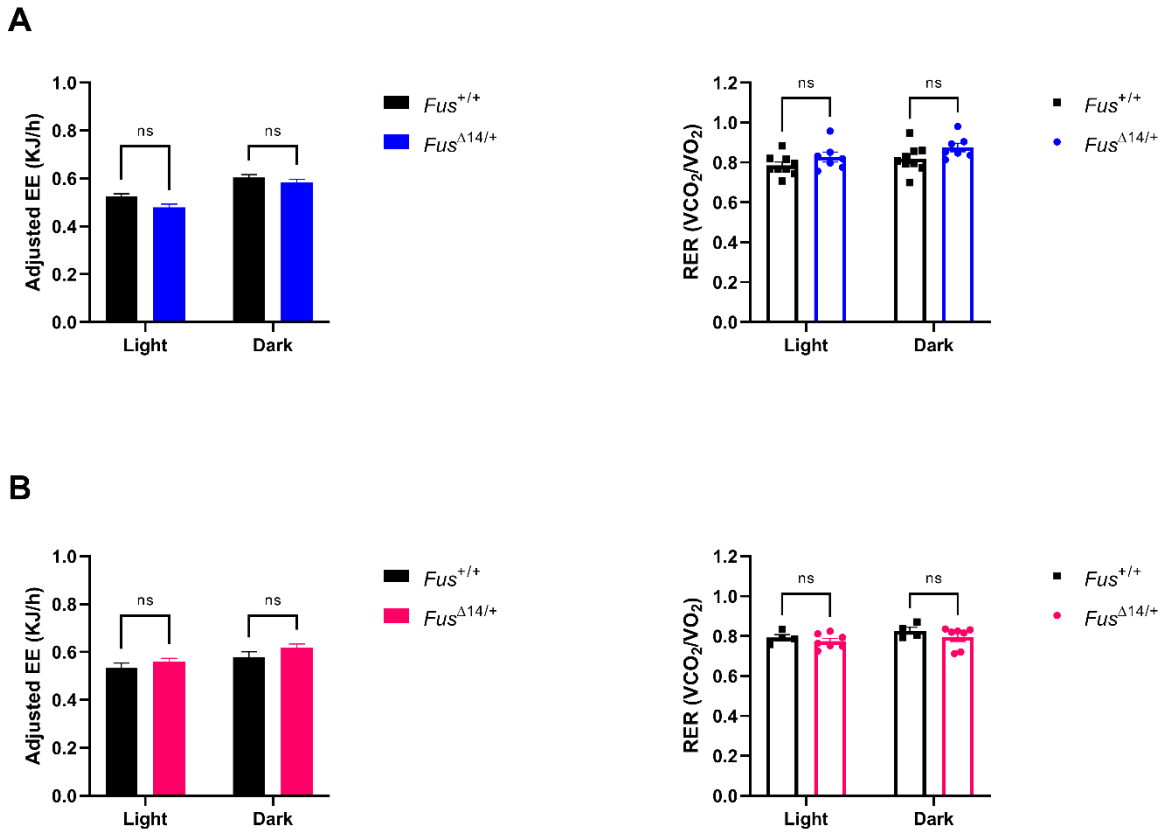


Figure 3.18. Indirect calorimetry analysis of *Fus*$^{\Delta 14}$ mice on different genetic backgrounds. Graphs show indirect calorimetry parameters from 12-month old male mice on the C57BL/6J (**A**) and hybrid (**B**) background. No genotype differences in any of the measured parameters. EE was corrected by lean mass using 2-way ANCOVA to give an adjusted EE mean value. Parameters are separated by time (light and dark). Light: 12- 5pm and 7- 10am. Dark: 6pm- 6am. Data shown as mean. Error bars denote SEM of data. Data was analysed using 2-way ANOVA followed by Tukey's multiple comparisons test to compare between genotypes in each phase. C57BL/6J: n=9 *Fus*$^{+/+}$ and n=7 *Fus*$^{\Delta 14/+}$. Hybrid: n=4 *Fus*$^{+/+}$ and n=7 *Fus*$^{\Delta 14/+}$. ns= not significant.

3.3 Discussion

3.3.1 *Fus*$^{\Delta 14}$ mutation causes widespread effects

The *Fus*$^{\Delta 14}$ mutation in homozygosity produces severe phenotypes (Table 3.3). On the congenic C57BL/6J background, the mutation caused perinatal lethality in homozygous mice. Homozygous lethality has been reported in other mouse models carrying *Fus* mutations (Sanjuan-Ruiz et al., 2021), demonstrating the essential role of this protein in developmental processes. While this lethality is rescued on a hybrid background, homozygous mice had a shorter lifespan compared to their littermate controls due to sudden fatal seizures. Seizures have also been documented in other *Fus* mouse models (Korobeynikov et al., 2022).

Test		Findings
Transcriptomic		Dysregulation in multiple tissues
Muscle		Upregulation of slow-twitch fibres
Brain	**Structural**	Thinner brains
	Behavioural/cognition	Innate behavioural deficits/apathy
Metabolic	**Body weight**	Weighed less from birth
	EchoMRI	Increased fat mass and reduced lean mass
	TSE	Hypometabolic and a fat fuel preference
	Hepatic lipid droplet staining	Increased lipid droplets around the blood vessels
	Plasma lipid profile	No change
	***In vitro* adipogenesis**	Increased adipogenesis
	***In vivo* lipolysis**	No change
	IPGTT	Slower glucose uptake

Table 3.3. Summary of male *Fus*$^{\Delta 14/\Delta 14}$ phenotypes on the hybrid background. Table summaries the changes seen in male *Fus*$^{\Delta 14/\Delta 14}$ mice, compared to control *Fus*$^{+/+}$ mice, at 9 weeks of age.

Systemic transcriptomic analysis revealed that the *Fus*$^{\Delta 14}$ mutation caused dysregulation in several tissues. Commonalities were seen between most tissues, mainly in the downregulation of *Fus* and *Hist1h1c*. Downregulation in *FUS* transcript levels is expected in this model as less wild-type FUS was seen in heterozygous mice (Devoy et al., 2017). However, the RNA-seq did not pick up the mutant transcript because the alignment software did not take the humanised C-terminal into account. Additional qRT-PCR analysis showed an upregulation of total *Fus* gene levels in the spinal cords and TA muscles of homozygous male

mice at 9 weeks of age, indicating increased mutant *Fus* gene expression (**Appendix A6**). This finding corroborates the dysregulated FUS autoregulation effect previously observed by this mutation (Humphrey et al., 2020). This molecular effect is shared with other NLS *Fus* mutations. In physiological conditions, FUS shuttles between the nucleus and cytoplasm. FUS binds to its own intron 6 and 7 to promote nucleus retention, reducing the amount of cytoplasmic *FUS* mRNA available for translation. When there are low levels of FUS, intron retention is reduced and cytoplasmic *FUS* transcripts increase. In NLS *Fus* mutations, mutant FUS is not transported to the nucleus as effectively thus reducing its ability to regulate its own protein levels. This causes a vicious cycle of ever-increasing cytoplasmic FUS levels which may underline the toxic effects observed in this model. Mutant FUS mislocalisation to the cytoplasm has been reported in the lumbar spinal motor neurons of $Fus^{\Delta 14}$ heterozygous mice (Devoy et al., 2017). Like other FUS NLS models, the $Fus^{\Delta 14}$ mutation causes cytoplasmic mislocalisation without nuclear depletion or protein aggregates (Scekic-Zahirovic et al., 2021).

Hist1h1c belongs to the histone H1 family, which binds to linker DNA between nucleosomes and plays a role in the compaction of chromatin into higher order structures (B.-R. Zhou et al., 2013). Downregulation of this gene was also seen in the brains of mice expressing a truncated FUS protein lacking the NLS (Scekic-Zahirovic et al., 2016). This indicates additional shared effects of mutations targeting the NLS region of FUS. The role of *Hist1h1c* in NDDs remains unknown as its research predominately relates to cancer and inflammation.

Gene ontology analysis revealed shared neuronal and peripheral links. Terms linked to the extracellular matrix were significantly enriched in the spinal cords and

TA muscles of homozygous mice. These pathways were also dysregulated in the spinal cords of other mouse models carrying *Fus* NLS mutations (Humphrey et al., 2020). This suggests that *Fus* NLS mutations may cause structural changes in these tissues, leading to a specific phenotype profile.

3.3.1.1 Brain structure and function

Despite these commonalities, the *Fus*$^{\Delta 14}$ mutation also caused tissue-specific effects. The brain was the most transcriptionally dysregulated tissue, and this correlated with significant alterations in brain structure and function. Notable brain morphological changes were accompanied by microscopic changes. The Corrochano group observed thinner cortical layers, and fewer neurons, in the brains of homozygous mice. While cortical thinning is a key feature of ALS, it is usually seen at a later time-point (Agosta et al., 2012). The presence of cortical thinning at 9 weeks of age may explain the sudden fatal seizures (Galovic et al., 2019). The *Fus*$^{\Delta 14}$ mutation may be directly acting on excitatory or inhibitory neurons, therefore additional molecular characterisation of neurons and interneurons is needed. Homozygous mice showed innate behaviour deficits and apathy. These findings are reproducible as these mice buried less marbles in a different facility. The Corrochano group also observed deficits in recognition memory. The hippocampus and cortex are implicated in these tests (R. M. J. Deacon, 2006; Deacon et al., 2002; Tanimizu et al., 2018) suggesting that these brain regions are particularly vulnerable to the *Fus*$^{\Delta 14}$ mutation. Neuronal changes and behavioural impairments have been observed in a mouse with truncated FUS protein lacking the NLS (*Fus*$^{\Delta NLS}$) (Scekic-Zahirovic et al., 2021).

These early brain structural and functional alterations point to a developmental origin. FUS is known to play an important role in development and postnatal life.

FUS is involved in DNA damage response and repair machinery, and complete KO causes perinatal lethality (Shang & Huang, 2016). Behavioural deficits were seen as early as 9 weeks of age in a transgenic FUS mouse model (*FUS*$^{\Delta NLS}$) (Ito et al., 2020). Patients who have juvenile forms of FUS-ALS display developmental delays (Bäumer et al., 2010; Mochizuki et al., 2012; Zou et al., 2016). Not all *FUS* mutations cause developmental problems but those that significantly target the NLS region cause a severe phenotype.

Neurodevelopmental effects are seen in other NDDs. Despite HD having a late manifestation, neuronal abnormalities (cortex, neural progenitor cells, ciliogensis and cell cycle) were seen in human foetuses (Barnat et al., 2020). Proteins implicated in the pathogenesis of NDDs (e.g., Aβ, PINK and MAPT/tau) are involved in nervous system development in prenatal and early postnatal life (Schor & Bianchi, 2021). This changes the way researchers approach NDDs. Treatments may need to be administered early, possibly *in utero*. IVF with pre-implantation screening should occur, although many *FUS* mutations arise *de novo*.

3.3.1.2 Muscle

The second most transcriptionally altered tissue was the TA muscle. GO terms related to the extracellular matrix and muscle composition were significantly enriched, indicating that the *Fus*$^{\Delta 14}$ mutation caused structural changes in the muscles. Muscle from homozygous mice showed significant upregulation of the slow-twitch fibre gene (*Myh7*) and downregulation of a fast-twitch fibre gene (*Myh2*), suggesting an increase in slow-fibre muscle composition. Muscle histological analysis showed more slow-twitch (type 1) fibres in the TA muscles of homozygous mice, at 3 months of age (unpublished data, Fratta group). Literature has shown that an increase in slow-twitch fibres may temporarily compensate for

the loss of fast-twitch fibres seen in early ALS disease (Nijssen et al., 2017). This may explain the lack of motor phenotypes seen at this early time-point.

The Fratta group observed extensive neuromuscular changes in homozygous mice at 3 months of age (data unpublished). *In vivo* muscle physiology readings showed a reduction in TA force. Lumbrical muscle innervation deficits were coupled with reductions in NMJ sizes. At the spinal level, reductions in EDL motor units and L4-L5 motor neurons were seen. These neuromuscular changes were not accompanied by grip strength deficits (when corrected by weight). Motor symptoms will likely develop at a later time-point, however, this cannot be studied as homozygous mice have a reduced lifespan.

3.3.1.3 Systemic metabolism

The *Fus*$^{\Delta 14}$ mutation in homozygosity caused extensive systemic metabolic alterations. The transcriptomic data hinted at these effects as GO terms related to lipid metabolism were significantly enriched in the liver (the main lipid regulation organ). Despite homozygous mice being proportionately smaller than their control littermates, they had increased fat stores. These fat depots were caused by increased adipogenesis, with FUS directly acting on adipocytes in a cell-autonomous manner. These fat depots caused downstream effects, like altered glucose handling and hepatic lipid accumulation.

It is important to know the significance of these fat stores and the role they play in disease. A progressive reduction in glucose metabolism was seen in a pre-symptomatic *SOD1* mutant mouse. Loss of glycolytic metabolism, coupled with a higher energy need, resulted in the muscles switching to lipids as an alternative energy source (Palamiuc et al., 2015). Data from this project points to a similar compensatory mechanism in *Fus*$^{\Delta 14}$ homozygous mice at 9 weeks of age.

Impaired glucose handling in homozygous mice caused adaptive changes in the TA muscles, in the form of more slow-twitch fibres. These fibres are known to display low fatigability, high oxidative capacity and a preference for FFAs as a substrate for energy production (Baskin et al., 2015). Therefore, the fat depots provide fuel. Despite these compensatory mechanisms, significant neuromuscular changes occurred at 3 months of age. This suggests that these muscle metabolic changes may exacerbate disease progression. This skeletal-muscle metabolic reprogramming was also detected in pre-symptomatic *SOD1*^{G93A} mice, and this predated hypermetabolism and neuromuscular changes in the symptomatic stage. Chronic treatment of a fatty acid β-oxidation inhibitor decreased energy expenditure and temporarily improved locomotor symptoms (Scaricamazza et al., 2020). Muscle LD accumulation has been documented in ALS patients, especially in patients with *FUS* mutations (Zhou et al., 2022). Partial improvements were seen in a jALS patient, carrying a NLS *FUS* mutation (P525L), after the administration of drugs that target lipid metabolism (riboflavin and levocarnitine) (Zhou et al., 2020). The patient initially presented a dropped neck and could partially lift his head one week after treatment. Targeting early muscle metabolism using drugs, with better pharmacokinetic and pharmacodynamics profiles, may provide therapeutic benefits in ALS patients.

Hypometabolism was observed in homozygous mice, indicating an abnormally low metabolic rate. While indirect calorimetry analysis refers to whole-body metabolism, brain hypometabolism has been observed in NDDs with cognitive dysfunction, e.g., Alzheimer's disease (Costantini et al., 2008). The brain has a high energy demand (accounts for 20% of the body's energy consumption), which is met by glucose metabolism (Garrett & Niccoli, 2022). This process is measured

by tracking radioactive glucose tracer (18-fluoro-deoxy-glucose) using positron emission tomography (FDG-PET) (Meeter et al., 2017). Brain hypometabolism has also been reported in FTD, where FUS pathology (inclusions) has been observed. Hypometabolism was detected in cortical and subcortical regions of bv-FTD patients (Jeong et al., 2005), while sv-FTD patients showed hypometabolism in the right caudate nucleus, insula and bilateral orbitofrontal areas (Diehl-Schmid et al., 2006). The affected regions correlated to the disease symptoms, e.g., executive dysfunction in bv-FTD and language problems in sv-FTD. Slow glucose uptake in homozygous mice shows that the *FUS*$^{\Delta 14}$ mutation downregulates glucose metabolism, possibly by directly acting on insulin-signalling pathways. Additionally, cytoplasmic FUS has been shown to interact with several glycolytic proteins like pyruvate kinase (PK), phosphoglycerate kinase 1 (PGK) and glucose-6-phosphate isomerase (GPI) (Wang et al., 2015) The *Fus*$^{\Delta 14}$ mutation increases cytoplasmic FUS concentrations, which could sequester these proteins. Systemic glucose dysregulation in *Fus*$^{\Delta 14}$ homozygous mice could reduce glucose availability in their brain causing neuronal dysfunction, and possibly contributing to the observed behavioural deficits and seizures in these mice (Zilberter & Zilberter, 2017). As a result, FDG-PET scans could be conducted in this mutant line to confirm brain hypometabolism.

3.3.2 Genetic background effects

Possible interactions between the mouse genetic background and the *Fus*$^{\Delta 14}$ mutation were demonstrated by the ability to rescue perinatal lethality on a hybrid background (C57BL/6J x DBA/2J). Metabolic comparisons of heterozygous mice across the congenic inbred and hybrid backgrounds revealed additional background differences. Heterozygous mice on the hybrid and DBA/2J

backgrounds showed similar early body composition profiles (increased fat mass and reduced lean mass). However, these changes were time-specific in DBA/2J mice, while mice on the hybrid background maintained these genotype differences in later life (up to 12-months). This metabolic phenotype was absent in heterozygous mice on the C57BL/6J background. While the DBA/2J background may be contributing to some of the observed phenotypes, there are specific hybrid background interactions that may be influencing *Fus*$^{\Delta 14}$ mutation effects. In addition, there could be background effects that this mutation is exacerbating. For example, juvenile mice on the DBA/2J background are known to have auditory seizures, which may be contributing to the fatal seizures in homozygous mice (Jawahar et al., 2011). While it is difficult to determine the significance and extent of these background changes without repeating all the experiments conducted on the hybrid background, it demonstrates that genetic background interacts with the *Fus*$^{\Delta 14}$ mutation to alter phenotypes.

Genetic background differences have been extensively documented in the literature. Differences in disease presentation and progression were reported between C57BL/6J and B6SJL mice carrying the *SOD1*^{G93A} mutation (Mancuso et al., 2012). Genetic backgrounds are known to contribute to phenotypes in mouse models due to modifier loci and interacting genes at sites distinct from the target mutation (Montagutelli, 2000). These modifier genes may interact with or modify the mutation's effect. Genetic modifiers may explain the heterogeneity of phenotypes seen across mouse backgrounds and in human populations. In the clinic, this translates to individuals carrying the same mutation but not developing the disease (incomplete penetrance) or displaying different clinical symptoms (variable expressivity) (Hou et al., 2019). The low population frequencies of

genetic modifiers and their heterogenic nature mean that they are difficult to identify. Additionally, research has shown that highly complex modifier interactions lead to genetic background effects, and they can be confounded by additional genetic and environmental factors (Mullis et al., 2018).

Through the use of animal studies, it has been shown that genetic modifiers can alter the expression of the target gene. For example, they can: (i) alter the expression of genes involved in the target pathway, (ii) alter DNA transcription rates or mRNA stability, (iii) alter DNA methylation or chromatin structure through epigenetic effects, and (iv) alter gene copy number (Erickson, 1996). Traditionally, genetic modifiers have been identified through gene mapping and positional cloning approaches. Mapping begins with identifying two strains that harbour the same mutation but display different phenotypes. F2 intercrosses between these strains will produce F2 mice that undergo genome-wide analysis, using DNA markers that are polymorphic between the two strains (Linder, 2006). Currently, whole genome sequencing techniques are used to identify genetic variation (Keane et al., 2011).

While identifying mouse modifier genes is beyond the scope of this project, phenotypic differences between genetic backgrounds raises interesting points about animal research. Inbred lines are commonly used in research because these mice are purported to show less within-strain phenotypic variability, therefore the target mutation’s effects can be studied. However, growing evidence shows that inbred and outbred mice display comparable phenotypic variation (Jensen et al., 2016). It has been suggested that phenotypic variability in inbred mice is due to their unnatural fixed allelic states and interactions. Therefore, they have a single-state response to environmental stressors. Outbred mice have

multiple allelic variants in each biological pathway which could have a stabilising effect on phenotypic readouts (Tuttle et al., 2018). Outbred mice are better equipped to handle environmental and experimental changes. Additionally, heterogeneity in genetic backgrounds exists in patients, making outbred mice more clinically relevant. Using wild-derived strains can also improve the reproducibility and translatability of mouse research through increasing genetic heterogeneity (Yoshiki & Moriwaki, 2006).

Using F2 hybrid backgrounds (cross-breeding two inbred strains) increases the genetic heterogeneity of the hybrid offspring (Sloin et al., 2022). The variation of alleles means that the offspring: survive longer, are resistant to environmental factors and have more reproductive success than their parental strains (Sprott & Ramirez, 1997).

Continuing the use of inbred mice means that genetic background effects need to be controlled. Observing consistent phenotypes in multiple congenic backgrounds ensures that mutation specific effects are being observed (Montagutelli, 2000). Researchers should know the endogenous traits of inbred strains so mutant phenotypes can be accurately interpreted. This knowledge should be used in the mouse background selection process. Some behavioural phenotypes of inbred mouse strains have been characterised (Crawley et al., 1997), however a centralised database containing all phenotypes is needed for future mouse research.

3.3.3 Conclusion

The *Fus*$^{\Delta 14}$ mutation in homozygosity caused a severe phenotype profile, evidenced by the widespread effects and reduced lifespan. Significant early alterations were seen in brain structure and function, as well as neuromuscular

changes (Fratta group). These changes point to a developmental origin and are reflective of jALS cases. This mutation also caused systemic metabolic dysregulation which may contribute to the cognitive and motor phenotypes. As a result, *Fus*$^{\Delta 14}$ homozygous mouse is a good model to study FUS specific pathological mechanisms (**Figure 3.19**).

Genetic backgrounds interact with the *Fus*$^{\Delta 14}$ mutation to alter metabolic phenotypes. Additional characterisation experiments (motor and behavioural) are needed to understand the extent of this interaction and potential modifier genes. However, reproducible phenotypes in other NLS *Fus* mutation models indicates that the observed phenotypes in the hybrid background are strongly influenced by the *Fus*$^{\Delta 14}$ mutation.

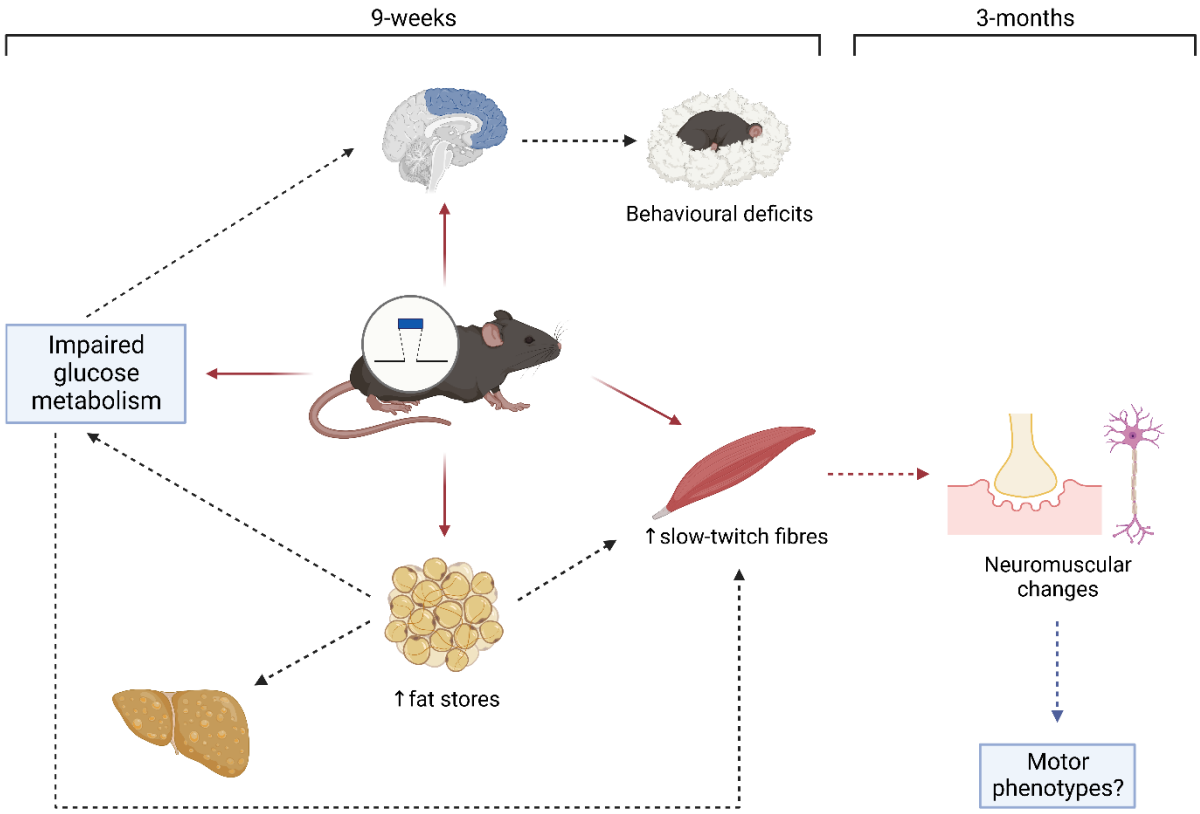


Figure 3.19. *FUS*$^{\Delta 14}$ mutation caused systemic effects in homozygosity. Homozygous mice were proportionately smaller than their littermate controls and had a reduced lifespan (~12-weeks). RNA-sequencing data showed widespread alterations, with the brain and muscle being the most transcriptionally dysregulated tissues. Follow-up experiments revealed that this mutation caused brain morphological changes (narrower brains), which were accompanied by cortical thinning and fewer neurons. These brain structural changes may underline the observed behavioural deficits and seizures. Early brain-related changes suggest developmental mutation effects. Significant metabolic alterations were observed in homozygous mice. Increased fat depots caused downstream effects, like fatty liver and impaired glucose uptake. Alterations in glucose handling, coupled with hypometabolism, suggest impaired glucose metabolism. This negatively affected the two energy-dependent organs in the body (muscle and brain). In the muscle, early compensatory mechanisms occurred. There was a switch to a 'slow-twitch' muscle fibres which are known to have a fat fuel preference. Muscle metabolic switch preceded significant neuromuscular changes at 3 months of age. In the brain, reduced glucose may affect brain structure and function but this was not confirmed in this model. Figure created using BioRender.com.

Results II

Investigating the systemic effects of the *Tardbp*^{M323K} mutation in homozygosity

4 Investigating the systemic effects of the *Tardbp*^{M323K} mutation in homozygosity

4.1 Introduction

TDP-43 pathology is implicated several NDDs, collectively referred to as “TDP-43 proteinopathies”. The precise TDP-43 pathological mechanism remains unknown. A number of molecular processes have been proposed in the pathogenesis, falling under LOF and/or GOF (de Boer et al., 2021). However, the transgenic overexpression and conditional deletion mouse models commonly used in this field may not be the best models to study TDP-43 pathology. TDP-43, along with FUS, is extremely dosage sensitive and slight changes in wild-type levels can cause severe phenotypes. For example, elevated TDP-43 levels are enough to induce toxic effects (Mitchell et al., 2015), while ‘knocking-down’ TDP-43 causes embryonic lethality (Xu et al., 2010). Additionally, overexpression models cannot be used to study LOF effects, while conditional KO models ignore GOF effects. As a result, the phenotypes observed in transgenic models may not be representative of underlying pathomechanisms. Models that express mutant proteins at physiological levels may be a better tool to accurately study TDP-43 pathomechanisms.

This chapter aims to understand the systemic effects of *TARDBP* mutations since TDP-43 is expressed in many tissues and is involved in numerous RNA metabolism processes (Birsa et al., 2020). Therefore, *TARDBP* mutations are expected to cause widespread effects. Although rare, the majority of *TARDBP* mutations are seen in familial cases of ALS so motor characterisation is the focus of *in vivo* research. However, TDP-43 pathology is widely found in sporadic NDDs

with cognitive decline, e.g., ALS-FTD, FTD and Alzheimer's disease (Wilson et al., 2013). Metabolic dysregulation is also observed in these conditions, especially across the ALS-FTD spectrum.

For this project, the systemic pathological mechanisms of TDP-43 were investigated through the characterisation of the *Tardbp*^{M323K} mouse. This mouse contains a point mutation in the endogenous mouse *Tardbp* gene and expresses TDP-43 at physiological levels. Previous characterisation of the knock-in *Tardbp*^{M323K} homozygous mouse revealed a late neuromuscular and motor phenotype in both sexes (Fratta et al., 2018; Oliveira, 2014); progression from 18 months of age. Preliminary behavioural tests hinted to neuronal dysfunction in the form of associative learning problems and a classical PPI deficit (Oliveira, 2014), however, further characterisation was needed to validate this mouse as an ALS-FTD model. A longitudinal pipeline was designed to identify motor, neuromuscular, cognitive/behavioural and metabolic phenotypes (**Figure 4.1**). Males were omitted due to possible underpowering of tests. Male homozygous mice are known to be aggressive, and this behaviour is seen in FTD patients (Grochmal-Bach et al., 2009). While aggression/personality changes is a valuable readout, potential welfare concerns could result in the early culls of male mice. The Corrochano group had the time and resources to support multiple cohorts, therefore they were able to conduct a parallel longitudinal study to characterise male *Tardbp*^{M323K} mice. Previous characterisation of heterozygous mice revealed no significant phenotypes (Oliveira, 2014) so they were omitted from this study.

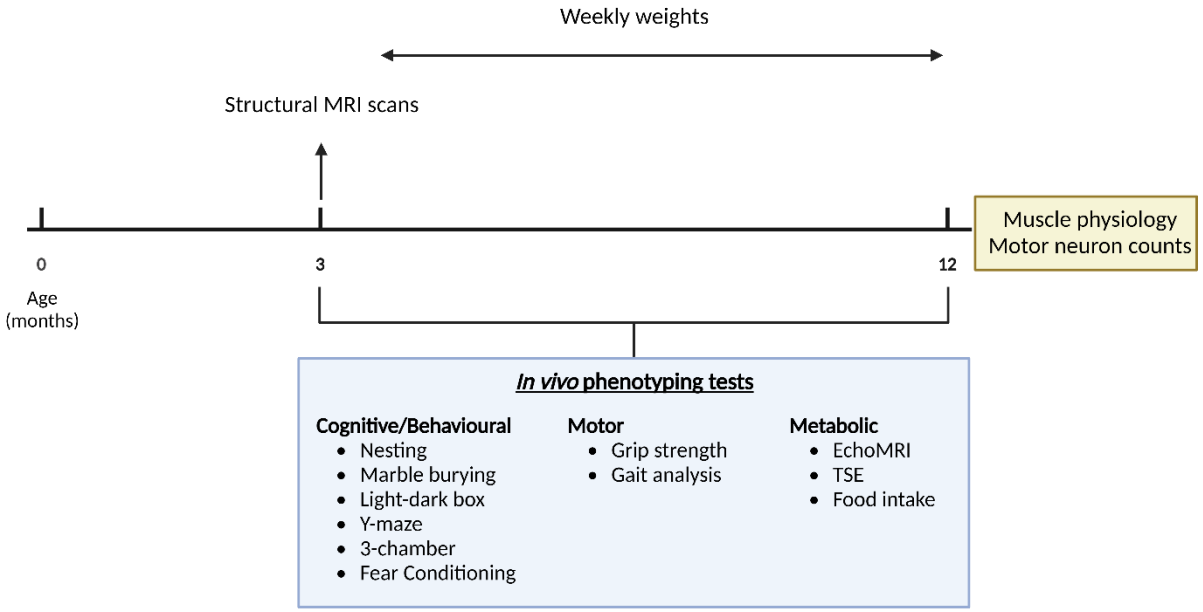


Figure 4.1. Phenotyping pipeline to characterise the *Tardbp*^{M323K} mouse. Female wild-type (*Tardbp*$^{+/+}$) and homozygous (*Tardbp*$^{M323K/M323K}$) mice were longitudinally studied for motor, cognitive/behavioural and metabolic phenotypes. *In vivo* phenotyping tests were conducted at 3 and 12-months to identify any progressive changes. Each genotype group has a sample size of ~12. At the end of this study, these mice underwent *in vivo* muscle physiology experiments at UCL and their spinal cords were collected for motor neuron counts. Different cohorts were used for the weekly weights and structural MRI scans. Structural MRI scans were conducted at 3 months of age, at the Mouse Imaging Centre (Toronto, Canada). Figure created using BioRender.com.

4.2 Results

4.2.1 Metabolic alterations in *Tardbp*$^{M323K/M323K}$ mice

4.2.1.1 *Tardbp*$^{M323K/M323K}$ mice weighed more than littermate controls, but this was not statistically significant

Mice were weighed weekly to monitor development and possible disease progression. Body weights were collected longitudinally (19 to 51-weeks) and analysed using 2-way ANOVA repeated measures and Bonferroni correction of multiple testing to evaluate genotype differences at each time-point.

From 35-weeks, *Tardbp*$^{M323K/M323K}$ appeared to weigh more than control *Tardbp*$^{+/+}$ littermates (**Figure 4.2**); *Tardbp*$^{M323K/M323K}$ gained weight at a faster rate. However, this trend was not statistically significant after repeated measures analysis (**Table 4.1**).

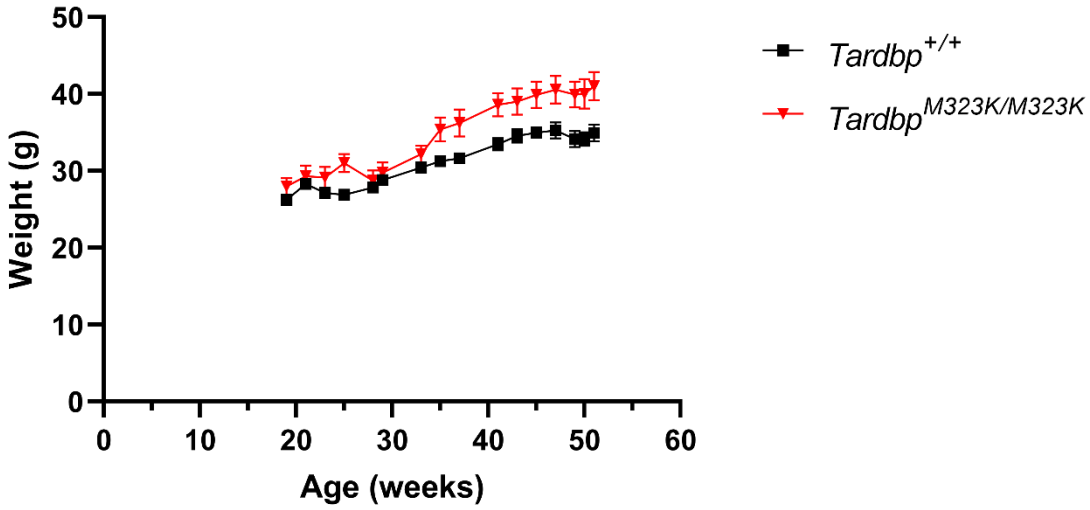


Figure 4.2. Body weights of female *Tardbp*^{M323K} mice. Graphs showing weekly weights of female *Tardbp*$^{+/+}$ and *Tardbp*$^{M323K/M323K}$ mice. *Tardbp*$^{M323K/M323K}$ weighed more than control littermates but this was not statistically significant. Data shown as mean. Error bars denote SEM of data. Data analysed using 2-way ANOVA repeated measures and Bonferroni correction of multiple testing to evaluate genotype differences at each time-point. n numbers for each time-point can be found in **Table 4.1**.

Age (weeks)	Genotype						Adjusted p-value
	Tardbp$^{+/+}$			*Tardbp*$^{M323K/M323K}$			
	Mean weight (grams)	SEM	n	Mean weight (grams)	SEM	*n*	
19	26.24	0.41	9	27.96	1.11	12	>0.9999
21	28.32	0.52	9	29.31	1.36	12	>0.9999
23	27.15	0.28	9	29.14	1.37	12	>0.9999
25	26.90	0.28	9	31.00	1.18	12	0.08350
28	27.86	0.52	9	28.71	1.34	12	>0.9999
29	28.80	0.63	9	29.77	1.34	12	>0.9999
33	30.44	0.51	9	32.19	1.07	12	>0.9999
35	31.28	0.62	9	35.41	1.54	12	0.41490
37	31.66	0.28	9	36.23	1.75	12	0.40200
41	33.46	0.80	9	38.59	1.53	12	0.14240
43	34.58	0.88	9	39.02	1.70	12	0.53960
45	34.98	0.72	9	39.90	1.73	12	0.31270
47	35.28	1.05	9	40.56	1.80	12	0.34660
49	34.16	1.03	9	39.95	1.66	12	0.13580
50	34.13	0.90	9	40.01	1.93	12	0.22620
51	34.93	1.09	9	41.02	1.83	12	0.17200

Table 4.1. Mean body weights of female *Tardbp*^{M323K} mice and statistical analysis. Table showing mean weights, SEM, n numbers and adjusted p-values of female *Tardbp*$^{+/+}$ and *Tardbp*$^{M323K/M323K}$ mice.

4.2.1.2 *Tardbp*$^{M323K/M323K}$ mice had increased fat mass at 3 months of age

While body weight is a useful marker for overall disease state, it does not give much information on body composition. It is difficult to determine the cause of the increased body weights in *Tardbp*$^{M323K/M323K}$ mice. EchoMRI was used to measure changes in fat and lean mass at 3 and 12 months of age. Data was analysed using 2-way ANOVA followed by Tukey's multiple comparisons test to compare between genotypes at each time-point, and between time-points within genotypes.

Tardbp$^{M323K/M323K}$ mice had significantly increased fat mass at 3 months of age, compared to control *Tardbp*$^{+/+}$ littermates (p<0.05, **Figure 4.3**). While the same trend was observed at 12-months, it was not statistically significant. At both time-points, there were no genotype differences in lean mass. Over time, both genotypes displayed the expected age-related increases in fat mass and decreases in lean mass (p<0.001) (Moulias et al., 1999).

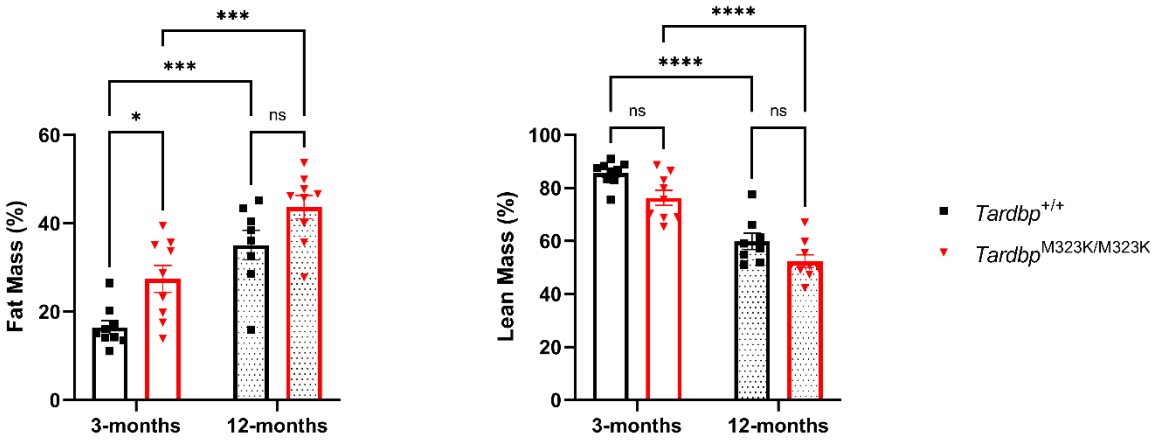


Figure 4.3. Body composition of female *Tardbp*^{M323K} mice. Graphs show data from female mice at 3 (blank bars) and 12-months (dotted bars). *Tardbp*$^{M323K/M323K}$ mice had increased fat mass at 3 months of age but not at 12-months. No genotypes differences in lean mass, at both time-points. All mice showed increased fat mass and reduced lean mass over time. Fat and lean mass corrected for individual animal's body weight. Data shown as mean. Error bars denote SEM of data. Data analysed using 2-way ANOVA followed by Tukey's multiple comparisons test to compare between genotypes at each time-point, and between time-points within genotypes. n=9 *Tardbp*$^{+/+}$ and n=9 *Tardbp*$^{M323K/M323K}$. ns= not significant. *p<0.05. ***p<0.001. ***p<0.0001.

4.2.1.3 Elevated EE rates in *Tardbp*$^{M323K/M323K}$ mice at 12 months of age

Literature has shown that ALS-FTD spectrum diseases are associated with a higher prevalence of metabolic alterations. These metabolic changes are reported in symptomatic patients therefore it is unclear if they occur in the pre-symptomatic stage. The benefit of this longitudinal study is that characterisation was conducted at an early time-point (3-months) so initial disease changes could be observed. While differences exist across the spectrum, hypermetabolism has been reported at both ends (Ahmed, Irish, Piguet, et al., 2016). EE is an indicator of whole-body metabolism so indirect calorimetry was used to measure this parameter. This metabolic test also provides the RER, which is an indicator of fuel preference. Mice were placed in a metabolic cage and the amount of oxygen used and carbon dioxide released by the body is measured to determine these parameters. EE measurements were corrected by lean mass using 2-way ANCOVA to give adjusted mean EE values. Diurnal differences meant that all parameters were separated into dark (6pm- 6am) and light (12- 5pm and 7- 10am) phase. Data was analysed using 2-way ANOVA followed by Tukey's multiple comparisons test to compare between genotypes in each time-point, and between time-points within genotypes.

At 12 months of age, *Tardbp*$^{M323K/M323K}$ mice had elevated EE rates in the light and dark phase, compared to control *Tardbp*$^{+/+}$ littermates ($p<0.001$, **Figure 4.4A**), suggesting hypermetabolism. This genotype difference was not seen at 3-months. No genotype differences were reported in RER (**Figure 4.4B**). Over time, all mice showed increased EE rates and RER.

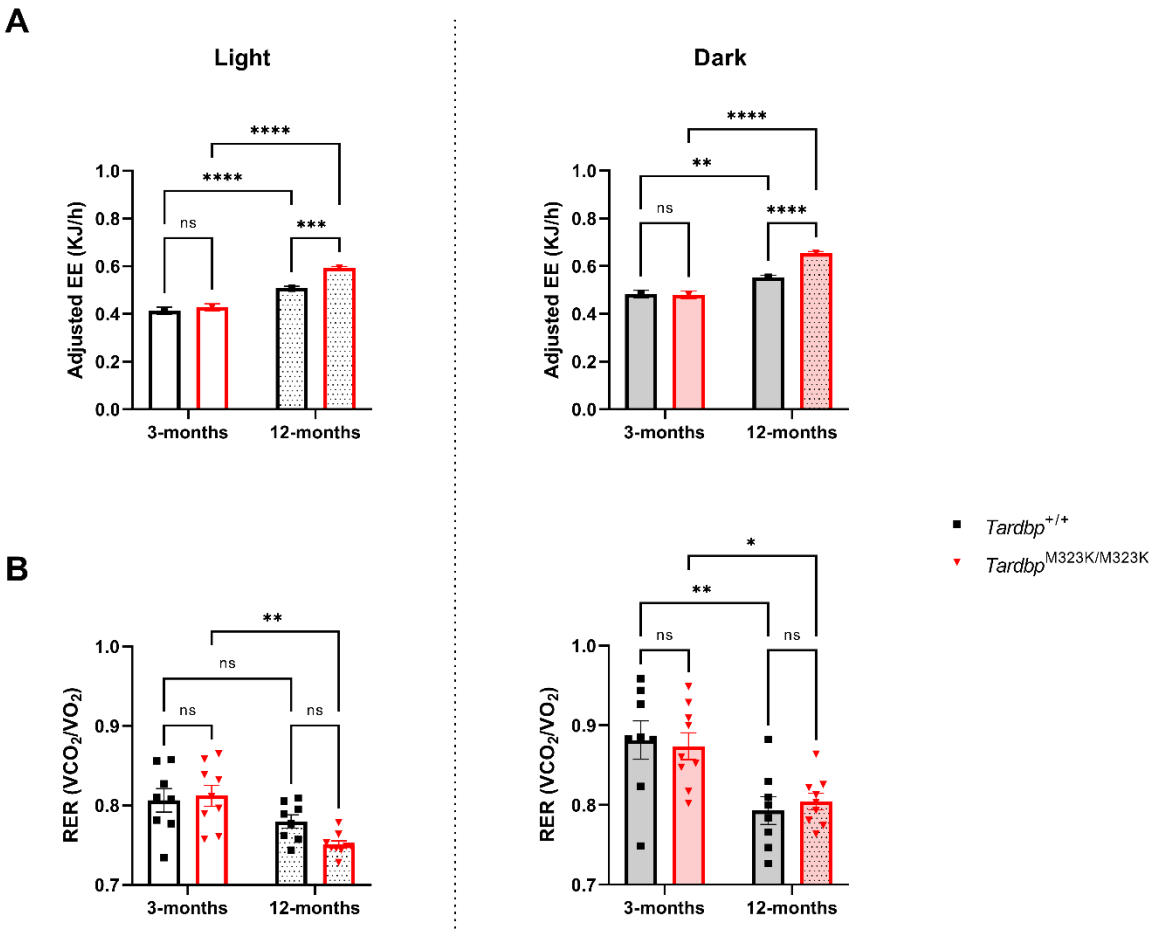


Figure 4.4. Indirect calorimetry analysis on female *Tardbp*^{M323K} mice. Graphs show energy expenditure (EE) (**A**) and respiratory exchange ratio (RER) (**B**) measurements from female mice at 3 (blank bars) and 12-months (dotted bars). *Tardbp*$^{M323K/M323K}$ mice had elevated EE rates at 12 months of age. EE corrected by lean mass using 2-way ANCOVA to give an adjusted EE mean value. Parameters are separated by time (light and dark). Light (graphs with white bars): 12- 5pm and 7- 10am. Dark (graphs with shaded bars): 6pm- 6am. Data shown as mean. Error bars denote SEM of data. Data was analysed using 2-way ANOVA followed by Tukey's multiple comparisons test to compare between genotypes in each time-point, and between time-points within genotypes. n=8 *Tardbp*$^{+/+}$ and n=9 *Tardbp*$^{M323K/M323K}$. ns= not significant. *p<0.05. **p<0.01. ***p<0.001. ***p<0.0001.

4.2.1.4 No evidence of hyperphagsia in *Tardbp*$^{M323K/M323K}$ mice

Differences in food intake are reported across the ALS-FTD spectrum, with increased caloric intake and binge-eating reported in FTD patients (Mendez et al., 2008). Therefore, total food intake was measured in these mice. A feeding period of 24-hours was assessed. Due to licensing constraints, this test was only conducted at 12-months. There were no genotype differences in food intake at 12 months of age (**Figure 4.5**).

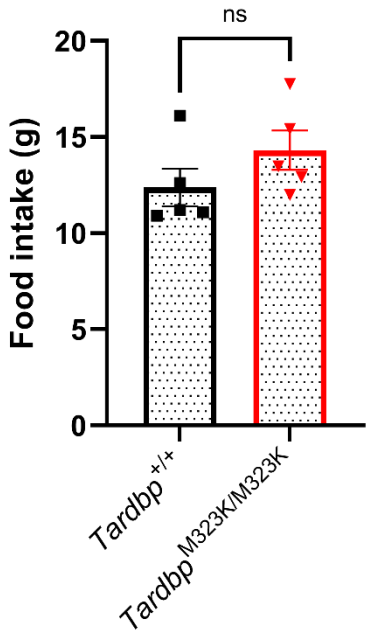


Figure 4.5. Food intake analysis of *Tardbp*^{M323K} mice. Graph shows data from female mice at 12-months (dotted bars). Food intake per cage/ 2. Data shown as mean. Error bars denote SEM of data. Data was analysed using unpaired t-test to compare between genotypes. n=5 *Tardbp*$^{+/+}$ and n=5 *Tardbp*$^{M323K/M323K}$. ns= not significant.

4.2.2 Motor phenotypes in *Tardbp*$^{M323K/M323K}$ mice

Previous *in vivo* characterisation revealed late neuromuscular and motor phenotypes in *Tardbp*$^{M323K/M323K}$ mice. A grip strength deficit was observed at 24 months of age in females *Tardbp*$^{M323K/M323K}$ mice, but not at 7-months (Fratta et al., 2018) However, it remains unknown precisely when these motor phenotypes develop. In this study, grip-strength and gait pattern were measured at 12-months. Data was analysed using unpaired t-test to compare between genotypes.

Tardbp$^{M323K/M323K}$ mice displayed a significant 20.43% grip strength deficit at 12 months of age ($p<0.05$, **Figure 4.6**). Gait abnormalities were also observed at this time-point (**Figure 4.7**). *Tardbp*$^{M323K/M323K}$ mice had a reduced front and hind limb stance duration, compared to control *Tardbp*$^{+/+}$ littermates ($p<0.05$), as well as a reduced front limb step length ($p<0.01$). Increased hind limb stride length and swing duration ($p<0.05$) were also observed in *Tardbp*$^{M323K/M323K}$ mice.

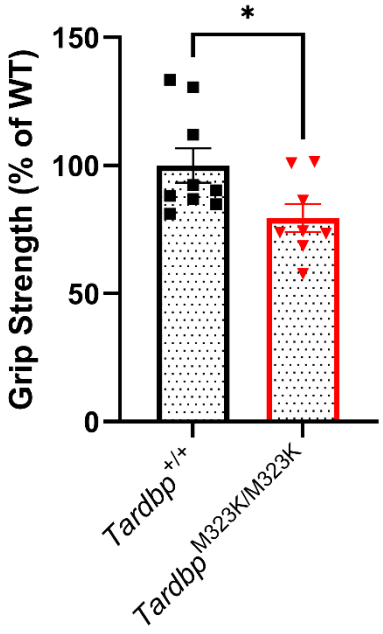


Figure 4.6. Fore and hind limb grip strength analysis of female *Tardbp*^{M323K} mice. Graph shows data from female mice at 12-months (dotted bars). *Tardbp*$^{M323K/M323K}$ mice had a grip strength deficit. Combined limb grip strength force was corrected for individual animal's body weight, and then expressed as related to the *Tardbp*$^{+/+}$ average measurements. Data shown as mean. Error bars denote SEM of data. Data analysed using unpaired t-test to compare between genotypes. n=9 *Tardbp*$^{+/+}$ and n=8 *Tardbp*$^{M323K/M323K}$. *p<0.05.

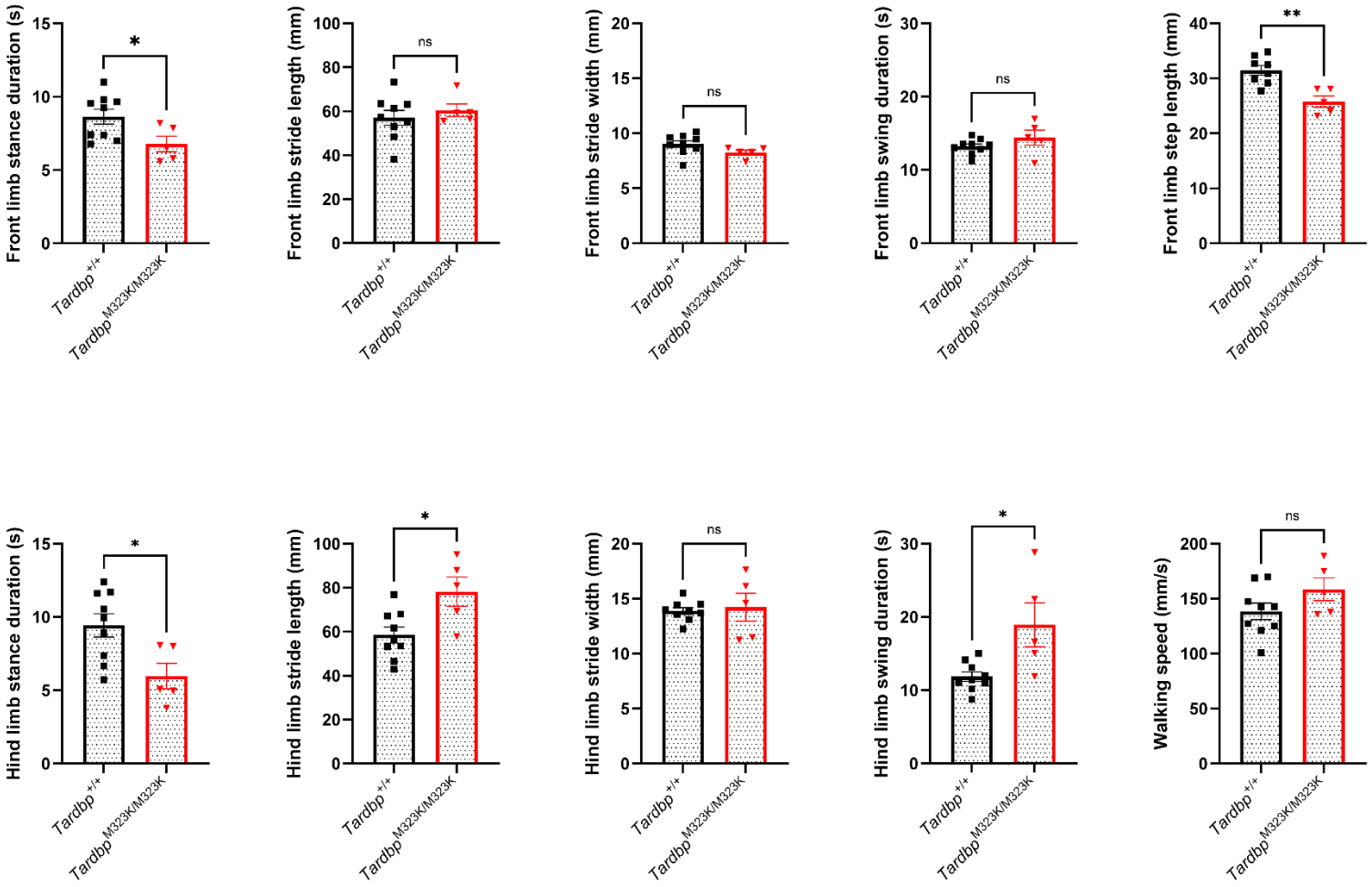


Figure 4.7. Gait analysis of female *Tardbp*^{M323K} mice. Graphs show parameters from the Mousewalker test conducted at 12-months (dotted bars). Gait abnormalities were seen in *Tardbp*$^{M323K/M323K}$ mice. Data shown as mean. Error bars denote SEM of data. Data analysed using unpaired t-test to compare between genotypes. n=9 *Tardbp*$^{+/+}$ and n=5 *Tardbp*$^{M323K/M323K}$. ns= not significant. *p<0.05. **p<0.01.

4.2.3 Neuromuscular analysis in *Tardbp*$^{M323K/M323K}$ mice

To determine if the motor phenotypes observed in *Tardbp*$^{M323K/M323K}$ mice correlate to changes in muscle function, a series of *in vivo* muscle physiology experiments were conducted at the end of the longitudinal study (~13 months). Muscle force (twitch and tetanic) in the TA and EDL muscles was measured, as well as EDL motor unit survival (MUNE). These experiments were conducted at UCL, under the supervision of Dr Mhoriam Ahmed. Motor neuron counts were performed on histological sections of L4- L5 regions of the lumbar spinal cord. Data was analysed using unpaired t-test to compare between genotypes. At 12 months of age, there were no genotype differences in any of the muscle physiology readings or in the motor neurons counts (**Figure 4.8**).

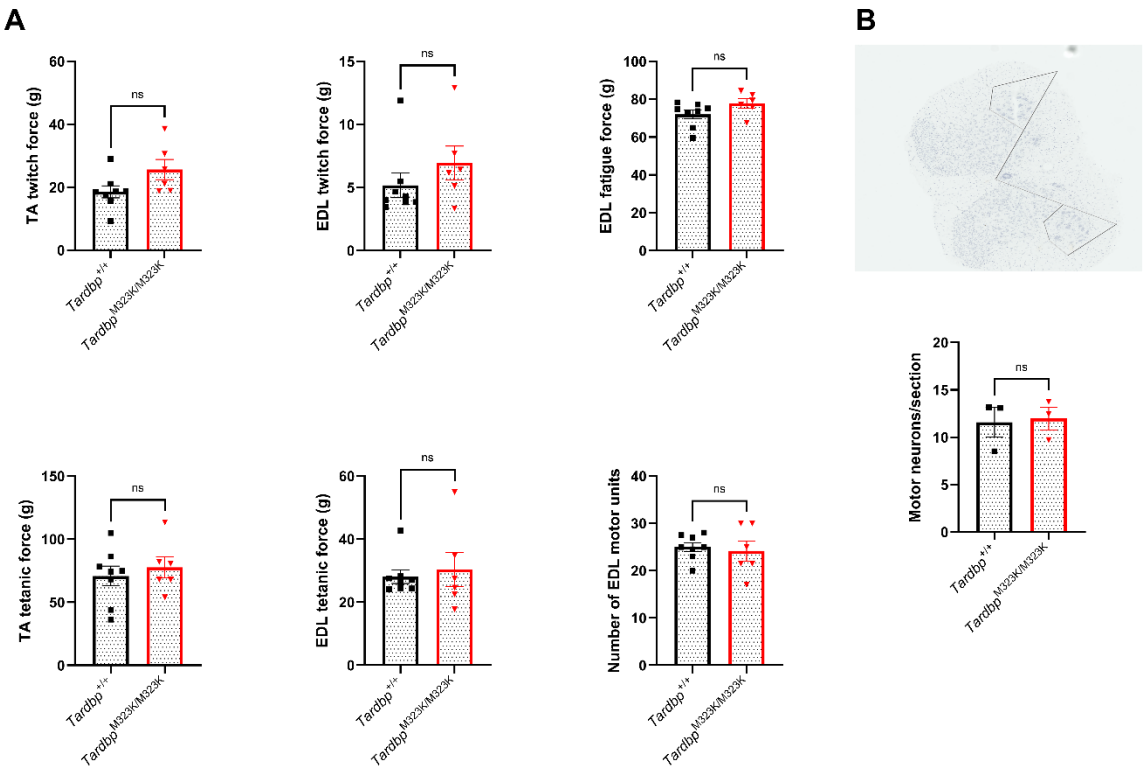


Figure 4.8. Neuromuscular analysis of female *Tardbp*^{M323K} mice. Graphs show parameters from *in vivo* muscle physiology experiments (**A**) and motor neuron (MN) counts of L4- L5 region of lumbar spinal cords (**B**) at ~13-months (dotted bars). B) Representative image of transverse sections (20µm) cut from regions L4 to L5 of the lumbar spinal cord for MN counts. Sections were stained with Gallocyanin. Sciatic MN clustered ventrolaterally (within the shapes) were counted. No genotype differences in both experiments. Data shown as mean. Error bars denote SEM of data. Data analysed using unpaired t-test to compare between genotypes. A (muscle physiology): n=8 *Tardbp*$^{+/+}$ and n=6 *Tardbp*$^{M323K/M323K}$. B (motor neuron counts): n=3 *Tardbp*$^{+/+}$ and n=3 *Tardbp*$^{M323K/M323K}$. ns= not significant.

4.2.4 Behavioural and cognitive impairments in *Tardbp*$^{M323K/M323K}$ mice

A number of *in vivo* behavioural tests were conducted to investigate this mutation's role in cognitive function. Other mouse models carrying a similar *Tardbp* mutation (*Tardbp*^{Q331K} mouse) have reported behavioural alterations (White et al., 2018), therefore, it was important to assess if the *Tardbp*^{M323K} mutation had a similar effect. A range of behavioural tests were used to assess different cognitive and behavioural processes.

4.2.4.1 Early innate rodent behaviour deficits

Initial cognitive investigations involved quick observational tests related to normal rodent behaviours, like nesting and burying. Both tests were conducted at 3 and 12-months. Data was analysed using multiple Mann-Whitney U tests to compare between genotypes at each time-point.

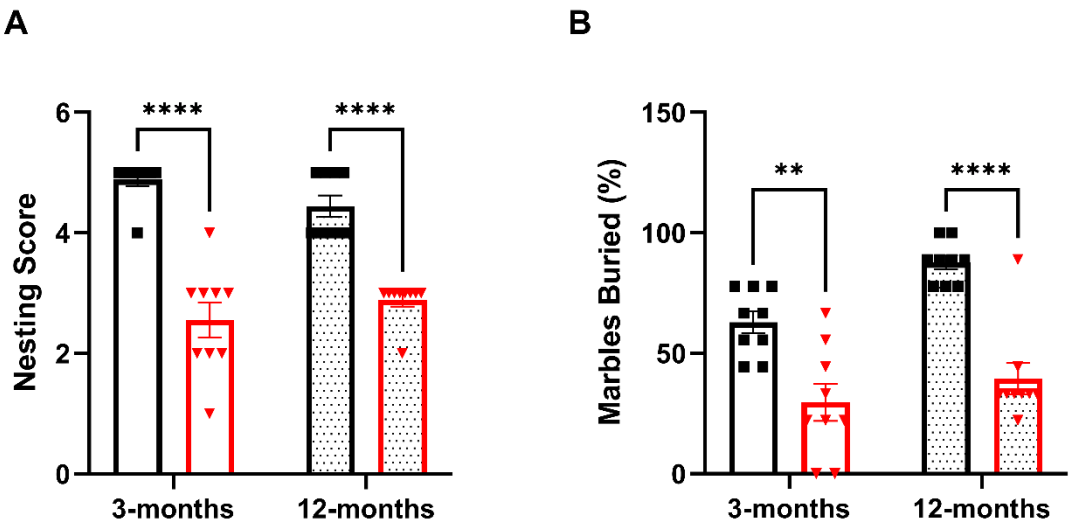


Figure 4.9. Innate rodent behaviour analysis of female *Tardbp*^{M323K} mice. Graphs show data from the nesting (**A**) and marble burying (**B**) tests conducted at 3 (blank bars) and 12-months (dotted bars). *Tardbp*$^{M323K/M323K}$ mice had a lower nesting score and buried less marbles from 3 months of age. Data shown as mean. Error bars denote SEM of data. Data analysed using multiple Mann-Whitney U tests to compare between genotypes at each time-point. n=9 *Tardbp*$^{+/+}$ and n=9 *Tardbp*$^{M323K/M323K}$. **p<0.01. ****p<0.0001.

From 3 months of age, *Tardbp*$^{M323K/M323K}$ mice had a lower nesting score compared to control *Tardbp*$^{+/+}$ littermates ($p<0.0001$, **Figure 4.9**). These mice continued to show significantly lower nesting scores at 12 months of age ($p<0.0001$). *Tardbp*$^{M323/M323K}$ mice also buried fewer marbles from 3 months of age ($p<0.01$) compared to control littermates. This innate behaviour deficit was still present at 12 months of age ($p<0.0001$). Dysregulation in these innate rodent behaviours meant that additional cognitive tests were undertaken.

4.2.4.2 Late onset anxiety-like phenotype

The light-dark box test assesses anxiety-related phenotypes. It also utilises normal rodent behaviours as mice have an innate aversion to brightly-lit/open spaces, which conflicts with their exploratory tendencies (Crawley, 1985). The percentage of time spent in the light zone and proportion of frequency in the light zone were recorded. Data was analysed using 2-way ANOVA followed by Tukey's multiple comparisons test to compare between genotypes at each time-point, and between time-points within genotypes.

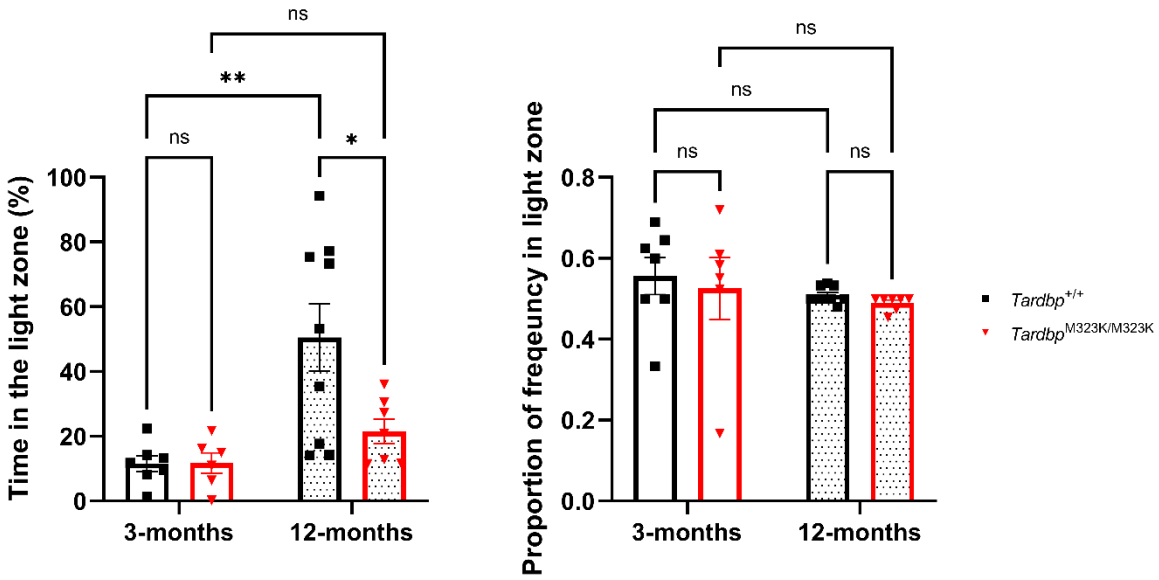


Figure 4.10. Light-dark box test in female *Tardbp*^{M323K} mice. Graphs show data from female mice at 3 (blank bars) and 12-months (dotted bars). *Tardbp*$^{M323K/M323K}$ mice spent less time in the light zone at 12 months of age. Proportion of frequency in light zone: frequency in light zone/ (frequency in light zone + frequency in dark zone). A ratio of 0.5 indicates equal entries in both zones, while a higher frequency indicates more time entered in the light zone. Data shown as mean. Error bars denote SEM of data. Data analysed using 2-way ANOVA followed by Tukey's multiple comparisons test to compare between genotypes at each time-point, and between time-points within genotypes. n=9 *Tardbp*$^{+/+}$ and n=9 *Tardbp*$^{M323K/M323K}$. ns= not significant. *p<0.05. ***p<0.001.

At 12 months of age, *Tardbp*$^{M323K/M323K}$ mice spent less time in the light zone, compared to control *Tardbp*$^{+/+}$ littermates (p<0.05, **Figure 4.10**). This was not seen at 3-months indicating a late onset phenotype. Unlike *Tardbp*$^{+/+}$ mice, the aversion/fear response to the light zone outweighed the exploratory drive in *Tardbp*$^{M323K/M323K}$ mice, suggesting an anxiety-like phenotype. Over time, *Tardbp*$^{+/+}$ mice spent significantly more time in the light zone (p<0.05), suggesting possible habituation to the test. No changes over time were reported in *Tardbp*$^{M323K/M323K}$ mice. At both time-points, the zone entry preference was not altered between the genotypes; mice from both groups entered the light and dark zone at similar frequencies. This did not change over time.

4.2.4.3 Unaltered spatial working memory

The y-maze test was used to assess spatial working memory, specifically spatial reference memory. This test was conducted since global executive dysfunction was observed in FTD patients (Convery et al., 2019) The percentage of time spent in the novel arm and proportion of frequency in the novel arm were recorded. Data was analysed using 2-way ANOVA followed by Tukey's multiple comparisons test to compare between genotypes at each time-point, and between time-points within genotypes.

At both time-points, there were no genotype differences in the measured parameters. Additionally, there were no differences over time within genotypes (**Figure 4.11**). The *Tardbp*^{M323K} mutation has no effect on spatial reference memory.

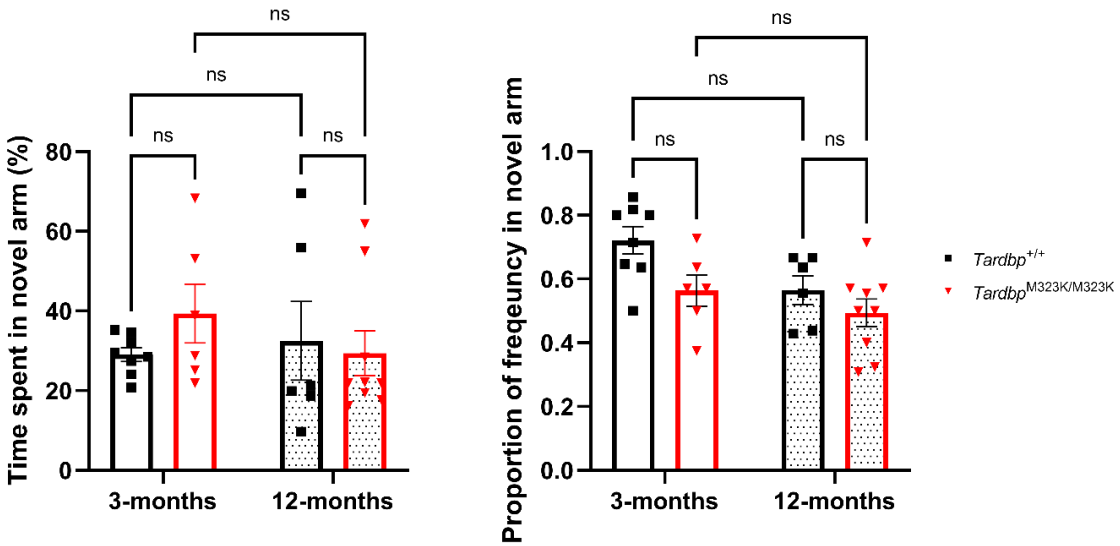


Figure 4.11. Y-maze (forced alteration) test in female *Tardbp*^{M323K} mice. Graphs show data from female mice at 3 (blank bars) and 12-months (dotted bars). No genotype differences at both time-points. Proportion of frequency in novel: frequency in novel/ (frequency in novel arm + frequency in familiar arm). A ratio of 0.5 indicates equal entries in both arms, while a higher frequency indicates more time entered in the novel arm. Data shown as mean. Error bars denote SEM of data. Data analysed using 2-way ANOVA followed by Tukey's multiple comparisons test to compare between genotypes at each time-point, and between time-points within genotypes. 3-months: n=8 *Tardbp*$^{+/+}$ and n=7 *Tardbp*$^{M323K/M323K}$. 12-months: n=7 *Tardbp*$^{+/+}$ and n=9 *Tardbp*$^{M323K/M323K}$. ns= not significant.

4.2.4.4 Unaltered levels of sociability

Personality changes and diminished social interest has been described in FTD patients (Bott et al., 2014). Therefore, general sociability and social novelty were assessed in these mice using the 3-chamber test. Mice were placed in an arena with chambers containing either a novel object or novel mouse. The time spent in each chamber was recorded, as well as the frequencies into each chamber. Due to time constraints, this test was only conducted at 12-months. Data was analysed using 2-way ANOVA followed by Tukey multiple comparisons test to compare between genotypes within object/mouse, and between object and mouse within genotypes.

All mice spent more time interacting with the novel mouse than the novel object (**Figure 4.12**) which is expected as they are social animals. However, there were no genotype differences in any of the measured parameters.

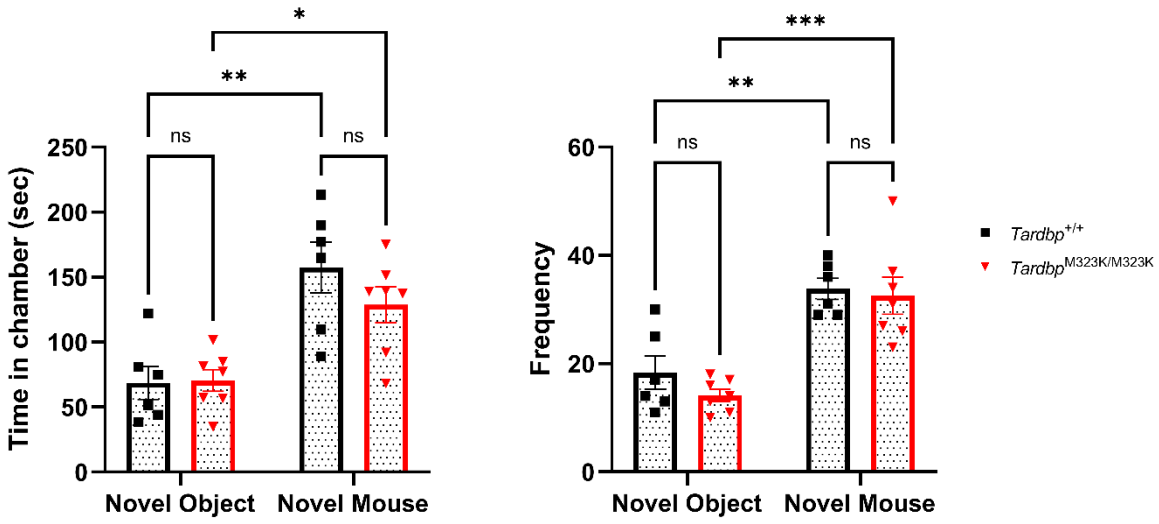


Figure 4.12. 3-chamber test in female *Tardbp*^{M323K} mice. Graphs show parameters from the 3-chamber test at 12-months (dotted bars). No genotype differences in any of the measured parameters. Data shown as mean. Error bars denote SEM of data. Data analysed using 2-way ANOVA followed by Tukey multiple comparisons test to compare between genotypes within object/mouse, and between object and mouse within genotypes. n=6 *Tardbp*$^{+/+}$ and n=7 *Tardbp*$^{M323K/M323K}$. ns= not significant. *p<0.05. **p<0.01. ***p<0.001.

4.2.4.5 Impaired context learning

A key neuropsychological feature of FTD is executive dysfunction, therefore learning and memory were assessed in these mice using the fear conditioning test. This test was spilt into two subtests, context and cue. In the context test, the freezing times (%) before the aversive unconditioned stimuli (sound coupled with shock) and after the animal is placed in the same environment (context) were recorded. In the cue test, the animal was placed in a new environment. The freezing times (%) before (baseline) and after a sound (cue) were recorded. Data was analysed using 2-way ANOVA followed by Sidak's multiple comparisons test to compare between genotypes in each test condition (baseline and context/cue), and between time-points within genotypes to assess if the test worked.

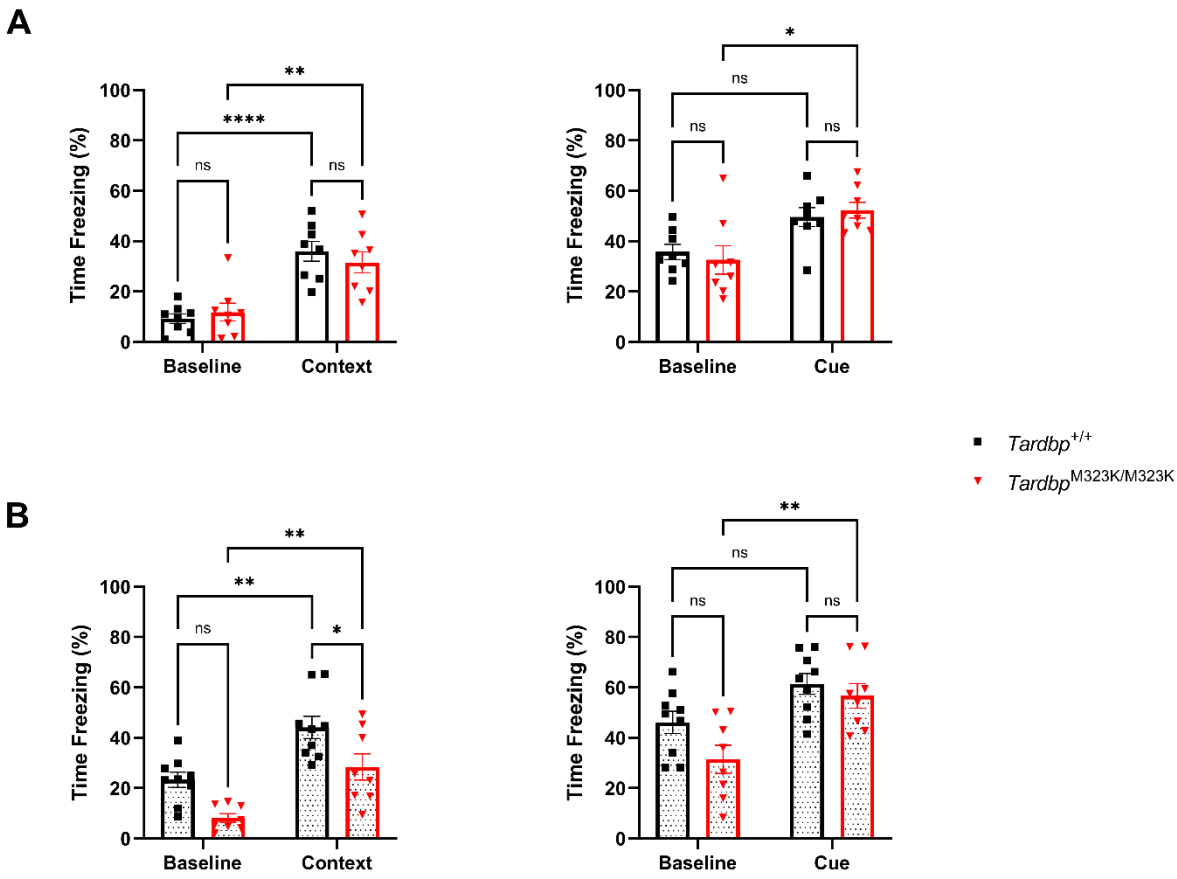


Figure 4.13. Fear conditioning test in female *Tardbp*^{M323K} mice. Graphs show data from 3 (**A**) and 12-months (**B**) (dotted bars). *Tardbp*$^{M323K/M323K}$ mice spent less time freezing in the context test at 12 months of age. Data shown as mean. Error bars denote SEM of data. Data analysed using 2-way ANOVA followed by Sidak's multiple comparisons test to compare between genotypes at each time-point, and between time-points within genotypes. 3-months: n=8 *Tardbp*$^{+/+}$ and n=8 *Tardbp*$^{M323K/M323K}$. 12-months: n=9 *Tardbp*$^{+/+}$ and n=8 *Tardbp*$^{M323K/M323K}$. ns= not significant. *p<0.05. **p<0.01. ****p<0.0001.

At 12 months of age, *Tardbp*$^{M323K/M323K}$ spent less time freezing in the context test, compared to control *Tardbp*$^{+/+}$ mice (p<0.05, **Figure 4.13**). This was not seen at 3-months indicating a late onset phenotype. Mice from all genotypes froze more in the context, compared to baseline, indicating that this test worked. Genotype differences were not reported in the cue test, at both time-points. It should be noted that unlike *Tardbp*$^{M323K/M323K}$ mice, *Tardbp*$^{+/+}$ mice did not show the expected increase in freezing time in the cue test compared to baseline readings. This

suggests that the test did not work in these mice therefore genotype comparisons cannot be made.

4.2.5 Early structural brain alterations in *Tardbp*$^{M323K/M323K}$ mice

The next step was to determine if the *in vivo* behavioural and cognitive deficits observed in *Tardbp*$^{M323K/M323K}$ mice correlated to structural brain changes. Structural MRI scans were conducted to identify brain regions vulnerable to the *Tardbp*^{M323K} mutation. These scans were previously done at 12-months by collaborators (data unavailable). In this study, these scans were repeated at 3-months since cognitive and behavioural deficits were already present at this time-point. Brains from perfused female mice (*Tardbp*$^{+/+}$ and *Tardbp*$^{M323K/M323K}$) were sent to collaborators at the Mouse Imaging Centre (Toronto, Canada) for scanning and analysis.

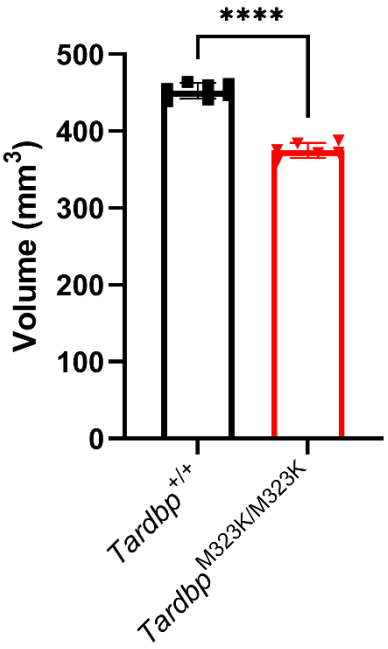


Figure 4.14. Brain volumes of female *Tardbp*^{M323K} mice. Graph shows data from 3-months. *Tardbp*$^{M323K/M323K}$ mice had a reduced brain volume compared to control *Tardbp*$^{+/+}$ littermates. Data shown as mean. Error bars denote SEM of data. Data analysed using unpaired t-test to compare between genotypes. n=7 *Tardbp*$^{+/+}$ and n=6 *Tardbp*$^{M323K/M323K}$. ****p<0.0001.

At 3 months of age, *Tardbp*$^{M323K/M323K}$ mice had a reduced whole brain volume compared to control *Tardbp*$^{+/+}$ littermates ($p<0.0001$, **Figure 4.14**). When directly compared to control mice, significant reduction in absolute volumes were observed in all brain regions of *Tardbp*$^{M323K/M323K}$ mice (**Figure 4.15, Appendix C1**). When volumes relative to the whole brain size were taken into account (global scaling), eighty-nine regions showed statistically significant volume changes between *Tardbp*$^{M323K/M323K}$ and control *Tardbp*$^{+/+}$ mice after multiple comparisons at 5% false discovery rate (FDR) (**Figure 4.16B, Appendix C2**). A mixture of atrophy and hypertrophy were seen in *Tardbp*$^{M323K/M323K}$ mice. Widespread reduction in white matter volumes were detected. The thalamus (subcortical grey matter) displayed reduced volumes. Reduced volumes were also seen in cerebellar regions, like the *flocculus* and *nucleus interpositus*.

Tardbp$^{M323K/M323K}$ mice also displayed significant volume increases in various cerebral brain areas. The hippocampus, cortex and sub-cortical grey matter (nucleus accumbens) showed the most significant volume increases. Volume increases were also seen in other cerebral grey matter regions, like the amygdala and hypothalamus (mammillary bodies). As a whole, the midbrain showed hypertrophy but specific regions (periaqueductal grey) had reduced volumes. The only region in the ventricular system that showed volume differences was the third ventricle (hypertrophy). No volume differences were seen in the brainstem.

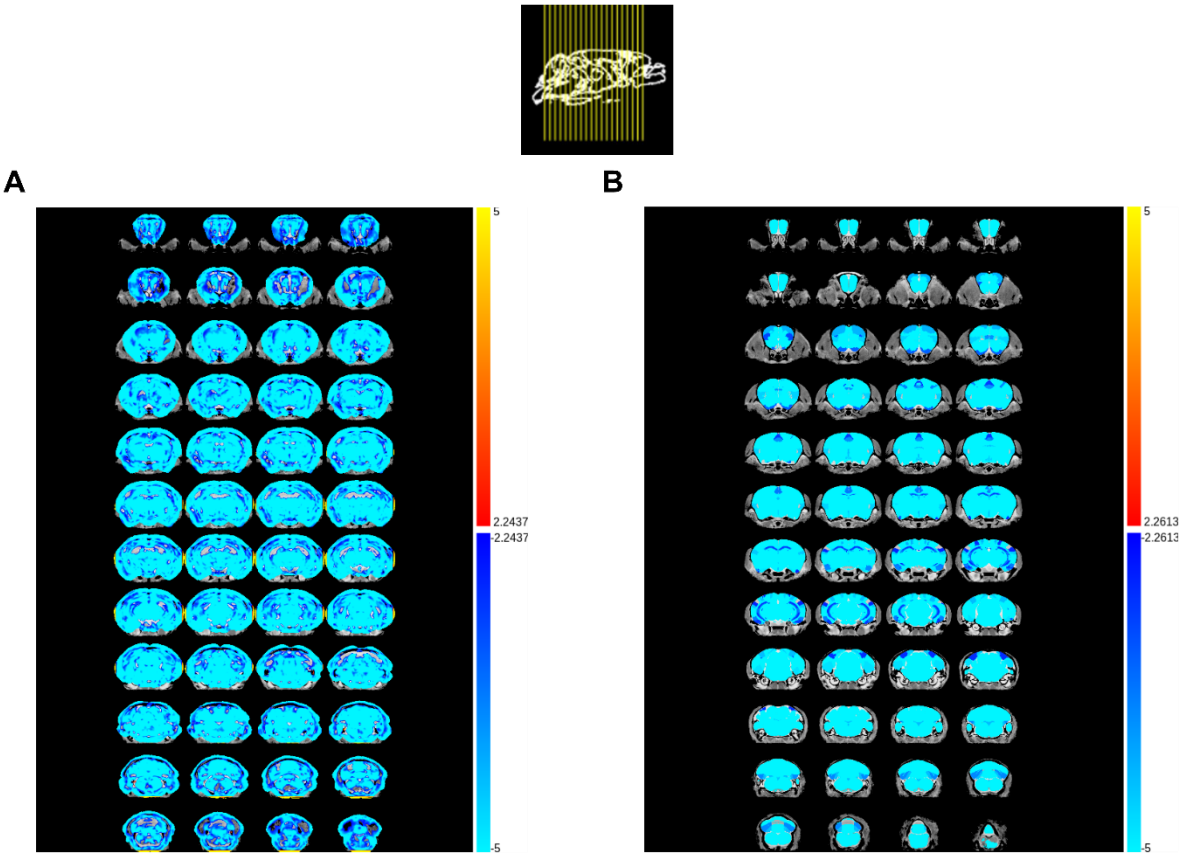


Figure 4.15. Structural MRI scans of female *Tardbp*$^{M323K/M323K}$ mice (absolute changes). Jacobian determinant maps show voxel-wise volume analysis (**A**) and structure-wise volume analysis (**B**) of coronal brain scans from 3-month old female mice. Structure-wise volumes (mm^3) were extracted using the DSURQE mouse brain atlas; this allowed volume comparison of the 182 pre-defined region between the genotype groups. These scans show local volume changes therefore *Tardbp*$^{M323K/M323K}$ volumes were directly compared to *Tardbp*$^{+/+}$ mice. Atrophic regions are shown in blue. Hypertrophic regions are shown in red/yellow. The opacity of the colour indicates statistical significance (the lighter the colour, the more statistically significant). T-statistic used. False discovery rate of 5%. Maps produced by the Mouse Imaging Centre (Toronto, Canada).

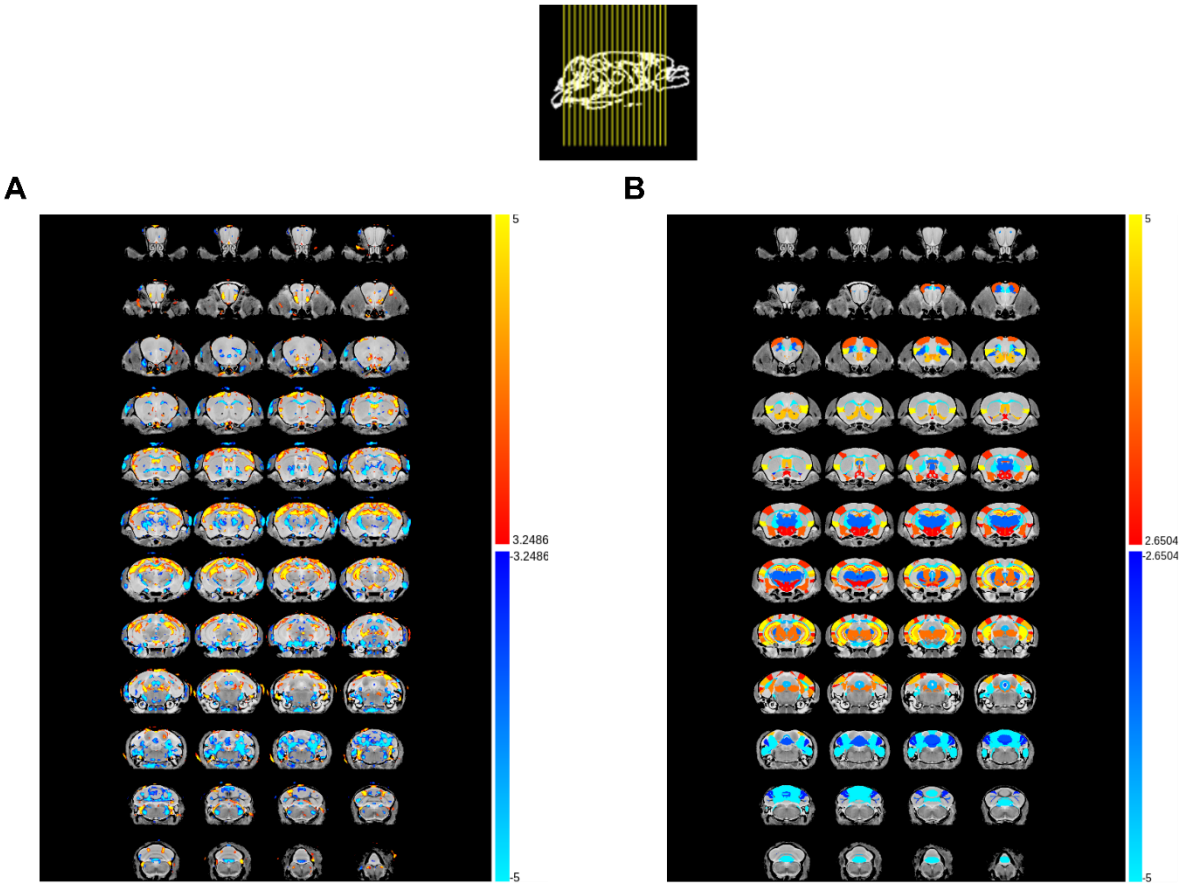


Figure 4.16. Structural MRI scans of female *Tardbp*$^{M323K/M323K}$ mice (relative changes). Jacobian determinant maps show voxel-wise volume analysis (**A**) and structure-wise volume analysis (**B**) of coronal brain scans from 3-month old female mice. Structure-wise volumes (mm^3) were extracted using the DSURQE mouse brain atlas; this allowed volume comparison of the 182 pre-defined region between the genotype groups. *Tardbp*$^{M323K/M323K}$ mice had a reduced brain volume therefore global scaling differences were taken into account to calculate the relative Jacobian determinant. Atrophic regions are shown in blue. Hypertrophic regions are shown in red/yellow. The opacity of the colour indicates statistical significance (the lighter the colour, the more statistically significant). T-statistic used. False discovery rate of 5%. Maps produced by the Mouse Imaging Centre (Toronto, Canada).

4.3 Discussion

This phenotyping pipeline revealed novel cognitive and metabolic effects caused by the *Tardbp*^{M323K} mutation (**Table 4.2**). These new findings, coupled with the motor phenotypes, reintroduces the *Tardbp*^{M323K} mouse as a model of ALS-FTD.

Test		Time-point (months)		Conclusion
		3	12	
Motor	**Grip strength**	N/A	↓	Grip deficits
	Gait analysis	N/A	↕	Altered gait pattern
Neuromuscular	**Muscle physiology**	N/A	−	No neuromuscular changes observed
	Motor neuron counts	N/A	−	
Cognitive	**Nesting**	↓	↓	Early innate behaviour deficits
	Marble burying	↓	↓	
	Light-dark box	−	↓	Late onset anxiety phenotype
	Y-maze	−	−	No change in spatial memory
	3-chamber	N/A	−	No change in sociability
	Fear conditioning	−	↓	Late onset learning and memory deficits
	Structural MRI scans	↕	↕	Early structural brain changes
Metabolic	**Weights**	↑		Increased body weights
	EchoMRI	↑ fat mass	−	Altered body composition
	TSE	−	↑ EE	Progressive hypermetabolism
	Food intake	N/A	−	No hyperphagsia

Table 4.2. Summary of *Tardbp*$^{M323K/M323K}$ phenotypes. Table summaries changes seen in female *Tardbp*$^{M323K/M323K}$ mice, compared to control *Tardbp*$^{+/+}$ mice. N/A means not applicable (test not done), ↑ means an increase, ↓ means a decrease, − means no change and ↕ means multiple parameters are altered in either direction.

4.3.1 Earlier motor phenotypes

This mutation has been shown to cause a late neuromuscular phenotype, coupled with grip strength deficits at 24 months of age in female homozygous mice (Fratta et al., 2018; Oliveira, 2014). This longitudinal study revealed motor deficits at 12 months of age, earlier than previously reported. This points to a progressive motor phenotype in these mice. Gait abnormalities were measured in the Mousewalker test. The hind limb stance phase was shorter than the swing phase meaning that the hind limbs spent more time off the ground, suggesting a limp in these mice. This gait pattern is referred to as an antalgic gait as it is caused by pain (Pirker & Katzenschlager, 2017). It should be noted that these gait abnormalities were subtle and could not be observed when handling the mice.

Despite clear motor phenotypes at 12-months, this was not accompanied by neuromuscular changes. No changes were observed in any of the *in vivo* muscle physiology readings. Additionally, there were no genotype differences in motor neuron counts, although the n numbers were really low. Denervation in neuromuscular junctions (NMJs) are reported in a number of pre-symptomatic ALS mouse models (Fischer et al., 2004). In early disease changes, nerve terminals and motor neuron junctions are significantly degraded, while cells bodies remain intact. This is referred to the ‘dying-back’ theory in ALS literature (Dadon-Nachum et al., 2011). Therefore, motor neurons being unaffected at this time-point fits with this theory. However, differences were expected in the muscle physiology readings, especially in MUNE. It is entirely probable that these *in vivo* readings might not be sensitive enough to pick up early changes in the NMJs. The ‘NMJ-Analyser’ uses machine learning to quantitatively define healthy and aberrant neuromuscular synapses. It was used to analyse the NMJs of *Tardbp*^{M323K}

homozygous mice at 12 months of age. While NMJ denervation did not occur at this time-point, the NMJ analyser was able to detect early structural changes in the pre-synaptic terminals (Mejia Maza et al., 2021).

Structural MRI scans revealed hypertrophy in the cortex, which contrasts clinical data as cortical thinning is normally seen in ALS patients (Verstraete et al., 2012). Cortical thinning, particularly in the precentral gyrus, is associated with the speed of disease progression; patients with more cortical thinning have a faster disease progression (motor symptoms and death) (Agosta et al., 2012). Since motor symptoms are progressive in this model, and are considerably mild at 12 months of ago, it makes sense that cortical thinning is absent at this time-point. Hypertrophy in these regions might reflect early compensatory mechanisms within the motor and extra-motor network, or even developmental effects from the mutation.

4.3.2 Novel behavioural and cognitive deficits

A key part of this project was to determine the role of the *Tardbp*^{M323K} mutation on cognitive processes. As previously mentioned, TDP-43 pathology is seen in conditions with cognitive impairment like ALS, FTD, LATE and CARTS (de Boer et al., 2021). Unsurprisingly, this longitudinal study revealed widespread cognitive deficits in homozygous mice.

Initial observational tests showed early innate behavioural deficits in homozygous mice. The exact function of the marble burying test is controversial, with the previously accepted dogma being that it measures anxiety and obsessive-compulsive disorder. Since burying, burrowing and digging are all normal behaviours in rodents, the marble burying test is actually a measure of mouse wellbeing (Wolmarans de et al., 2016). Nesting is another normal rodent behaviour

used for heat conservation, shelter and reproduction (R. M. J. Deacon, 2006). Deficits in these behaviours also suggests apathy, which is seen in up to 90% of FTD patients (Johnson & Kumfor, 2018). The hippocampus is implicated in both tests; agents that target this region (benzodiazepines and 5-HT active compounds) inhibit burying (R. M. Deacon, 2006), while hippocampal lesions affect rodent nesting behaviours (Deacon et al., 2002). In addition, significant structural hippocampal abnormalities were seen in the MRI scans. Hippocampal pathology has been observed across the ALS-FTD spectrum, in FTD patients (Laakso et al., 2000) and ALS patients with cognitive impairment (Christidi et al., 2018). This data and literature supports the role of TDP-43 in hippocampal processes. TDP-43 immunoreactivity has been detected in a large number of patients with hippocampal sclerosis (Amador-Ortiz et al., 2007). This condition is characterised by significant neuronal cell loss and gliosis in the hippocampus. Epidemiology studies have found that TDP-43 pathology is associated with an increased risk of developing this condition (Nag et al., 2015). It is unclear how the *Tardbp*^{M323K} mutation affects the hippocampus as cytoplasmic TDP-43 inclusions are not yet seen; it is entirely possible that they might develop later as a consequence.

The early onset of innate behaviour deficits indicates that the *Tardbp*^{M323K} mutation causes developmental effects. Coupled with the abnormalities seen in the MRI scans, it is clear that TDP-43 is important for brain structural development and function. The role of TDP-43 in CNS development has been described in literature. TDP-43 is expressed throughout embryonic development at high levels, but progressively decreases during postnatal development (Sephton et al., 2010). Embryonic lethality is observed in TDP-43 KO mice (Sephton et al., 2012). In adult

mice, TDP-43 protein levels are almost undetectable in some peripheral tissues. However, protein levels are sustained in tissues implicated in NDDs like the brain, cerebellum and spinal cord (Huang et al., 2010). Within the brain, TDP-43 is largely present in the hippocampus and cortex. Therefore, *TARDBP* mutations alter the regulation and normal function of TDP-43 in development giving rise to pathological changes, distinct from degeneration. Specific brain regions (e.g., hippocampus and cortex) may be more vulnerable, giving rise to earlier phenotypes.

A number of late cognitive phenotypes were seen in the homozygous mice, such as an anxiety-like phenotype and impaired associative learning and memory. The prevalence of anxiety symptoms increases in ALS patients, before and after disease onset (Zucchi et al., 2019), while executive dysfunction is a key characteristic of FTD (Olney et al., 2017). These later onset deficits support the role of TDP-43 pathology in neurodegenerative processes, as it is already implicated in AD and ageing (Nag et al., 2018). Widespread white atrophy seen in the MRI scans may be responsible for the global cognitive impairment and anxiety seen in these mice (Hirono et al., 2000). However, early changes in cerebral grey matter regions may also underline these phenotypes. The hippocampus and amygdala have been shown to be involved in conditioned fear learning and extinction (Maren, 2008; Maren & Quirk, 2004), and both these regions displayed significant hypertrophy in the structural MRI scans. Due to the delayed onset of this phenotype, hypertrophy in these regions may reflect earlier disease mechanisms that would precede neuronal loss and atrophy, like inflammation (DiSabato et al., 2016; Tan et al., 2012). Structural MRI scans were conducted at 12-months by collaborators (Wellcome Centre for Integrative Neuroimaging,

Oxford). Similar brain structural changes to the 3-month time-point were observed. e.g., reduced brain volume, white matter atrophy and hypertrophy in the hippocampus and cortex. However, age-related analysis needs to be conducted to identify progressive structural changes.

This mutation appears to have specific brain functional effects as not all cognitive processes were disrupted. Homozygous mice displayed normal spatial working memory. This is consistent with clinical FTD cases as this process is relatively spared in patients (Bott et al., 2014); it may appear at a later time-point. No sociability changes were reported but this could be sex-dependent as male homozygous mice are known to be aggressive.

4.3.3 Metabolic alterations

Distinct and overlapping metabolic alterations have been documented in ALS and FTD, with less research being conducted in FTD (Ahmed, Irish, Piguet, et al., 2016). Body mass has been shown to delineate ALS from FTD (Ahmed et al., 2014); ALS patients with some cognitive/behavioural impairments have a high BMI compared to pure-ALS patients, and FTD patients have high BMIs. *Tardbp*^{M323K} homozygous mice appeared to weigh more than their littermate controls. While this trend is not statistically significant, it has been observed in cohorts from other research groups. However, BMI is only based on height and weight. It does not give any information on body composition which is a better indicator of metabolic status. Homozygous mice showed increased fat mass from 3 months of age. The increased body weights and fat stores places the *Tardbp*^{M323K} homozygous mouse towards the FTD region of the spectrum.

Hypermetabolism coincides with the appearance of motor symptoms. In the clinic, hypermetabolism is seen across the ALS-FTD spectrum (Ahmed, Irish, Piguet, et

al., 2016). It is observed in ~40% of ALS patients and is associated with a faster disease progression (Steyn et al., 2018). However, hypermetabolism occurs in patients without alterations in body weight and BMI (Ioannides et al., 2017). It has been suggested that the skeletal muscle is responsible for hypermetabolism (Loeffler et al., 2016). Denervation of muscles have been shown to cause increased oxygen utilisation and overall increased respiratory muscle expenditure in late-stage ALS (Kasarskis et al., 1996). Therefore, the *Tardbp*^{M323K} mutation may increase the energy demand of muscles, contributing to muscle pathology and motor phenotypes. The hypothalamus is responsible for regulating energy balance through humoral and neuronal mechanisms (Tran et al., 2022) and research has shown dysregulation in hypothalamic networks in ALS patients (Gorges et al., 2017) and mouse models (Bayer et al., 2021). Structural MRI scans revealed early hypertrophy in specific regions within this network. Due to the delayed onset of this phenotype, hypothalamus hypertrophy may reflect early disease mechanisms that would precede neuronal loss and atrophy; similar to the late cognitive phenotypes.

4.3.4 Model considerations

4.3.4.1 Face validity

Within animal behavioural science, there are concerns about the validity and interpretation of mouse data. This is due to problems with reproducibility across different research units. Both the experimenter and laboratory environment can have an effect (Nigri et al., 2022). To circumvent this, parts of this study were repeated in different animal units using a standardised approach. This study is part of a wider characterisation project, involving several international animal units. The Corrochano group also identified early innate behaviour deficits (marble

burying) and motor phenotypes (grip strength) in female homozygous mice. Achieving these reproducible results provides future researchers confidence when using this model to understand disease mechanisms or validating novel treatments.

This phenotyping pipeline used female mice to study the effects of the *Tardbp*^{M323K} mutation. Therefore, it was important to determine if this mutation caused sex-differences in the phenotypes. Male homozygous mice also showed early innate behavioural deficits. Unlike females, male homozygous mice weighed significantly less than their littermate controls and this was accompanied by earlier motor phenotypes (grip strength deficit at 6-months versus 12-months in females). This suggests that the *Tardbp*^{M323K} mutation has a more severe effect in male mice, indicating sexual dimorphism. Sex has already been shown to independently influence ALS-FTD development and progression. Males are more susceptible than women to develop the disease and have a worse prognosis (Pape & Grose, 2020; Rooney et al., 2017). Sex-hormonal differences may be contributing factors as oestrogen has been shown to be protective in animal models of ALS (Choi et al., 2008; Groeneveld et al., 2004).

Collaborators were able to conduct additional tests to support this project. The NOR test revealed deficits in spatial working memory, which is seen in late bv-FTD as the prefrontal cortex degenerates (Poos et al., 2018; van Asselen et al., 2006). Homozygous mice showed an increased ‘sweet’ food preference, which mirrors the eating behavioural habits observed in FTD patients (Ahmed, Irish, Henning, et al., 2016).

4.3.4.2 Construct validity

This longitudinal study demonstrated that the *Tardbp*^{M323K} mouse is a good model of ALS-FTD. However, there are some criticisms related to the construct validity of this model that future researchers should know.

While the *Tardbp*^{M323K} mutation is not found in patients, it lies in the LCD region of TDP-43 where the majority of ALS-linked mutations are found (Chien et al., 2021). Additionally, this mutation causes a gain-of-splicing function which is seen in the fibroblasts of patients carrying other LCD *TARDBP* mutations (Fratta et al., 2018). The *Tardbp*^{Q331K} mutation causes a similar splicing GOF effect in mice (White et al., 2018) and this mutation was identified in a patient who developed limb-onset ALS at 72 years of age (Sreedharan et al., 2008).

Another criticism of this model is the absence of traditional TDP-43 pathology. ALS-FTD phenotypes are present in this model without: (i) loss of TDP-43 in the nuclei, (ii) accumulation of TDP-43 aggregates, and (iii) accumulation of insoluble TDP-43. This phenomena has been observed in other *Tardbp* mutation mouse models, transgenic (Arnold et al., 2013) and knock-in (White et al., 2018). This suggests that these processes are not necessary in early disease mechanisms and these *Tardbp* mutations produce ALS-FTD related phenotypes through a different mechanism. Therefore, the *Tardbp*^{M323K} homozygous mouse is well-suited for early disease mechanistic studies.

The *Tardbp*^{M323K} mutation causes a splicing GOF effect on exons that are constitutively included. This causes abnormal skipping of these exons (“skiptic” exons), leading to the downregulation of genes harbouring these skiptic exons (Fratta et al., 2018). About 16% of these downregulated genes are involved in the ubiquitin proteasome pathway, implicating altered CNS proteostasis as a possible

neurodegeneration mechanism (Ling et al., 2013). This mutation also alters the modulation of alternative splicing, which may be responsible for the abnormal autoregulation of TDP-43. TDP-43 can autoregulate its nuclear levels via alternative splicing once it is bound the *Tardbp* pre-mRNA 3'UTR (Koike et al., 2021). The *Tardbp*^{M323K} mutation disturbs normal TDP-43 alterative splicing function. This causes upregulation of *Tardbp* mRNA levels in the spinal cords of homozygous mice throughout life, even though loss of nuclear TDP-43 is not observed (Fratta et al., 2018). While TDP-43 protein levels remained unchanged in most *Tardbp*^{M323K} tissues, upregulation was seen in the frontal cortex of homozygous mice at 12 months of age (unpublished data, Corrochano group). Increased intracellular levels of TDP-43 are known to have direct and indirect toxic effects. Elevated levels in the forebrain can cause FTD neurological problems (Tsai et al., 2010), therefore elevated cortical TDP-43 levels may be directly causing the cognitive phenotypes in *Tardbp*^{M323K} homozygous mice. Elevated intracellular TDP-43 levels can also lead to aggregate formation (Xu et al., 2010), which may occur at a later time-point in *Tardbp*^{M323K} homozygous mice.

4.3.5 Comparison to the *Tardbp*^{Q331K} mouse

There is a need in literature for more physiological ALS-FTD models which recapitulate TDP-43 relevant mechanisms. The main comparable mouse is the knock-in *Tardbp*^{Q331K} mouse. Both mutant lines contain a mutation in the C-terminal LCD of TDP-43 and display a splicing GOF, while expressing mutant proteins at endogenous levels (White et al., 2018).

Tardbp^{Q331K} homozygous mice have increased body weights compared to control littermates. Unlike *Tardbp*^{M323K} mice, this weight gain is speculated to be caused by hyperphagsia. No other metabolic phenotyping tests were conducted in these

mice. Motor phenotypes and NMJ abnormalities were not observed in *Tardbp*^{Q331K} homozygous mice (up to 16-months). Similar to *Tardbp*^{M323K} mice, executive dysfunction and memory impairment were also seen in *Tardbp*^{Q331K} homozygous mice.

Structural MRI scans were also performed on *Tardbp*^{Q331K} homozygous mice at 7 months of age. Atrophy was seen in brain regions implicated in FTD, and these changes correlated to the observed cognitive/behavioural phenotypes (Lin et al., 2021). Both *Tardbp*^{Q331K} and *Tardbp*^{M323K} homozygous mice showed atrophy in white matter, thalamus and cerebellum. *Tardbp*^{Q331K} mice showed ventricular and brainstem atrophy, while volumes in these regions remained unchanged in *Tardbp*^{M323K} mice. A major brain structural difference between these mutant lines is in the hippocampus and cortex. Both mutant lines displayed cognitive/behavioural phenotypes which implicated these brain regions, however opposite volumetric changes were observed. *Tardbp*^{Q331K} mice displayed atrophy in these regions, while *Tardbp*^{M323K} mice displayed hypertrophy. Time-point could be a cause for this difference, however hypertrophy in these regions were still seen at 12-months in *Tardbp*^{M323K} mice. Additionally, cognitive deficits were present in *Tardbp*^{M323K} homozygous mice when the structural MRI scans were conducted so comparisons can be made between the lines. Despite sharing a mutation function, it appears that each mutation affects these brain regions differently to achieve neuronal dysfunction. Like *Tardbp*^{M323K} mice, behavioural phenotypes were also less severe in female *Tardbp*^{Q331K} mice compared to males (Watkins et al., 2020), confirming sexual dimorphism in ALS-FTD related disorders.

The *Tardbp*^{Q331K} mouse displayed cognitive/behavioural phenotypes that were accompanied by structural brain changes. The lack of motor and neuromuscular phenotypes, even at a later time-point, suggests that this mouse is a model of FTD-like phenotypes. The *Tardbp*^{M323K} mutation is more severe as it causes a range of motor, cognitive/behavioural and metabolic effects that is reflective of ALS-FTD.

4.3.6 Conclusion

The *Tardbp*^{M323K} mutation produces systemic effects (**Figure 4.17**). The phenotyping pipeline revealed novel cognitive/behavioural effects, as well as metabolic alterations. The early presentation of some cognitive/behavioural effects suggest that the mutation affects developmental processes. The phenotypes observed in this mouse correlated to the clinical symptoms seen across the ALS-FTD spectrum. As a result, the *Tardbp*^{M323K} mouse is a novel ALS-FTD model which recapitulates TDP-43 mechanisms. This model can be used to understand ALS-FTD disease pathomechanisms, as well as a tool to test new therapeutics. The validation of this model meant that it was used to investigate the effect of diet-induced metabolic changes in modulating motor and cognitive phenotypes in the ALS-FTD spectrum (next chapter).

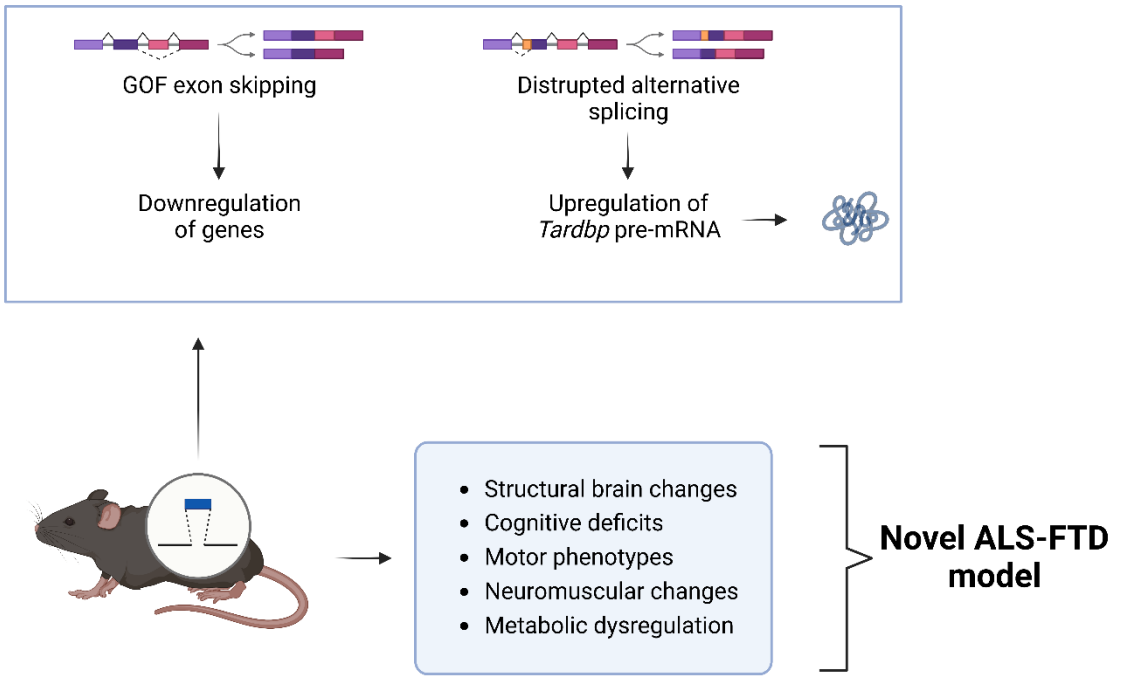


Figure 4.17. The knock-in *Tardbp*^{M323K} mouse is a novel ALS-FTD model. Previous characterisation of homozygous mice revealed that this mutation affects splicing. It causes a splicing gain-of-function effect on exons that are constitutively included, leading to abnormal skipping of these exons ("skiptic" exons).This causes downregulation of 44 genes, which are mainly involved in the ubiquitin proteasome pathway. This mutation also affects alternative splicing, leading to dysregulation of TDP-43 autoregulation. This causes upregulation of *Tardbp* pre-mRNA in the spinal cords of homozygous mice throughout life (Fratta et al., 2018). While TDP-43 levels are unaltered in most tissues at 12 months of age, it is possible that protein levels may increase as the disease progress, causing direct TDP-43 toxic effects or protein aggregation. The molecular effects of the mutation may be responsible for the systemic phenotypes observed in homozygous mice. Structural MRI scans revealed early brain abnormalities, which correlated to behavioural and cognitive deficits. This points to a developmental effect of the *Tardbp*^{M323K} mutation. Some cognitive deficits were present at a later time-point. Homozygous mice also displayed a mid-late motor phenotype, coupled with subtle neuromuscular changes (Mejia Maza et al., 2021). At a later time-point, there was evidence of hypermetabolism and an increased sweet food preference. These systemic phenotypes correlate to clinical symptoms seen in the ALS-FTD cases. Figure created using BioRender.com.

Results III

Shifting ALS-FTD spectrum phenotypes using diet

5 Shifting ALS-FTD spectrum phenotypes using diet

5.1 Introduction

Observational studies have shown that in NDDs with cognitive and behavioural symptoms, such as Alzheimer's disease and FTD, patients often display increased body weights (Emmerzaal et al., 2015). Conversely patients with NDDs that mainly affect motor function, like Huntington's disease and ALS, display weight loss (Ashrafian et al., 2013). These differences in body weights are evident in the ALS-FTD spectrum disorders, where weight may delineate the clinical forms within the spectrum. Studies have found that the majority of limb and bulbar onset ALS patients have a normal weight or underweight. However, ALS patients with cognitive impairments or FTD are frequently overweight or obese (Ahmed et al., 2014). Such alterations in body weight have been considered as the consequence of disease, but recent studies support the hypothesis that weight/BMI may influence the clinical presentations of these disorders. Therefore, BMI may also be a good indicator of disease prognosis and could help delineate the metabolic profile across ALS-FTD spectrum diseases.

Weight, adiposity and metabolic alterations are observed across the ALS-FTD spectrum (Ahmed, Irish, Piguet, et al., 2016; Juan Miguel Godoy-Corchuelo et al., 2022). These parameters have been shown to influence disease processes, with distinct and overlapping alterations. This information can help in the stratification of patients in clinical trials, thus enabling more personalised and effective treatments. However, the causal association of weight with clinical symptoms is not clear. This chapter aims to explore the hypothesis that metabolic status can

influence clinical outcomes within the ALS-FTD spectrum. Patients could potentially modify their disease phenotype, as well as progression, using environmental factors, namely diet. Diet has been shown to have a direct effect on systemic and neuronal metabolism (Gómez-Pinilla, 2008). The specific hypothesis is that diet will modify general metabolism like weight and body composition, and that will induce phenotypic sifts in the *Tardbp*^{M323K} homozygous mouse. Specifically, a HFD will exacerbate cognitive phenotypes through changes in metabolic status (compared to standard chow diet, or a control low fat diet) and possibly ameliorate motor phenotypes.

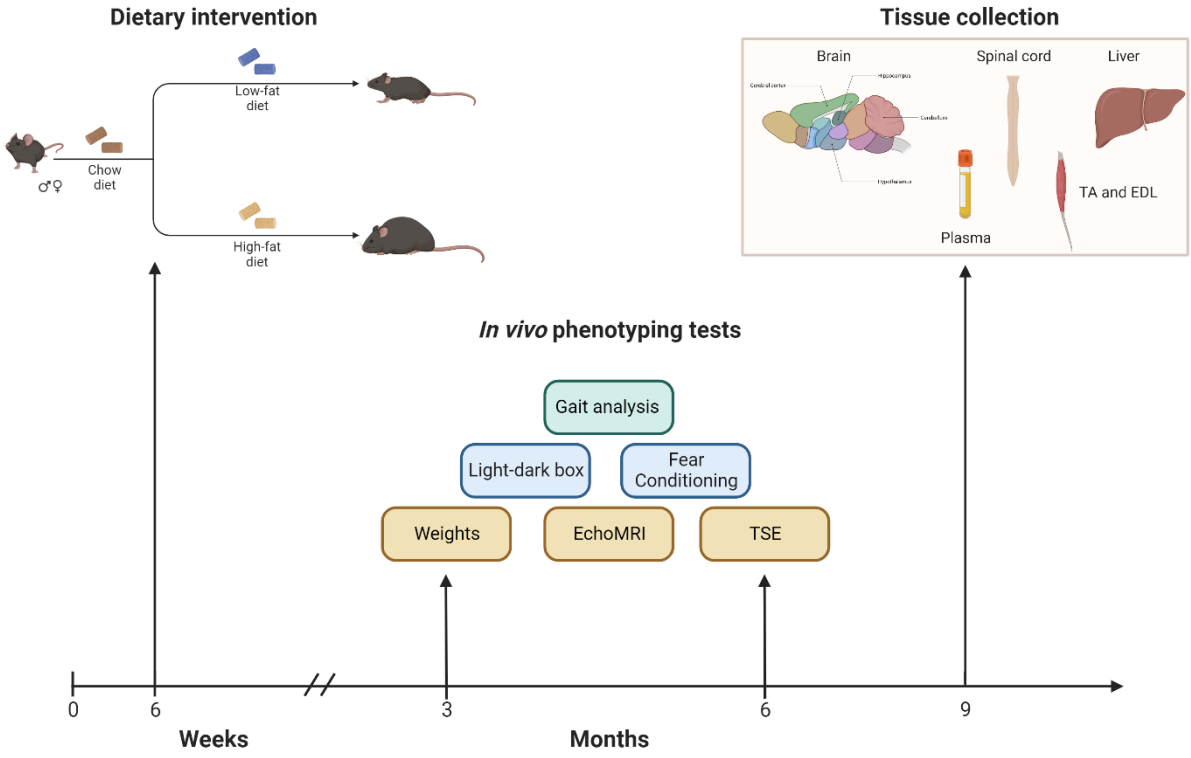


Figure 5.1. Diet study pipeline. Mice were fed standard chow diet till 6 weeks of age to avoid diet-related developmental problems. Wild-type (*Tardbp*$^{+/+}$) and homozygous (*Tardbp*$^{M323K/M323K}$) mice were randomly allocated into 2 different diet groups: low-fat (10% fat) or high-fat (45% fat), each matched with 17% sucrose. In total, there were 4 groups for each sex. Based on power calculations, each group had a sample size of ~12. At 3 and 6-months, mice underwent *in vivo* phenotyping testing (metabolic, motor and cognitive). At 9-months, mice were sacrificed and a range of tissues were collected for future molecular work. Figure created using BioRender.com.

The *Tardbp*^{M323K} mouse was selected because it is a physiological model that presents both motor and cognitive phenotypes. The potential modulatory effects of metabolic changes, induced by HFD, on cognitive and motor phenotypes was investigated in *Tardbp*^{M323K} homozygous mice. The LFD was used as a control, with 10% of calories from fat. The HFD used in this study had 45% of the calories from fat, unlike the classical 60% fat, to avoid morbid obesity in the mice. The diets were administered, *ad libitum*, from 6 weeks of age. This time-point was early enough to identify initial phenotypes but still allowed for normal nervous system development. Metabolic, motor and cognitive phenotypes were studied using a range of *in vivo* behavioural tests at an early and late time-point (**Figure 5.1**). Both male and female *Tardbp*^{M323K} mice were used in this diet study, which was important as previous characterisation of the *Tardbp*^{M323K} homozygous mouse revealed sexual dimorphism.

5.2 Results

5.2.1 Diet effects on mutation-driven metabolic phenotypes

5.2.1.1 Body weight

Mice were weighed weekly to monitor the effect of diets on disease progression. Body weights were collected longitudinally, starting from diet intervention (6-weeks), and analysed using 2-way ANOVA mixed-effects analysis and Bonferroni correction of multiple testing to evaluate genotype differences within each diet group.

Males:

There was little variation in male body weights between the groups, except for *Tardbp*$^{+/+}$ mice in the HFD group (**Figure 5.2**). These mice weighed more than mice in the other groups from 18-weeks, and this was statistically significant when directly compared to male *Tardbp*$^{M323K/M323K}$ on HFD ($p<0.05$ from 22-weeks, **Table 5.1**). At 12 and 16-weeks, *Tardbp*$^{M323K/M323K}$ mice in the LFD group weighed more than *Tardbp*$^{+/+}$ mice. However, there were no genotype weight differences in the LFD group at any other time-point.

Females:

Opposite weight trends were seen in female mice. Firstly, all mice in the HFD group weighed more than mice on the LFD, regardless of genotype (**Figure 5.3**). Secondly, female *Tardbp*$^{M323K/M323K}$ mice in both diet groups weighed significantly more than control *Tardbp*$^{+/+}$ littermates. From 22-weeks, *Tardbp*$^{M323K/M323K}$ mice in the LFD group consistently weighed more than controls ($p<0.05$, **Table 5.2**). *Tardbp*$^{M323K/M323K}$ mice in the HFD group weighed significantly more than controls

from the start of the experiment ($p<0.05$) but by 36-weeks, no weight differences were seen between the genotypes.

♂

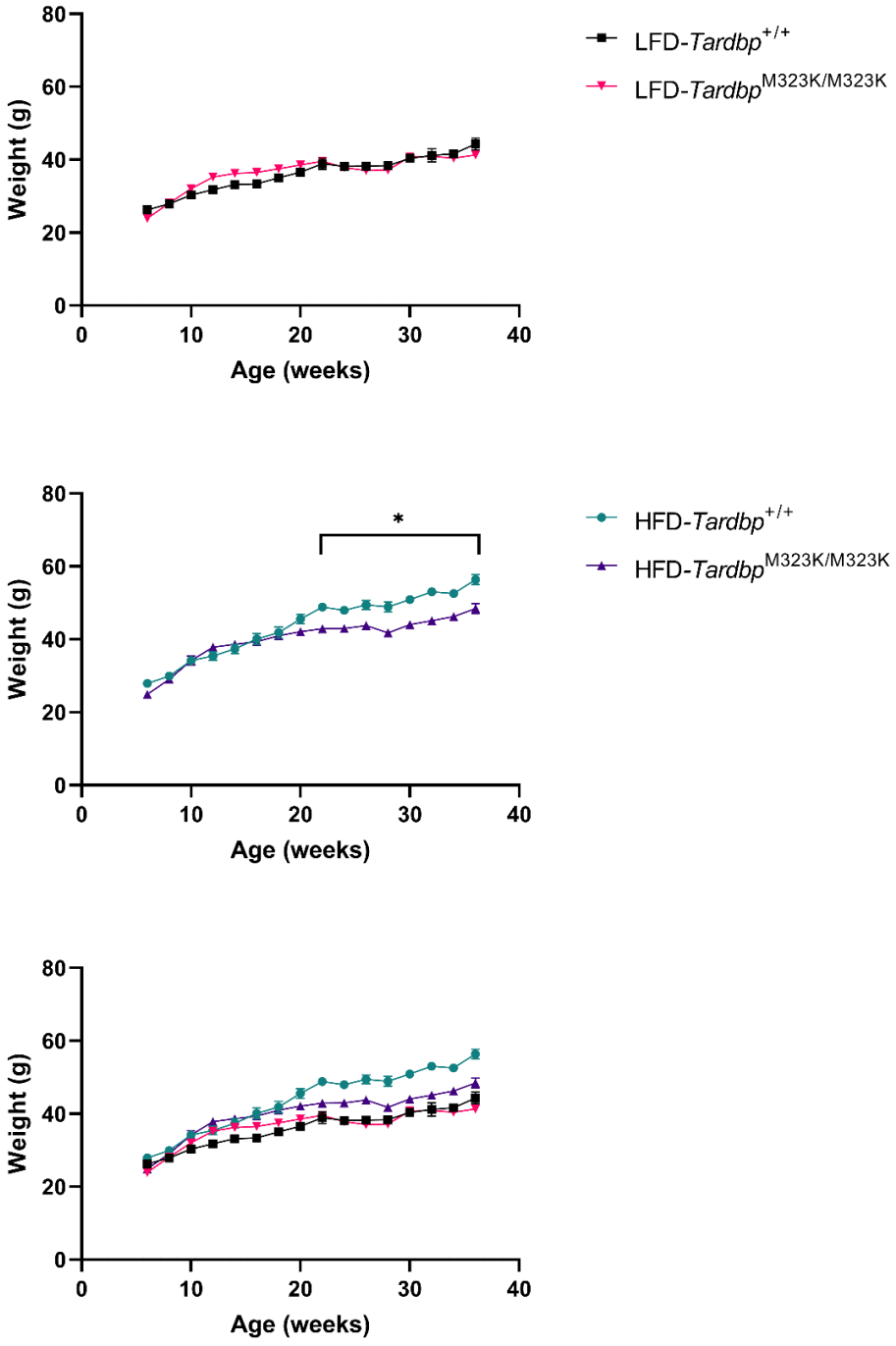


Figure 5.2. Body weights of male *Tardbp*^{M323K} mice in diet study. Graphs showing weekly weights of male *Tardbp*$^{+/+}$ and *Tardbp*$^{M323K/M323K}$ mice in low-fat diet (LFD) and high-fat diet (HFD) groups. No significant changes reported between genotypes of mice in the LFD group. *Tardbp*$^{+/+}$ mice in the HFD group weighed more than *Tardbp*$^{M323K/M323K}$ from 22-weeks. Data shown as mean. Error bars denote SEM of data. Data analysed using 2-way ANOVA mixed-effects analysis and Bonferroni correction of multiple testing to evaluate genotype differences within each diet group. N numbers for each time-point can be found in **Table 5.1**. *p<0.05.

Males LFD							
Age (weeks)	**Genotype**						**Adjusted p-value**
	***Tardbp*$^{+/+}$**			***Tardbp*$^{M323K/M323K}$**			
	Mean weight (grams)	**SEM**	**n**	**Mean weight (grams)**	**SEM**	***n***	
6	26.26	0.37	10	23.88	0.51	12	0.44110
8	27.88	0.43	11	28.10	0.69	13	>0.9999
10	30.30	0.73	7	32.04	0.86	13	0.81690
12	31.78	0.70	11	35.24	0.67	13	**0.01350**
14	33.17	0.68	11	36.22	0.35	13	0.05000
16	33.33	0.79	11	36.53	0.44	13	**0.03230**
18	35.01	1.00	11	37.49	0.63	13	0.25770
20	36.55	1.06	11	38.55	0.47	13	0.83300
22	38.87	1.56	7	39.54	0.38	13	>0.9999
24	38.19	0.87	11	37.82	0.60	13	>0.9999
26	38.26	1.05	11	37.05	0.69	13	>0.9999
28	38.38	0.89	11	37.13	0.49	13	>0.9999
30	40.39	1.01	11	40.75	0.53	13	>0.9999
32	41.18	1.80	6	40.90	0.54	13	>0.9999
34	41.65	1.09	10	40.42	0.59	12	>0.9999
36	44.31	1.61	6	41.33	0.76	12	0.23750

Males HFD							
Age (weeks)	**Genotype**						**Adjusted p-value**
	***Tardbp*$^{+/+}$**			***Tardbp*$^{M323K/M323K}$**			
	Mean weight (grams)	**SEM**	**n**	**Mean weight (grams)**	**SEM**	***n***	
6	27.87	0.72	11	24.91	0.67	9	0.13970
8	29.92	0.80	11	29.02	0.89	12	>0.9999
10	34.17	1.10	8	34.18	1.19	11	>0.9999
12	35.47	1.22	11	37.81	0.96	12	>0.9999
14	37.38	1.28	11	38.65	0.62	12	>0.9999
16	40.07	1.52	11	39.37	0.76	12	>0.9999
18	41.86	1.55	11	40.94	0.47	12	>0.9999
20	45.54	1.37	11	42.13	0.57	12	0.19810
22	48.83	0.62	8	42.91	0.54	11	**0.03120**
24	47.97	0.90	11	42.94	0.58	12	**0.00390**
26	49.42	1.22	11	43.79	0.63	12	**0.00070**
28	48.87	1.34	11	41.80	0.67	12	**<0.0001**
30	50.88	1.00	11	44.06	0.52	10	**<0.0001**
32	53.04	1.03	8	45.10	0.53	9	**0.00020**
34	52.54	1.06	11	46.20	0.64	10	**0.00010**
36	56.39	1.36	8	48.44	1.34	8	**0.00020**

Table 5.1. Mean body weights of male *Tardbp*^{M323K} mice in diet study and statistical analysis. Tables showing mean weights, SEM, n numbers and adjusted p-values of male *Tardbp*$^{+/+}$ and *Tardbp*$^{M323K/M323K}$ mice in low-fat diet (LFD) and high-fat diet (HFD) groups. Adjusted p-values in bold red indicate statistical significance.

♀

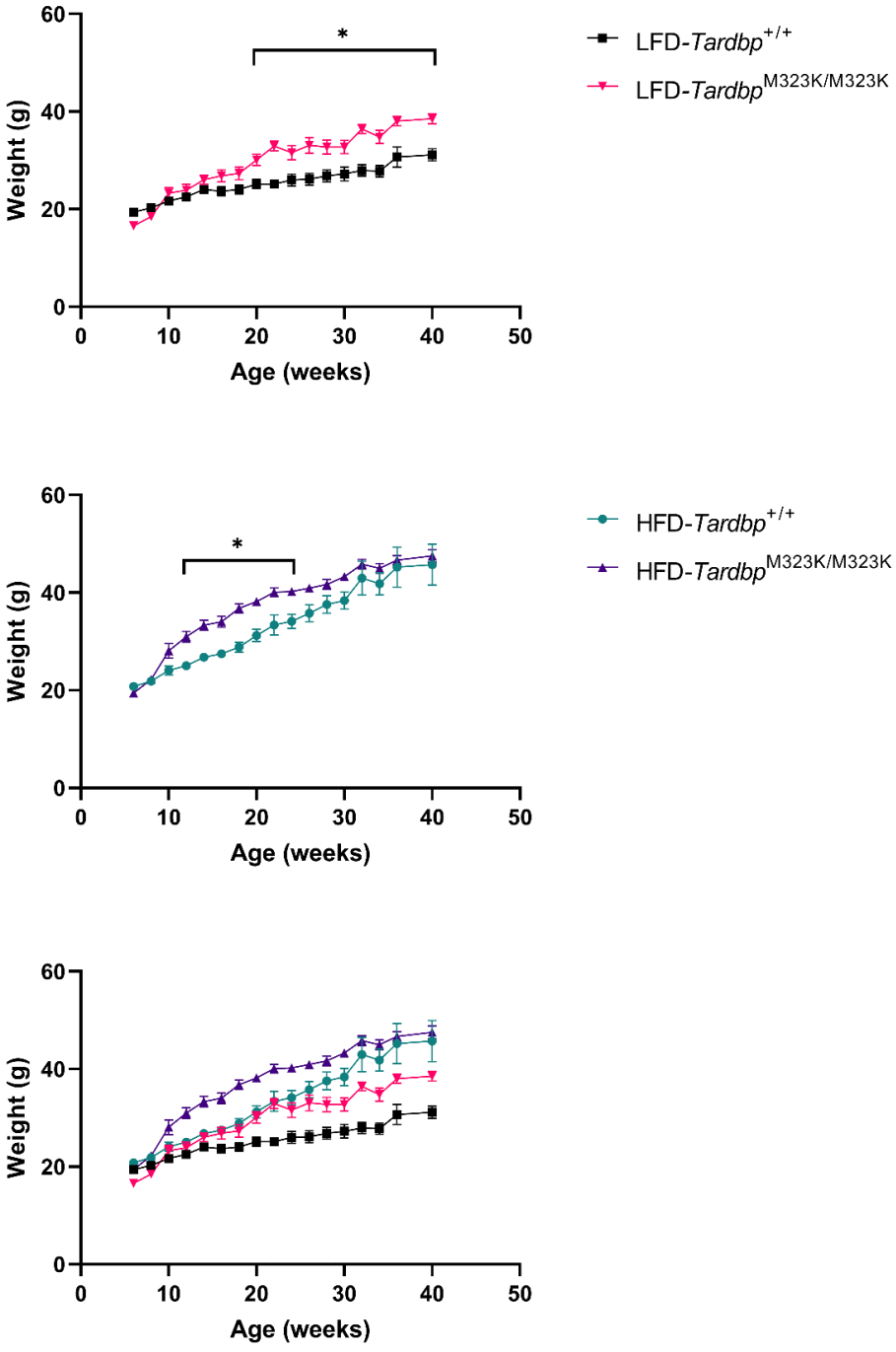


Figure 5.3. Body weights of female *Tardbp*^{M323K} mice in diet study. Graphs showing weekly weights of female *Tardbp*$^{+/+}$ and *Tardbp*$^{M323K/M323K}$ mice in low-fat diet (LFD) and high-fat diet (HFD) groups. All mice in the HFD group weighed more than mice in the LFD group. *Tardbp*$^{M323K/M323K}$ mice in both diet groups weighed more than littermate controls. Data shown as mean. Error bars denote SEM of data. Data analysed using 2-way ANOVA mixed-effects analysis and Bonferroni correction of multiple testing to evaluate genotype differences within each diet group. N numbers for each time-point can be found in **Table 5.2**. *p<0.05.

Females LFD							
Age (weeks)	Genotype						Adjusted p-value
	Tardbp$^{+/+}$			*Tardbp*$^{M323K/M323K}$			
	Mean weight (grams)	SEM	n	Mean weight (grams)	SEM	*n*	
6	19.37	0.39	11	16.56	0.41	11	>0.9999
8	20.28	0.43	11	18.47	0.52	11	>0.9999
10	21.70	0.73	4	23.27	1.13	6	>0.9999
12	22.53	0.63	11	23.85	1.22	11	>0.9999
14	24.05	0.86	11	26.03	0.90	11	>0.9999
16	23.66	0.92	11	26.82	1.22	11	0.77160
18	24.02	0.91	11	27.34	1.30	11	0.60130
20	25.10	0.99	11	30.07	1.15	11	**0.02910**
22	25.13	0.81	4	32.92	1.02	6	**0.00580**
24	25.99	1.19	11	31.59	1.48	11	**0.00700**
26	26.13	1.19	11	33.08	1.59	11	**0.00020**
28	26.83	1.19	11	32.71	1.48	11	**0.00370**
30	27.24	1.40	11	32.74	1.39	11	**0.00890**
32	27.91	1.19	4	36.43	0.88	6	**0.00110**
34	27.75	1.17	11	34.77	1.37	11	**0.00020**
36	30.68	2.03	4	38.04	0.95	6	**0.01400**
40	31.14	1.25	4	38.55	1.02	6	**0.01270**

Females HFD							
Age (weeks)	Genotype						Adjusted p-value
	Tardbp$^{+/+}$			*Tardbp*$^{M323K/M323K}$			
	Mean weight (grams)	SEM	n	Mean weight (grams)	SEM	*n*	
6	20.78	0.47	11	19.45	0.70	11	>0.9999
8	21.88	0.48	11	22.22	0.71	11	>0.9999
10	24.06	0.89	6	28.08	1.48	7	0.68850
12	25.03	0.75	11	30.99	1.11	11	**0.01240**
14	26.76	0.58	11	33.33	1.04	11	**0.00350**
16	27.49	0.79	11	34.01	1.10	11	**0.00390**
18	28.81	0.99	11	36.77	0.94	11	**0.00010**
20	31.22	1.27	11	38.19	0.79	11	**0.00140**
22	33.38	2.04	6	40.07	0.88	7	**0.01080**
24	34.10	1.46	11	40.24	0.69	11	**0.00880**
26	35.80	1.73	11	40.94	0.84	11	0.05980
28	37.55	1.83	11	41.67	0.99	11	0.32420
30	38.38	1.75	11	43.25	0.88	11	0.09560
32	42.99	3.51	5	45.81	1.00	7	0.97460
34	41.82	2.27	11	44.97	0.99	11	>0.9999
36	45.22	4.12	6	46.67	0.95	7	>0.9999
40	45.72	4.19	6	47.51	1.30	6	>0.9999

Table 5.2. Mean body weights of female Tardbp^{M323K} mice in diet study and statistical analysis. Tables showing mean weights, SEM, n numbers and adjusted p-values of female

Tardbp$^{+/+}$ and *Tardbp*$^{M323K/M323K}$ mice in low-fat diet (LFD) and high-fat diet (HFD) groups. Adjusted p-values in bold red indicate statistical significance.

5.2.1.2 Body composition

The next step was to determine if the observed weight differences between genotypes and diets correlated with differences in body composition. Body composition was assessed by EchoMRI at 3 and 6 months. For each diet group, data was analysed using 2-way ANOVA followed by Tukey's multiple comparisons test to compare between genotypes in each time-point, and between time-points within genotypes.

Males:

Male *Tardbp*$^{M323K/M323K}$ mice in the LFD group had significantly increased fat mass at 3 months of age ($p<0.0001$, **Figure 5.4A**) compared to control *Tardbp*$^{+/+}$ littermates. *Tardbp*$^{M323K/M323K}$ mice in this group also had a slightly reduced lean mass at 3-months ($p<0.0001$). However, these body composition differences were no longer evident by 6 months of age.

Despite male *Tardbp*$^{M323K/M323K}$ mice in the HFD group weighing less than control littermates by 22-weeks, no changes in body composition were seen any time-point.

In both diet groups, male *Tardbp*$^{+/+}$ mice displayed normal increases in fat mass and decreases in lean mass over time (as seen in ageing *Tardbp*^{M323K} mice on a standard chow diet, results chapter 2). This expected trend was not seen in *Tardbp*$^{M323K/M323K}$ mice.

Females:

In both diet groups, *Tardbp*$^{M323K/M323K}$ mice had significantly increased fat mass than control *Tardbp*$^{+/+}$ littermates. These differences were seen at 3 and 6-months (**Figure 5.5**). *Tardbp*$^{M323K/M323K}$ mice in both diet groups also had significantly less lean mass at 3 months of age. While the trend was still present in these mice at 6-months, it was statistically significant only in *Tardbp*$^{M323K/M323K}$ mice in the HFD group ($p<0.0001$, **Figure 5.4A**).

Only *Tardbp*$^{M323K/M323K}$ mice on the LFD and *Tardbp*$^{+/+}$ on the HFD displayed normal increases in fat mass and decreases in lean mass over time.

♂

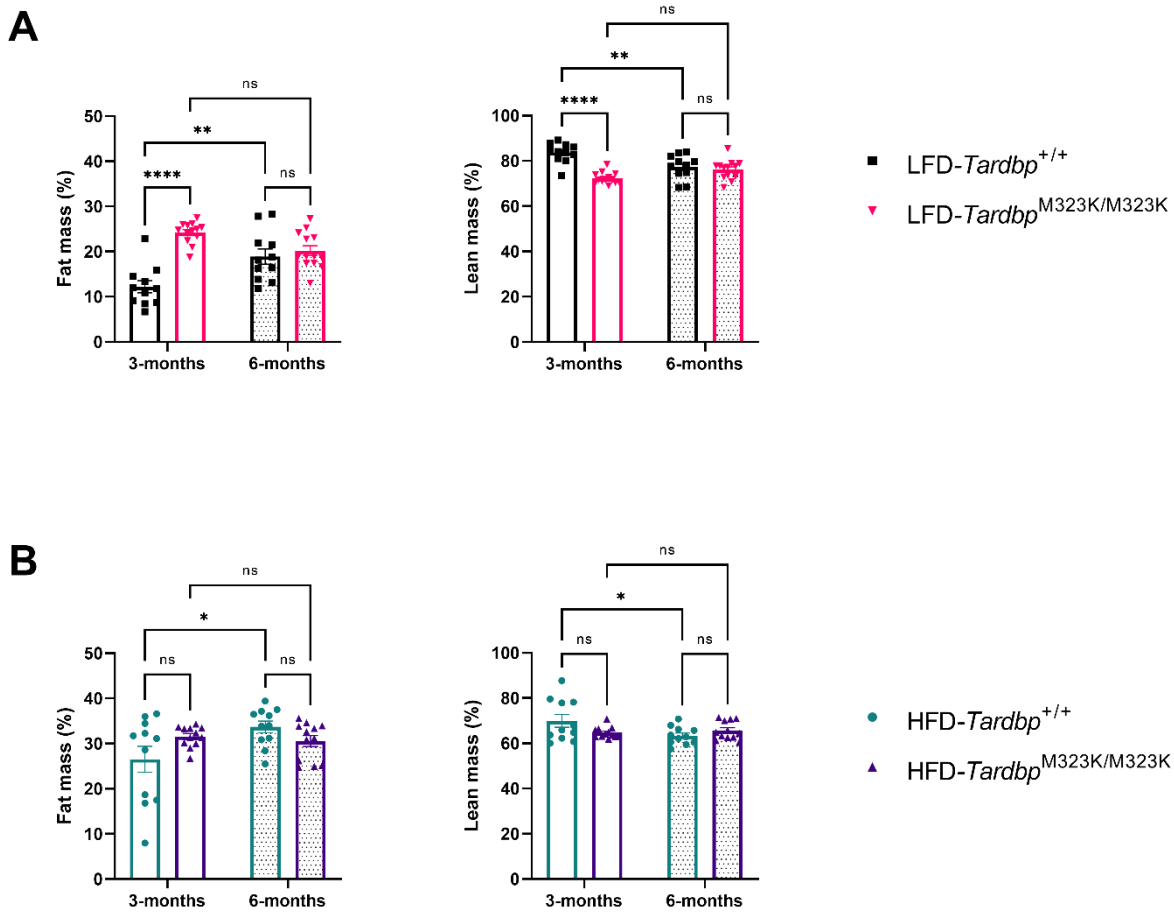


Figure 5.4. Body composition of male *Tardbp*^{M323K} mice in diet study. Graphs show data from male mice in the low-fat (**A**) and high-fat diet group (**B**) at 3 and 6-months. *Tardbp*$^{M323K/M323K}$ mice in the LFD group had increased fat mass at 3 months of age, compared to control littermates. They also had reduced lean mass at this time-point. No genotypes differences in the HFD group. All *Tardbp*$^{+/+}$ mice showed increased fat mass and reduced lean mass over time. Fat and lean mass corrected for individual animal's weight. Data shown as mean. Error bars denote SEM of data. Dotted bars indicate the 6-month time-point. Data analysed using 2-way ANOVA followed by Tukey's multiple comparisons test to compare between genotypes in each time-point, and between time-points within genotypes. LFD: n=11 *Tardbp*$^{+/+}$ and n=13 *Tardbp*$^{M323K/M323K}$. HFD: n= 11 *Tardbp*$^{+/+}$ and n=12 *Tardbp*$^{M323K/M323K}$. ns= not significant. *p<0.05. **p<0.01. ***p<0.001. ***p<0.0001.

♀

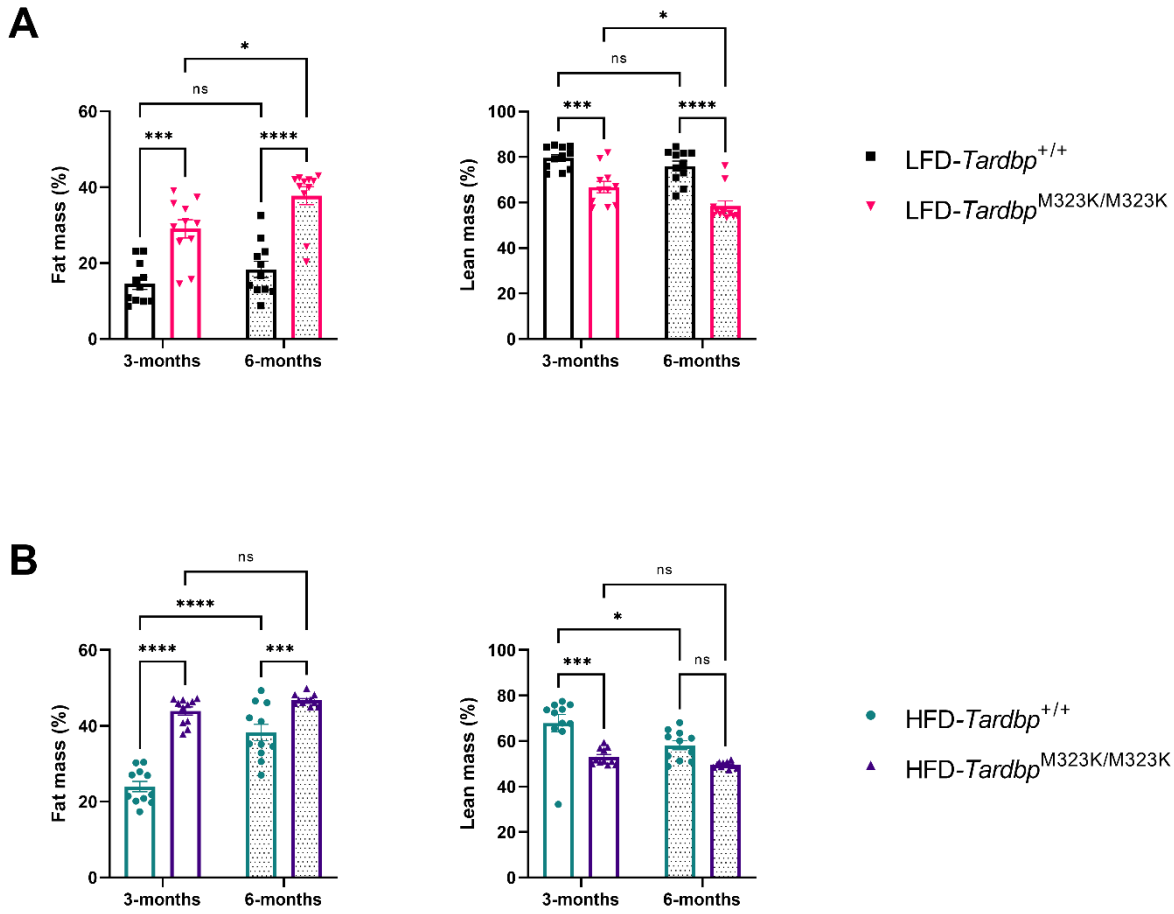


Figure 5.5. Body composition of female *Tardbp*^{M323K} mice in diet study. Graphs show data from female mice in the low-fat (**A**) and high-fat diet group (**B**) at 3 and 6-months. *Tardbp*$^{M323K/M323K}$ mice in both diet groups showed increased fat mass and reduced lean mass from 3 months of age. Fat and lean mass corrected for individual animal's weight. Data shown as mean. Error bars denote SEM of data. Dotted bars indicate the 6-month time-point. Data analysed using 2-way ANOVA followed by Tukey's multiple comparisons test to compare between genotypes at each time-point, and between time-points within genotypes. LFD: n=11 *Tardbp*$^{+/+}$ and n=11 *Tardbp*$^{M323K/M323K}$. HFD: n= 11 *Tardbp*$^{+/+}$ and n=11 *Tardbp*$^{M323K/M323K}$. ns= not significant. *p<0.05. **p<0.01. ***p<0.001. ***p<0.0001.

5.2.1.3 Indirect calorimetry

Indirect calorimetry was performed to determine if diet affected energy expenditure EE and RER. EE is an indicator of whole-body metabolism, while RER gives information on fuel preference. Mice were placed in a metabolic cage and the amount of oxygen used and carbon dioxide released by the body was measured to determine EE and RER. EE measurements were corrected by lean mass using 2-way ANCOVA to give adjusted mean EE values. Diurnal differences meant that all parameters were separated into dark (6pm- 6am) and light (12- 5pm and 7-10am) phases. For each time-point and phase, data was analysed using 2-way ANOVA followed by Tukey's multiple comparisons test to compare between genotypes in each time-point, and between time-points within genotypes.

Males:

In both diet groups, male *Tardbp*$^{M323K/M323K}$ mice displayed elevated EE rates in the dark phase at 3 months of age, compared to control *Tardbp*$^{+/+}$ littermates (**Figure 5.6**). However, only *Tardbp*$^{M323K/M323K}$ mice in the HFD group continued to show elevated EE rates in the dark phase at 6-months ($p<0.01$, **Figure 5.6A**). Elevated EE rates point to hypermetabolism. No genotype differences in the light EE rates were observed in either diet groups. Male *Tardbp*$^{+/+}$ mice in the LFD group showed increased EE rates over time (light and dark phase). No changes were observed over time in *Tardbp*$^{M323K/M323K}$ mice from the LFD group. No changes were observed over time within any of the genotypes in the HFD group.

Tardbp$^{M323K/M323K}$ mice in the LFD group had significantly lower RER in the light phase compared to *Tardbp*$^{+/+}$ mice at 3 months of age ($p<0.05$, **Figure 5.6A**), indicating a fat fuel preference. This was not seen at 6-months or in the dark phase. No RER genotype differences were seen in male mice in the HFD group.

Only *Tardbp*$^{M323K/M323K}$ mice in the LFD group showed increased light and dark RER over time. Both genotypes in the HFD group showed increased RER over time, but only in the light phase.

.

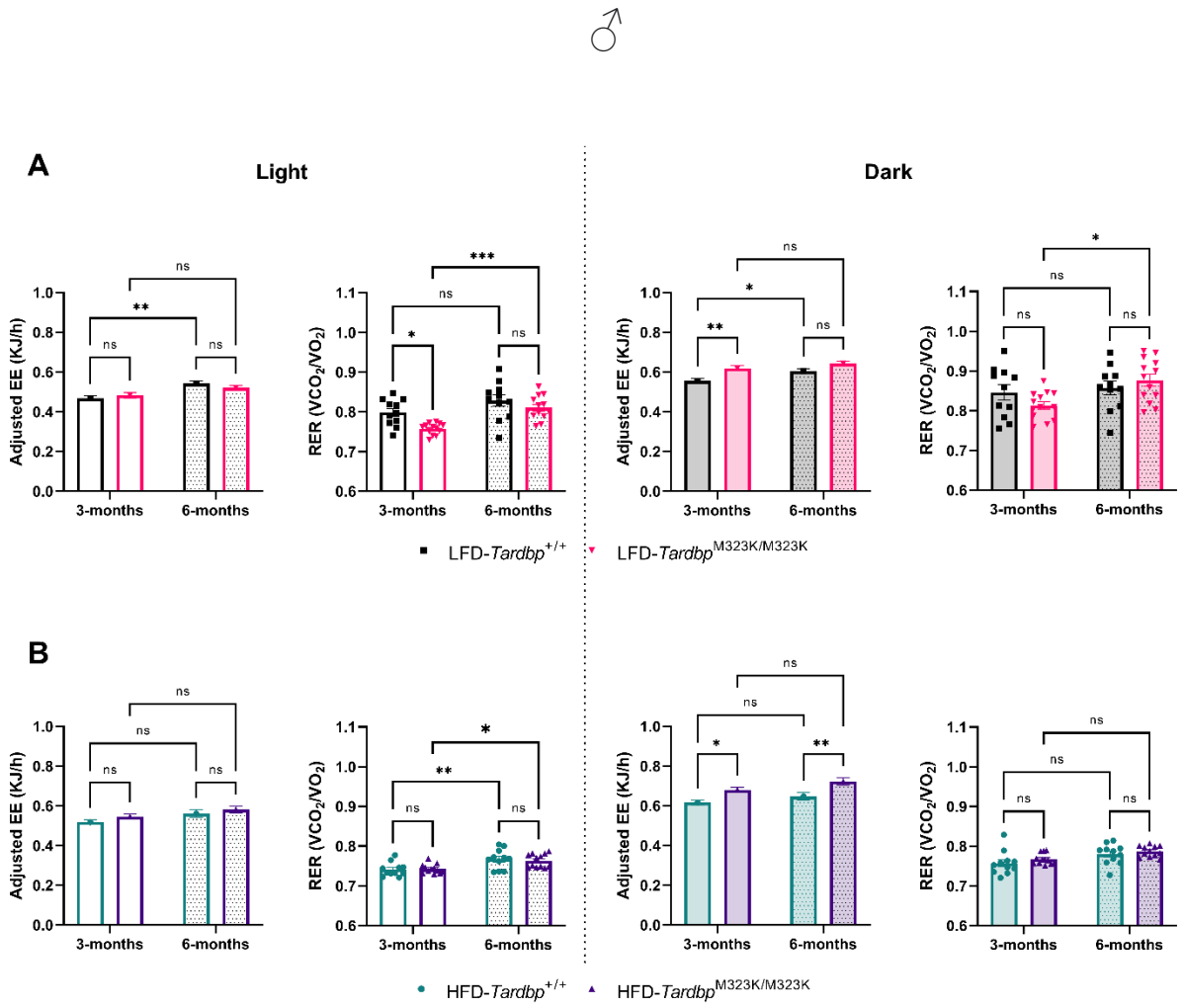


Figure 5.6. Indirect calorimetry analysis of male *Tardbp*^{M323K} mice in diet study. Graphs show energy expenditure (EE) and respiratory exchange ratio (RER) measurements from male mice in the low-fat (A) and high-fat diet group (B) at 3 and 6-months. *Tardbp*$^{M323K/M323K}$ mice had elevated dark EE rates at both time-points in the HFD group, but only at 3-months in the LFD group. *Tardbp*$^{M323K/M323K}$ mice in the LFD group had reduced light RER at 3 months of age.

EE corrected by lean mass using 2-way ANCOVA to give an adjusted EE mean value. Parameters are separated by time (light and dark). Dark (graphs with shaded bars): 6pm- 6am. Light (graphs with white bars): 12- 5pm and 7- 10am. Data shown as mean. Error bars denote SEM of data. Dotted bars indicate the 6-month time-point. Data analysed using 2-way ANOVA followed by Tukey's multiple comparisons test to compare between genotypes in each diet group, and between diet groups within genotypes. LFD: n=11 *Tardbp*$^{+/+}$ and n=13 *Tardbp*$^{M323K/M323K}$. HFD: n= 11 *Tardbp*$^{+/+}$ and n=12 *Tardbp*$^{M323K/M323K}$. ns= not significant. *p<0.05. **p<0.01. ***p<0.001. ***p<0.0001.

Females:

Female *Tardbp*$^{M323K/M323K}$ mice in the HFD group showed slightly elevated EE rates in the dark phase, compared to control *Tardbp*$^{+/+}$ littermates. This was seen at both 3 ($p<0.05$) and 6-months ($p<0.001$, **Figure 5.7B**). *Tardbp*$^{M323K/M323K}$ mice in the LFD showed elevated EE, in the dark phase, at 6 months of age ($p<0.01$, **Figure 5.7A**). In both diet groups, no genotype differences were seen in EE during the light phase. *Tardbp*$^{M323K/M323K}$ mice in the LFD group showed increased EE rates over time ($p<0.05$), while *Tardbp*$^{+/+}$ mice showed elevated EE rates over time only in the dark phase ($p<0.05$). Both genotypes in the HFD group showed elevated EE rates, in the dark phase, over time ($p<0.01$) but only *Tardbp*$^{M323K/M323K}$ mice showed this trend in the light phase.

Similar to males, female *Tardbp*$^{M323K/M323K}$ mice in the HFD group had a significantly lower dark RER compared to control *Tardbp*$^{+/+}$ littermates at 3 months of age ($p<0.01$, **Figure 3.7B**). These differences were no longer evident by 6 months of age. No other RER genotype differences were observed in females. Additionally, no changes over time were reported in any of the genotypes.

♀

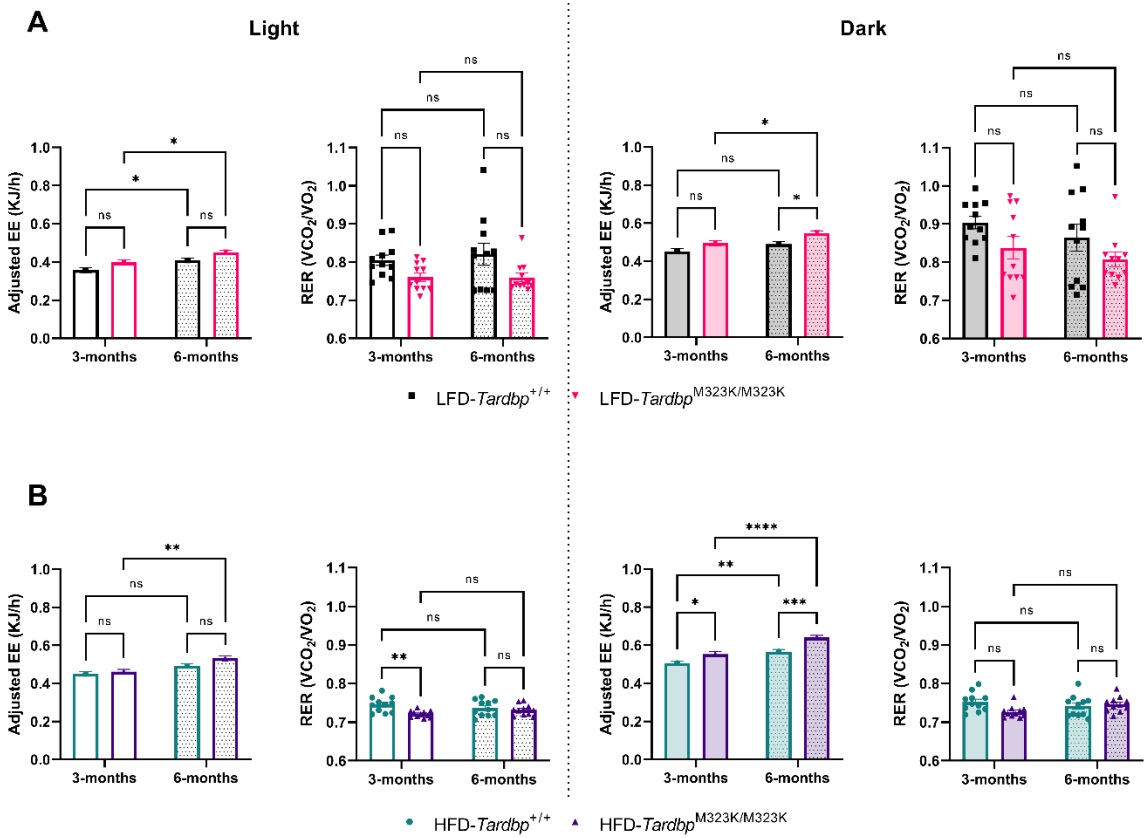


Figure 5.7. Indirect calorimetry analysis of female *Tardbp*^{M323K} mice in diet study. Graphs show energy expenditure (EE) and respiratory exchange ratio (RER) measurements from mice in the low-fat (A) and high-fat diet group (B) at 3 and 6-months. *Tardbp*$^{M323K/M323K}$ mice in the HFD group had elevated dark EE levels at both time-points, but only at 6-months in the LFD group.*Tardbp*$^{M323K/M323K}$ mice in the HFD group had reduced RER at 3-months. EE corrected by

lean mass using 2-way ANCOVA to give an adjusted EE mean value. Parameters are separated by time (light and dark). Dark (graphs with shaded bars): 6pm- 6am. Light (graphs with white bars): 12- 5pm and 7- 10am. Data shown as mean. Error bars denote SEM of data. Dotted bars indicate the 6-month time-point. Data analysed using 2-way ANOVA followed by Tukey's multiple comparisons test to compare between genotypes in each diet group, and between diet groups within genotypes. LFD: n=11 *Tardbp*$^{+/+}$ and n=11 *Tardbp*$^{M323K/M323K}$. HFD: n= 11 *Tardbp*$^{+/+}$ and n=11 *Tardbp*$^{M323K/M323K}$. ns= not significant. *p<0.05. **p<0.01. ***p<0.001. ***p<0.0001.

5.2.2 Diet effects on mutation-driven cognitive phenotypes

This section investigated if diet could shift motor and cognitive phenotypes seen in the ALS-FTD spectrum. Phenotyping tests were conducted at 3 and 6-months. From the previous chapter, tests known to detect a progressive phenotype in this mutant line were selected to evaluate the cognitive modulatory effects of diet. This was intended to provide a readout to evaluate the potential worsening or delay of already observed phenotypes by diet. A parallel diet study was conducted by the Corrochano group. They were able to conduct additional motor and cognitive tests that will be included in the discussion.

5.2.2.1 Light-dark box

This test was selected since it detected a progressive anxiety-like phenotype in *Tardbp*$^{M323K/M323K}$ mice on the standard chow-diet. The percentage of time spent in the light zone and proportion of frequency in the light zone were recorded. For each time-point, data was analysed using 2-way ANOVA followed by Tukey's multiple comparisons test to compare between genotypes in each time-point, and between time-points within genotypes. Since this experiment did not work in males at 3-months, data was collected only at 6-months. As a result, the male data was analysed using unpaired t-test to compare between genotypes within diet groups.

Males:

Male *Tardbp*$^{M323K/M323K}$ mice in the LFD group spent more time in the light zone at 6 months of age compared to control *Tardbp*$^{+/+}$ mice ($p<0.05$, **Figure 5.8A**). The zone entry preference was not altered between the genotypes; mice from both groups entered the light and dark zone at equal frequencies. No genotype differences were reported in male mice in the HFD diet group (**Figure 5.8B**).

Females:

At both time-points, there were no genotype differences in the LFD and HFD groups (**Figure 5.9**). Female *Tardbp*$^{+/+}$ mice in the LFD group entered the light zone more frequently at 6 months of age, compared to 3-months ($p<0.01$, **Figure 5.9A**), suggesting possible habituation to the test. No other significant time differences were observed within genotypes.

♂

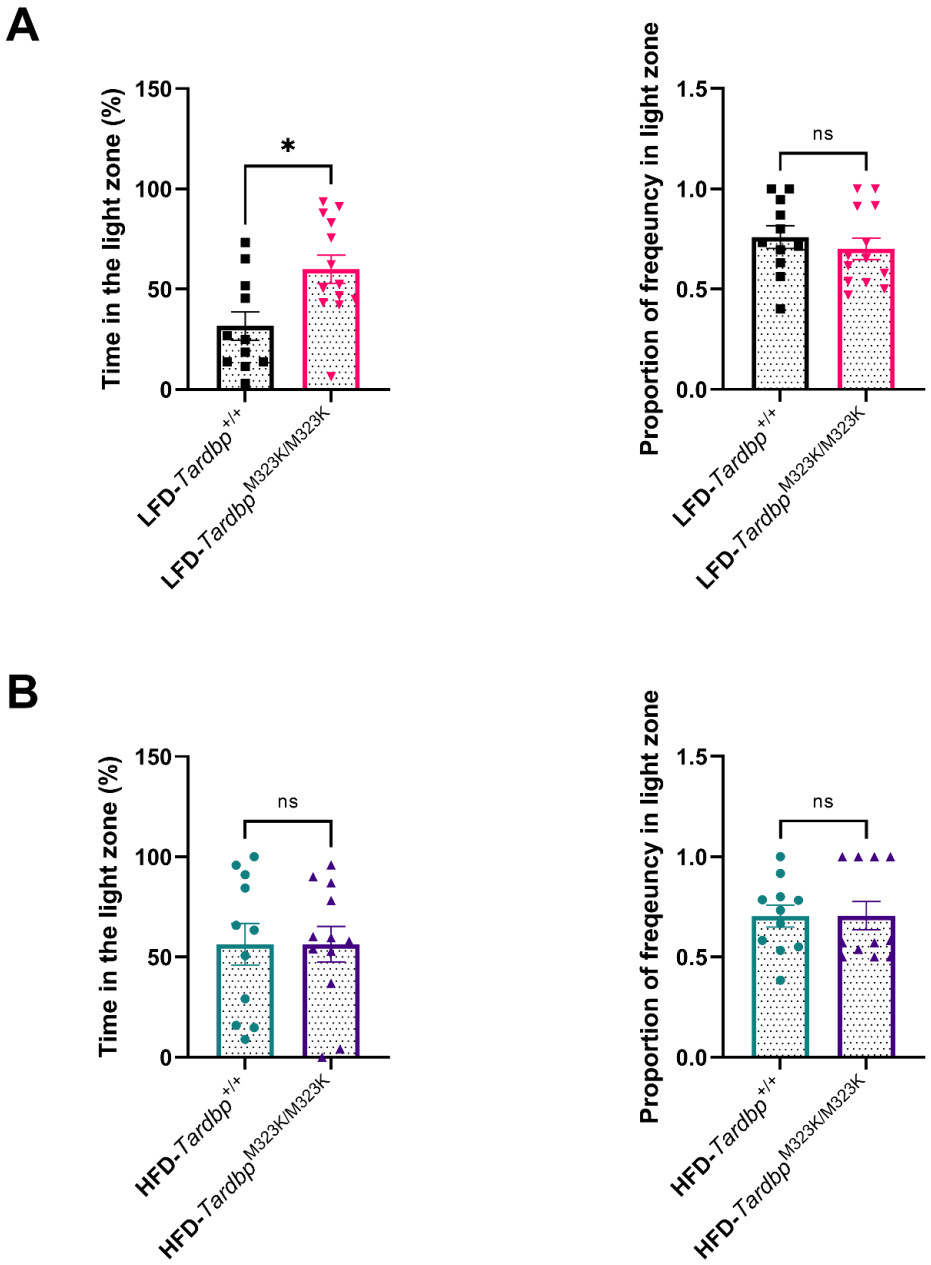


Figure 5.8. Light-dark box test in male *Tardbp*^{M323K} mice in diet study. Graphs show data from mice in the low-fat (**A**) and high-fat diet group (**B**) at 6-months (dotted bars). *Tardbp*$^{M323K/M323K}$ mice in the LFD group spent more time in the light zone compared to control littermates, at 3 months of age. Proportion of frequency in light zone: frequency in light zone/ (frequency in light zone + frequency in dark zone). A ratio of 0.5 indicates equal entries in both zones, while a higher frequency indicates more time entered in the light zone. Data shown as mean. Error bars denote SEM of data. Data analysed using unpaired t-test to compare between genotypes within diet group at 6-months. LFD: n=11 *Tardbp*$^{+/+}$ and n=13 *Tardbp*$^{M323K/M323K}$. HFD: n= 11 *Tardbp*$^{+/+}$ and n=12 *Tardbp*$^{M323K/M323K}$. ns= not significant. *p<0.05.

♀

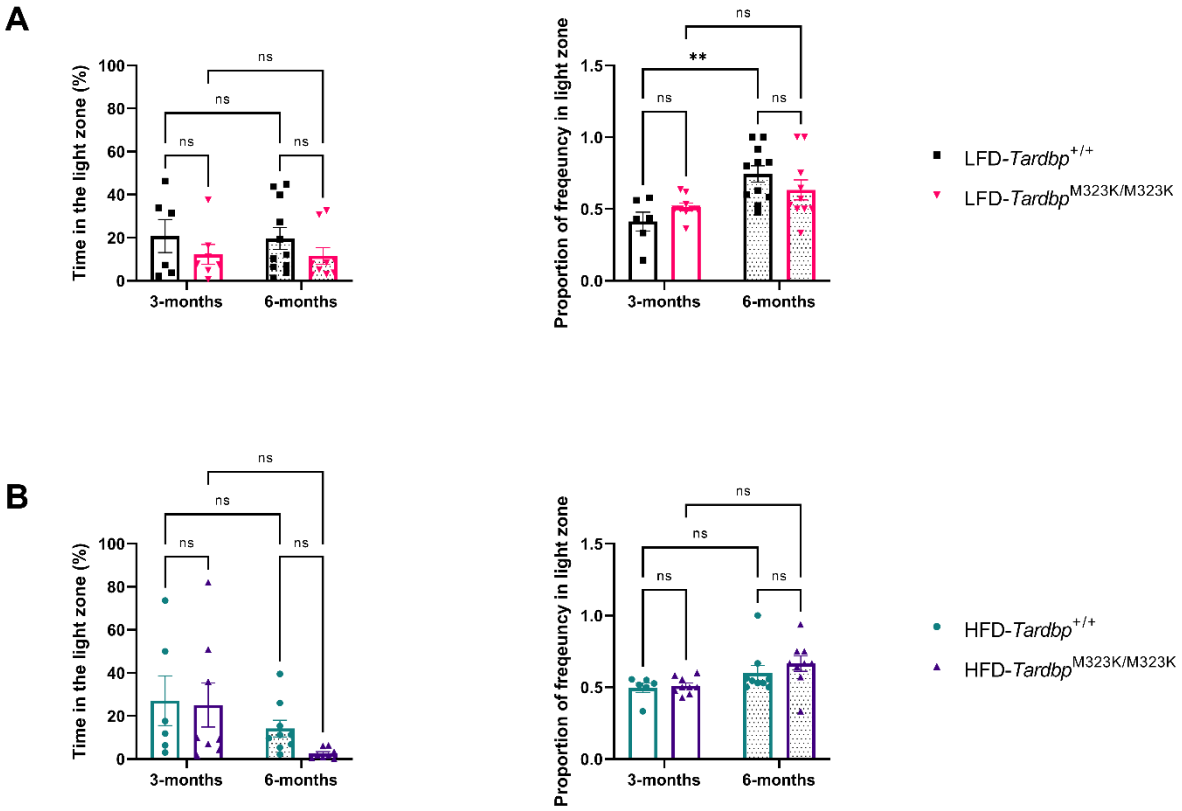


Figure 5.9. Light-dark box test in female *Tardbp*^{M323K} mice in diet study. Graphs show data from mice in the low-fat (**A**) and high-fat diet group (**B**) at 3 and 6-months. In both diet groups, there were no genotype differences. Proportion of frequency in light zone: frequency in light zone/ (frequency in light zone + frequency in dark zone). A ratio of 0.5 indicates equal entries in both zones, while a higher frequency indicates more time entered in the light zone. Data shown as mean. Error bars denote SEM of data. Dotted bars indicate the 6-month time-point. Data analysed using 2-way ANOVA followed by Tukey's multiple comparisons test to compare between genotypes at each time-point, and between time-points within genotypes. LFD (3-months): n=6 *Tardbp*$^{+/+}$ and n=9 *Tardbp*$^{M323K/M323K}$. HFD (3-months): n= 6 *Tardbp*$^{+/+}$ and n=9 *Tardbp*$^{M323K/M323K}$. LFD (6-months): n=11 *Tardbp*$^{+/+}$ and n=11 *Tardbp*$^{M323K/M323K}$. HFD (6-months): n= 11 *Tardbp*$^{+/+}$ and n=11 *Tardbp*$^{M323K/M323K}$. ns= not significant.

5.2.2.2 Fear conditioning

This test identified progressive, associative learning impairments in *Tardbp*$^{M323K/M323K}$ mice on the standard chow diet, specifically deficits in context learning. This test was split into two subtests, context and cue. In the context test, the freezing times (%) before the aversive unconditioned stimuli (sound coupled with shock) and after the animal is placed in the same environment (context) were recorded. In the cue test, the animal was placed in a new environment. The freezing times (%) before (baseline) and after a sound (cue) were recorded. The % freezing time difference for each test was then calculated for analysis. For each time-point, data was analysed using 2-way ANOVA followed by Tukey's multiple comparisons test to compare between genotypes in each time-point, and between time-points within genotypes.

Males:

At 3 months of age, male *Tardbp*$^{M323K/M323K}$ mice on the LFD spent more time freezing after the cue compared to control *Tardbp*$^{+/+}$ littermates ($p<0.01$, **Fig 5.10A**). This difference was still observed at 6-months ($p<0.0001$). There were no changes in cue freezing over time in any of the genotypes. Male mice in the LFD group did not show genotype differences in the context test. Male mice in the HFD group did not show genotypes differences in the context and cue test (**Figure 5.10B**).

Females:

In both diet groups, there were no genotype differences in the context and cue test (**Figure 5.11**).

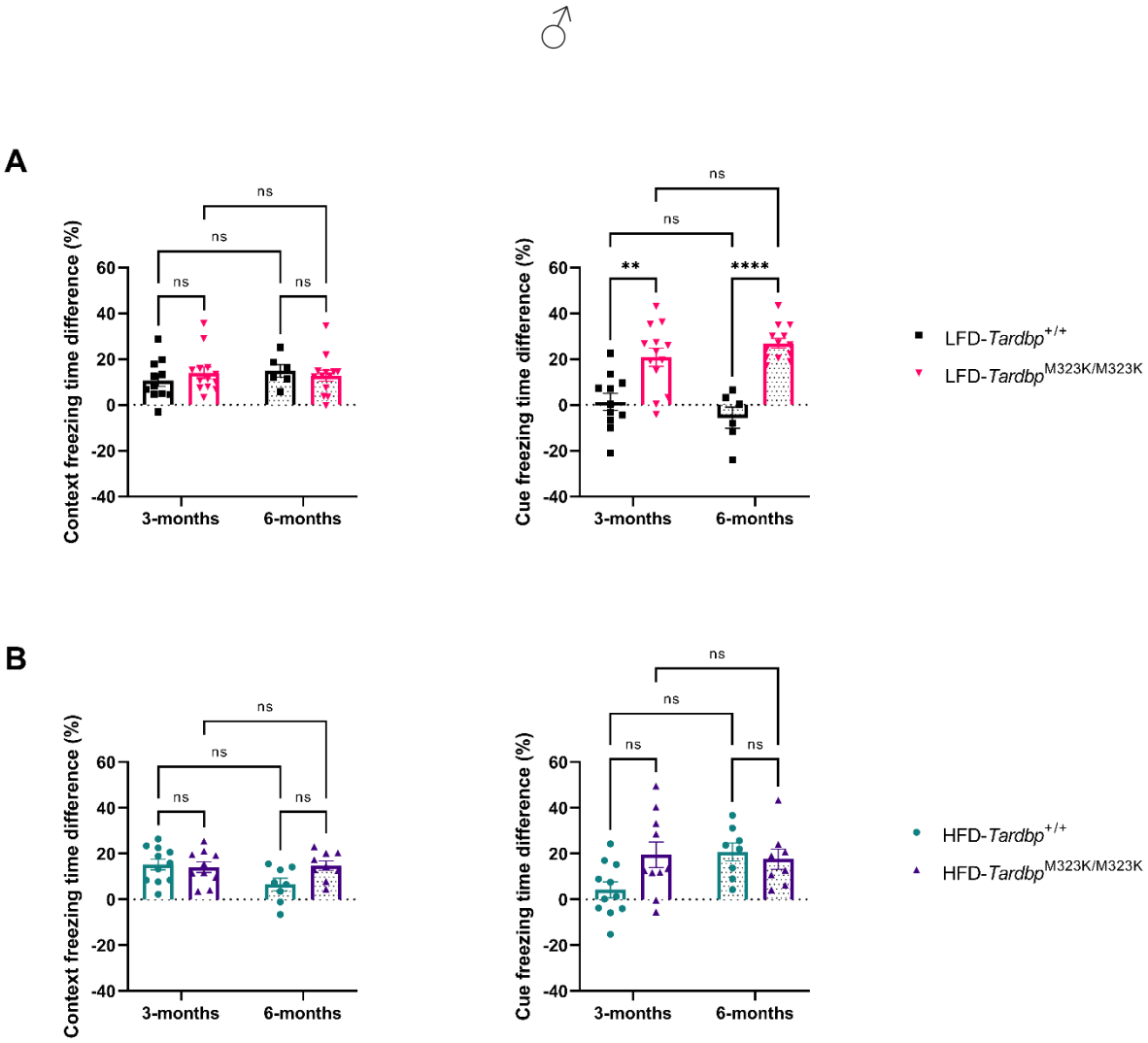


Figure 5.10. Fear conditioning test in male *Tardbp*^{M323K} mice in the diet study. Graphs show cue and context data from mice in the low-fat (**A**) and high-fat diet group (**B**) at 3 and 6-months. *Tardbp*$^{M323K/M323K}$ mice in the LFD group spent more time freezing in the cue test, compared to control littermates. Freezing time difference is the % change between test (context or cue) and baseline freezing. Data shown as mean. Error bars denote SEM of data. Dotted bars indicate the 6-month time-point. Data analysed using 2-way ANOVA followed by Tukey's multiple comparisons test to compare between genotypes at each time-point, and between time-points within genotypes. LFD (3-months): n=11 *Tardbp*$^{+/+}$ and n=13 *Tardbp*$^{M323K/M323K}$. HFD (3-months): n= 11 *Tardbp*$^{+/+}$ and n=10 *Tardbp*$^{M323K/M323K}$. LFD (6-months): n=6 *Tardbp*$^{+/+}$ and n=13 *Tardbp*$^{M323K/M323K}$. HFD (6-months): n= 8 *Tardbp*$^{+/+}$ and n=9 *Tardbp*$^{M323K/M323K}$. ns= not significant.

♀

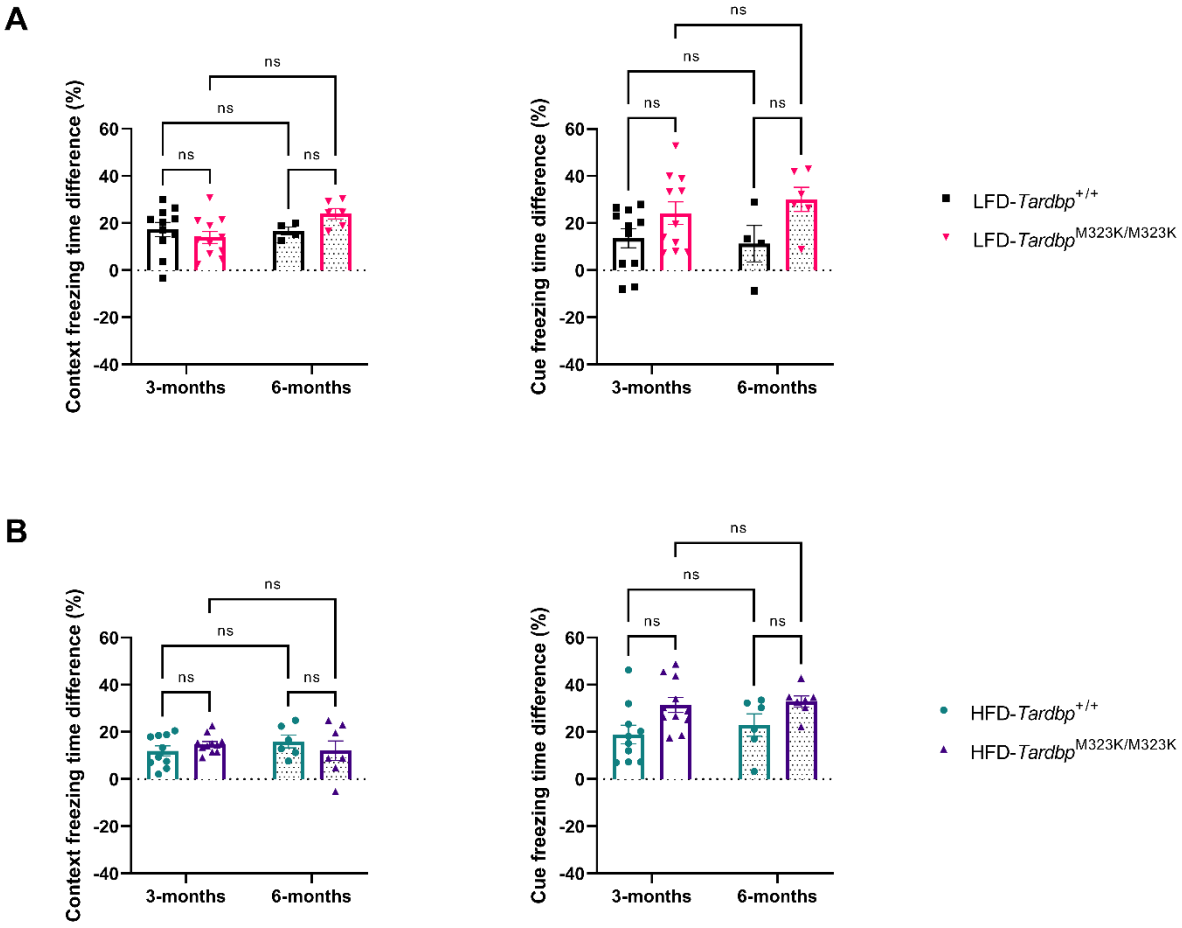


Figure 5.11. Fear conditioning test in female *Tardbp*^{M323K} mice in the diet study. Graphs show cue and context data from mice in the low-fat (**A**) and high-fat diet group (**B**) at 3 and 6-months. No genotype differences in both diet groups. Freezing time difference is the % change between test (context or cue) and baseline freezing. Data shown as mean. Error bars denote SEM of data. Dotted bars indicate the 6-month time-point. Data analysed using 2-way ANOVA followed by Tukey's multiple comparisons test to compare between genotypes at each time-point, and between time-points within genotypes. LFD (3-months): n=11 *Tardbp*$^{+/+}$ and n=11 *Tardbp*$^{M323K/M323K}$. HFD (3-months): n= 10 *Tardbp*$^{+/+}$ and n=11 *Tardbp*$^{M323K/M323K}$. LFD (6-months): n=4 *Tardbp*$^{+/+}$ and n=6 *Tardbp*$^{M323K/M323K}$. HFD (6-months): n= 6 *Tardbp*$^{+/+}$ and n=7 *Tardbp*$^{M323K/M323K}$. ns= not significant.

5.2.3 Diet effects on mutation-driven motor phenotypes

Late neuromuscular changes were seen in *Tardbp*$^{M323K/M323K}$ mice on the standard chow-diet, coupled with *in vivo* motor phenotypes. Unlike other locomotor behavioural tests, the Mousewalker test provides a detailed kinematic information on gait patterns. *Tardbp*$^{M323K/M323K}$ mice on the standard chow-diet showed abnormalities in a number of gait parameters at 12 months of age. As a result, this was the only motor phenotyping test used in this study. This test was only conducted at 6-months to reduce stress; this test was conducted in the dark, which caused hyperactivity and fighting among male mice. Thus, the data was analysed using unpaired t-test to compare between genotypes within diet groups.

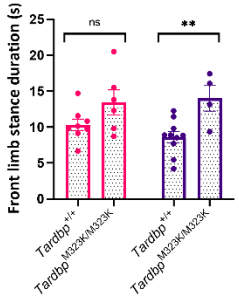
Males:

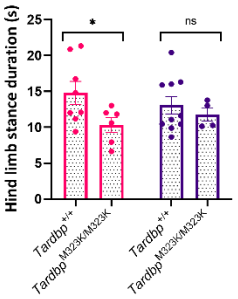
Male *Tardbp*$^{M323K/M323K}$ mice in the LFD group had a reduced hind limb stance duration ($p<0.05$) and increased hind limb swing duration ($p<0.05$, **Figure 5.10**) compared to control *Tardbp*$^{+/+}$ littermates. No differences were reported in other gait parameters within the male LFD group. Male *Tardbp*$^{M323K/M323K}$ mice in the HFD group also had increased hind limb swing duration compared to *Tardbp*$^{+/+}$ mice, but the opposite effect was seen in the front limbs ($p<0.05$). *Tardbp*$^{M323K/M323K}$ mice also had an increased front limb stance duration ($p<0.01$). No other differences were reported in the other gait parameters within the male HFD group. It should be noted that there was a reduced male sample size in this test due to increased cage fighting.

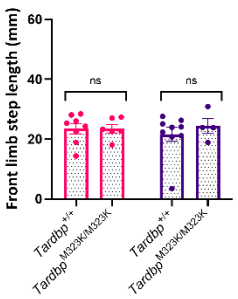
Females:

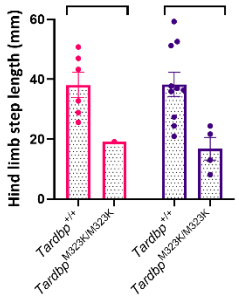
Female *Tardbp*$^{M323K/M323K}$ mice in the LFD group had an increased front limb stance compared to control *Tardbp*$^{+/+}$ mice ($p<0.01$, **Figure 5.11**). *Tardbp*$^{M323K/M323K}$ mice in this diet group also had increased front and hind limb swing duration, as well as a reduced walking speed ($p<0.05$). No genotypes differences were reported in the other gait parameters within the female LFD group. Similar to the LFD group, female *Tardbp*$^{M323K/M323K}$ mice in the HFD group also had an increased front limb stance duration, increased hind limb swing duration and reduced walking speed ($p<0.05$). These mice also had an increased hind limb stride width compared to *Tardbp*$^{+/+}$ mice ($p<0.0001$). No genotype differences were reported in the other gait parameters within the female HFD group.

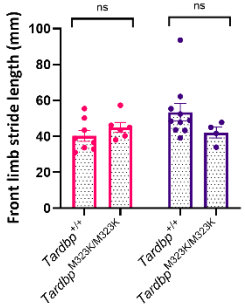
♂

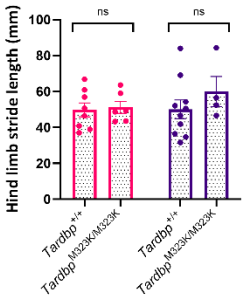

Front limb stance duration (s)
ns
**
Tardbp +/+
Tardbp M323K/M323K

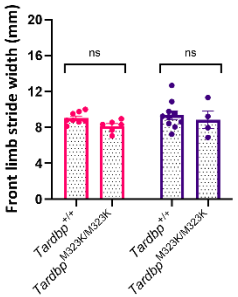

Hind limb stance duration (s)
*
ns
Tardbp +/+
Tardbp M323K/M323K

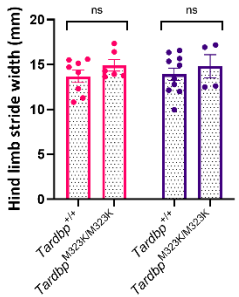

Front limb step length (mm)
ns
ns
Tardbp +/+
Tardbp M323K/M323K

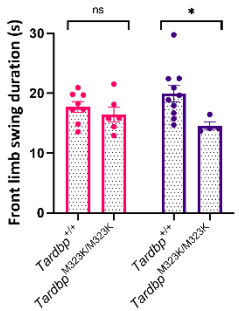

Hind limb step length (mm)
ns
**
Tardbp +/+
Tardbp M323K/M323K

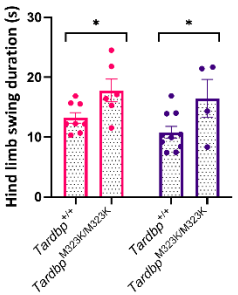

Front limb stride length (mm)
ns
ns
Tardbp +/+
Tardbp M323K/M323K

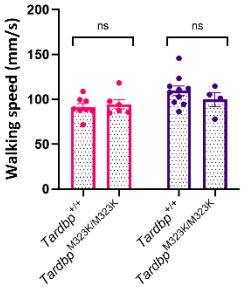

Hind limb stride length (mm)
ns
ns
Tardbp +/+
Tardbp M323K/M323K


Front limb stride width (mm)
ns
ns
Tardbp +/+
Tardbp M323K/M323K


Hind limb stride width (mm)
ns
ns
Tardbp +/+
Tardbp M323K/M323K


Front limb swing duration (s)
ns
*
Tardbp +/+
Tardbp M323K/M323K


Hind limb swing duration (s)
*
*
Tardbp +/+
Tardbp M323K/M323K


Walking speed (mm/s)
ns
ns
Tardbp +/+
Tardbp M323K/M323K

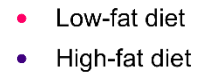
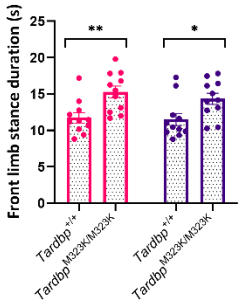
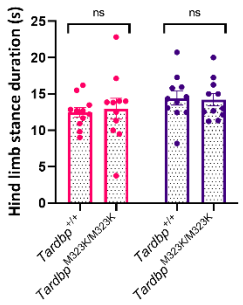
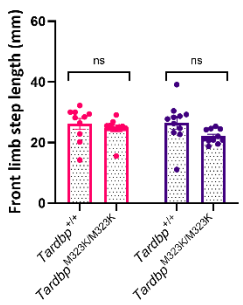

Low-fat diet
High-fat diet

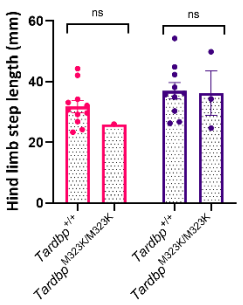
Figure 5.12. Gait analysis of male *Tardbp*^{M323K} mice in the diet study. Graphs show parameters from the Mousewalker test conducted at 6-months (dotted bars). For each animal, parameters are from the mean gait cycle. Gait abnormalities were seen in *Tardbp*$^{M323K/M323K}$ mice in both diet groups. Data shown as mean. Error bars denote SEM of data. Data analysed using 2-way ANOVA followed by Tukey's multiple comparisons test to compare between genotypes in each diet group, and between diet groups within genotypes. LFD: n=8 *Tardbp*$^{+/+}$ and n=6 *Tardbp*$^{M323K/M323K}$. HFD: n= 10 *Tardbp*$^{+/+}$ and n=4 *Tardbp*$^{M323K/M323K}$. ns= not significant. *p<0.05. **p<0.01.

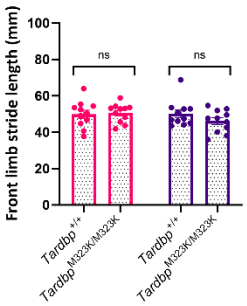
♀

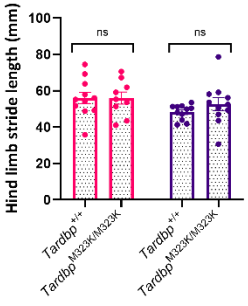

Front limb stance duration (s)
**
*
Tardbp+/+
TardbpM323K/M323K

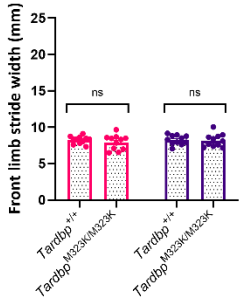

Hind limb stance duration (s)
ns
ns
Tardbp+/+
TardbpM323K/M323K

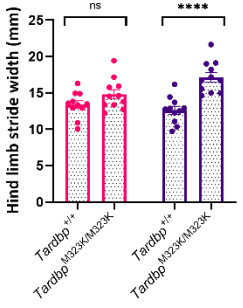

Front limb step length (mm)
ns
ns
Tardbp+/+
TardbpM323K/M323K

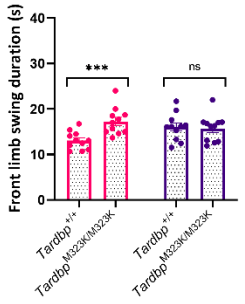

Hind limb step length (mm)
ns
ns
Tardbp+/+
TardbpM323K/M323K

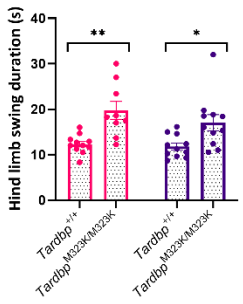

Front limb stride length (mm)
ns
ns
Tardbp+/+
TardbpM323K/M323K

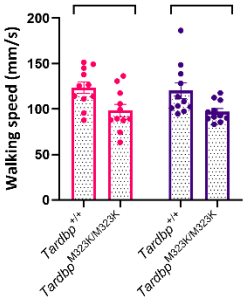

Hind limb stride length (mm)
ns
ns
Tardbp+/+
TardbpM323K/M323K


Front limb stride width (mm)
ns
ns
Tardbp+/+
TardbpM323K/M323K


Hind limb stride width (mm)
ns
****
Tardbp+/+
TardbpM323K/M323K


Front limb swing duration (s)
***
ns
Tardbp+/+
TardbpM323K/M323K


Hind limb swing duration (s)
**
*
Tardbp+/+
TardbpM323K/M323K


Walking speed (mm/s)
*
*
Tardbp+/+
TardbpM323K/M323K

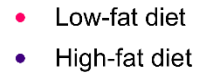

Low-fat diet
High-fat diet

Figure 5.13. Gait analysis of female *Tardbp*^{M323K} mice in the diet study. Graphs show parameters from the Mousewalker test conducted at 6-months (dotted bars). For each animal, parameters are from the mean gait cycle. Gait abnormalities were seen in *Tardbp*$^{M323K/M323K}$ mice in both diet groups. Data shown as mean. Error bars denote SEM of data. Data analysed using 2-way ANOVA followed by Tukey's multiple comparisons test to compare between genotypes in each diet group, and between diet groups within genotypes. LFD: n=11 *Tardbp*$^{+/+}$ and n=11 *Tardbp*$^{M323K/M323K}$. HFD: n= 11 *Tardbp*$^{+/+}$ and n=11 *Tardbp*$^{M323K/M323K}$. ns= not significant. *p<0.05. **p<0.01. ****p<0.0001.

5.3 Discussion

5.3.1 Summary

5.3.1.1 Metabolic

This study shows that diet interacts with the *Tardbp*^{M323K} mutation to modulate phenotypes. Differences were observed between the diet, sex and time. These changes are summarised in **Table 5.3**.

Tests	Diet			
	Low-fat		High-fat	
	Male	Female	Male	Female
Weights	−	↑	↓	↑
Fat mass	↑ at 3M	↑	−	↑
Lean mass	↓ at 3M	↓	−	↓
EE	↑ at 3M	↑ at 6M	↑	↑
RER	↓ at 3M	−	−	↓ at 3M
Light-dark box	↑ at 3M	−	−	−
Context	−	−	−	−
Cue	↑	−	−	−
Gait	↕	↕	↕	↕

Table 5.3. Summary of phenotypes in the diet study. Changes found in male and female *Tardbp*$^{M323K/M323K}$ mice compared to control *Tardbp*$^{+/+}$ mice. ↑ means an increase in parameters, ↓ means a decrease in parameters, − means no change and ↕ means multiple parameters are altered in either direction. 3M= 3-months. 6M= 6-months. If 3M or 6M accompanies a symbol, that particular phenotype was only present at that time-point. If no time-point is indicated, that phenotype was present at both time-points. Gait analysis was only conducted at 6-months. In-depth summary of gait parameters are found in **Table 5.4**.

The *Tardbp*^{M323K} mutation in homozygosity has been shown to produce sex-differences in body weight (previous chapter). When fed the standard chow diet, female homozygous mice weighed more than their littermate controls, while males weighed less. The mutation's effect was conserved across all diet groups in females and males on HFD. The normal *Tardbp*^{M323K} male weight effect was not seen in the LFD group as no significant weight differences were detected between the genotypes.

The increased body weights in female homozygous mice correlated to increased fat mass and reduced lean mass. These body composition changes were also seen in female homozygous mice fed the standard chow diet. However, things were more complicated in males. Despite male homozygous mice in the HFD group weighing significantly less than controls, there were no body composition changes. On the other hand, there were no genotype weight differences in the LFD group but male homozygous mice had increased fat mass and decreased lean mass; a similar body composition to female homozygous mice. This data further confirms that body weight/BMI indexes do not give an accurate depiction of body composition.

In females, body composition changes appear to be independent of EE rates as females homozygous mice weighed more than controls despite being hypermetabolic. Therefore, it is important to measure food intake to investigate hyperphagsia. Hypermetabolism correlated to the reduced body weights observed in male homozygous mice fed the HFD. Interestingly, both diets accelerated the mutation's effect on energy expenditure. When fed the standard chow diet, hypermetabolism was observed in homozygous mice at 12 months of age. In the diet studies, this phenotype was seen at 3-months in males. In the females,

hypermetabolism was detected at 3-months in the HFD, and at 6-months in the LFD group. Both diets cause a general worsening of the mouse's metabolic state, with HFD having a greater effect in female mice. In ALS, hypermetabolism is associated with greater functional decline and shorter survival (Steyn et al., 2018), as well as alterations in muscle energy demand (Loeffler et al., 2016). Therefore, diet may be hastening these disease processes.

Increased fat depots indicates that the body uses more fats for fuel. This was confirmed by the fat fuel preference seen in diet groups with increased fat mass; all female homozygous mice and male homozygous mice in the LFD group. Similar to *FUS*$^{\Delta 14}$ homozygous mice, this might be a compensatory mechanism to meet the high energy demands in a disease state, as evidenced by hypermetabolism (Palamiuc et al., 2015). Alterations in glucose metabolism could also contribute to the observed fat fuel preference. IPGTT and further blood/plasma analysis is needed to determine glucose and lipid homeostasis.

5.3.1.2 Cognitive

Late anxiety-like phenotypes and executive functioning deficits were observed in female homozygous mice fed the standard chow diet. Genotype differences were not seen in these cognitive readouts in female mice, in either diet group. This shows that diet did not modulate the mutation's cognitive effects in female mice.

The HFD and LFD did not modulate the mutation's cognitive effects in male mice. Interestingly, the LFD modulated cognitive effects in wild-type mice. Compare to homozygous mice, wild-type mice spent less time in the light zone indicating that the LFD causes anxiety-like phenotypes (Crawley, 1985). The absence of this phenotype at a later time-point may be due to test habituation. Male wild-type mice in the LFD group also spend less time freezing in the cue test compared to

homozygous mice. This test measures learning and memory as the animal needs to associate the aversive unconditioned stimuli (shock) to the conditioned stimuli (context- environment or cue- sound) (Shoji et al., 2014). Data from this test suggests that the LFD causes learning and memory deficits.

5.3.1.3 Motor

The previous chapter showed that this mutation in homozygosity caused gait abnormalities at 12 months of age, including reduced front and hind limb stance duration, reduced front limb step length and increased hind limb stride length. This gait pattern was absent in female homozygous mice in both diet groups (**Table 5.4**). Female homozygous mice in both diet groups displayed increased stance and swing duration, coupled with the reduced walking speed, indicating a slower walking pattern. This could be caused by a number of factors, however weight is the most logical answer as these mice weighed more than their littermate controls (possible confounder). Increased body weight may be hiding possible gait abnormalities therefore it is difficult to determine if diet modulates the mutation's motor effects in female mice.

Male homozygous mice in the LFD group continued to show unique phenotypes. These mice displayed similar gait abnormalities to female homozygous mice fed the standard chow diet. They had a hind limb stance phase that was shorter than the swing phase meaning the hind limbs spent more time off the ground so more weight-bearing on the front limbs, suggesting a limp. This gait pattern is referred to as antalgic gait as it is caused by pain (Pirker & Katzenschlager, 2017). While front limb gait abnormalities were present in male homozygous mice fed the HFD, their stance and swing duration were similar. A change specific to this group was

the shorter hind limb step distances. However, it is difficult to assign these changes to a known gait pattern.

The time-point at which these metabolic and cognitive effects occurred differed between diet, sexes and test. For example, many phenotypes in males in the LFD group were observed only at 3 months of age, just as mice start to become mature adults (Dutta & Sengupta, 2016), while other changes occurred at both time-points suggesting that age interacts with diet and the mutation. The time of diet intervention in the clinic will heavily depend on the type of diet, sex of the individual and symptom.

Gait parameter	Diet			
	Low-fat		High-fat	
	Male	Female	Male	Female
Front limb stance duration	−	↑	↑	↑
Hind limb stance duration	↓	−	−	−
Front limb step length	−	−	−	−
Hind limb step length	−	−	↓	−
Front limb stride length	−	−	−	−
Hind limb stride length	−	−	−	−
Front limb stride width	−	−	−	−
Hind length stride width	−	−	−	↑
Front limb swing duration	−	↑	↓	−
Hind limb swing duration	↑	↑	↑	↑
Walking speed	−	↓	−	↓

Table 5.4. Summary of gait parameters from the diet study. Changes found in *Tardbp*$^{M323K/M323K}$ mice compared to control *Tardbp*$^{+/+}$ mice. Test was conducted at 6-months. ↑ means an increase, ↓ means a decrease and − means no change.

5.3.2 Can diet shift phenotypes in the ALS-FTD spectrum?

The conservation of female weight, body composition and EE between different diet groups (standard chow, LFD and HFD) shows that diet does not modulate female *Tardbp*^{M323K} metabolic effects. This is not surprising as TDP-43 has been shown to play an important role in metabolic regulation. Postnatal TDP-43 KO in mice caused weight loss, reduced fat mass and reduced survival. When overexpressed, mice have an increased fat mass and adipocyte hypertrophy (Stallings et al., 2013). Mutant TDP-43 may cause metabolic alterations in the ALS-FTD spectrum possibly through mitochondrial dysfunction. Mice carrying TDP-43 mutations have been shown to disrupt mitochondrial morphology and physiology, impairing electron transport chain (ETC) activity. This leads to the accumulation of reactive oxygen species and calcium buffering defects (Floare & Allen, 2020). This could explain why diet has little effect on changing metabolic phenotypes in female *Tardbp*^{M323K} mice. However, diet modulates weight and body composition in male homozygous mice as phenotypic differences were observed between mice in the standard chow, LFD and HFD. Changes in metabolic parameters, caused by diet, may explain the motor and cognitive phenotypes differences observed in male mice across the different diets.

In males, diet did not modulate the *Tardbp*^{M323K} mutation-driven cognitive effects. However, the LFD caused behavioural deficits in wild-type mice, in a sex dependent manner. Male wild-type mice fed the LFD showed anxiety-like phenotypes and deficits in associative learning; similar phenotypes seen in homozygous mice fed the standard chow diet. The LFD did not have an effect on mutant mice. The *in vivo* cognitive tests used in this study were not conducted in male mice on a standard chow diet, therefore it is difficult to determine if diet

delays any cognitive deficits in mutant mice. The parallel diet study conducted by the Corrochano group used cognitive behavioural tests previously used in the characterisation of male *Tardbp*^{M323K} mice. Both diets caused deficits in the marble burying and NOR test, at similar time-point to the standard chow diet.

A worsening of mutation-driven cognitive phenotypes were expected in the HFD groups as diet caused significant metabolic alterations. However, this data showed that HFD did not modulate cognitive alterations in *Tardbp*^{M323K} mice. The expected behavioural deficits and cognitive dysfunction associated with HFD may have occurred in wild-type mice to match homozygous mice (Han et al., 2020), but it did not cause genotype differences. This creates doubt over the validity of the diet composition. The HFD used in this study was 45% fat (45% of calories from fat), while other HFD in literature are 60% fat (Speakman, 2019). One particular study showed that a 60% fat HFD caused deficits in episodic, spatial and contextual memory deficits in C57BL/6J mice (McLean et al., 2018). A lower fat composition was selected for this project's HFD to avoid potential welfare and confounding effects of diet-induced morbid obesity. Considering that a shorter phenotyping pipeline was used for this study (6-months), retrospectively it might have been better to use a higher fat diet (60%) to accelerate any potential phenotypes.

Diet modulated *Tardbp*^{M323K} mutation motor effects, in a sex-dependent manner. Males in both diet groups displayed gait abnormalities but distinct patterns. The LFD caused an expected worsening of motor phenotypes; male homozygous mice in this group displayed a limp at 6 months of age, which was absent in homozygous mice in the HFD group. A limp was observed in homozygous mice fed a standard chow-diet at a later time-point, therefore changes in diet (LFD) accelerated the mutation's motor effect. This motor phenotype was accompanied

by hypermetabolism, suggesting that muscle metabolic reprogramming has already occurred in these mice; similar to *FUS*$^{\Delta 14}$ homozygous mice. Hypermetabolism indicates an increased energy demand from the muscles, which is usually coupled with altered glucose metabolism. To compensate, muscles switch to lipids as an alternative fuel (Palamiuc et al., 2015; Scaricamazza et al., 2020). Homozygous mice in the LFD group showed an early fat fuel preference and increased fat stores, before the observed limp phenotype. This metabolic switch is known exacerbate disease progression.

In contrast, female homozygous mice in both diet groups had similar gait patterns. The slow stride pattern observed in these mice can be explained by the weight gain caused by this mutation in females, which could mask any possible gait abnormalities. Therefore, it is difficult to conclusively determine diet's effect on female mutation-driven motor phenotypes. However, neither diets accelerated the mutation's gait effects as a limp was not present.

Sex differences in the LFD group point to sex hormones as being contributing factors. Epidemiological studies implicate oestrogen and progesterone to be protective against ALS, and this has been confirmed in *in vivo* animal models. The neuroprotective effects of oestrogen have been demonstrated in numerous pre-clinical studies (Arevalo et al., 2015; Choi et al., 2008; Groeneveld et al., 2004). These hormonal influences may explain the lack of motor deficits in female homozygous mice fed the LFD, compared to male mice in this group which showed significant alterations.

This chapter demonstrates that diet can modulate certain ALS-FTD spectrum phenotypes. This data suggests the LFD exacerbates *Tardbp*^{M323K} motor phenotypes in a sex-dependent manner. In males, a LFD modulated metabolic

phenotypes (body composition, EE and RER) which may underline the motor phenotypes. The extent and mechanisms of this modulation remains unknown until the completion of the wider study.

5.3.3 Future experiments

Due to the large-scale nature of this study (both sexes and different diets), limited *in vivo* behavioural tests were conducted. This study was part of an international, ongoing study. The main aim of this particular study was to provide valuable metabolic readings (body composition, EE and RER) to supplement the wider characterisation study conducted by the Corrochano group in Spain. As a result, additional work and analysis is needed to create a complete picture.

A wide range of tissues were collected at the end of the study (9-months) for future molecular characterisation work. This included perfused tissues for imaging work, fresh frozen tissues for RNA and protein work, and plasma for clinical chemistry and lipidomics. These tissues will be used to understand the molecular mechanisms that underlie diet's ability to modulate *Tardbp*^{M323K} phenotypes. The following points will be answered at the end of the study:

I. Diet's effect on additional metabolic parameters- Plasma lipid panel and glucose tolerance test.
II. Diet's effect on additional cognitive/behavioural parameters.
III. Diet's effect on additional motor and neuromuscular parameters.
IV. Diet's effect on TDP-43 pathology. TDP-43 autoregulation and nuclear protein level effects. Does it trigger aggregate formation? Additional splicing changes?
V. Candidate pathways/mechanisms- Plasma and tissue lipidomics will guide further experiments.

Discussion

6 Final discussion

6.1 Main findings and contributions to the field

6.1.1 Widespread systemic effects of *Fus* and *Tardbp* mutations

The aim of this project was to uncover the systemic pathological effects of *FUS* and *TARDBP* mutations. Both genes encode for RNA-binding proteins and have shared physiological roles in RNA metabolism (Lagier-Tourenne & Cleveland, 2009; Lagier-Tourenne et al., 2010). Dysregulation of these processes, coupled with cytoplasmic mislocalisation and protein aggregates, have been identified in ALS-FTD spectrum disorders (I. R. A. Mackenzie et al., 2010). Despite ALS and FTD being considered primarily neurological disorders, new evidence suggests that they are multi-system disorders. This is not surprising as FUS and TDP-43 are widely expressed in various tissues (Suk & Rousseaux, 2020; Vance et al., 2009). However, most of the research into the pathological effects of these proteins has been focused in neuronal tissues. The RNA-binding properties and pathomechanisms of FUS and TDP-43 in peripheral tissues are unknown. Therefore, it is possible that peripheral alterations induced by these proteins could directly contribute to disease aetiology.

A limitation of commonly used transgenic models is that wild-type/mutant FUS and TDP-43 levels, which are physiologically tightly autoregulated, are significantly increased or decreased. Therefore, the phenotypes observed in these models may be confounded by non-physiological expression changes (de Boer et al., 2021). This project characterised physiological mouse models, carrying disease relevant mutations, to uncover a broad range of phenotypes including significant metabolic dysregulation.

Metabolic alterations have been heavily documented in ALS-FTD spectrum disorders. While clinical and pre-clinical data have pointed towards the disease-modifying effects of these alterations (Jawaid et al., 2018), their exact pathomechanisms have remained unsolved. In addition to identifying systemic pathological effects, this project discovered mechanisms by which metabolic dysregulation influenced key ALS-FTD spectrum phenotypes.

6.1.1.1 *Fus*$^{\Delta 14}$ mutation

Transcriptomic analysis of multiple tissues revealed that the *Fus*$^{\Delta 14}$ mutation caused widespread dysregulation. While there were some commonalities between tissues, this mutation affected each tissue differently. The brain and muscle were the most transcriptionally dysregulated tissues and this correlated to the observed phenotypes. The *Fus*$^{\Delta 14}$ mutation in homozygosity significantly affected brain structure and function. This caused obvious effects in homozygous mice, such as being proportionately smaller and abnormal 'anxiety-like'/hyperactive behaviours. These mice also had a reduced lifespan caused by sudden lethal seizures. Clear brain morphological changes were observed as early as 9 weeks of age, coupled with innate behaviour deficits. This not surprising as FUS plays an important role in synapse formation and regulation. In ALS models, rodents exhibited a reduction in dendritic spine numbers in the cortical and motor neurons (Sephton & Yu, 2015), indicating that the *Fus*$^{\Delta 14}$ mutation is also affecting these neuronal processes.

The *Fus*$^{\Delta 14}$ mutation caused early muscle remodelling which preceded neuromuscular changes and possible future motor phenotypes. GO terms related to the extracellular matrix and muscle composition were significantly enriched. Gene expression and histological analysis identified increased slow-twitch fibre

composition in the TA muscles of homozygous mice. Slow-twitch fibres display low fatigability, high oxidative capacity and preference for FFAs as a substrate for fuel (Baskin et al., 2015). These muscular changes occurred in response to the systemic metabolic effects of the *Fus*$^{\Delta 14}$ mutation. Impaired glucose uptake and hypometabolism point to altered glucose metabolism, which negatively affects muscles. ALS-related mechanisms increase the energy demand of skeletal muscles (Kasarskis et al., 1996; Palamiuc et al., 2015) and this demand cannot be met by the usual glycolytic pathways (Richter & Hargreaves, 2013). As a result, the muscles switch to lipids as an alternative fuel. The increased fat depots in *Fus*$^{\Delta 14}$ homozygous mice act as fuel supplies for this process. Despite these compensatory mechanisms, significant neuromuscular changes occurred at 3 months of age. These muscular metabolic changes may exacerbate disease progression. Muscle metabolic reprogramming was also detected in the pre-symptomatic *Sod1*^{G93A} mouse, and it predated hypermetabolism and neuromuscular changes in the symptomatic stage. Chronic treatment of a fatty acid β-oxidation inhibitor decreased energy expenditure and temporarily improved locomotor symptoms (Scaricamazza et al., 2020). Targeting early muscle metabolic pathways using drugs may provide a therapeutic benefit in ALS patients. Additional research is needed to optimise the pharmacokinetic and pharmacodynamics profiles of candidate drug treatments to improve efficacy.

The early nature of these phenotypes supports the developmental role of FUS. These phenotypes strongly correlate to clinical cases of juvenile-ALS (FUS-jALS) which are typically *FUS* mutation linked. FUS-jALS has a rapid disease progression, with death usually occurring within 1-2 years (Lehky & Grunseich, 2021). Clinicians have advocated for the screening of *FUS* mutations in children

presenting ALS symptoms. These children may initially present with learning disabilities and mild motor developmental delays (Picher-Martel et al., 2020). This project places metabolic dysregulation as an early indicator of FUS-jALS, as well as a pathomechanism in FUS-linked conditions.

6.1.1.2 *Tardbp*^{M323K} mutation

Like the *Fus*$^{\Delta 14}$ mouse, additional characterisation of the *Tardbp*^{M323K} mutation in homozygosity revealed widespread phenotypes. Structural brain MRI scans revealed structural brain abnormalities which were linked to the innate behaviours deficits and altered executive functioning observed in the behavioural tests. These behavioural and cognitive phenotypes correlated to FTD clinical symptoms (Convery et al., 2019) and supported a role for TDP-43 in normal neuronal development and function (Sephton et al., 2012). The *Tardbp*^{M323K} mutation in homozygosity also produced late neuromuscular changes and motor phenotypes.

An overlooked parameter in FTD research is metabolism. *Tardbp*^{M323K} homozygous mice displayed increased body weights, hypermetabolism and a sweet food preference- all of which have been observed in FTD patients (Ahmed, Irish, Piguet, et al., 2016). Hypermetabolism was observed in *Tardbp*^{M323K} mice at a later time-point, when homozygous mice displayed significant motor alterations (Dupuis et al., 2011), further highlighting that muscle metabolic alterations influence ALS-FTD motor phenotypes. Structural MRI scans revealed abnormalities in the hypothalamus, which may underlie these phenotypes as this brain region usually regulates appetite and energy patterns (Timper & Brüning, 2017).

Previous characterisation of this mutation revealed interesting molecular phenotypes (Fratta et al., 2018). The *Tardbp*^{M323K} mutation caused a splicing GOF

effect on constitutively included exons, leading to the downregulation of genes containing ‘skiptic’ exons. A majority of these genes were involved in CNS proteostasis, a pathomechanism implicated in neurodegeneration. While the *Tardbp*^{M323K} mutation is not found in patients (Chien et al., 2021), this splicing GOF was also identified in fibroblasts derived from ALS patients with *TARDBP* mutations, supporting the construct validity of this model. The *Tardbp*^{M323K} mutation also altered the modulation of alternative splicing, which caused abnormal autoregulation of TDP-43. Disrupted TDP-43 autoregulation has been identified in ALS motor neurons (Koyama et al., 2016), further supporting the construct validity of this model. Complete characterisation of the *Tardbp*^{M323K} homozygous mouse revealed that it is a novel ALS-FTD model, which recapitulates TDP-43 relevant mechanisms. There are limited ALS-FTD mouse models with TDP-43 pathology, therefore the *Tardbp*^{M323K} mouse fills this gap in the field. It can be used by researchers to understand ALS-FTD disease related mechanisms, as well as a tool to investigate biomarkers and novel treatments. This model is freely available via the European Mutant Mouse Achieve (EMMA).

6.1.2 Protein aggregates are not necessary in early disease mechanisms

ALS-FTD phenotypes were observed in *Tardbp*^{M323K} homozygous mice without the traditional TDP-43 pathology seen in post-mortem samples from late-stage disease patients (Fratta et al., 2018). The *Fus*$^{\Delta 14}$ mutation caused cytoplasmic FUS mislocalisation but systemic dysregulation occurred without cytoplasmic protein aggregation (Devoy et al., 2017). A similar phenomenon was observed in other *Fus* mutations (Sahadevan et al., 2021; Scekic-Zahirovic et al., 2021). These observations suggest that traditional protein pathology is not necessary in early disease mechanisms and that disease is initiated through different mechanisms.

Disruptions in the physiological roles of FUS and TDP-43 appears to be underlying mutation effects. The *Fus*$^{\Delta 14}$ and *Tardbp*^{M323K} mutation affected alternative splicing, leading to deficits in autoregulation (Humphrey et al., 2020; Koike et al., 2021). The *Tardbp*^{M323K} mutation caused additional splicing defects, specifically a splicing GOF. These findings show that these models are well suited for early disease mechanistic studies.

Despite both models sharing significant molecular and phenotypic characteristics, there are differences. The *Fus*$^{\Delta 14}$ mutation in homozygosity is severe, whereas the *Tardbp*^{M323K} mutation is milder in comparison. These mutations also target the brain differently, e.g., cortical thinning versus cortical atrophy. This could be due to differences in RNA-binding and splicing functions. This has already been confirmed in the brain as TDP-43 and FUS affected the processing and expressing levels of largely distinct sets of RNAs (Lagier-Tourenne et al., 2012; Ling et al., 2013). It is likely that this trend is present in other tissues therefore systemic transcriptomic comparisons between these mutations may be insightful.

6.1.3 Sex-differences in *Fus* and *Tardbp* mutations

The *Fus*$^{\Delta 14}$ mutation in homozygosity was more severe in females as they died earlier from seizures. While some phenotypes were conserved between the sexes, it is difficult to determine if this was the case in other parameters as characterisation was mostly conducted in males. Sexual dimorphism was also seen in *Tardbp*^{M323K} homozygous mice. Differences in body weight and earlier motor phenotypes suggests that this mutation, in homozygosity, was more severe in males. Additionally, diet modulated motor phenotypes in male *Tardbp*^{M323K} homozygous mice.

There is extensive evidence of sexual dimorphism in ALS. Males are more susceptible than women to develop the disease and have a worse prognosis (Pape & Grose, 2020). However, there are fewer FTD epidemiological studies making it difficult to accurately determine a sex association. A higher prevalence of bulbar ALS with cognitive impairment was seen in males (Portet et al., 2001). Behavioural phenotypes were less severe in female *Tardbp*^{Q331K} mice, compared to males (Watkins et al., 2020). The neuroprotective effects of oestrogen may underline the sex-differences in ALS-FTD spectrum disorders (Arevalo et al., 2015), however further studies using *Tardbp*^{M323K} mice can help unravel exactly how oestrogen protects against ALS-FTD disease.

Sexual dimorphism is varied and complex in other NDDs. In Parkinson's disease, males have a greater risk and prevalence, with a delayed onset in females. In Alzheimer's disease, age-specific risk and incidence is greater in females. Females also have a faster disease progression in Huntington's disease (Ullah et al., 2019). Therefore, each NDD pathology may interact with sex hormones in a different manner. Despite these clear sex-differences, female mice are significantly underrepresented in animal research (Beery & Zucker, 2011) which affects the translatability of research as females are included in clinical trials and beyond.

6.1.4 Genetic background effects

Possible interactions between genetic background and mutation were first highlighted when *Fus*$^{\Delta 14}$ and *Tardbp*^{M323K} homozygous embryonic lethality was rescued on a hybrid background. This was confirmed in the *Fus*$^{\Delta 14}$ mutant line when differences in body composition were observed between heterozygous mice on different genetic backgrounds. While the full extent and significance of this

interaction remains unknown, it raised important points about mouse research. It has been estimated that between 50- 90% of published pre-clinical data is irreproducible (von Kortzfleisch et al., 2020). Phenotypic differences between genetic backgrounds contributes to poor reproducibility and translatability of mouse research. As a result, it is important to determine how much of the observed mouse phenotypes are influenced by the mutation, and/or the genetic background. This can be done by validating observations across multiple genetic backgrounds and having a good grasp of the endogenous traits of inbred strains. It should be noted that motor and cognitive phenotypes observed in *Fus*$^{\Delta 14}$ homozygous mice were also observed in different research units (experimental heterogeneity) (Voelkl et al., 2018), and in other mouse models carrying NLS *FUS* mutations.

6.1.5 Diet can modulate mutation phenotypes

This project demonstrated that a LFD can modulate *Tardbp*^{M323K} motor phenotypes, in a sex-dependent manner. The LFD produced different metabolic phenotypes in male homozygous mice, compared to those fed a HFD. These metabolic differences (weight, body composition and fuel preference) may underlie the modulation of phenotypes. The LFD caused an expected worsening of motor phenotypes as it did not correct for disease energy imbalance. The mice presented a limp, which was coupled with hypermetabolism. A fat fuel preference and increased fat stores were observed before the motor phenotypes indicating that muscle metabolic reprogramming had already occurred (Scaricamazza et al., 2020)

Dietary effects on cognitive phenotypes are complicated. A worsening of mutation-driven cognitive phenotypes was expected on the HFD. However, this project

showed that HFD did not modulate mutation cognitive phenotypes in any of the sexes. This may be explained by the fat composition of the diet; traditional HFDs have more calories from fat (60% compared to 40%). In males, the LFD caused cognitive deficits in wild-type mice but not in mutant mice. It is important to note that limited *in vivo* phenotyping tests were conducted in this study therefore it is difficult to accurately determine the full extent of diet modulation on mutation phenotypes.

6.2 Future experiments

This thesis has contributed important findings in the field of ALS-FTD research. In the process, new questions and ideas were raised that were beyond the scope of this project's timeline.

Characterisation of *Fus*$^{\Delta 14}$ and *Tardbp*^{M323K} mice revealed widespread mutation effects in homozygosity. However, the molecular mechanisms behind these effects remains unknown. The systemic transcriptomic data in *Fus*$^{\Delta 14}$ homozygous mice provides a wealth of information on potential candidate pathways. RNA-sequencing was conducted on a range of *Fus*$^{\Delta 14}$ tissues, which revealed commonalties and differences that can be investigated further. The *Hist1h1c* gene was commonly dysregulated in 4 tissues (neuronal and peripheral). Characterising the role of this protein may reveal a conserved, systemic pathomechanism of *FUS* mutations. GO terms related to the mitochondria were significantly enriched in the brain and TA muscle, and this may underline metabolic alterations seen in these mice. Mitochondrial deficits are thought to underline the skeletal muscle metabolic switch, through the impairment of complex 1 activity and a decline in ATP synthesis (Scaricamazza et al., 2020).

Conservation of *Fus*$^{\Delta 14}$ cognitive, motor and metabolic phenotypes with other NLS *Fus* mutation mouse models means that RNA-sequencing data should be combined to identify communal FUS pathomechanisms. This has already been conducted using *Fus*$^{\Delta 14}$ spinal cords from E17.5 mouse embryos compared to other NLS *Fus* mutations (*Fus*^{P525L} and *Fus*$^{\Delta NLS}$), which revealed a shared NLS mutation effect on autoregulation through intron retention (Humphrey et al., 2020). However, repeating this joint analysis at 9-weeks will assess splicing in depth in an adult stage mouse. Comparisons can also be made with other ALS gene mutations, e.g., *Tardbp* and *Sod1*, to reveal communal disease effects. These findings may reveal broader pathomechanisms that can be targeted to provide a therapeutic benefit to a wider population group. The widespread effects of the *Fus*$^{\Delta 14}$ mutation will hopefully encourage other researchers to conduct RNA-sequencing on tissues beyond neuronal and muscle, allowing systemic comparisons to be made. The full transcriptomic dataset (DEGs from each tissue) is available in **Appendix A** and will be readily available for other researchers after the paper publication.

The extent of brain structure alterations remains unknown in both mutant lines. Brain structure was assessed in *Fus*$^{\Delta 14}$ mice via simple measurements. Structural MRI scans will give a more in-depth analysis of the anatomical properties as specific brain region volumes can be calculated. Structural MRI scans were conducted on the brains of *Tardbp*^{M323K} mice at 3 and 12-months. The datasets from each time-point need to be combined for age-related analysis to identify any progressive changes. This work is currently being done by Aurea Martins Bach (Wellcome Centre for Integrative Neuroimaging, Oxford).

The majority of experiments were done on a F1 hybrid background. Additional experiments are needed to understand the genetic background and mutation interactions, e.g., additional characterisation and identifying modifier genes. However, both mutations share molecular and behavioural phenotypes with other related mutations, e.g., comparable effects between *Fus*$^{\Delta 14}$ and other NLS mutations, as well as between *Tardbp*^{M323K} and *Tardbp*^{Q331K} mutations. This demonstrates good reproducibility in physiological models. However, data interpretations should always consider genetic backgrounds and the endogenous traits of inbred strains should be take into account in the selection process of new studies. Going forward, additional measures need to be taken to improve reproducibility and translatability of mouse research, e.g., increasing genetic and experimental heterogeneity.

Currently, the diet study is incomplete. The experiments conducted in this project are part of a larger, on-going study. As a result, additional work and analysis is needed to fully understand how diet modulates ALS-FTD phenotypes. Additional motor and cognitive phenotype readouts are needed to understand the extent of diet modulation. Molecular characterisation experiments will determine diet's effects on TDP-43 pathology, e.g., mislocalisation, aggregate formation and splicing effects of the mutation. Plasma and tissue lipidomic experiments will be conducted on mice from all diets (standard chow, LFD and HFD) to identify candidate pathways. These experiments will be conducted by the Corrochano group.

6.3 Concluding remarks

Through the characterisation of physiological mouse models, this project demonstrated that *FUS* and *TARDBP* mutations caused systemic pathological effects. Some of these peripheral pathomechanisms significantly influenced disease aetiology. For example, muscle metabolic reprogramming. Within the ALS-FTD field, this opens up a whole new area of possible therapeutic targets that will hopefully bring us closer to finding a cure for these diseases, as well as methods to modify disease progression and phenotypes. Data from this project supports the growing view that NDDs are multi-system disorders therefore future research should always focus on the pleiotropic effects of mutations.

Characterisation of these models identified additional significant discoveries. Protein inclusions and other pathological changes associated with traditional proteinopathies are not vital in early disease mechanisms. Both mutations produced significant widespread effects through alterations in RNA-processing. The *Tardbp*^{M323K} homozygous mouse modelled ALS-FTD, while the *Fus*$^{\Delta 14}$ homozygous mouse modelled aspects of jALS. The construct and face validity of these models support their use to study disease related mechanisms, as well as tools to investigate biomarkers and novel treatments. Sex and genetic background interactions with mutations highlighted ways to improve the translatability of mouse research, e.g., the need to include both sexes in studies and the importance of strain selection.

This thesis challenged current paradigms in the quest to better understand the pathological mechanisms underpinning ALS-FTD spectrum disorders. The hope is

that future researchers will build on this knowledge to bring us closer to finding cures for these devastating diseases.

References

7 References

Abe, K., Aoki, M., Tsuji, S., Itoyama, Y., Sobue, G., Togo, M., Hamada, C., Tanaka, M., Akimoto, M., Nakamura, K., Takahashi, F., Kondo, K., Yoshino, H., Abe, K., Aoki, M., Tsuji, S., Itoyama, Y., Sobue, G., Togo, M., . . . Yoshino, H. (2017). Safety and efficacy of edaravone in well defined patients with amyotrophic lateral sclerosis: a randomised, double-blind, placebo-controlled trial. *The Lancet Neurology*, *16*(7), 505-512. https://doi.org/https://doi.org/10.1016/S1474-4422(17)30115-1

Abramzon, Y. A., Fratta, P., Traynor, B. J., & Chia, R. (2020). The Overlapping Genetics of Amyotrophic Lateral Sclerosis and Frontotemporal Dementia [Review]. *Frontiers in Neuroscience*, *14*. https://doi.org/10.3389/fnins.2020.00042

Acevedo-Arozena, A., Kalmar, B., Essa, S., Ricketts, T., Joyce, P., Kent, R., Rowe, C., Parker, A., Gray, A., Hafezparast, M., Thorpe, J. R., Greensmith, L., & Fisher, E. M. (2011). A comprehensive assessment of the SOD1G93A low-copy transgenic mouse, which models human amyotrophic lateral sclerosis. *Dis Model Mech*, *4*(5), 686-700. https://doi.org/10.1242/dmm.007237

Acevedo-Arozena, A., Wells, S., Potter, P., Kelly, M., Cox, R. D., & Brown, S. D. (2008). ENU mutagenesis, a way forward to understand gene function. *Annu Rev Genomics Hum Genet*, *9*, 49-69. https://doi.org/10.1146/annurev.genom.9.081307.164224

Agosta, F., Valsasina, P., Riva, N., Copetti, M., Messina, M. J., Prelle, A., Comi, G., & Filippi, M. (2012). The cortical signature of amyotrophic lateral sclerosis. *PLoS One*, *7*(8), e42816. https://doi.org/10.1371/journal.pone.0042816

Ahmed, R. M. (2021). Metabolism in frontotemporal dementia. *Alzheimer's & Dementia*, *17*(S6), e055309. https://doi.org/https://doi.org/10.1002/alz.055309

Ahmed, R. M., Highton-Williamson, E., Caga, J., Thornton, N., Ramsey, E., Zoing, M., Kim, W. S., Halliday, G. M., Piguet, O., Hodges, J. R., Farooqi, I. S., & Kiernan, M. C. (2018). Lipid Metabolism and Survival Across the Frontotemporal Dementia-Amyotrophic Lateral Sclerosis Spectrum: Relationships to Eating Behavior and Cognition. *Journal of Alzheimer's Disease*, *61*, 773-783. https://doi.org/10.3233/JAD-170660

Ahmed, R. M., Irish, M., Henning, E., Dermody, N., Bartley, L., Kiernan, M. C., Piguet, O., Farooqi, S., & Hodges, J. R. (2016). Assessment of Eating Behavior Disturbance and Associated Neural Networks in Frontotemporal Dementia. *JAMA Neurol*, *73*(3), 282-290. https://doi.org/10.1001/jamaneurol.2015.4478

Ahmed, R. M., Irish, M., Piguet, O., Halliday, G. M., Ittner, L. M., Farooqi, S., Hodges, J. R., & Kiernan, M. C. (2016). Amyotrophic lateral sclerosis and frontotemporal dementia: distinct and overlapping changes in eating behaviour and metabolism. *The Lancet. Neurology*, *15*(3), 332-342. https://doi.org/10.1016/s1474-4422(15)00380-4

Ahmed, R. M., Irish, M., van Eersel, J., Ittner, A., Ke, Y. D., Volkerling, A., van der Hoven, J., Tanaka, K., Karl, T., Kassiou, M., Kril, J. J., Piguet, O., Götz, J., Kiernan, M. C., Halliday, G. M., Hodges, J. R., & Ittner, L. M. (2017). Mouse models of frontotemporal dementia: A comparison of phenotypes with clinical symptomatology. *Neuroscience & Biobehavioral Reviews*, *74*, 126-138. https://doi.org/https://doi.org/10.1016/j.neubiorev.2017.01.004

Ahmed, R. M., Landin-Romero, R., Liang, C. T., Keogh, J. M., Henning, E., Strikwerda-Brown, C., Devenney, E. M., Hodges, J. R., Kiernan, M. C., Farooqi, I. S., & Piguet, O. (2019). Neural

networks associated with body composition in frontotemporal dementia. *Ann Clin Transl Neurol*, *6*(9), 1707-1717. https://doi.org/10.1002/acn3.50869

Ahmed, R. M., Mioshi, E., Caga, J., Shibata, M., Zoing, M., Bartley, L., Piguet, O., Hodges, J. R., & Kiernan, M. C. (2014). Body mass index delineates ALS from FTD: implications for metabolic health. *J Neurol*, *261*(9), 1774-1780. https://doi.org/10.1007/s00415-014-7416-6

Al-Obeidi, E., Al-Tahan, S., Surampalli, A., Goyal, N., Wang, A. K., Hermann, A., Omizo, M., Smith, C., Mozaffar, T., & Kimonis, V. (2018). Genotype-phenotype study in patients with valosin-containing protein mutations associated with multisystem proteinopathy. *Clin Genet*, *93*(1), 119-125. https://doi.org/10.1111/cge.13095

Alexander, G. M., Erwin, K. L., Byers, N., Deitch, J. S., Augelli, B. J., Blankenhorn, E. P., & Heiman-Patterson, T. D. (2004). Effect of transgene copy number on survival in the G93A SOD1 transgenic mouse model of ALS. *Brain Res Mol Brain Res*, *130*(1-2), 7-15. https://doi.org/10.1016/j.molbrainres.2004.07.002

Amador-Ortiz, C., Lin, W. L., Ahmed, Z., Personett, D., Davies, P., Duara, R., Graff-Radford, N. R., Hutton, M. L., & Dickson, D. W. (2007). TDP-43 immunoreactivity in hippocampal sclerosis and Alzheimer's disease. *Ann Neurol*, *61*(5), 435-445. https://doi.org/10.1002/ana.21154

Andersen, P. M. (2006). Amyotrophic lateral sclerosis associated with mutations in the CuZn superoxide dismutase gene. *Curr Neurol Neurosci Rep*, *6*(1), 37-46. https://doi.org/10.1007/s11910-996-0008-9

Anderson, P., & Kedersha, N. (2009). RNA granules: post-transcriptional and epigenetic modulators of gene expression. *Nature Reviews Molecular Cell Biology*, *10*(6), 430-436. https://doi.org/10.1038/nrm2694

Arevalo, M.-A., Azcoitia, I., & Garcia-Segura, L. M. (2015). The neuroprotective actions of oestradiol and oestrogen receptors. *Nature Reviews Neuroscience*, *16*(1), 17-29. https://doi.org/10.1038/nrn3856

Arnold, E. S., Ling, S. C., Huelga, S. C., Lagier-Tourenne, C., Polymenidou, M., Ditsworth, D., Kordasiewicz, H. B., McAlonis-Downes, M., Platoshyn, O., Parone, P. A., Da Cruz, S., Clutario, K. M., Swing, D., Tessarollo, L., Marsala, M., Shaw, C. E., Yeo, G. W., & Cleveland, D. W. (2013). ALS-linked TDP-43 mutations produce aberrant RNA splicing and adult-onset motor neuron disease without aggregation or loss of nuclear TDP-43. *Proc Natl Acad Sci U S A*, *110*(8), E736-745. https://doi.org/10.1073/pnas.1222809110

Ashrafian, H., Harling, L., Darzi, A., & Athanasiou, T. (2013). Neurodegenerative disease and obesity: what is the role of weight loss and bariatric interventions? *Metabolic Brain Disease*, *28*(3), 341-353. https://doi.org/10.1007/s11011-013-9412-4

Ayala, Y. M., De Conti, L., Avendaño-Vázquez, S. E., Dhir, A., Romano, M., D'Ambrogio, A., Tollervey, J., Ule, J., Baralle, M., Buratti, E., & Baralle, F. E. (2011). TDP-43 regulates its mRNA levels through a negative feedback loop. *EMBO J*, *30*(2), 277-288. https://doi.org/10.1038/emboj.2010.310

Ayala, Y. M., Zago, P., D'Ambrogio, A., Xu, Y. F., Petrucelli, L., Buratti, E., & Baralle, F. E. (2008). Structural determinants of the cellular localization and shuttling of TDP-43. *J Cell Sci*, *121*(Pt 22), 3778-3785. https://doi.org/10.1242/jcs.038950

Baltadzhieva, R., Gurevich, T., & Korczyn, A. D. (2005). Autonomic impairment in amyotrophic lateral sclerosis. *Curr Opin Neurol*, *18*(5), 487-493. https://doi.org/10.1097/01.wco.0000183114.76056.0e

Bannwarth, S., Ait-El-Mkadem, S., Chaussenot, A., Genin, E. C., Lacas-Gervais, S., Fragaki, K., Berg-Alonso, L., Kageyama, Y., Serre, V., Moore, D. G., Verschueren, A., Rouzier, C., Le Ber, I., Augé, G., Cochaud, C., Lespinasse, F., N'Guyen, K., de Septenville, A., Brice, A., . . . Paquis-Flucklinger, V. (2014). A mitochondrial origin for frontotemporal dementia and amyotrophic lateral sclerosis through CHCHD10 involvement. *Brain*, *137*(Pt 8), 2329-2345. https://doi.org/10.1093/brain/awu138

Barnat, M., Capizzi, M., Aparicio, E., Boluda, S., Wennagel, D., Kacher, R., Kassem, R., Lenoir, S., Agasse, F., Braz, B. Y., Liu, J. P., Ighil, J., Tessier, A., Zeitlin, S. O., Duyckaerts, C., Dommergues, M., Durr, A., & Humbert, S. (2020). Huntington's disease alters human neurodevelopment. *Science*, *369*(6505), 787-793. https://doi.org/10.1126/science.aax3338

Baskin, Kedryn K., Winders, Benjamin R., & Olson, Eric N. (2015). Muscle as a "Mediator" of Systemic Metabolism. *Cell Metabolism*, *21*(2), 237-248. https://doi.org/https://doi.org/10.1016/j.cmet.2014.12.021

Bäumer, D., Hilton, D., Paine, S. M., Turner, M. R., Lowe, J., Talbot, K., & Ansorge, O. (2010). Juvenile ALS with basophilic inclusions is a FUS proteinopathy with FUS mutations. *Neurology*, *75*(7), 611-618. https://doi.org/10.1212/WNL.0b013e3181ed9cde

Bayer, D., Antonucci, S., Müller, H. P., Saad, R., Dupuis, L., Rasche, V., Böckers, T. M., Ludolph, A. C., Kassubek, J., & Roselli, F. (2021). Disruption of orbitofrontal-hypothalamic projections in a murine ALS model and in human patients. *Transl Neurodegener*, *10*(1), 17. https://doi.org/10.1186/s40035-021-00241-6

Beck, J., Lloyd, S., Hafezparast, M., Lennon-Pierce, M., Eppig, J., Festing, M., & Fisher, E. (2000). Genealogies of mouse inbred strains. *Nature genetics*, *24*, 23-25. https://doi.org/10.1038/71641

Beck, J., Poulter, M., Hensman, D., Rohrer, J. D., Mahoney, C. J., Adamson, G., Campbell, T., Uphill, J., Borg, A., Fratta, P., Orrell, R. W., Malaspina, A., Rowe, J., Brown, J., Hodges, J., Sidle, K., Polke, J. M., Houlden, H., Schott, J. M., . . . Mead, S. (2013). Large C9orf72 hexanucleotide repeat expansions are seen in multiple neurodegenerative syndromes and are more frequent than expected in the UK population. *Am J Hum Genet*, *92*(3), 345-353. https://doi.org/10.1016/j.ajhg.2013.01.011

Beery, A. K., & Zucker, I. (2011). Sex bias in neuroscience and biomedical research. *Neurosci Biobehav Rev*, *35*(3), 565-572. https://doi.org/10.1016/j.neubiorev.2010.07.002

Bensimon, G., Lacomblez, L., & Meininger, V. (1994). A controlled trial of riluzole in amyotrophic lateral sclerosis. ALS/Riluzole Study Group. *N Engl J Med*, *330*(9), 585-591. https://doi.org/10.1056/nejm199403033300901

Benson, B. C., Shaw, P. J., Azzouz, M., Highley, J. R., & Hautbergue, G. M. (2021). Proteinopathies as Hallmarks of Impaired Gene Expression, Proteostasis and Mitochondrial Function in Amyotrophic Lateral Sclerosis. *Front Neurosci*, *15*, 783624. https://doi.org/10.3389/fnins.2021.783624

Bertolotti, A., Lutz, Y., Heard, D. J., Chambon, P., & Tora, L. (1996). hTAF(II)68, a novel RNA/ssDNA-binding protein with homology to the pro-oncoproteins TLS/FUS and EWS is associated with both TFIID and RNA polymerase II. *EMBO J*, *15*(18), 5022-5031.

Birsa, N., Bentham, M. P., & Fratta, P. (2020). Cytoplasmic functions of TDP-43 and FUS and their role in ALS. *Seminars in Cell & Developmental Biology*, *99*, 193-201. https://doi.org/https://doi.org/10.1016/j.semcdb.2019.05.023

Boeynaems, S., Alberti, S., Fawzi, N. L., Mittag, T., Polymenidou, M., Rousseau, F., Schymkowitz, J., Shorter, J., Wolozin, B., Van Den Bosch, L., Tompa, P., & Fuxreiter, M. (2018). Protein Phase Separation: A New Phase in Cell Biology. *Trends Cell Biol*, *28*(6), 420-435. https://doi.org/10.1016/j.tcb.2018.02.004

Bott, N. T., Radke, A., Stephens, M. L., & Kramer, J. H. (2014). Frontotemporal dementia: diagnosis, deficits and management. *Neurodegener Dis Manag*, *4*(6), 439-454. https://doi.org/10.2217/nmt.14.34

Brooks, B. R., Miller, R. G., Swash, M., & Munsat, T. L. (2000). El Escorial revisited: revised criteria for the diagnosis of amyotrophic lateral sclerosis. *Amyotroph Lateral Scler Other Motor Neuron Disord*, *1*(5), 293-299. https://doi.org/10.1080/146608200300079536

Brown, A.-L., Wilkins, O. G., Keuss, M. J., Hill, S. E., Zanovello, M., Lee, W. C., Bampton, A., Lee, F. C. Y., Masino, L., Qi, Y. A., Bryce-Smith, S., Gatt, A., Hallegger, M., Fagegaltier, D., Phatnani, H., Phatnani, H., Kwan, J., Sareen, D., Broach, J. R., . . . Consortium, N. A. (2022). TDP-43 loss and ALS-risk SNPs drive mis-splicing and depletion of UNC13A. *Nature*, *603*(7899), 131-137. https://doi.org/10.1038/s41586-022-04436-3

Brown, A.-L., Wilkins, O. G., Keuss, M. J., Hill, S. E., Zanovello, M., Lee, W. C., Lee, F. C. Y., Masino, L., Qi, Y. A., Bryce-Smith, S., Bampton, A., Gatt, A., Phatnani, H., Schiavo, G., Fisher, E. M. C., Raj, T., Secrier, M., Lashley, T., Ule, J., . . . Fratta, P. (2021). Common ALS/FTD risk variants in UNC13A exacerbate its cryptic splicing and loss upon TDP-43 mislocalization. *bioRxiv*, 2021.2004.2002.438170. https://doi.org/10.1101/2021.04.02.438170

Bryda, E. C. (2013). The Mighty Mouse: the impact of rodents on advances in biomedical research. *Mo Med*, *110*(3), 207-211.

Buratti, E., Dörk, T., Zuccato, E., Pagani, F., Romano, M., & Baralle, F. E. (2001). Nuclear factor TDP-43 and SR proteins promote in vitro and in vivo CFTR exon 9 skipping. *EMBO J*, *20*(7), 1774-1784. https://doi.org/10.1093/emboj/20.7.1774

Burrell, J. R., Kiernan, M. C., Vucic, S., & Hodges, J. R. (2011). Motor neuron dysfunction in frontotemporal dementia. *Brain*, *134*(Pt 9), 2582-2594. https://doi.org/10.1093/brain/awr195

Carey, J. L., & Guo, L. (2022). Liquid-Liquid Phase Separation of TDP-43 and FUS in Physiology and Pathology of Neurodegenerative Diseases [Review]. *Frontiers in Molecular Biosciences*, *9*. https://doi.org/10.3389/fmolb.2022.826719

Chang, A., Xiang, X., Wang, J., Lee, C., Arakhamia, T., Simjanoska, M., Wang, C., Carlomagno, Y., Zhang, G., Dhingra, S., Thierry, M., Perneel, J., Heeman, B., Forgrave, L. M., DeTure, M., DeMarco, M. L., Cook, C. N., Rademakers, R., Dickson, D. W., . . . Fitzpatrick, A. W. P. (2022). Homotypic fibrillization of TMEM106B across diverse neurodegenerative diseases. *Cell*, *185*(8), 1346-1355.e1315. https://doi.org/https://doi.org/10.1016/j.cell.2022.02.026

Chang, C. Y., Ting, H. C., Liu, C. A., Su, H. L., Chiou, T. W., Lin, S. Z., Harn, H. J., & Ho, T. J. (2020). Induced Pluripotent Stem Cell (iPSC)-Based Neurodegenerative Disease Models for Phenotype Recapitulation and Drug Screening. *Molecules*, *25*(8). https://doi.org/10.3390/molecules25082000

Charcot, J.-M. (1965). Sclerose des cordons lateraux de la moelle epinere chez femmehysterique atteinte de contracture peranemte des quatre membres. *Bull Soc Med Hop Paris*, *2*(2), 24.

Chebib, J., Jackson, B. C., López-Cortegano, E., Tautz, D., & Keightley, P. D. (2021). Inbred lab mice are not isogenic: genetic variation within inbred strains used to infer the mutation rate per nucleotide site. *Heredity*, *126*(1), 107-116. https://doi.org/10.1038/s41437-020-00361-1

Chen, S., Sayana, P., Zhang, X., & Le, W. (2013). Genetics of amyotrophic lateral sclerosis: an update. *Molecular Neurodegeneration*, *8*(1), 28. https://doi.org/10.1186/1750-1326-8-28

Chien, H. M., Lee, C. C., & Huang, J. J. (2021). The Different Faces of the TDP-43 Low-Complexity Domain: The Formation of Liquid Droplets and Amyloid Fibrils. *Int J Mol Sci*, *22*(15). https://doi.org/10.3390/ijms22158213

Chiò, A., Logroscino, G., Traynor, B. J., Collins, J., Simeone, J. C., Goldstein, L. A., & White, L. A. (2013). Global epidemiology of amyotrophic lateral sclerosis: a systematic review of the published literature. *Neuroepidemiology*, *41*(2), 118-130. https://doi.org/10.1159/000351153

Choi, C. I., Lee, Y. D., Gwag, B. J., Cho, S. I., Kim, S. S., & Suh-Kim, H. (2008). Effects of estrogen on lifespan and motor functions in female hSOD1 G93A transgenic mice. *J Neurol Sci*, *268*(1-2), 40-47. https://doi.org/10.1016/j.jns.2007.10.024

Christidi, F., Karavasilis, E., Velonakis, G., Ferentinos, P., Rentzos, M., Kelekis, N., Evdokimidis, I., & Bede, P. (2018). The Clinical and Radiological Spectrum of Hippocampal Pathology in Amyotrophic Lateral Sclerosis. *Front Neurol*, *9*, 523. https://doi.org/10.3389/fneur.2018.00523

Chung, C. G., Lee, H., & Lee, S. B. (2018). Mechanisms of protein toxicity in neurodegenerative diseases. *Cell Mol Life Sci*, *75*(17), 3159-3180. https://doi.org/10.1007/s00018-018-2854-4

Colombrita, C., Onesto, E., Megiorni, F., Pizzuti, A., Baralle, F. E., Buratti, E., Silani, V., & Ratti, A. (2012). TDP-43 and FUS RNA-binding proteins bind distinct sets of cytoplasmic messenger RNAs and differently regulate their post-transcriptional fate in motoneuron-like cells. *J Biol Chem*, *287*(19), 15635-15647. https://doi.org/10.1074/jbc.M111.333450

Convery, R., Mead, S., & Rohrer, J. D. (2019). Review: Clinical, genetic and neuroimaging features of frontotemporal dementia [https://doi.org/10.1111/nan.12535]. *Neuropathology and Applied Neurobiology*, *45*(1), 6-18. https://doi.org/https://doi.org/10.1111/nan.12535

Costantini, L. C., Barr, L. J., Vogel, J. L., & Henderson, S. T. (2008). Hypometabolism as a therapeutic target in Alzheimer's disease. *BMC Neurosci*, *9 Suppl 2*(Suppl 2), S16. https://doi.org/10.1186/1471-2202-9-s2-s16

Crawley, J. N. (1985). Exploratory behavior models of anxiety in mice. *Neurosci Biobehav Rev*, *9*(1), 37-44. https://doi.org/10.1016/0149-7634(85)90030-2

Crawley, J. N., Belknap, J. K., Collins, A., Crabbe, J. C., Frankel, W., Henderson, N., Hitzemann, R. J., Maxson, S. C., Miner, L. L., Silva, A. J., Wehner, J. M., Wynshaw-Boris, A., & Paylor, R. (1997). Behavioral phenotypes of inbred mouse strains: implications and recommendations for molecular studies. *Psychopharmacology*, *132*(2), 107-124. https://doi.org/10.1007/s002130050327

Crown, A., McAlary, L., Fagerli, E., Brown, H., Yerbury, J. J., Galaleldeen, A., Cashman, N. R., Borchelt, D. R., & Ayers, J. I. (2020). Tryptophan residue 32 in human Cu-Zn superoxide

dismutase modulates prion-like propagation and strain selection. *PLoS One*, *15*(1), e0227655. https://doi.org/10.1371/journal.pone.0227655

Cruts, M., Gijselinck, I., van der Zee, J., Engelborghs, S., Wils, H., Pirici, D., Rademakers, R., Vandenberghe, R., Dermaut, B., Martin, J. J., van Duijn, C., Peeters, K., Sciot, R., Santens, P., De Pooter, T., Mattheijssens, M., Van den Broeck, M., Cuijt, I., Vennekens, K., . . . Van Broeckhoven, C. (2006). Null mutations in progranulin cause ubiquitin-positive frontotemporal dementia linked to chromosome 17q21. *Nature*, *442*(7105), 920-924. https://doi.org/10.1038/nature05017

D'Ovidio, F., d'Errico, A., Carnà, P., Calvo, A., Costa, G., & Chiò, A. (2018). The role of pre-morbid diabetes on developing amyotrophic lateral sclerosis. *Eur J Neurol*, *25*(1), 164-170. https://doi.org/10.1111/ene.13465

Da Cruz, S., & Cleveland, D. W. (2011). Understanding the role of TDP-43 and FUS/TLS in ALS and beyond. *Curr Opin Neurobiol*, *21*(6), 904-919. https://doi.org/10.1016/j.conb.2011.05.029

Dadon-Nachum, M., Melamed, E., & Offen, D. (2011). The "Dying-Back" Phenomenon of Motor Neurons in ALS. *Journal of Molecular Neuroscience*, *43*(3), 470-477. https://doi.org/10.1007/s12031-010-9467-1

Davidson, Y., Kelley, T., Mackenzie, I. R., Pickering-Brown, S., Du Plessis, D., Neary, D., Snowden, J. S., & Mann, D. M. (2007). Ubiquitinated pathological lesions in frontotemporal lobar degeneration contain the TAR DNA-binding protein, TDP-43. *Acta Neuropathol*, *113*(5), 521-533. https://doi.org/10.1007/s00401-006-0189-y

de Boer, E. M. J., Orie, V. K., Williams, T., Baker, M. R., De Oliveira, H. M., Polvikoski, T., Silsby, M., Menon, P., van den Bos, M., Halliday, G. M., van den Berg, L. H., Van Den Bosch, L., van Damme, P., Kiernan, M. C., van Es, M. A., & Vucic, S. (2021). TDP-43 proteinopathies: a new wave of neurodegenerative diseases. *Journal of Neurology, Neurosurgery & Psychiatry*, *92*(1), 86. https://doi.org/10.1136/jnnp-2020-322983

De Giorgio, F., Maduro, C., Fisher, E. M. C., & Acevedo-Arozena, A. (2019). Transgenic and physiological mouse models give insights into different aspects of amyotrophic lateral sclerosis. *Dis Model Mech*, *12*(1). https://doi.org/10.1242/dmm.037424

Deacon, R. M. (2006). Assessing nest building in mice. *Nat Protoc*, *1*(3), 1117-1119. https://doi.org/10.1038/nprot.2006.170

Deacon, R. M. J. (2006). Digging and marble burying in mice: simple methods for in vivo identification of biological impacts. *Nature Protocols*, *1*(1), 122-124. https://doi.org/10.1038/nprot.2006.20

Deacon, R. M. J., Croucher, A., & Rawlins, J. N. P. (2002). Hippocampal cytotoxic lesion effects on species-typical behaviours in mice. *Behavioural Brain Research*, *132*(2), 203-213. https://doi.org/https://doi.org/10.1016/S0166-4328(01)00401-6

DeJesus-Hernandez, M., Mackenzie, I. R., Boeve, B. F., Boxer, A. L., Baker, M., Rutherford, N. J., Nicholson, A. M., Finch, N. A., Flynn, H., Adamson, J., Kouri, N., Wojtas, A., Sengdy, P., Hsiung, G. Y., Karydas, A., Seeley, W. W., Josephs, K. A., Coppola, G., Geschwind, D. H., . . . Rademakers, R. (2011). Expanded GGGGCC hexanucleotide repeat in noncoding region of C9ORF72 causes chromosome 9p-linked FTD and ALS. *Neuron*, *72*(2), 245-256. https://doi.org/10.1016/j.neuron.2011.09.011

Deng, H., Gao, K., & Jankovic, J. (2014). The role of FUS gene variants in neurodegenerative diseases. *Nature Reviews Neurology*, *10*(6), 337-348. https://doi.org/10.1038/nrneurol.2014.78

Deng, H. X., Chen, W., Hong, S. T., Boycott, K. M., Gorrie, G. H., Siddique, N., Yang, Y., Fecto, F., Shi, Y., Zhai, H., Jiang, H., Hirano, M., Rampersaud, E., Jansen, G. H., Donkervoort, S., Bigio, E. H., Brooks, B. R., Ajroud, K., Sufit, R. L., . . . Siddique, T. (2011). Mutations in UBQLN2 cause dominant X-linked juvenile and adult-onset ALS and ALS/dementia. *Nature*, *477*(7363), 211-215. https://doi.org/10.1038/nature10353

Desai, J., & Swash, M. (1999). Extrapyramidal involvement in amyotrophic lateral sclerosis: backward falls and retropulsion. *J Neurol Neurosurg Psychiatry*, *67*(2), 214-216. https://doi.org/10.1136/jnnp.67.2.214

Desport, J.-C., Torny, F., Lacoste, M., Preux, P.-M., & Couratier, P. (2005). Hypermetabolism in ALS: correlations with clinical and paraclinical parameters. *Neurodegenerative Diseases*, *2*(3-4), 202-207.

Desport, J. C., Preux, P. M., Truong, T. C., Vallat, J. M., Sautereau, D., & Couratier, P. (1999). Nutritional status is a prognostic factor for survival in ALS patients. *Neurology*, *53*(5), 1059-1063. https://doi.org/10.1212/wnl.53.5.1059

Devoy, A., Kalmar, B., Stewart, M., Park, H., Burke, B., Noy, S. J., Redhead, Y., Humphrey, J., Lo, K., Jaeger, J., Mejia Maza, A., Sivakumar, P., Bertolin, C., Soraru, G., Plagnol, V., Greensmith, L., Acevedo Arozena, A., Isaacs, A. M., Davies, B., . . . Fisher, E. M. C. (2017). Humanized mutant FUS drives progressive motor neuron degeneration without aggregation in 'FUSDelta14' knockin mice. *Brain*, *140*(11), 2797-2805. https://doi.org/10.1093/brain/awx248

Devoy, A., Price, G., De Giorgio, F., Bunton-Stasyshyn, R., Thompson, D., Gasco, S., Allan, A., Codner, G. F., Nair, R. R., Tibbit, C., McLeod, R., Ali, Z., Noda, J., Marrero-Gagliardi, A., Brito-Armas, J. M., Williams, C., Öztürk, M. M., Simon, M., O'Neill, E., . . . Cunningham, T. J. (2021). Generation and analysis of innovative genomically humanized knockin SOD1, TARDBP (TDP-43), and FUS mouse models. *iScience*, *24*(12), 103463. https://doi.org/https://doi.org/10.1016/j.isci.2021.103463

Diehl-Schmid, J., Grimmer, T., Drzezga, A., Bornschein, S., Perneczky, R., Forstl, H., Schwaiger, M., & Kurz, A. (2006). Longitudinal changes of cerebral glucose metabolism in semantic dementia. *Dement Geriatr Cogn Disord*, *22*(4), 346-351. https://doi.org/10.1159/000095624

DiSabato, D. J., Quan, N., & Godbout, J. P. (2016). Neuroinflammation: the devil is in the details. *J Neurochem*, *139 Suppl 2*(Suppl 2), 136-153. https://doi.org/10.1111/jnc.13607

Dorst, J., Kühnlein, P., Hendrich, C., Kassubek, J., Sperfeld, A. D., & Ludolph, A. C. (2011). Patients with elevated triglyceride and cholesterol serum levels have a prolonged survival in amyotrophic lateral sclerosis. *J Neurol*, *258*(4), 613-617. https://doi.org/10.1007/s00415-010-5805-z

Doudna, J. A., & Charpentier, E. (2014). The new frontier of genome engineering with CRISPR-Cas9. *Science*, *346*(6213), 1258096. https://doi.org/doi:10.1126/science.1258096

Duffy, C. M., Hofmeister, J. J., Nixon, J. P., & Butterick, T. A. (2019). High fat diet increases cognitive decline and neuroinflammation in a model of orexin loss. *Neurobiol Learn Mem*, *157*, 41-47. https://doi.org/10.1016/j.nlm.2018.11.008

Dupuis, L., Corcia, P., Fergani, A., Gonzalez De Aguilar, J. L., Bonnefont-Rousselot, D., Bittar, R., Seilhean, D., Hauw, J. J., Lacomblez, L., Loeffler, J. P., & Meininger, V. (2008). Dyslipidemia is a protective factor in amyotrophic lateral sclerosis. *Neurology*, *70*(13), 1004-1009. https://doi.org/10.1212/01.wnl.0000285080.70324.27

Dupuis, L., Oudart, H., René, F., Gonzalez de Aguilar, J. L., & Loeffler, J. P. (2004). Evidence for defective energy homeostasis in amyotrophic lateral sclerosis: benefit of a high-energy diet in a transgenic mouse model. *Proc Natl Acad Sci U S A*, *101*(30), 11159-11164. https://doi.org/10.1073/pnas.0402026101

Dupuis, L., Pradat, P.-F., Ludolph, A. C., & Loeffler, J.-P. (2011). Energy metabolism in amyotrophic lateral sclerosis. *The Lancet. Neurology*, *10*(1), 75-82. https://doi.org/10.1016/s1474-4422(10)70224-6

Efimova, A. D., Ovchinnikov, R. K., Roman, A. Y., Maltsev, A. V., Grigoriev, V. V., Kovrazhkina, E. A., & Skvortsova, V. I. (2017). The FUS protein: Physiological functions and a role in amyotrophic lateral sclerosis. *Molecular Biology*, *51*(3), 341-351. https://doi.org/10.1134/S0026893317020091

Elden, A. C., Kim, H. J., Hart, M. P., Chen-Plotkin, A. S., Johnson, B. S., Fang, X., Armakola, M., Geser, F., Greene, R., Lu, M. M., Padmanabhan, A., Clay-Falcone, D., McCluskey, L., Elman, L., Juhr, D., Gruber, P. J., Rüb, U., Auburger, G., Trojanowski, J. Q., . . . Gitler, A. D. (2010). Ataxin-2 intermediate-length polyglutamine expansions are associated with increased risk for ALS. *Nature*, *466*(7310), 1069-1075. https://doi.org/10.1038/nature09320

Emmerzaal, T. L., Kiliaan, A. J., & Gustafson, D. R. (2015). 2003-2013: a decade of body mass index, Alzheimer's disease, and dementia. *J Alzheimers Dis*, *43*(3), 739-755. https://doi.org/10.3233/jad-141086

Erickson, R. P. (1996). Mouse models of human genetic disease: which mouse is more like a man? *Bioessays*, *18*(12), 993-998. https://doi.org/10.1002/bies.950181209

Fecto, F., Yan, J., Vemula, S. P., Liu, E., Yang, Y., Chen, W., Zheng, J. G., Shi, Y., Siddique, N., Arrat, H., Donkervoort, S., Ajroud-Driss, S., Sufit, R. L., Heller, S. L., Deng, H. X., & Siddique, T. (2011). SQSTM1 mutations in familial and sporadic amyotrophic lateral sclerosis. *Arch Neurol*, *68*(11), 1440-1446. https://doi.org/10.1001/archneurol.2011.250

Fiesel, F. C., Voigt, A., Weber, S. S., Van den Haute, C., Waldenmaier, A., Görner, K., Walter, M., Anderson, M. L., Kern, J. V., Rasse, T. M., Schmidt, T., Springer, W., Kirchner, R., Bonin, M., Neumann, M., Baekelandt, V., Alunni-Fabbroni, M., Schulz, J. B., & Kahle, P. J. (2010). Knockdown of transactive response DNA-binding protein (TDP-43) downregulates histone deacetylase 6. *EMBO J*, *29*(1), 209-221. https://doi.org/10.1038/emboj.2009.324

Fiorillo, C., Astrea, G., Savarese, M., Cassandrini, D., Brisca, G., Trucco, F., Pedemonte, M., Trovato, R., Ruggiero, L., Vercelli, L., D'Amico, A., Tasca, G., Pane, M., Fanin, M., Bello, L., Broda, P., Musumeci, O., Rodolico, C., Messina, S., . . . on behalf of the Italian Network on Congenital, M. (2016). MYH7-related myopathies: clinical, histopathological and imaging findings in a cohort of Italian patients. *Orphanet Journal of Rare Diseases*, *11*(1), 91. https://doi.org/10.1186/s13023-016-0476-1

Fischer, L. R., Culver, D. G., Tennant, P., Davis, A. A., Wang, M., Castellano-Sanchez, A., Khan, J., Polak, M. A., & Glass, J. D. (2004). Amyotrophic lateral sclerosis is a distal axonopathy: evidence in mice and man. *Experimental Neurology*, *185*(2), 232-240. https://doi.org/https://doi.org/10.1016/j.expneurol.2003.10.004

Floare, M. L., & Allen, S. P. (2020). Why TDP-43? Why Not? Mechanisms of Metabolic Dysfunction in Amyotrophic Lateral Sclerosis. *Neurosci Insights*, *15*, 2633105520957302. https://doi.org/10.1177/2633105520957302

Flurkey, K., Currer, J. M., Leiter, E. H., & Witham, B. (2009). *The Jackson Laboratory handbook on genetically standardized mice* (6th ed.). Jackson Laboratory.

Fratta, P., Sivakumar, P., Humphrey, J., Lo, K., Ricketts, T., Oliveira, H., Brito-Armas, J. M., Kalmar, B., Ule, A., Yu, Y., Birsa, N., Bodo, C., Collins, T., Conicella, A. E., Mejia Maza, A., Marrero-Gagliardi, A., Stewart, M., Mianne, J., Corrochano, S., . . . Acevedo-Arozena, A. (2018). Mice with endogenous TDP-43 mutations exhibit gain of splicing function and characteristics of amyotrophic lateral sclerosis. *EMBO J*, *37*(11). https://doi.org/10.15252/embj.201798684

Freeman, L. R., Haley-Zitlin, V., Rosenberger, D. S., & Granholm, A. C. (2014). Damaging effects of a high-fat diet to the brain and cognition: a review of proposed mechanisms. *Nutr Neurosci*, *17*(6), 241-251. https://doi.org/10.1179/1476830513y.0000000092

Freibaum, B. D., & Taylor, J. P. (2017). The Role of Dipeptide Repeats in C9ORF72-Related ALS-FTD. *Front Mol Neurosci*, *10*, 35. https://doi.org/10.3389/fnmol.2017.00035

Fujii, R., Okabe, S., Urushido, T., Inoue, K., Yoshimura, A., Tachibana, T., Nishikawa, T., Hicks, G. G., & Takumi, T. (2005). The RNA binding protein TLS is translocated to dendritic spines by mGluR5 activation and regulates spine morphology. *Curr Biol*, *15*(6), 587-593. https://doi.org/10.1016/j.cub.2005.01.058

Fujii, R., & Takumi, T. (2005). TLS facilitates transport of mRNA encoding an actin-stabilizing protein to dendritic spines. *J Cell Sci*, *118*(Pt 24), 5755-5765. https://doi.org/10.1242/jcs.02692

Galovic, M., van Dooren, V. Q. H., Postma, T. S., Vos, S. B., Caciagli, L., Borzì, G., Cueva Rosillo, J., Vuong, K. A., de Tisi, J., Nachev, P., Duncan, J. S., & Koepp, M. J. (2019). Progressive Cortical Thinning in Patients With Focal Epilepsy. *JAMA Neurology*, *76*(10), 1230-1239. https://doi.org/10.1001/jamaneurol.2019.1708

Gao, F.-B., Almeida, S., & Lopez-Gonzalez, R. (2017). Dysregulated molecular pathways in amyotrophic lateral sclerosis–frontotemporal dementia spectrum disorder. *The EMBO Journal*, *36*(20), 2931-2950. https://doi.org/https://doi.org/10.15252/embj.201797568

Garrett, L. R., & Niccoli, T. (2022). Frontotemporal Dementia and Glucose Metabolism [Review]. *Frontiers in Neuroscience*, *16*. https://doi.org/10.3389/fnins.2022.812222

Geser, F., Martinez-Lage, M., Robinson, J., Uryu, K., Neumann, M., Brandmeir, N. J., Xie, S. X., Kwong, L. K., Elman, L., McCluskey, L., Clark, C. M., Malunda, J., Miller, B. L., Zimmerman, E. A., Qian, J., Van Deerlin, V., Grossman, M., Lee, V. M., & Trojanowski, J. Q. (2009). Clinical and pathological continuum of multisystem TDP-43 proteinopathies. *Arch Neurol*, *66*(2), 180-189. https://doi.org/10.1001/archneurol.2008.558

Godoy-Corchuelo, J. M., Fernández-Beltrán, L. C., Ali, Z., Gil-Moreno, M. J., López-Carbonero, J. I., Guerrero-Sola, A., Larrad-Sainz, A., Matias-Guiu, J., Matias-Guiu, J. A., Cunningham, T. J., & Corrochano, S. (2022). Lipid Metabolic Alterations in the ALS-FTD Spectrum of Disorders. *Biomedicines*, *10*(5). https://doi.org/10.3390/biomedicines10051105

Godoy-Corchuelo, J. M., Fernández-Beltrán, L. C., Ali, Z., Gil-Moreno, M. J., López-Carbonero, J. I., Guerrero-Sola, A., Larrad-Sainz, A., Matias-Guiu, J., Matias-Guiu, J. A., Cunningham, T. J.,

& Corrochano, S. (2022). Lipid Metabolic Alterations in the ALS–FTD Spectrum of Disorders. *Biomedicines*, *10*(5), 1105. https://www.mdpi.com/2227-9059/10/5/1105

Golimstok, A., Cámpora, N., Rojas, J. I., Fernandez, M. C., Elizondo, C., Soriano, E., & Cristiano, E. (2014). Cardiovascular risk factors and frontotemporal dementia: a case-control study. *Transl Neurodegener*, *3*, 13. https://doi.org/10.1186/2047-9158-3-13

Gómez-Pinilla, F. (2008). Brain foods: the effects of nutrients on brain function. *Nat Rev Neurosci*, *9*(7), 568-578. https://doi.org/10.1038/nrn2421

Goodwin, L. O., Splinter, E., Davis, T. L., Urban, R., He, H., Braun, R. E., Chesler, E. J., Kumar, V., van Min, M., Ndukum, J., Philip, V. M., Reinholdt, L. G., Svenson, K., White, J. K., Sasner, M., Lutz, C., & Murray, S. A. (2019). Large-scale discovery of mouse transgenic integration sites reveals frequent structural variation and insertional mutagenesis. *Genome Res*, *29*(3), 494-505. https://doi.org/10.1101/gr.233866.117

Gorges, M., Vercruysse, P., Müller, H. P., Huppertz, H. J., Rosenbohm, A., Nagel, G., Weydt, P., Petersén, Å., Ludolph, A. C., Kassubek, J., & Dupuis, L. (2017). Hypothalamic atrophy is related to body mass index and age at onset in amyotrophic lateral sclerosis. *J Neurol Neurosurg Psychiatry*, *88*(12), 1033-1041. https://doi.org/10.1136/jnnp-2017-315795

Green, E. L. (1981). *Genetics and probability in animal breeding experiments : a primer and reference book on probability, segregation, assortment, linkage and mating systems for biomedical scientists who breed and use genetically defined laboratory animals for research*. Oxford University Press.

Green, P., Wiseman, M., Crow, Y. J., Houlden, H., Riphagen, S., Lin, J. P., Raymond, F. L., Childs, A. M., Sheridan, E., Edwards, S., & Josifova, D. J. (2010). Brown-Vialetto-Van Laere syndrome, a ponto-bulbar palsy with deafness, is caused by mutations in c20orf54. *Am J Hum Genet*, *86*(3), 485-489. https://doi.org/10.1016/j.ajhg.2010.02.006

Grochmal-Bach, B., Bidzan, L., Pachalska, M., Bidzan, M., Łukaszewska, B., & Pufal, A. (2009). Aggressive and impulsive behaviors in Frontotemporal dementia and Alzheimer's disease. *Med Sci Monit*, *15*(5), Cr248-254.

Groeneveld, G. J., Van Muiswinkel, F. L., Sturkenboom, J. M., Wokke, J. H., Bär, P. R., & Van den Berg, L. H. (2004). Ovariectomy and 17beta-estradiol modulate disease progression of a mouse model of ALS. *Brain Res*, *1021*(1), 128-131. https://doi.org/10.1016/j.brainres.2004.06.024

Gurney, M. E., Pu, H., Chiu, A. Y., Dal Canto, M. C., Polchow, C. Y., Alexander, D. D., Caliendo, J., Hentati, A., Kwon, Y. W., Deng, H. X., & et al. (1994). Motor neuron degeneration in mice that express a human Cu,Zn superoxide dismutase mutation. *Science*, *264*(5166), 1772-1775. https://doi.org/10.1126/science.8209258

Han, J., Nepal, P., Odelade, A., Freely, F. D., Belton, D. M., Graves, J. L., Jr., & Maldonado-Devincci, A. M. (2020). High-Fat Diet-Induced Weight Gain, Behavioral Deficits, and Dopamine Changes in Young C57BL/6J Mice. *Front Nutr*, *7*, 591161. https://doi.org/10.3389/fnut.2020.591161

Han, T. W., Kato, M., Xie, S., Wu, L. C., Mirzaei, H., Pei, J., Chen, M., Xie, Y., Allen, J., Xiao, G., & McKnight, S. L. (2012). Cell-free formation of RNA granules: bound RNAs identify features and components of cellular assemblies. *Cell*, *149*(4), 768-779. https://doi.org/10.1016/j.cell.2012.04.016

Haruyama, N., Cho, A., & Kulkarni, A. B. (2009). Overview: engineering transgenic constructs and mice. *Curr Protoc Cell Biol*, *Chapter 19*, Unit 19.10. https://doi.org/10.1002/0471143030.cb1910s42

Hicks, G. G., Singh, N., Nashabi, A., Mai, S., Bozek, G., Klewes, L., Arapovic, D., White, E. K., Koury, M. J., Oltz, E. M., Van Kaer, L., & Ruley, H. E. (2000). Fus deficiency in mice results in defective B-lymphocyte development and activation, high levels of chromosomal instability and perinatal death. *Nat Genet*, *24*(2), 175-179. https://doi.org/10.1038/72842

Hirono, N., Kitagaki, H., Kazui, H., Hashimoto, M., & Mori, E. (2000). Impact of white matter changes on clinical manifestation of Alzheimer's disease: A quantitative study. *Stroke*, *31*(9), 2182-2188. https://doi.org/10.1161/01.str.31.9.2182

Hoell, J. I., Larsson, E., Runge, S., Nusbaum, J. D., Duggimpudi, S., Farazi, T. A., Hafner, M., Borkhardt, A., Sander, C., & Tuschl, T. (2011). RNA targets of wild-type and mutant FET family proteins. *Nature Structural & Molecular Biology*, *18*(12), 1428-1431. https://doi.org/10.1038/nsmb.2163

Hou, J., Tan, G., Fink, G. R., Andrews, B. J., & Boone, C. (2019). Complex modifier landscape underlying genetic background effects. *Proceedings of the National Academy of Sciences*, *116*(11), 5045-5054. https://doi.org/doi:10.1073/pnas.1820915116

Hu, W. T., Seelaar, H., Josephs, K. A., Knopman, D. S., Boeve, B. F., Sorenson, E. J., McCluskey, L., Elman, L., Schelhaas, H. J., Parisi, J. E., Kuesters, B., Lee, V. M., Trojanowski, J. Q., Petersen, R. C., van Swieten, J. C., & Grossman, M. (2009). Survival profiles of patients with frontotemporal dementia and motor neuron disease. *Arch Neurol*, *66*(11), 1359-1364. https://doi.org/10.1001/archneurol.2009.253

Huang, C., Xia, P. Y., & Zhou, H. (2010). Sustained expression of TDP-43 and FUS in motor neurons in rodent's lifetime. *Int J Biol Sci*, *6*(4), 396-406. https://doi.org/10.7150/ijbs.6.396

Humphrey, J., Birsa, N., Milioto, C., McLaughlin, M., Ule, A. M., Robaldo, D., Eberle, A. B., Kräuchi, R., Bentham, M., Brown, A.-L., Jarvis, S., Bodo, C., Garone, Maria G., Devoy, A., Soraru, G., Rosa, A., Bozzoni, I., Fisher, E. M. C., Mühlemann, O., . . . Fratta, P. (2020). FUS ALS-causative mutations impair FUS autoregulation and splicing factor networks through intron retention. *Nucleic Acids Research*, *48*(12), 6889-6905. https://doi.org/10.1093/nar/gkaa410

Igaz, L. M., Kwong, L. K., Lee, E. B., Chen-Plotkin, A., Swanson, E., Unger, T., Malunda, J., Xu, Y., Winton, M. J., Trojanowski, J. Q., & Lee, V. M. (2011). Dysregulation of the ALS-associated gene TDP-43 leads to neuronal death and degeneration in mice. *J Clin Invest*, *121*(2), 726-738. https://doi.org/10.1172/jci44867

Ikeda, K., Hirayama, T., Takazawa, T., Kawabe, K., & Iwasaki, Y. (2012). Relationships between disease progression and serum levels of lipid, urate, creatinine and ferritin in Japanese patients with amyotrophic lateral sclerosis: a cross-sectional study. *Intern Med*, *51*(12), 1501-1508. https://doi.org/10.2169/internalmedicine.51.7465

Ingre, C., Roos, P. M., Piehl, F., Kamel, F., & Fang, F. (2015). Risk factors for amyotrophic lateral sclerosis. *Clin Epidemiol*, *7*, 181-193. https://doi.org/10.2147/clep.S37505

Ioannides, Z. A., Ngo, S. T., Henderson, R. D., McCombe, P. A., & Steyn, F. J. (2017). Hypermetabolism in motor neurone disease is associated with a greater functional decline but not weight loss. *Journal of Neurology, Neurosurgery & Psychiatry*, *88*(5), e1. https://doi.org/10.1136/jnnp-2017-316074.18

Isaacs, J. D., Dean, A. F., Shaw, C. E., Al-Chalabi, A., Mills, K. R., & Leigh, P. N. (2007). Amyotrophic lateral sclerosis with sensory neuropathy: part of a multisystem disorder? *J Neurol Neurosurg Psychiatry*, *78*(7), 750-753. https://doi.org/10.1136/jnnp.2006.098798

Ishigaki, S., Masuda, A., Fujioka, Y., Iguchi, Y., Katsuno, M., Shibata, A., Urano, F., Sobue, G., & Ohno, K. (2012). Position-dependent FUS-RNA interactions regulate alternative splicing events and transcriptions. *Sci Rep*, *2*, 529. https://doi.org/10.1038/srep00529

Ito, D., Taguchi, R., Deguchi, M., Ogasawara, H., & Inoue, E. (2020). Extensive splicing changes in an ALS/FTD transgenic mouse model overexpressing cytoplasmic fused in sarcoma. *Scientific Reports*, *10*(1), 4857. https://doi.org/10.1038/s41598-020-61676-x

Janssens, J., Wils, H., Kleinberger, G., Joris, G., Cuijt, I., Ceuterick-de Groote, C., Van Broeckhoven, C., & Kumar-Singh, S. (2013). Overexpression of ALS-associated p.M337V human TDP-43 in mice worsens disease features compared to wild-type human TDP-43 mice. *Mol Neurobiol*, *48*(1), 22-35. https://doi.org/10.1007/s12035-013-8427-5

Jawahar, M. C., Sari, C. I., Wilson, Y. M., Lawrence, A. J., Brodnicki, T., & Murphy, M. (2011). Audiogenic seizure proneness requires the contribution of two susceptibility loci in mice. *neurogenetics*, *12*(3), 253-257. https://doi.org/10.1007/s10048-011-0289-2

Jawaid, A., Khan, R., Polymenidou, M., & Schulz, P. E. (2018). Disease-modifying effects of metabolic perturbations in ALS/FTLD. *Molecular Neurodegeneration*, *13*(1), 63. https://doi.org/10.1186/s13024-018-0294-0

Jawaid, A., Salamone, A. R., Strutt, A. M., Murthy, S. B., Wheaton, M., McDowell, E. J., Simpson, E., Appel, S. H., York, M. K., & Schulz, P. E. (2010). ALS disease onset may occur later in patients with pre-morbid diabetes mellitus. *Eur J Neurol*, *17*(5), 733-739. https://doi.org/10.1111/j.1468-1331.2009.02923.x

Jensen, V. S., Porsgaard, T., Lykkesfeldt, J., & Hvid, H. (2016). Rodent model choice has major impact on variability of standard preclinical readouts associated with diabetes and obesity research. *Am J Transl Res*, *8*(8), 3574-3584.

Jeong, Y., Cho, S. S., Park, J. M., Kang, S. J., Lee, J. S., Kang, E., Na, D. L., & Kim, S. E. (2005). ¹⁸F-FDG PET Findings in Frontotemporal Dementia: An SPM Analysis of 29 Patients. *Journal of Nuclear Medicine*, *46*(2), 233-239. https://jnm.snmjournals.org/content/jnumed/46/2/233.full.pdf

Jiang, Y. X., Cao, Q., Sawaya, M. R., Abskharon, R., Ge, P., DeTure, M., Dickson, D. W., Fu, J. Y., Ogorzalek Loo, R. R., Loo, J. A., & Eisenberg, D. S. (2022). Amyloid fibrils in FTLD-TDP are composed of TMEM106B and not TDP-43. *Nature*, *605*(7909), 304-309. https://doi.org/10.1038/s41586-022-04670-9

JM, C. (1874). Amyotrophies spinales deuteropathiques sclérose latérale amyotrophique & Sclérose latérale amyotrophique. *Bureaux du Progrès Médical*, *2*, 234-266.

John, S. W., Smith, R. S., Savinova, O. V., Hawes, N. L., Chang, B., Turnbull, D., Davisson, M., Roderick, T. H., & Heckenlively, J. R. (1998). Essential iris atrophy, pigment dispersion, and glaucoma in DBA/2J mice. *Invest Ophthalmol Vis Sci*, *39*(6), 951-962.

Johnson, B. S., Snead, D., Lee, J. J., McCaffery, J. M., Shorter, J., & Gitler, A. D. (2009). TDP-43 is intrinsically aggregation-prone, and amyotrophic lateral sclerosis-linked mutations accelerate aggregation and increase toxicity. *J Biol Chem*, *284*(30), 20329-20339. https://doi.org/10.1074/jbc.M109.010264

Johnson, E., & Kumfor, F. (2018). Overcoming apathy in frontotemporal dementia: challenges and future directions. *Current Opinion in Behavioral Sciences*, *22*, 82-89. https://doi.org/https://doi.org/10.1016/j.cobeha.2018.01.022

Johnson, J. O., Mandrioli, J., Benatar, M., Abramzon, Y., Van Deerlin, V. M., Trojanowski, J. Q., Gibbs, J. R., Brunetti, M., Gronka, S., Wuu, J., Ding, J., McCluskey, L., Martinez-Lage, M., Falcone, D., Hernandez, D. G., Arepalli, S., Chong, S., Schymick, J. C., Rothstein, J., . . . Traynor, B. J. (2010). Exome sequencing reveals VCP mutations as a cause of familial ALS. *Neuron*, *68*(5), 857-864. https://doi.org/10.1016/j.neuron.2010.11.036

Josephs, K. A., Stroh, A., Dugger, B., & Dickson, D. W. (2009). Evaluation of subcortical pathology and clinical correlations in FTLD-U subtypes. *Acta Neuropathol*, *118*(3), 349-358. https://doi.org/10.1007/s00401-009-0547-7

Jovičić, A., Mertens, J., Boeynaems, S., Bogaert, E., Chai, N., Yamada, S. B., Paul, J. W., 3rd, Sun, S., Herdy, J. R., Bieri, G., Kramer, N. J., Gage, F. H., Van Den Bosch, L., Robberecht, W., & Gitler, A. D. (2015). Modifiers of C9orf72 dipeptide repeat toxicity connect nucleocytoplasmic transport defects to FTD/ALS. *Nat Neurosci*, *18*(9), 1226-1229. https://doi.org/10.1038/nn.4085

Kabashi, E., Valdmanis, P. N., Dion, P., Spiegelman, D., McConkey, B. J., Vande Velde, C., Bouchard, J. P., Lacomblez, L., Pochigaeva, K., Salachas, F., Pradat, P. F., Camu, W., Meininger, V., Dupre, N., & Rouleau, G. A. (2008). TARDBP mutations in individuals with sporadic and familial amyotrophic lateral sclerosis. *Nat Genet*, *40*(5), 572-574. https://doi.org/10.1038/ng.132

Karagiannis, P., & Inoue, H. (2020). ALS, a cellular whodunit on motor neuron degeneration. *Mol Cell Neurosci*, *107*, 103524. https://doi.org/10.1016/j.mcn.2020.103524

Kasarskis, E. J., Berryman, S., Vanderleest, J. G., Schneider, A. R., & McClain, C. J. (1996). Nutritional status of patients with amyotrophic lateral sclerosis: relation to the proximity of death. *The American Journal of Clinical Nutrition*, *63*(1), 130-137. https://doi.org/10.1093/ajcn/63.1.130

Keane, T. M., Goodstadt, L., Danecek, P., White, M. A., Wong, K., Yalcin, B., Heger, A., Agam, A., Slater, G., Goodson, M., Furlotte, N. A., Eskin, E., Nellåker, C., Whitley, H., Cleak, J., Janowitz, D., Hernandez-Pliego, P., Edwards, A., Belgard, T. G., . . . Adams, D. J. (2011). Mouse genomic variation and its effect on phenotypes and gene regulation. *Nature*, *477*(7364), 289-294. https://doi.org/10.1038/nature10413

Keating, S. S., San Gil, R., Swanson, M. E. V., Scotter, E. L., & Walker, A. K. (2022). TDP-43 pathology: From noxious assembly to therapeutic removal. *Progress in Neurobiology*, *211*, 102229. https://doi.org/https://doi.org/10.1016/j.pneurobio.2022.102229

Kiebler, M. A., & Bassell, G. J. (2006). Neuronal RNA granules: movers and makers. *Neuron*, *51*(6), 685-690. https://doi.org/10.1016/j.neuron.2006.08.021

Kim, H. J., Raphael, A. R., LaDow, E. S., McGurk, L., Weber, R. A., Trojanowski, J. Q., Lee, V. M., Finkbeiner, S., Gitler, A. D., & Bonini, N. M. (2014). Therapeutic modulation of eIF2α phosphorylation rescues TDP-43 toxicity in amyotrophic lateral sclerosis disease models. *Nat Genet*, *46*(2), 152-160. https://doi.org/10.1038/ng.2853

Kinkel, A. D., Fernyhough, M. E., Helterline, D. L., Vierck, J. L., Oberg, K. S., Vance, T. J., Hausman, G. J., Hill, R. A., & Dodson, M. V. (2004). Oil red-O stains non-adipogenic cells: a precautionary note. *Cytotechnology*, *46*(1), 49-56. https://doi.org/10.1007/s10616-004-3903-4

Kino, Y., Washizu, C., Kurosawa, M., Yamada, M., Miyazaki, H., Akagi, T., Hashikawa, T., Doi, H., Takumi, T., Hicks, G. G., Hattori, N., Shimogori, T., & Nukina, N. (2015). FUS/TLS deficiency causes behavioral and pathological abnormalities distinct from amyotrophic lateral sclerosis. *Acta Neuropathologica Communications*, *3*(1), 24. https://doi.org/10.1186/s40478-015-0202-6

Klim, J. R., Williams, L. A., Limone, F., Guerra San Juan, I., Davis-Dusenbery, B. N., Mordes, D. A., Burberry, A., Steinbaugh, M. J., Gamage, K. K., Kirchner, R., Moccia, R., Cassel, S. H., Chen, K., Wainger, B. J., Woolf, C. J., & Eggan, K. (2019). ALS-implicated protein TDP-43 sustains levels of STMN2, a mediator of motor neuron growth and repair. *Nature Neuroscience*, *22*(2), 167-179. https://doi.org/10.1038/s41593-018-0300-4

Koike, Y., Sugai, A., Hara, N., Ito, J., Yokoseki, A., Ishihara, T., Yamagishi, T., Tsuboguchi, S., Tada, M., Ikeuchi, T., Kakita, A., & Onodera, O. (2021). Age-related demethylation of the TDP-43 autoregulatory region in the human motor cortex. *Communications Biology*, *4*(1), 1107. https://doi.org/10.1038/s42003-021-02621-0

Korobeynikov, V. A., Lyashchenko, A. K., Blanco-Redondo, B., Jafar-Nejad, P., & Shneider, N. A. (2022). Antisense oligonucleotide silencing of FUS expression as a therapeutic approach in amyotrophic lateral sclerosis. *Nat Med*, *28*(1), 104-116. https://doi.org/10.1038/s41591-021-01615-z

Koyama, A., Sugai, A., Kato, T., Ishihara, T., Shiga, A., Toyoshima, Y., Koyama, M., Konno, T., Hirokawa, S., Yokoseki, A., Nishizawa, M., Kakita, A., Takahashi, H., & Onodera, O. (2016). Increased cytoplasmic TARDBP mRNA in affected spinal motor neurons in ALS caused by abnormal autoregulation of TDP-43. *Nucleic Acids Research*, *44*(12), 5820-5836. https://doi.org/10.1093/nar/gkw499

Kraemer, B. C., Schuck, T., Wheeler, J. M., Robinson, L. C., Trojanowski, J. Q., Lee, V. M., & Schellenberg, G. D. (2010). Loss of murine TDP-43 disrupts motor function and plays an essential role in embryogenesis. *Acta Neuropathol*, *119*(4), 409-419. https://doi.org/10.1007/s00401-010-0659-0

Kwiatkowski, T. J., Jr., Bosco, D. A., Leclerc, A. L., Tamrazian, E., Vanderburg, C. R., Russ, C., Davis, A., Gilchrist, J., Kasarskis, E. J., Munsat, T., Valdmanis, P., Rouleau, G. A., Hosler, B. A., Cortelli, P., de Jong, P. J., Yoshinaga, Y., Haines, J. L., Pericak-Vance, M. A., Yan, J., . . . Brown, R. H., Jr. (2009). Mutations in the FUS/TLS gene on chromosome 16 cause familial amyotrophic lateral sclerosis. *Science*, *323*(5918), 1205-1208. https://doi.org/10.1126/science.1166066

Laakso, M. P., Frisoni, G. B., Könönen, M., Mikkonen, M., Beltramello, A., Geroldi, C., Bianchetti, A., Trabucchi, M., Soininen, H., & Aronen, H. J. (2000). Hippocampus and entorhinal cortex in frontotemporal dementia and Alzheimer's disease: a morphometric MRI study. *Biol Psychiatry*, *47*(12), 1056-1063. https://doi.org/10.1016/s0006-3223(99)00306-6

Lagier-Tourenne, C., & Cleveland, D. W. (2009). Rethinking ALS: the FUS about TDP-43. *Cell*, *136*(6), 1001-1004. https://doi.org/10.1016/j.cell.2009.03.006

Lagier-Tourenne, C., Polymenidou, M., & Cleveland, D. W. (2010). TDP-43 and FUS/TLS: emerging roles in RNA processing and neurodegeneration. *Human Molecular Genetics*, *19*(R1), R46-R64. https://doi.org/10.1093/hmg/ddq137

Lagier-Tourenne, C., Polymenidou, M., Hutt, K. R., Vu, A. Q., Baughn, M., Huelga, S. C., Clutario, K. M., Ling, S. C., Liang, T. Y., Mazur, C., Wancewicz, E., Kim, A. S., Watt, A., Freier, S., Hicks, G. G., Donohue, J. P., Shiue, L., Bennett, C. F., Ravits, J., . . . Yeo, G. W. (2012). Divergent

roles of ALS-linked proteins FUS/TLS and TDP-43 intersect in processing long pre-mRNAs. *Nat Neurosci*, *15*(11), 1488-1497. https://doi.org/10.1038/nn.3230

Lamb, R., Rohrer, J. D., Real, R., Lubbe, S. J., Waite, A. J., Blake, D. J., Walters, R. J., Lashley, T., Revesz, T., Holton, J. L., & Morris, H. R. (2019). A novel TBK1 mutation in a family with diverse frontotemporal dementia spectrum disorders. *Cold Spring Harb Mol Case Stud*, *5*(3). https://doi.org/10.1101/mcs.a003913

Lanson, N. A., & Pandey, U. B. (2012). FUS-related proteinopathies: Lessons from animal models. *Brain Research*, *1462*, 44-60. https://doi.org/https://doi.org/10.1016/j.brainres.2012.01.039

Law, W. J., Cann, K. L., & Hicks, G. G. (2006). TLS, EWS and TAF15: a model for transcriptional integration of gene expression. *Briefings in Functional Genomics*, *5*(1), 8-14. https://doi.org/10.1093/bfgp/ell015

Leavitt, A. D., & Hamlett, I. (2011). Homologous recombination in human embryonic stem cells: a tool for advancing cell therapy and understanding and treating human disease. *Clin Transl Sci*, *4*(4), 298-305. https://doi.org/10.1111/j.1752-8062.2011.00281.x

Lehky, T., & Grunseich, C. (2021). Juvenile Amyotrophic Lateral Sclerosis: A Review. *Genes (Basel)*, *12*(12). https://doi.org/10.3390/genes12121935

Li, Y. R., King, O. D., Shorter, J., & Gitler, A. D. (2013). Stress granules as crucibles of ALS pathogenesis. *J Cell Biol*, *201*(3), 361-372. https://doi.org/10.1083/jcb.201302044

Lin, Z., Kim, E., Ahmed, M., Han, G., Simmons, C., Redhead, Y., Bartlett, J., Pena Altamira, L. E., Callaghan, I., White, M. A., Singh, N., Sawiak, S., Spires-Jones, T., Vernon, A. C., Coleman, M. P., Green, J., Henstridge, C., Davies, J. S., Cash, D., & Sreedharan, J. (2021). MRI-guided histology of TDP-43 knock-in mice implicates parvalbumin interneuron loss, impaired neurogenesis and aberrant neurodevelopment in amyotrophic lateral sclerosis-frontotemporal dementia. *Brain Communications*, *3*(2), fcab114. https://doi.org/10.1093/braincomms/fcab114

Lindauer, E., Dupuis, L., Müller, H. P., Neumann, H., Ludolph, A. C., & Kassubek, J. (2013). Adipose Tissue Distribution Predicts Survival in Amyotrophic Lateral Sclerosis. *PLoS One*, *8*(6), e67783. https://doi.org/10.1371/journal.pone.0067783

Linder, C. C. (2001). The influence of genetic background on spontaneous and genetically engineered mouse models of complex diseases. *Lab Anim (NY)*, *30*(5), 34-39.

Linder, C. C. (2006). Genetic Variables That Influence Phenotype. *ILAR Journal*, *47*(2), 132-140. https://doi.org/10.1093/ilar.47.2.132

Lindquist, S. G., Duno, M., Batbayli, M., Puschmann, A., Braendgaard, H., Mardosiene, S., Svenstrup, K., Pinborg, L. H., Vestergaard, K., Hjermind, L. E., Stokholm, J., Andersen, B. B., Johannsen, P., & Nielsen, J. E. (2013). Corticobasal and ataxia syndromes widen the spectrum of C9ORF72 hexanucleotide expansion disease. *Clin Genet*, *83*(3), 279-283. https://doi.org/10.1111/j.1399-0004.2012.01903.x

Ling, S. C., Polymenidou, M., & Cleveland, D. W. (2013). Converging mechanisms in ALS and FTD: disrupted RNA and protein homeostasis. *Neuron*, *79*(3), 416-438. https://doi.org/10.1016/j.neuron.2013.07.033

Loeffler, J.-P., Picchiarelli, G., Dupuis, L., & Gonzalez De Aguilar, J.-L. (2016). The Role of Skeletal Muscle in Amyotrophic Lateral Sclerosis. *Brain Pathology*, *26*(2), 227-236. https://doi.org/https://doi.org/10.1111/bpa.12350

Loughlin, F. E., Lukavsky, P. J., Kazeeva, T., Reber, S., Hock, E. M., Colombo, M., Von Schroetter, C., Pauli, P., Cléry, A., Mühlemann, O., Polymenidou, M., Ruepp, M. D., & Allain, F. H. (2019). The Solution Structure of FUS Bound to RNA Reveals a Bipartite Mode of RNA Recognition with Both Sequence and Shape Specificity. *Mol Cell*, *73*(3), 490-504.e496. https://doi.org/10.1016/j.molcel.2018.11.012

Ludolph, A. C., Dorst, J., Dreyhaupt, J., Weishaupt, J. H., Kassubek, J., Weiland, U., Meyer, T., Petri, S., Hermann, A., Emmer, A., Grosskreutz, J., Grehl, T., Zeller, D., Boentert, M., Schrank, B., Prudlo, J., Winkler, A. S., Gorbulev, S., Roselli, F., . . . Group, f. t. L.-A. S. (2020). Effect of High-Caloric Nutrition on Survival in Amyotrophic Lateral Sclerosis. *Annals of Neurology*, *87*(2), 206-216. https://doi.org/https://doi.org/10.1002/ana.25661

Lutz, C. (2018). Mouse models of ALS: Past, present and future. *Brain Res*, *1693*(Pt A), 1-10. https://doi.org/10.1016/j.brainres.2018.03.024

Lyon, M. F., & Searle, A. G. (1989). *Genetic variants and strains of the laboratory mouse*. Oxford University Press.

Ma, X. R., Prudencio, M., Koike, Y., Vatsavayai, S. C., Kim, G., Harbinski, F., Briner, A., Rodriguez, C. M., Guo, C., Akiyama, T., Schmidt, H. B., Cummings, B. B., Wyatt, D. W., Kurylo, K., Miller, G., Mekhoubad, S., Sallee, N., Mekonnen, G., Ganser, L., . . . Gitler, A. D. (2022). TDP-43 represses cryptic exon inclusion in the FTD–ALS gene UNC13A. *Nature*, *603*(7899), 124-130. https://doi.org/10.1038/s41586-022-04424-7

Ma, Y. L., & Li, Z. P. (2019). [Jean-Martin Charcot, discovery and nomenclature of amyotrophic lateral sclerosis]. *Zhonghua Yi Shi Za Zhi*, *49*(1), 14-18. https://doi.org/10.3760/cma.j.issn.0255-7053.2019.01.003

Mackenzie, I. R., Bigio, E. H., Ince, P. G., Geser, F., Neumann, M., Cairns, N. J., Kwong, L. K., Forman, M. S., Ravits, J., Stewart, H., Eisen, A., McClusky, L., Kretzschmar, H. A., Monoranu, C. M., Highley, J. R., Kirby, J., Siddique, T., Shaw, P. J., Lee, V. M., & Trojanowski, J. Q. (2007). Pathological TDP-43 distinguishes sporadic amyotrophic lateral sclerosis from amyotrophic lateral sclerosis with SOD1 mutations. *Ann Neurol*, *61*(5), 427-434. https://doi.org/10.1002/ana.21147

Mackenzie, I. R., Munoz, D. G., Kusaka, H., Yokota, O., Ishihara, K., Roeber, S., Kretzschmar, H. A., Cairns, N. J., & Neumann, M. (2011). Distinct pathological subtypes of FTLD-FUS. *Acta Neuropathol*, *121*(2), 207-218. https://doi.org/10.1007/s00401-010-0764-0

Mackenzie, I. R., Neumann, M., Baborie, A., Sampathu, D. M., Du Plessis, D., Jaros, E., Perry, R. H., Trojanowski, J. Q., Mann, D. M., & Lee, V. M. (2011). A harmonized classification system for FTLD-TDP pathology. *Acta Neuropathol*, *122*(1), 111-113. https://doi.org/10.1007/s00401-011-0845-8

Mackenzie, I. R., Neumann, M., Bigio, E. H., Cairns, N. J., Alafuzoff, I., Kril, J., Kovacs, G. G., Ghetti, B., Halliday, G., Holm, I. E., Ince, P. G., Kamphorst, W., Revesz, T., Rozemuller, A. J., Kumar-Singh, S., Akiyama, H., Baborie, A., Spina, S., Dickson, D. W., . . . Mann, D. M. (2010). Nomenclature and nosology for neuropathologic subtypes of frontotemporal lobar degeneration: an update. *Acta Neuropathol*, *119*(1), 1-4. https://doi.org/10.1007/s00401-009-0612-2

Mackenzie, I. R. A., Rademakers, R., & Neumann, M. (2010). TDP-43 and FUS in amyotrophic lateral sclerosis and frontotemporal dementia. *The Lancet Neurology*, *9*(10), 995-1007. https://doi.org/https://doi.org/10.1016/S1474-4422(10)70195-2

Mancuso, R., Oliván, S., Mancera, P., Pastén-Zamorano, A., Manzano, R., Casas, C., Osta, R., & Navarro, X. (2012). Effect of genetic background on onset and disease progression in the SOD1-G93A model of amyotrophic lateral sclerosis. *Amyotroph Lateral Scler*, *13*(3), 302-310. https://doi.org/10.3109/17482968.2012.662688

Manjaly, Z. R., Scott, K. M., Abhinav, K., Wijesekera, L., Ganesalingam, J., Goldstein, L. H., Janssen, A., Dougherty, A., Willey, E., Stanton, B. R., Turner, M. R., Ampong, M. A., Sakel, M., Orrell, R. W., Howard, R., Shaw, C. E., Leigh, P. N., & Al-Chalabi, A. (2010). The sex ratio in amyotrophic lateral sclerosis: A population based study. *Amyotroph Lateral Scler*, *11*(5), 439-442. https://doi.org/10.3109/17482961003610853

Maren, S. (2008). Pavlovian fear conditioning as a behavioral assay for hippocampus and amygdala function: cautions and caveats. *Eur J Neurosci*, *28*(8), 1661-1666. https://doi.org/10.1111/j.1460-9568.2008.06485.x

Maren, S., & Quirk, G. J. (2004). Neuronal signalling of fear memory. *Nature Reviews Neuroscience*, *5*(11), 844-852. https://doi.org/10.1038/nrn1535

Mariosa, D., Kamel, F., Bellocco, R., Ye, W., & Fang, F. (2015). Association between diabetes and amyotrophic lateral sclerosis in Sweden. *Eur J Neurol*, *22*(11), 1436-1442. https://doi.org/10.1111/ene.12632

Maruyama, H., Morino, H., Ito, H., Izumi, Y., Kato, H., Watanabe, Y., Kinoshita, Y., Kamada, M., Nodera, H., Suzuki, H., Komure, O., Matsuura, S., Kobatake, K., Morimoto, N., Abe, K., Suzuki, N., Aoki, M., Kawata, A., Hirai, T., . . . Kawakami, H. (2010). Mutations of optineurin in amyotrophic lateral sclerosis. *Nature*, *465*(7295), 223-226. https://doi.org/10.1038/nature08971

Masopust, D., Sivula, C. P., & Jameson, S. C. (2017). Of Mice, Dirty Mice, and Men: Using Mice To Understand Human Immunology. *The Journal of Immunology*, *199*(2), 383. https://doi.org/10.4049/jimmunol.1700453

McCombe, P. A., & Henderson, R. D. (2010). Effects of gender in amyotrophic lateral sclerosis. *Gender Medicine*, *7*(6), 557-570. https://doi.org/https://doi.org/10.1016/j.genm.2010.11.010

McLean, F. H., Grant, C., Morris, A. C., Horgan, G. W., Polanski, A. J., Allan, K., Campbell, F. M., Langston, R. F., & Williams, L. M. (2018). Rapid and reversible impairment of episodic memory by a high-fat diet in mice. *Scientific Reports*, *8*(1), 11976. https://doi.org/10.1038/s41598-018-30265-4

Meeter, L. H., Kaat, L. D., Rohrer, J. D., & van Swieten, J. C. (2017). Imaging and fluid biomarkers in frontotemporal dementia. *Nat Rev Neurol*, *13*(7), 406-419. https://doi.org/10.1038/nrneurol.2017.75

Mejia Maza, A., Jarvis, S., Lee, W. C., Cunningham, T. J., Schiavo, G., Secrier, M., Fratta, P., Sleigh, J. N., Fisher, E. M. C., & Sudre, C. H. (2021). NMJ-Analyser identifies subtle early changes in mouse models of neuromuscular disease. *Sci Rep*, *11*(1), 12251. https://doi.org/10.1038/s41598-021-91094-6

Mendes, C. S., Bartos, I., Márka, Z., Akay, T., Márka, S., & Mann, R. S. (2015). Quantification of gait parameters in freely walking rodents. *BMC Biology*, *13*(1), 50. https://doi.org/10.1186/s12915-015-0154-0

Mitchell, J. C., Constable, R., So, E., Vance, C., Scotter, E., Glover, L., Hortobagyi, T., Arnold, E. S., Ling, S. C., McAlonis, M., Da Cruz, S., Polymenidou, M., Tessarolo, L., Cleveland, D. W., &

Shaw, C. E. (2015). Wild type human TDP-43 potentiates ALS-linked mutant TDP-43 driven progressive motor and cortical neuron degeneration with pathological features of ALS. *Acta Neuropathol Commun*, *3*, 36. https://doi.org/10.1186/s40478-015-0212-4

Mitchell, J. C., McGoldrick, P., Vance, C., Hortobagyi, T., Sreedharan, J., Rogelj, B., Tudor, E. L., Smith, B. N., Klasen, C., Miller, C. C., Cooper, J. D., Greensmith, L., & Shaw, C. E. (2013). Overexpression of human wild-type FUS causes progressive motor neuron degeneration in an age- and dose-dependent fashion. *Acta Neuropathol*, *125*(2), 273-288. https://doi.org/10.1007/s00401-012-1043-z

Mochizuki, Y., Isozaki, E., Takao, M., Hashimoto, T., Shibuya, M., Arai, M., Hosokawa, M., Kawata, A., Oyanagi, K., Mihara, B., & Mizutani, T. (2012). Familial ALS with FUS P525L mutation: two Japanese sisters with multiple systems involvement. *J Neurol Sci*, *323*(1-2), 85-92. https://doi.org/10.1016/j.jns.2012.08.016

Mohandas, E., & Rajmohan, V. (2009). Frontotemporal dementia: An updated overview. *Indian J Psychiatry*, *51 Suppl 1*(Suppl1), S65-69.

Molliex, A., Temirov, J., Lee, J., Coughlin, M., Kanagaraj, A. P., Kim, H. J., Mittag, T., & Taylor, J. P. (2015). Phase separation by low complexity domains promotes stress granule assembly and drives pathological fibrillization. *Cell*, *163*(1), 123-133. https://doi.org/10.1016/j.cell.2015.09.015

Monaco, G., van Dam, S., Casal Novo Ribeiro, J. L., Larbi, A., & de Magalhães, J. P. (2015). A comparison of human and mouse gene co-expression networks reveals conservation and divergence at the tissue, pathway and disease levels. *BMC Evol Biol*, *15*, 259. https://doi.org/10.1186/s12862-015-0534-7

Montagutelli, X. (2000). Effect of the Genetic Background on the Phenotype of Mouse Mutations. *Journal of the American Society of Nephrology*, *11*(suppl 2), S101. https://doi.org/10.1681/ASN.V11suppl_2s101

Morrice, J. R., Gregory-Evans, C. Y., & Shaw, C. A. (2018). Animal models of amyotrophic lateral sclerosis: A comparison of model validity. *Neural Regen Res*, *13*(12), 2050-2054. https://doi.org/10.4103/1673-5374.241445

Moulias, R., Meaume, S., & Raynaud-Simon, A. (1999). Sarcopenia, hypermetabolism, and aging. *Z Gerontol Geriatr*, *32*(6), 425-432. https://doi.org/10.1007/s003910050140

Mullis, M. N., Matsui, T., Schell, R., Foree, R., & Ehrenreich, I. M. (2018). The complex underpinnings of genetic background effects. *Nature Communications*, *9*(1), 3548. https://doi.org/10.1038/s41467-018-06023-5

Nag, S., Yu, L., Boyle, P. A., Leurgans, S. E., Bennett, D. A., & Schneider, J. A. (2018). TDP-43 pathology in anterior temporal pole cortex in aging and Alzheimer's disease. *Acta Neuropathol Commun*, *6*(1), 33. https://doi.org/10.1186/s40478-018-0531-3

Nag, S., Yu, L., Capuano, A. W., Wilson, R. S., Leurgans, S. E., Bennett, D. A., & Schneider, J. A. (2015). Hippocampal sclerosis and TDP-43 pathology in aging and Alzheimer disease. *Ann Neurol*, *77*(6), 942-952. https://doi.org/10.1002/ana.24388

Nagano, S., Takahashi, Y., Yamamoto, K., Masutani, H., Fujiwara, N., Urushitani, M., & Araki, T. (2015). A cysteine residue affects the conformational state and neuronal toxicity of mutant SOD1 in mice: relevance to the pathogenesis of ALS. *Hum Mol Genet*, *24*(12), 3427-3439. https://doi.org/10.1093/hmg/ddv093

Nakaya, T., Alexiou, P., Maragkakis, M., Chang, A., & Mourelatos, Z. (2013). FUS regulates genes coding for RNA-binding proteins in neurons by binding to their highly conserved introns. *Rna*, *19*(4), 498-509. https://doi.org/10.1261/rna.037804.112

Neary, D., Snowden, J., & Mann, D. (2005). Frontotemporal dementia. *The Lancet Neurology*, *4*(11), 771-780. https://doi.org/https://doi.org/10.1016/S1474-4422(05)70223-4

Nelson, P. T., Dickson, D. W., Trojanowski, J. Q., Jack, C. R., Boyle, P. A., Arfanakis, K., Rademakers, R., Alafuzoff, I., Attems, J., Brayne, C., Coyle-Gilchrist, I. T. S., Chui, H. C., Fardo, D. W., Flanagan, M. E., Halliday, G., Hokkanen, S. R. K., Hunter, S., Jicha, G. A., Katsumata, Y., . . . Schneider, J. A. (2019). Limbic-predominant age-related TDP-43 encephalopathy (LATE): consensus working group report. *Brain*, *142*(6), 1503-1527. https://doi.org/10.1093/brain/awz099

Neumann, M., Rademakers, R., Roeber, S., Baker, M., Kretzschmar, H. A., & Mackenzie, I. R. (2009). A new subtype of frontotemporal lobar degeneration with FUS pathology. *Brain*, *132*(Pt 11), 2922-2931. https://doi.org/10.1093/brain/awp214

Neumann, M., Roeber, S., Kretzschmar, H. A., Rademakers, R., Baker, M., & Mackenzie, I. R. (2009). Abundant FUS-immunoreactive pathology in neuronal intermediate filament inclusion disease. *Acta Neuropathol*, *118*(5), 605-616. https://doi.org/10.1007/s00401-009-0581-5

Neumann, M., Sampathu, D. M., Kwong, L. K., Truax, A. C., Micsenyi, M. C., Chou, T. T., Bruce, J., Schuck, T., Grossman, M., Clark, C. M., McCluskey, L. F., Miller, B. L., Masliah, E., Mackenzie, I. R., Feldman, H., Feiden, W., Kretzschmar, H. A., Trojanowski, J. Q., & Lee, V. M. (2006). Ubiquitinated TDP-43 in frontotemporal lobar degeneration and amyotrophic lateral sclerosis. *Science*, *314*(5796), 130-133. https://doi.org/10.1126/science.1134108

Nguyen, P., Leray, V., Diez, M., Serisier, S., Le Bloc'h, J., Siliart, B., & Dumon, H. (2008). Liver lipid metabolism. *J Anim Physiol Anim Nutr (Berl)*, *92*(3), 272-283. https://doi.org/10.1111/j.1439-0396.2007.00752.x

Nigri, M., Åhlgren, J., Wolfer, D. P., & Voikar, V. (2022). Role of Environment and Experimenter in Reproducibility of Behavioral Studies With Laboratory Mice [Original Research]. *Frontiers in Behavioral Neuroscience*, *16*. https://doi.org/10.3389/fnbeh.2022.835444

Nijssen, J., Comley, L. H., & Hedlund, E. (2017). Motor neuron vulnerability and resistance in amyotrophic lateral sclerosis. *Acta Neuropathol*, *133*(6), 863-885. https://doi.org/10.1007/s00401-017-1708-8

Nolan, M., Talbot, K., & Ansorge, O. (2016). Pathogenesis of FUS-associated ALS and FTD: insights from rodent models. *Acta Neuropathologica Communications*, *4*(1), 99. https://doi.org/10.1186/s40478-016-0358-8

Nonaka, T., Masuda-Suzukake, M., Arai, T., Hasegawa, Y., Akatsu, H., Obi, T., Yoshida, M., Murayama, S., Mann, D. M., Akiyama, H., & Hasegawa, M. (2013). Prion-like properties of pathological TDP-43 aggregates from diseased brains. *Cell Rep*, *4*(1), 124-134. https://doi.org/10.1016/j.celrep.2013.06.007

Oliveira, H. D. S. J. M. D. (2014). *Investigating TDP43 biological dysfunction through the characterisation of Tardbp ENU mouse mutants: implications for Neurodegeneration* University of Oxford].

Olney, N. T., Spina, S., & Miller, B. L. (2017). Frontotemporal Dementia. *Neurol Clin*, *35*(2), 339-374. https://doi.org/10.1016/j.ncl.2017.01.008

Onyike, C. U., & Diehl-Schmid, J. (2013). The epidemiology of frontotemporal dementia. *Int Rev Psychiatry*, *25*(2), 130-137. https://doi.org/10.3109/09540261.2013.776523

Paganoni, S., Hendrix, S., Dickson, S. P., Knowlton, N., Macklin, E. A., Berry, J. D., Elliott, M. A., Maiser, S., Karam, C., Caress, J. B., Owegi, M. A., Quick, A., Wymer, J., Goutman, S. A., Heitzman, D., Heiman-Patterson, T. D., Jackson, C. E., Quinn, C., Rothstein, J. D., . . . Cudkowicz, M. E. (2021). Long-term survival of participants in the CENTAUR trial of sodium phenylbutyrate-taurursodiol in amyotrophic lateral sclerosis. *Muscle Nerve*, *63*(1), 31-39. https://doi.org/10.1002/mus.27091

Paganoni, S., Macklin, E. A., Hendrix, S., Berry, J. D., Elliott, M. A., Maiser, S., Karam, C., Caress, J. B., Owegi, M. A., Quick, A., Wymer, J., Goutman, S. A., Heitzman, D., Heiman-Patterson, T., Jackson, C. E., Quinn, C., Rothstein, J. D., Kasarskis, E. J., Katz, J., . . . Cudkowicz, M. E. (2020). Trial of Sodium Phenylbutyrate–Taurursodiol for Amyotrophic Lateral Sclerosis. *New England Journal of Medicine*, *383*(10), 919-930. https://doi.org/10.1056/NEJMoa1916945

Palamiuc, L., Schlagowski, A., Ngo, S. T., Vernay, A., Dirrig-Grosch, S., Henriques, A., Boutillier, A. L., Zoll, J., Echaniz-Laguna, A., Loeffler, J. P., & René, F. (2015). A metabolic switch toward lipid use in glycolytic muscle is an early pathologic event in a mouse model of amyotrophic lateral sclerosis. *EMBO Mol Med*, *7*(5), 526-546. https://doi.org/10.15252/emmm.201404433

Pape, J. A., & Grose, J. H. (2020). The effects of diet and sex in amyotrophic lateral sclerosis. *Revue Neurologique*, *176*(5), 301-315. https://doi.org/https://doi.org/10.1016/j.neurol.2019.09.008

Parkinson, N., Ince, P. G., Smith, M. O., Highley, R., Skibinski, G., Andersen, P. M., Morrison, K. E., Pall, H. S., Hardiman, O., Collinge, J., Shaw, P. J., & Fisher, E. M. (2006). ALS phenotypes with mutations in CHMP2B (charged multivesicular body protein 2B). *Neurology*, *67*(6), 1074-1077. https://doi.org/10.1212/01.wnl.0000231510.89311.8b

Patel, P., & Abate, N. (2013). Body fat distribution and insulin resistance. *Nutrients*, *5*(6), 2019-2027. https://doi.org/10.3390/nu5062019

Pearce, J. M. S. (2003). Pick's disease. *Journal of Neurology, Neurosurgery & Psychiatry*, *74*(2), 169. https://doi.org/10.1136/jnnp.74.2.169

Peirce, J. L., Derr, R., Shendure, J., Kolata, T., & Silver, L. M. (1998). A major influence of sex-specific loci on alcohol preference in C57Bl/6 and DBA/2 inbred mice. *Mamm Genome*, *9*(12), 942-948. https://doi.org/10.1007/s003359900904

Picher-Martel, V., Brunet, F., Dupré, N., & Chrestian, N. (2020). The Occurrence of FUS Mutations in Pediatric Amyotrophic Lateral Sclerosis: A Case Report and Review of the Literature. *Journal of Child Neurology*, *35*(8), 556-562. https://doi.org/10.1177/0883073820915099

Pirker, W., & Katzenschlager, R. (2017). Gait disorders in adults and the elderly : A clinical guide. *Wien Klin Wochenschr*, *129*(3-4), 81-95. https://doi.org/10.1007/s00508-016-1096-4

Polymenidou, M., & Cleveland, D. W. (2011). The seeds of neurodegeneration: prion-like spreading in ALS. *Cell*, *147*(3), 498-508. https://doi.org/10.1016/j.cell.2011.10.011

Polymenidou, M., Lagier-Tourenne, C., Hutt, K. R., Huelga, S. C., Moran, J., Liang, T. Y., Ling, S. C., Sun, E., Wancewicz, E., Mazur, C., Kordasiewicz, H., Sedaghat, Y., Donohue, J. P., Shiue, L., Bennett, C. F., Yeo, G. W., & Cleveland, D. W. (2011). Long pre-mRNA depletion and RNA

missplicing contribute to neuronal vulnerability from loss of TDP-43. *Nat Neurosci*, *14*(4), 459-468. https://doi.org/10.1038/nn.2779

Poos, J. M., Jiskoot, L. C., Papma, J. M., van Swieten, J. C., & van den Berg, E. (2018). Meta-analytic Review of Memory Impairment in Behavioral Variant Frontotemporal Dementia. *Journal of the International Neuropsychological Society*, *24*(6), 593-605. https://doi.org/10.1017/S1355617718000115

Portet, F., Cadilhac, C., Touchon, J., & Camu, W. (2001). Cognitive impairment in motor neuron disease with bulbar onset. *Amyotrophic Lateral Sclerosis and Other Motor Neuron Disorders*, *2*(1), 23-29. https://doi.org/10.1080/146608201300079382

Prasad, A., Bharathi, V., Sivalingam, V., Girdhar, A., & Patel, B. K. (2019). Molecular Mechanisms of TDP-43 Misfolding and Pathology in Amyotrophic Lateral Sclerosis [Review]. *Frontiers in Molecular Neuroscience*, *12*. https://doi.org/10.3389/fnmol.2019.00025

Radcliffe, C., & Clarke, J. L. (1862). An important case of paralysis and muscular atrophy, with disease of the nervous centres. *The British and Foreign Medico-Chirurgical Review*, *30*(59), 215.

Rademakers, R., Stewart, H., Dejesus-Hernandez, M., Krieger, C., Graff-Radford, N., Fabros, M., Briemberg, H., Cashman, N., Eisen, A., & Mackenzie, I. R. (2010). Fus gene mutations in familial and sporadic amyotrophic lateral sclerosis. *Muscle Nerve*, *42*(2), 170-176. https://doi.org/10.1002/mus.21665

Renton, A. E., Majounie, E., Waite, A., Simón-Sánchez, J., Rollinson, S., Gibbs, J. R., Schymick, J. C., Laaksovirta, H., van Swieten, J. C., Myllykangas, L., Kalimo, H., Paetau, A., Abramzon, Y., Remes, A. M., Kaganovich, A., Scholz, S. W., Duckworth, J., Ding, J., Harmer, D. W., . . . Traynor, B. J. (2011). A hexanucleotide repeat expansion in C9ORF72 is the cause of chromosome 9p21-linked ALS-FTD. *Neuron*, *72*(2), 257-268. https://doi.org/10.1016/j.neuron.2011.09.010

Richter, E. A., & Hargreaves, M. (2013). Exercise, GLUT4, and Skeletal Muscle Glucose Uptake. *Physiological Reviews*, *93*(3), 993-1017. https://doi.org/10.1152/physrev.00038.2012

Ricketts, T., McGoldrick, P., Fratta, P., de Oliveira, H. M., Kent, R., Phatak, V., Brandner, S., Blanco, G., Greensmith, L., Acevedo-Arozena, A., & Fisher, E. M. (2014). A nonsense mutation in mouse Tardbp affects TDP43 alternative splicing activity and causes limb-clasping and body tone defects. *PLoS One*, *9*(1), e85962. https://doi.org/10.1371/journal.pone.0085962

Rogelj, B., Easton, L. E., Bogu, G. K., Stanton, L. W., Rot, G., Curk, T., Zupan, B., Sugimoto, Y., Modic, M., Haberman, N., Tollervey, J., Fujii, R., Takumi, T., Shaw, C. E., & Ule, J. (2012). Widespread binding of FUS along nascent RNA regulates alternative splicing in the brain. *Scientific Reports*, *2*(1), 603. https://doi.org/10.1038/srep00603

Rohrer, J. D., Guerreiro, R., Vandrovcova, J., Uphill, J., Reiman, D., Beck, J., Isaacs, A. M., Authier, A., Ferrari, R., Fox, N. C., Mackenzie, I. R., Warren, J. D., de Silva, R., Holton, J., Revesz, T., Hardy, J., Mead, S., & Rossor, M. N. (2009). The heritability and genetics of frontotemporal lobar degeneration. *Neurology*, *73*(18), 1451-1456. https://doi.org/10.1212/WNL.0b013e3181bf997a

Rooney, J., Fogh, I., Westeneng, H. J., Vajda, A., McLaughlin, R., Heverin, M., Jones, A., van Eijk, R., Calvo, A., Mazzini, L., Shaw, C., Morrison, K., Shaw, P. J., Robberecht, W., Van Damme, P., Al-Chalabi, A., van den Berg, L., Chiò, A., Veldink, J., & Hardiman, O. (2017). C9orf72

expansion differentially affects males with spinal onset amyotrophic lateral sclerosis. *J Neurol Neurosurg Psychiatry*, *88*(4), 281. https://doi.org/10.1136/jnnp-2016-314093

Rosen, D. R., Siddique, T., Patterson, D., Figlewicz, D. A., Sapp, P., Hentati, A., Donaldson, D., Goto, J., O'Regan, J. P., Deng, H. X., & et al. (1993). Mutations in Cu/Zn superoxide dismutase gene are associated with familial amyotrophic lateral sclerosis. *Nature*, *362*(6415), 59-62. https://doi.org/10.1038/362059a0

Sahadevan, S., Hembach, K. M., Tantardini, E., Pérez-Berlanga, M., Hruska-Plochan, M., Megat, S., Weber, J., Schwarz, P., Dupuis, L., Robinson, M. D., De Rossi, P., & Polymenidou, M. (2021). Synaptic FUS accumulation triggers early misregulation of synaptic RNAs in a mouse model of ALS. *Nature Communications*, *12*(1), 3027. https://doi.org/10.1038/s41467-021-23188-8

Sanjuan-Ruiz, I., Govea-Perez, N., McAlonis-Downes, M., Dieterle, S., Megat, S., Dirrig-Grosch, S., Picchiarelli, G., Piol, D., Zhu, Q., Myers, B., Lee, C.-Z., Cleveland, D. W., Lagier-Tourenne, C., Da Cruz, S., & Dupuis, L. (2021). Wild-type FUS corrects ALS-like disease induced by cytoplasmic mutant FUS through autoregulation. *Molecular Neurodegeneration*, *16*(1), 61. https://doi.org/10.1186/s13024-021-00477-w

Saxon, J. A., Thompson, J. C., Jones, M., Harris, J. M., Richardson, A. M. T., Langheinrich, T., Neary, D., Mann, D. M. A., & Snowden, J. S. (2017). Examining the language and behavioural profile in FTD and ALS-FTD. *Journal of Neurology, Neurosurgery & Psychiatry*, *88*(8), 675. https://doi.org/10.1136/jnnp-2017-315667

Scaricamazza, S., Salvatori, I., Giacovazzo, G., Loeffler, J. P., Renè, F., Rosina, M., Quessada, C., Proietti, D., Heil, C., Rossi, S., Battistini, S., Giannini, F., Volpi, N., Steyn, F. J., Ngo, S. T., Ferraro, E., Madaro, L., Coccurello, R., Valle, C., & Ferri, A. (2020). Skeletal-Muscle Metabolic Reprogramming in ALS-SOD1(G93A) Mice Predates Disease Onset and Is A Promising Therapeutic Target. *iScience*, *23*(5), 101087. https://doi.org/10.1016/j.isci.2020.101087

Scekic-Zahirovic, J., Sanjuan-Ruiz, I., Kan, V., Megat, S., De Rossi, P., Dieterlé, S., Cassel, R., Jamet, M., Kessler, P., Wiesner, D., Tzeplaeff, L., Demais, V., Sahadevan, S., Hembach, K. M., Muller, H.-P., Picchiarelli, G., Mishra, N., Antonucci, S., Dirrig-Grosch, S., . . . Dupuis, L. (2021). Cytoplasmic FUS triggers early behavioral alterations linked to cortical neuronal hyperactivity and inhibitory synaptic defects. *Nature Communications*, *12*(1), 3028. https://doi.org/10.1038/s41467-021-23187-9

Scekic-Zahirovic, J., Sendscheid, O., El Oussini, H., Jambeau, M., Sun, Y., Mersmann, S., Wagner, M., Dieterlé, S., Sinniger, J., Dirrig-Grosch, S., Drenner, K., Birling, M.-C., Qiu, J., Zhou, Y., Li, H., Fu, X.-D., Rouaux, C., Shelkovnikova, T., Witting, A., . . . Dupuis, L. (2016). Toxic gain of function from mutant FUS protein is crucial to trigger cell autonomous motor neuron loss. *The EMBO Journal*, *35*(10), 1077-1097. https://doi.org/https://doi.org/10.15252/embj.201592559

Schor, N. F., & Bianchi, D. W. (2021). Neurodevelopmental Clues to Neurodegeneration. *Pediatric Neurology*, *123*, 67-76. https://doi.org/https://doi.org/10.1016/j.pediatrneurol.2021.07.012

Selman, C., & Swindell, W. R. (2018). Putting a strain on diversity. *EMBO J*, *37*(22). https://doi.org/10.15252/embj.2018100862

Sephton, C. F., Cenik, B., Cenik, B. K., Herz, J., & Yu, G. (2012). TDP-43 in central nervous system development and function: clues to TDP-43-associated neurodegeneration. *Biol Chem*, *393*(7), 589-594. https://doi.org/10.1515/hsz-2012-0115

Sephton, C. F., Cenik, C., Kucukural, A., Dammer, E. B., Cenik, B., Han, Y., Dewey, C. M., Roth, F. P., Herz, J., Peng, J., Moore, M. J., & Yu, G. (2011). Identification of neuronal RNA targets of TDP-43-containing ribonucleoprotein complexes. *J Biol Chem*, *286*(2), 1204-1215. https://doi.org/10.1074/jbc.M110.190884

Sephton, C. F., Good, S. K., Atkin, S., Dewey, C. M., Mayer, P., 3rd, Herz, J., & Yu, G. (2010). TDP-43 is a developmentally regulated protein essential for early embryonic development. *J Biol Chem*, *285*(9), 6826-6834. https://doi.org/10.1074/jbc.M109.061846

Sephton, C. F., Tang, A. A., Kulkarni, A., West, J., Brooks, M., Stubblefield, J. J., Liu, Y., Zhang, M. Q., Green, C. B., Huber, K. M., Huang, E. J., Herz, J., & Yu, G. (2014). Activity-dependent FUS dysregulation disrupts synaptic homeostasis. *Proc Natl Acad Sci U S A*, *111*(44), E4769-4778. https://doi.org/10.1073/pnas.1406162111

Sephton, C. F., & Yu, G. (2015). The function of RNA-binding proteins at the synapse: implications for neurodegeneration. *Cell Mol Life Sci*, *72*(19), 3621-3635. https://doi.org/10.1007/s00018-015-1943-x

Shan, X., Chiang, P. M., Price, D. L., & Wong, P. C. (2010). Altered distributions of Gemini of coiled bodies and mitochondria in motor neurons of TDP-43 transgenic mice. *Proc Natl Acad Sci U S A*, *107*(37), 16325-16330. https://doi.org/10.1073/pnas.1003459107

Shang, Y., & Huang, E. J. (2016). Mechanisms of FUS mutations in familial amyotrophic lateral sclerosis. *Brain Research*, *1647*, 65-78. https://doi.org/https://doi.org/10.1016/j.brainres.2016.03.036

Shiihashi, G., Ito, D., Yagi, T., Nihei, Y., Ebine, T., & Suzuki, N. (2016). Mislocated FUS is sufficient for gain-of-toxic-function amyotrophic lateral sclerosis phenotypes in mice. *Brain*, *139*(Pt 9), 2380-2394. https://doi.org/10.1093/brain/aww161

Shoji, H., Takao, K., Hattori, S., & Miyakawa, T. (2014). Contextual and cued fear conditioning test using a video analyzing system in mice. *J Vis Exp*(85). https://doi.org/10.3791/50871

Skibinski, G., Parkinson, N. J., Brown, J. M., Chakrabarti, L., Lloyd, S. L., Hummerich, H., Nielsen, J. E., Hodges, J. R., Spillantini, M. G., Thusgaard, T., Brandner, S., Brun, A., Rossor, M. N., Gade, A., Johannsen, P., Sørensen, S. A., Gydesen, S., Fisher, E. M., & Collinge, J. (2005). Mutations in the endosomal ESCRTIII-complex subunit CHMP2B in frontotemporal dementia. *Nat Genet*, *37*(8), 806-808. https://doi.org/10.1038/ng1609

Slanzi, A., Iannoto, G., Rossi, B., Zenaro, E., & Constantin, G. (2020). In vitro Models of Neurodegenerative Diseases [Review]. *Frontiers in Cell and Developmental Biology*, *8*. https://doi.org/10.3389/fcell.2020.00328

Sloin, H. E., Bikovski, L., Levi, A., Amber-Vitos, O., Katz, T., Spivak, L., Someck, S., Gattegno, R., Sivroni, S., Sjulson, L., & Stark, E. (2022). Hybrid offspring of C57BL/6J mice exhibit improved properties for neurobehavioral research. *bioRxiv*, 2022.2005.2003.490527. https://doi.org/10.1101/2022.05.03.490527

Smeyers, J., Banchi, E.-G., & Latouche, M. (2021). C9ORF72: What It Is, What It Does, and Why It Matters [Review]. *Frontiers in Cellular Neuroscience*, *15*. https://doi.org/10.3389/fncel.2021.661447

Speakman, J. R. (2019). Use of high-fat diets to study rodent obesity as a model of human obesity. *International Journal of Obesity*, *43*(8), 1491-1492. https://doi.org/10.1038/s41366-019-0363-7

Sprott, R. L., & Ramirez, I. (1997). Current Inbred and Hybrid Rat and Mouse Models for Gereontological Research. *Ilar j*, *38*(3), 104-109. https://doi.org/10.1093/ilar.38.3.104

Sreedharan, J., Blair, I. P., Tripathi, V. B., Hu, X., Vance, C., Rogelj, B., Ackerley, S., Durnall, J. C., Williams, K. L., Buratti, E., Baralle, F., de Belleroche, J., Mitchell, J. D., Leigh, P. N., Al-Chalabi, A., Miller, C. C., Nicholson, G., & Shaw, C. E. (2008). TDP-43 mutations in familial and sporadic amyotrophic lateral sclerosis. *Science*, *319*(5870), 1668-1672. https://doi.org/10.1126/science.1154584

Stallings, N. R., Puttaparthi, K., Dowling, K. J., Luther, C. M., Burns, D. K., Davis, K., & Elliott, J. L. (2013). TDP-43, an ALS linked protein, regulates fat deposition and glucose homeostasis. *PLoS One*, *8*(8), e71793. https://doi.org/10.1371/journal.pone.0071793

Stallings, N. R., Puttaparthi, K., Luther, C. M., Burns, D. K., & Elliott, J. L. (2010). Progressive motor weakness in transgenic mice expressing human TDP-43. *Neurobiol Dis*, *40*(2), 404-414. https://doi.org/10.1016/j.nbd.2010.06.017

Steyn, F. J., Ioannides, Z. A., van Eijk, R. P. A., Heggie, S., Thorpe, K. A., Ceslis, A., Heshmat, S., Henders, A. K., Wray, N. R., van den Berg, L. H., Henderson, R. D., McCombe, P. A., & Ngo, S. T. (2018). Hypermetabolism in ALS is associated with greater functional decline and shorter survival. *J Neurol Neurosurg Psychiatry*, *89*(10), 1016-1023. https://doi.org/10.1136/jnnp-2017-317887

Stottmann, R., & Beier, D. (2014). ENU Mutagenesis in the Mouse. *Curr Protoc Hum Genet*, *82*, 15.14.11-10. https://doi.org/10.1002/0471142905.hg1504s82

Suk, T. R., & Rousseaux, M. W. C. (2020). The role of TDP-43 mislocalization in amyotrophic lateral sclerosis. *Molecular Neurodegeneration*, *15*(1), 45. https://doi.org/10.1186/s13024-020-00397-1

Swarup, V., Phaneuf, D., Bareil, C., Robertson, J., Rouleau, G. A., Kriz, J., & Julien, J. P. (2011). Pathological hallmarks of amyotrophic lateral sclerosis/frontotemporal lobar degeneration in transgenic mice produced with TDP-43 genomic fragments. *Brain*, *134*(Pt 9), 2610-2626. https://doi.org/10.1093/brain/awr159

Swinnen, B., & Robberecht, W. (2014). The phenotypic variability of amyotrophic lateral sclerosis. *Nat Rev Neurol*, *10*(11), 661-670. https://doi.org/10.1038/nrneurol.2014.184

Tadenev, A. L. D., & Burgess, R. W. (2019). Model validity for preclinical studies in precision medicine: precisely how precise do we need to be? *Mammalian Genome*, *30*(5), 111-122. https://doi.org/10.1007/s00335-019-09798-0

Tajsharghi, H., Hammans, S., Lindberg, C., Lossos, A., Clarke, N. F., Mazanti, I., Waddell, L. B., Fellig, Y., Foulds, N., Katifi, H., Webster, R., Raheem, O., Udd, B., Argov, Z., & Oldfors, A. (2014). Recessive myosin myopathy with external ophthalmoplegia associated with MYH2 mutations. *Eur J Hum Genet*, *22*(6), 801-808. https://doi.org/10.1038/ejhg.2013.250

Taketo, M., Schroeder, A. C., Mobraaten, L. E., Gunning, K. B., Hanten, G., Fox, R. R., Roderick, T. H., Stewart, C. L., Lilly, F., Hansen, C. T., & et al. (1991). FVB/N: an inbred mouse strain preferable for transgenic analyses. *Proc Natl Acad Sci U S A*, *88*(6), 2065-2069. https://doi.org/10.1073/pnas.88.6.2065

Tan, K. W., Yeo, K. P., Wong, F. H., Lim, H. Y., Khoo, K. L., Abastado, J. P., & Angeli, V. (2012). Expansion of cortical and medullary sinuses restrains lymph node hypertrophy during prolonged inflammation. *J Immunol*, *188*(8), 4065-4080. https://doi.org/10.4049/jimmunol.1101854

Tanimizu, T., Kono, K., & Kida, S. (2018). Brain networks activated to form object recognition memory. *Brain Research Bulletin*, *141*, 27-34. https://doi.org/https://doi.org/10.1016/j.brainresbull.2017.05.017

Teyssou, E., Takeda, T., Lebon, V., Boillée, S., Doukouré, B., Bataillon, G., Sazdovitch, V., Cazeneuve, C., Meininger, V., LeGuern, E., Salachas, F., Seilhean, D., & Millecamps, S. (2013). Mutations in SQSTM1 encoding p62 in amyotrophic lateral sclerosis: genetics and neuropathology. *Acta Neuropathol*, *125*(4), 511-522. https://doi.org/10.1007/s00401-013-1090-0

Theunissen, F., Anderton, R. S., Mastaglia, F. L., Flynn, L. L., Winter, S. J., James, I., Bedlack, R., Hodgetts, S., Fletcher, S., Wilton, S. D., Laing, N. G., MacShane, M., Needham, M., Saunders, A., Mackay-Sim, A., Melamed, Z. e., Ravits, J., Cleveland, D. W., & Akkari, P. A. (2021). Novel STMN2 Variant Linked to Amyotrophic Lateral Sclerosis Risk and Clinical Phenotype [Original Research]. *Frontiers in Aging Neuroscience*, *13*. https://doi.org/10.3389/fnagi.2021.658226

Ticozzi, N., Silani, V., LeClerc, A. L., Keagle, P., Gellera, C., Ratti, A., Taroni, F., Kwiatkowski, T. J., Jr., McKenna-Yasek, D. M., Sapp, P. C., Brown, R. H., Jr., & Landers, J. E. (2009). Analysis of FUS gene mutation in familial amyotrophic lateral sclerosis within an Italian cohort. *Neurology*, *73*(15), 1180-1185. https://doi.org/10.1212/WNL.0b013e3181bbff05

Ticozzi, N., Vance, C., LeClerc, A. L., Keagle, P., Glass, J. D., McKenna-Yasek, D., Sapp, P. C., Silani, V., Bosco, D. A., Shaw, C. E., Brown Jr, R. H., & Landers, J. E. (2011). Mutational analysis reveals the FUS homolog TAF15 as a candidate gene for familial amyotrophic lateral sclerosis. *American Journal of Medical Genetics Part B: Neuropsychiatric Genetics*, *156*(3), 285-290. https://doi.org/https://doi.org/10.1002/ajmg.b.31158

Timper, K., & Brüning, J. C. (2017). Hypothalamic circuits regulating appetite and energy homeostasis: pathways to obesity. *Dis Model Mech*, *10*(6), 679-689. https://doi.org/10.1242/dmm.026609

Tollervey, J. R., Curk, T., Rogelj, B., Briese, M., Cereda, M., Kayikci, M., König, J., Hortobágyi, T., Nishimura, A. L., Zupunski, V., Patani, R., Chandran, S., Rot, G., Zupan, B., Shaw, C. E., & Ule, J. (2011). Characterizing the RNA targets and position-dependent splicing regulation by TDP-43. *Nat Neurosci*, *14*(4), 452-458. https://doi.org/10.1038/nn.2778

Tran, L. T., Park, S., Kim, S. K., Lee, J. S., Kim, K. W., & Kwon, O. (2022). Hypothalamic control of energy expenditure and thermogenesis. *Experimental & Molecular Medicine*, *54*(4), 358-369. https://doi.org/10.1038/s12276-022-00741-z

Tsai, K. J., Yang, C. H., Fang, Y. H., Cho, K. H., Chien, W. L., Wang, W. T., Wu, T. W., Lin, C. P., Fu, W. M., & Shen, C. K. (2010). Elevated expression of TDP-43 in the forebrain of mice is sufficient to cause neurological and pathological phenotypes mimicking FTLD-U. *J Exp Med*, *207*(8), 1661-1673. https://doi.org/10.1084/jem.20092164

Tuttle, A. H., Philip, V. M., Chesler, E. J., & Mogil, J. S. (2018). Comparing phenotypic variation between inbred and outbred mice. *Nature Methods*, *15*(12), 994-996. https://doi.org/10.1038/s41592-018-0224-7

Tyzack, G. E., Luisier, R., Taha, D. M., Neeves, J., Modic, M., Mitchell, J. S., Meyer, I., Greensmith, L., Newcombe, J., Ule, J., Luscombe, N. M., & Patani, R. (2019). Widespread FUS mislocalization is a molecular hallmark of amyotrophic lateral sclerosis. *Brain*, *142*(9), 2572-2580. https://doi.org/10.1093/brain/awz217

Uchimura, A., Higuchi, M., Minakuchi, Y., Ohno, M., Toyoda, A., Fujiyama, A., Miura, I., Wakana, S., Nishino, J., & Yagi, T. (2015). Germline mutation rates and the long-term phenotypic effects of mutation accumulation in wild-type laboratory mice and mutator mice. *Genome Res*, *25*(8), 1125-1134. https://doi.org/10.1101/gr.186148.114

Ullah, M. F., Ahmad, A., Bhat, S. H., Abu-Duhier, F. M., Barreto, G. E., & Ashraf, G. M. (2019). Impact of sex differences and gender specificity on behavioral characteristics and pathophysiology of neurodegenerative disorders. *Neuroscience & Biobehavioral Reviews*, *102*, 95-105. https://doi.org/https://doi.org/10.1016/j.neubiorev.2019.04.003

van Asselen, M., Kessels, R. P. C., Neggers, S. F. W., Kappelle, L. J., Frijns, C. J. M., & Postma, A. (2006). Brain areas involved in spatial working memory. *Neuropsychologia*, *44*(7), 1185-1194. https://doi.org/https://doi.org/10.1016/j.neuropsychologia.2005.10.005

Van Langenhove, T., van der Zee, J., & Van Broeckhoven, C. (2012). The molecular basis of the frontotemporal lobar degeneration-amyotrophic lateral sclerosis spectrum. *Ann Med*, *44*(8), 817-828. https://doi.org/10.3109/07853890.2012.665471

Van Mossevelde, S., van der Zee, J., Gijselinck, I., Engelborghs, S., Sieben, A., Van Langenhove, T., De Bleecker, J., Baets, J., Vandenbulcke, M., Van Laere, K., Ceyssens, S., Van den Broeck, M., Peeters, K., Mattheijssens, M., Cras, P., Vandenberghe, R., De Jonghe, P., Martin, J. J., De Deyn, P. P., . . . Van Broeckhoven, C. (2016). Clinical features of TBK1 carriers compared with C9orf72, GRN and non-mutation carriers in a Belgian cohort. *Brain*, *139*(Pt 2), 452-467. https://doi.org/10.1093/brain/awv358

Vance, C., Rogelj, B., Hortobágyi, T., De Vos, K. J., Nishimura, A. L., Sreedharan, J., Hu, X., Smith, B., Ruddy, D., Wright, P., Ganesalingam, J., Williams, K. L., Tripathi, V., Al-Saraj, S., Al-Chalabi, A., Leigh, P. N., Blair, I. P., Nicholson, G., de Belleroche, J., . . . Shaw, C. E. (2009). Mutations in FUS, an RNA processing protein, cause familial amyotrophic lateral sclerosis type 6. *Science*, *323*(5918), 1208-1211. https://doi.org/10.1126/science.1165942

Vance, C., Scotter, E. L., Nishimura, A. L., Troakes, C., Mitchell, J. C., Kathe, C., Urwin, H., Manser, C., Miller, C. C., Hortobágyi, T., Dragunow, M., Rogelj, B., & Shaw, C. E. (2013). ALS mutant FUS disrupts nuclear localization and sequesters wild-type FUS within cytoplasmic stress granules. *Hum Mol Genet*, *22*(13), 2676-2688. https://doi.org/10.1093/hmg/ddt117

Verstraete, E., Veldink, J. H., Hendrikse, J., Schelhaas, H. J., van den Heuvel, M. P., & van den Berg, L. H. (2012). Structural MRI reveals cortical thinning in amyotrophic lateral sclerosis. *J Neurol Neurosurg Psychiatry*, *83*(4), 383-388. https://doi.org/10.1136/jnnp-2011-300909

Voelkl, B., Vogt, L., Sena, E. S., & Würbel, H. (2018). Reproducibility of preclinical animal research improves with heterogeneity of study samples. *PLoS Biol*, *16*(2), e2003693. https://doi.org/10.1371/journal.pbio.2003693

von Kortzfleisch, V. T., Karp, N. A., Palme, R., Kaiser, S., Sachser, N., & Richter, S. H. (2020). Improving reproducibility in animal research by splitting the study population into several 'mini-experiments'. *Scientific Reports*, *10*(1), 16579. https://doi.org/10.1038/s41598-020-73503-4

Vossel, K. A., & Miller, B. L. (2008). New approaches to the treatment of frontotemporal lobar degeneration. *Curr Opin Neurol*, *21*(6), 708-716. https://doi.org/10.1097/WCO.0b013e328318444d

Waibel, S., Neumann, M., Rosenbohm, A., Birve, A., Volk, A. E., Weishaupt, J. H., Meyer, T., Müller, U., Andersen, P. M., & Ludolph, A. C. (2013). Truncating mutations in FUS/TLS give

rise to a more aggressive ALS-phenotype than missense mutations: a clinico-genetic study in Germany. *Eur J Neurol*, *20*(3), 540-546. https://doi.org/10.1111/ene.12031

Walker, A. K., Spiller, K. J., Ge, G., Zheng, A., Xu, Y., Zhou, M., Tripathy, K., Kwong, L. K., Trojanowski, J. Q., & Lee, V. M. (2015). Functional recovery in new mouse models of ALS/FTLD after clearance of pathological cytoplasmic TDP-43. *Acta Neuropathol*, *130*(5), 643-660. https://doi.org/10.1007/s00401-015-1460-x

Wang, I. F., Wu, L. S., Chang, H. Y., & Shen, C. K. (2008). TDP-43, the signature protein of FTLD-U, is a neuronal activity-responsive factor. *J Neurochem*, *105*(3), 797-806. https://doi.org/10.1111/j.1471-4159.2007.05190.x

Wang, P., Zhang, H., Wang, Y., Zhang, M., & Zhou, Y. (2020). Plasma cholesterol in Alzheimer's disease and frontotemporal dementia. *Transl Neurosci*, *11*(1), 116-123. https://doi.org/10.1515/tnsci-2020-0098

Wang, T., Jiang, X., Chen, G., & Xu, J. (2015). Interaction of amyotrophic lateral sclerosis/frontotemporal lobar degeneration-associated fused-in-sarcoma with proteins involved in metabolic and protein degradation pathways. *Neurobiol Aging*, *36*(1), 527-535. https://doi.org/10.1016/j.neurobiolaging.2014.07.044

Wang, Y., Duan, X., Zhou, X., Wang, R., Zhang, X., Cao, Z., Wang, X., Zhou, Z., Sun, Y., & Peng, D. (2022). ANXA11 mutations are associated with amyotrophic lateral sclerosis–frontotemporal dementia [Original Research]. *Frontiers in Neurology*, *13*. https://doi.org/10.3389/fneur.2022.886887

Watkins, J., Ghosh, A., Keerie, A. F. A., Alix, J. J. P., Mead, R. J., & Sreedharan, J. (2020). Female sex mitigates motor and behavioural phenotypes in TDP-43Q331K knock-in mice. *Scientific Reports*, *10*(1), 19220. https://doi.org/10.1038/s41598-020-76070-w

Weidberg, H., & Elazar, Z. (2011). TBK1 mediates crosstalk between the innate immune response and autophagy. *Sci Signal*, *4*(187), pe39. https://doi.org/10.1126/scisignal.2002355

Weishaupt, J. H., Hyman, T., & Dikic, I. (2016). Common Molecular Pathways in Amyotrophic Lateral Sclerosis and Frontotemporal Dementia. *Trends Mol Med*, *22*(9), 769-783. https://doi.org/10.1016/j.molmed.2016.07.005

White, M. A., Kim, E., Duffy, A., Adalbert, R., Phillips, B. U., Peters, O. M., Stephenson, J., Yang, S., Massenzio, F., Lin, Z., Andrews, S., Segonds-Pichon, A., Metterville, J., Saksida, L. M., Mead, R., Ribchester, R. R., Barhomi, Y., Serre, T., Coleman, M. P., . . . Sreedharan, J. (2018). TDP-43 gains function due to perturbed autoregulation in a Tardbp knock-in mouse model of ALS-FTD. *Nature Neuroscience*, *21*(4), 552-563. https://doi.org/10.1038/s41593-018-0113-5

Wills, A. M., Hubbard, J., Macklin, E. A., Glass, J., Tandan, R., Simpson, E. P., Brooks, B., Gelinas, D., Mitsumoto, H., Mozaffar, T., Hanes, G. P., Ladha, S. S., Heiman-Patterson, T., Katz, J., Lou, J. S., Mahoney, K., Grasso, D., Lawson, R., Yu, H., & Cudkowicz, M. (2014). Hypercaloric enteral nutrition in patients with amyotrophic lateral sclerosis: a randomised, double-blind, placebo-controlled phase 2 trial. *Lancet*, *383*(9934), 2065-2072. https://doi.org/10.1016/s0140-6736(14)60222-1

Wils, H., Kleinberger, G., Janssens, J., Pereson, S., Joris, G., Cuijt, I., Smits, V., Ceuterick-de Groote, C., Van Broeckhoven, C., & Kumar-Singh, S. (2010). TDP-43 transgenic mice develop spastic paralysis and neuronal inclusions characteristic of ALS and frontotemporal lobar degeneration. *Proc Natl Acad Sci U S A*, *107*(8), 3858-3863. https://doi.org/10.1073/pnas.0912417107

Wilson, R. S., Yu, L., Trojanowski, J. Q., Chen, E. Y., Boyle, P. A., Bennett, D. A., & Schneider, J. A. (2013). TDP-43 pathology, cognitive decline, and dementia in old age. *JAMA Neurol*, *70*(11), 1418-1424. https://doi.org/10.1001/jamaneurol.2013.3961

Witzel, S., Maier, A., Steinbach, R., Grosskreutz, J., Koch, J. C., Sarikidi, A., Petri, S., Günther, R., Wolf, J., Hermann, A., Prudlo, J., Cordts, I., Lingor, P., Löscher, W. N., Kohl, Z., Hagenacker, T., Ruckes, C., Koch, B., Spittel, S., . . . Network, G. M. N. D. (2022). Safety and Effectiveness of Long-term Intravenous Administration of Edaravone for Treatment of Patients With Amyotrophic Lateral Sclerosis. *JAMA Neurology*, *79*(2), 121-130. https://doi.org/10.1001/jamaneurol.2021.4893

Wolmarans de, W., Stein, D. J., & Harvey, B. H. (2016). Of mice and marbles: Novel perspectives on burying behavior as a screening test for psychiatric illness. *Cogn Affect Behav Neurosci*, *16*(3), 551-560. https://doi.org/10.3758/s13415-016-0413-8

Xu, L., Liu, T., Liu, L., Yao, X., Chen, L., Fan, D., Zhan, S., & Wang, S. (2020). Global variation in prevalence and incidence of amyotrophic lateral sclerosis: a systematic review and meta-analysis. *Journal of Neurology*, *267*(4), 944-953. https://doi.org/10.1007/s00415-019-09652-y

Xu, Y.-F., Gendron, T. F., Zhang, Y.-J., Lin, W.-L., Alton, S., Sheng, H., Casey, M. C., Tong, J., Knight, J., Yu, X., Rademakers, R., Boylan, K., Hutton, M., McGowan, E., Dickson, D. W., Lewis, J., & Petrucelli, L. (2010). Wild-Type Human TDP-43 Expression Causes TDP-43 Phosphorylation, Mitochondrial Aggregation, Motor Deficits, and Early Mortality in Transgenic Mice. *The Journal of Neuroscience*, *30*(32), 10851. https://doi.org/10.1523/JNEUROSCI.1630-10.2010

Xu, Y. F., Zhang, Y. J., Lin, W. L., Cao, X., Stetler, C., Dickson, D. W., Lewis, J., & Petrucelli, L. (2011). Expression of mutant TDP-43 induces neuronal dysfunction in transgenic mice. *Mol Neurodegener*, *6*, 73. https://doi.org/10.1186/1750-1326-6-73

Yoshiki, A., & Moriwaki, K. (2006). Mouse Phenome Research: Implications of Genetic Background. *ILAR Journal*, *47*(2), 94-102. https://doi.org/10.1093/ilar.47.2.94

Zarei, S., Carr, K., Reiley, L., Diaz, K., Guerra, O., Altamirano, P. F., Pagani, W., Lodin, D., Orozco, G., & Chinea, A. (2015). A comprehensive review of amyotrophic lateral sclerosis. *Surg Neurol Int*, *6*, 171. https://doi.org/10.4103/2152-7806.169561

Zhou, B.-R., Feng, H., Kato, H., Dai, L., Yang, Y., Zhou, Y., & Bai, Y. (2013). Structural insights into the histone H1-nucleosome complex. *Proceedings of the National Academy of Sciences*, *110*(48), 19390-19395. https://doi.org/doi:10.1073/pnas.1314905110

Zhou, B., Wang, H., Cai, Y., Wen, H., Wang, L., Zhu, M., Chen, Y., Yu, Y., Lu, X., Zhou, M., Fang, P., Li, X., & Hong, D. (2020). FUS P525L mutation causing amyotrophic lateral sclerosis and movement disorders. *Brain Behav*, *10*(6), e01625. https://doi.org/10.1002/brb3.1625

Zhou, B., Zheng, Y., Li, X., Dong, H., Yu, J., Zou, Y., Zhu, M., Yu, Y., Fang, X., Zhou, M., Zhang, W., Yuan, Y., Wang, Z., Deng, J., & Hong, D. (2022). FUS Mutation Causes Disordered Lipid Metabolism in Skeletal Muscle Associated with ALS. *Molecular Neurobiology*. https://doi.org/10.1007/s12035-022-03048-2

Zhou, Y., Liu, S., Liu, G., Oztürk, A., & Hicks, G. G. (2013). ALS-associated FUS mutations result in compromised FUS alternative splicing and autoregulation. *PLoS Genet*, *9*(10), e1003895. https://doi.org/10.1371/journal.pgen.1003895

Zhou, Y., Liu, S., Oztürk, A., & Hicks, G. G. (2014). FUS-regulated RNA metabolism and DNA damage repair: Implications for amyotrophic lateral sclerosis and frontotemporal dementia pathogenesis. *Rare Dis*, *2*, e29515. https://doi.org/10.4161/rdis.29515

Zhou, Z. D., Saw, W. T., & Tan, E. K. (2017). Mitochondrial CHCHD-Containing Proteins: Physiologic Functions and Link with Neurodegenerative Diseases. *Mol Neurobiol*, *54*(7), 5534-5546. https://doi.org/10.1007/s12035-016-0099-5

Zilberter, Y., & Zilberter, M. (2017). The vicious circle of hypometabolism in neurodegenerative diseases: Ways and mechanisms of metabolic correction. *Journal of Neuroscience Research*, *95*(11), 2217-2235. https://doi.org/https://doi.org/10.1002/jnr.24064

Zinszner, H., Sok, J., Immanuel, D., Yin, Y., & Ron, D. (1997). TLS (FUS) binds RNA in vivo and engages in nucleo-cytoplasmic shuttling. *J Cell Sci*, *110 (Pt 15)*, 1741-1750. https://doi.org/10.1242/jcs.110.15.1741

Zou, Z. Y., Liu, M. S., Li, X. G., & Cui, L. Y. (2016). Mutations in FUS are the most frequent genetic cause in juvenile sporadic ALS patients of Chinese origin. *Amyotroph Lateral Scler Frontotemporal Degener*, *17*(3-4), 249-252. https://doi.org/10.3109/21678421.2016.1143012

Zucchi, E., Ticozzi, N., & Mandrioli, J. (2019). Psychiatric Symptoms in Amyotrophic Lateral Sclerosis: Beyond a Motor Neuron Disorder [Review]. *Frontiers in Neuroscience*, *13*. https://doi.org/10.3389/fnins.2019.00175

Appendices

8 Appendices

Appendix A: RNA-seq tables of significantly differentiated genes (DEGs) in each tissue of the *Fus*$^{\Delta 14}$ homozygous mouse (**A1-5**), *Fus* gene expression in *Fus*$^{\Delta 14}$ tissues (**A6**) and quality of RNA samples used for transcriptomic analysis (**A7**).

Gene ID	EnsemblID	log2FoldChange	p-value	q-value
Rps15a-ps7	ENSMUSG00000081087	-4.664354444	4.72119E-25	7.54634E-21
Gm19963	ENSMUSG00000109404	-2.887155385	3.05804E-21	2.44398E-17
Gm42047	ENSMUSG00000110631	2.683138407	1.07531E-20	5.72926E-17
Rufy4	ENSMUSG00000061815	-1.864063923	3.9551E-12	1.58046E-08
AC114585.1	ENSMUSG00000115099	1.174573865	1.71222E-11	4.58852E-08
Gm14295	ENSMUSG00000078877	-0.959952296	1.72242E-11	4.58852E-08
Fus	ENSMUSG00000030795	0.86413938	7.70792E-11	1.76005E-07
Ddc	ENSMUSG00000020182	-0.79122857	2.2412E-10	4.47792E-07
Gm38300	ENSMUSG00000104279	-1.982905716	3.62501E-10	6.43802E-07
Serpind1	ENSMUSG00000022766	-1.018457116	7.59237E-10	1.21356E-06
B330016D10Rik	ENSMUSG00000048406	-1.259696804	5.86446E-09	8.5216E-06
Clgn	ENSMUSG00000002190	0.667729838	6.53307E-09	8.70204E-06
Hist1h1c	ENSMUSG00000036181	-0.962047104	8.22817E-09	1.01169E-05
Gm44645	ENSMUSG00000108601	-1.713132671	3.90869E-08	4.1651E-05
Hbb-bt	ENSMUSG00000073940	-1.558679006	3.90404E-08	4.1651E-05
Tdgf1	ENSMUSG00000032494	-0.933593859	4.23815E-08	4.23391E-05
Gpx3	ENSMUSG00000018339	-0.891044927	4.97748E-08	4.68E-05
Spp1	ENSMUSG00000029304	-0.754987466	1.70489E-07	0.000151395
Ggt5	ENSMUSG00000006344	-1.025417864	2.61601E-07	0.000220075
Gm44421	ENSMUSG00000107451	-0.974385729	2.877E-07	0.00022993
Yjefn3	ENSMUSG00000048967	-1.087939484	3.33554E-07	0.000253882
Txnl4a	ENSMUSG00000057130	-0.765345132	5.38122E-07	0.00039097
Fzd9	ENSMUSG00000049551	-0.814391475	5.69149E-07	0.000395534
Tgfb3	ENSMUSG00000021253	-0.576131111	6.05834E-07	0.000402916
Sez6l2	ENSMUSG00000030683	-0.464692621	6.30186E-07	0.000402916
Sfrp5	ENSMUSG00000018822	-0.780044294	8.65507E-07	0.000532087
Crlf1	ENSMUSG00000007888	-1.7633339	1.13079E-06	0.00066943
Ufsp1	ENSMUSG00000051502	-0.611475403	1.49659E-06	0.000854339

Sst	ENSMUSG00000004366	-0.837202671	1.80112E-06	0.000992728
C1qa	ENSMUSG00000036887	-0.761118713	1.87202E-06	0.000997415
Malsu1	ENSMUSG00000029815	-0.850693741	1.99376E-06	0.001028007
Agt	ENSMUSG00000031980	-0.701196779	2.36423E-06	0.001180935
Hist1h2be	ENSMUSG00000047246	-0.820463409	2.76519E-06	0.001339359
6330403L08Rik	ENSMUSG00000075585	-0.598184098	3.14563E-06	0.001471572
E430024I08Rik	ENSMUSG00000112964	1.118014403	3.22229E-06	0.001471572
Star	ENSMUSG00000031574	0.657499362	3.43344E-06	0.001483246
C1qb	ENSMUSG00000036905	-0.735017165	3.39924E-06	0.001483246
Alas2	ENSMUSG00000025270	-1.176364822	3.67841E-06	0.001547257
Igfbp4	ENSMUSG00000017493	-0.768946995	3.779E-06	0.001547739
F5	ENSMUSG00000026579	2.398256968	3.87322E-06	0.001547739
Pdlim1	ENSMUSG00000055044	-0.687574944	4.81766E-06	0.001878182
Tas1r1	ENSMUSG00000028950	1.066429976	5.17263E-06	0.001968557
Mt1	ENSMUSG00000031765	-0.940312992	5.55595E-06	0.002065262
Tcte2	ENSMUSG00000038347	1.06933631	5.98732E-06	0.002100989
Dgkk	ENSMUSG00000062393	0.657733728	5.92326E-06	0.002100989
Gm45426	ENSMUSG00000109792	1.301880148	6.04639E-06	0.002100989
Ackr1	ENSMUSG00000037872	-0.803172097	6.29545E-06	0.002140989
Gm47163	ENSMUSG00000111977	-0.562069484	7.65061E-06	0.002495659
Sh3d19	ENSMUSG00000028082	0.582908524	7.61222E-06	0.002495659
Prdx6	ENSMUSG00000026701	-0.682121528	9.57502E-06	0.003060941
Hoxb3	ENSMUSG00000048763	1.021010385	9.96968E-06	0.003124616
BC049352	ENSMUSG00000091996	1.213492139	1.29858E-05	0.003916307
Gm27030	ENSMUSG00000098221	-1.615755174	1.29561E-05	0.003916307
Rom1	ENSMUSG00000071648	-0.675009645	1.32715E-05	0.00392835
8430429K09Rik	ENSMUSG00000034587	0.642512915	1.43058E-05	0.004157521
Hspb1	ENSMUSG00000004951	-0.846270696	1.47187E-05	0.004201126
Tac2	ENSMUSG00000025400	-0.81490738	1.64456E-05	0.00454967
AC158605.1	ENSMUSG00000112110	1.334891271	1.65091E-05	0.00454967
Hnrnpa1	ENSMUSG00000046434	0.391970563	1.77291E-05	0.004723035
Hbb-bs	ENSMUSG00000052305	-1.565797614	1.76335E-05	0.004723035
Hist1h2bc	ENSMUSG00000018102	-0.889805282	1.84752E-05	0.004779822
Tmc7	ENSMUSG00000042246	0.753881784	1.88394E-05	0.004779822
Tshb	ENSMUSG00000027857	0.93542662	1.86237E-05	0.004779822
Rimklb	ENSMUSG00000040649	0.426694634	1.96431E-05	0.004905852

Hist2h3c2	ENSMUSG00000081058	-1.502651798	2.43502E-05	0.005987901
Nbl1	ENSMUSG00000041120	-0.693160822	2.47443E-05	0.00599261
Me2	ENSMUSG00000024556	0.529353418	2.5693E-05	0.006129514
4833423E24Rik	ENSMUSG00000075217	-0.544359015	2.67983E-05	0.006299188
Znhit2	ENSMUSG00000075227	-0.687562475	2.73902E-05	0.006344993
S100a11	ENSMUSG00000027907	-0.946244197	3.04217E-05	0.006946586
Atraid	ENSMUSG00000013622	-0.661876707	3.17436E-05	0.007146345
Cdon	ENSMUSG00000038119	0.648719466	3.32635E-05	0.007384499
Gm32122	ENSMUSG00000110633	-0.808578173	3.43464E-05	0.007520448
Ly6a	ENSMUSG00000075602	-0.820704273	3.4901E-05	0.007538624
Rcn3	ENSMUSG00000019539	-1.007096132	3.64618E-05	0.007709876
Traf3	ENSMUSG00000021277	0.477024991	3.66586E-05	0.007709876
Plekhh2	ENSMUSG00000040852	0.660598914	3.92104E-05	0.00813947
Trem2	ENSMUSG00000023992	-0.675335439	3.98738E-05	0.008171056
Lyz2	ENSMUSG00000069516	-0.842814091	4.82564E-05	0.009763682
Sdc4	ENSMUSG00000017009	-0.531368368	5.00778E-05	0.009927533
Catsperz	ENSMUSG00000050623	-1.197706165	5.03084E-05	0.009927533
C1qc	ENSMUSG00000036896	-0.65514571	5.78034E-05	0.011267435
Pgf	ENSMUSG00000004791	-0.614360198	5.95952E-05	0.011476749
Fam13c	ENSMUSG00000043259	0.772412064	6.05447E-05	0.011520791
Olig1	ENSMUSG00000046160	-0.556087704	6.56308E-05	0.012198171
Erbb3	ENSMUSG00000018166	0.592275074	6.55091E-05	0.012198171
Igf2bp3	ENSMUSG00000029814	1.332143761	6.7689E-05	0.012436111
Ly6c1	ENSMUSG00000079018	-0.6356273	7.16728E-05	0.013018379
Tmem256	ENSMUSG00000070394	-1.01939027	7.89906E-05	0.014186363
Mir99ahg	ENSMUSG00000090386	-1.03253834	8.04269E-05	0.014283814
Lhx1	ENSMUSG00000018698	0.804266101	8.20425E-05	0.014410638
Fth1	ENSMUSG00000024661	-0.764781267	8.29693E-05	0.014415016
Nudt18	ENSMUSG00000045211	-0.552149894	8.38987E-05	0.014419749
D130017N08Rik	ENSMUSG00000097287	0.443463262	8.98633E-05	0.015280577
Gstm7	ENSMUSG00000004035	-0.602132053	9.49754E-05	0.015849042
Gm9828	ENSMUSG00000048603	1.051395626	9.51894E-05	0.015849042
Usp16	ENSMUSG00000025616	0.458736565	9.88037E-05	0.016281214
Cck	ENSMUSG00000032532	-0.800962129	0.0001024	0.016701679
Slc25a12	ENSMUSG00000027010	-0.424060644	0.000104944	0.016943734
S100a10	ENSMUSG00000041959	-0.781151891	0.000108458	0.017335882

Gm42847	ENSMUSG00000106743	-0.789940867	0.00011186	0.01760581
Gpx4-ps2	ENSMUSG00000110841	-0.840481155	0.000112499	0.01760581
Aif1	ENSMUSG00000024397	-1.073511657	0.000113451	0.01760581
Htra1	ENSMUSG00000006205	-0.4183552	0.00011622	0.017862153
4632404H12Rik	ENSMUSG00000042579	0.622538791	0.000118469	0.017928679
Lrrc8a	ENSMUSG00000007476	-0.593627796	0.000120018	0.017928679
Medag	ENSMUSG00000029659	-0.695273089	0.000118955	0.017928679
Rdm1	ENSMUSG00000010362	-0.779397022	0.000122729	0.018163865
Gm18194	ENSMUSG00000109724	4.297730441	0.000127937	0.018422861
Bahcc1	ENSMUSG00000039741	0.57537014	0.000127883	0.018422861
Atp5l	ENSMUSG00000038717	-0.659760435	0.000126612	0.018422861
E330034L11Rik	ENSMUSG00000106383	0.877525848	0.000135636	0.019357136
Mrps10	ENSMUSG00000034729	-0.465024138	0.000141483	0.020012993
Smim27	ENSMUSG00000028407	-1.332381021	0.00014583	0.020446935
1600020E01Rik	ENSMUSG00000097048	-0.742648571	0.000150276	0.020706947
Mipep	ENSMUSG00000021993	-0.42159068	0.000149208	0.020706947
Tenm2	ENSMUSG00000049336	0.532611242	0.000152431	0.020824459
Mien1	ENSMUSG00000002580	-0.804167893	0.000156934	0.020903546
Pih1d1	ENSMUSG00000003423	-0.601565344	0.000156078	0.020903546
Slc2a4	ENSMUSG00000018566	-0.689629238	0.0001567	0.020903546
Ppargc1b	ENSMUSG00000033871	0.987838628	0.000160608	0.021195893
Ak6	ENSMUSG00000078941	-0.771533255	0.00016178	0.021195893
Tssc4	ENSMUSG00000045752	-0.689682173	0.000178933	0.023224332
Bcas1os2	ENSMUSG00000086999	1.419903216	0.000180169	0.023224332
Pold4	ENSMUSG00000024854	-0.731471714	0.00018744	0.023968344
Slx4	ENSMUSG00000039738	0.48018119	0.000188994	0.023975199
Mrps6	ENSMUSG00000039680	-0.757050021	0.000199698	0.024339304
Gpx4	ENSMUSG00000075706	-0.656533949	0.000199897	0.024339304
Grrp1	ENSMUSG00000050105	-1.020873262	0.000193996	0.024339304
Upp2	ENSMUSG00000026839	-0.41624948	0.000197343	0.024339304
A330048O09Rik	ENSMUSG00000097326	-0.969168766	0.000199655	0.024339304
A330049N07Rik	ENSMUSG00000111994	1.00438726	0.000201	0.024339304
Mt3	ENSMUSG00000031760	-0.825229383	0.000215295	0.025850323
Shisa8	ENSMUSG00000096883	-0.617873143	0.000216713	0.025850323
Ptgds	ENSMUSG00000015090	-0.609749004	0.000220231	0.025950646
Ndrg2	ENSMUSG00000004558	-0.433589877	0.00022518	0.025950646

Adra2c	ENSMUSG00000045318	-0.560742121	0.000225672	0.025950646
N4bp2	ENSMUSG00000037795	0.754115216	0.000224212	0.025950646
AC124739.2	ENSMUSG00000116775	-1.247301297	0.00022477	0.025950646
Gadd45g	ENSMUSG00000021453	-0.708788983	0.000230064	0.026266782
Xlr3b	ENSMUSG00000073125	1.20110059	0.000235204	0.026286559
Hipk4	ENSMUSG00000040424	-0.397861847	0.000234911	0.026286559
Tmem268	ENSMUSG00000045917	-0.410081857	0.000236816	0.026286559
Ccl17	ENSMUSG00000031780	-1.524155401	0.000234126	0.026286559
Calb2	ENSMUSG00000003657	-0.559651348	0.000240481	0.026509299
Apod	ENSMUSG00000022548	-0.558173208	0.000246736	0.026862884
Bcl9l	ENSMUSG00000063382	0.487167382	0.00024705	0.026862884
Arhgap18	ENSMUSG00000039031	0.641100762	0.000256032	0.027534751
Gng13	ENSMUSG00000025739	-0.994483459	0.000256674	0.027534751
Hexim2	ENSMUSG00000043372	-0.530732509	0.000273236	0.029116079
5930412G12Rik	ENSMUSG00000072591	-0.681443027	0.000275926	0.029207992
Gm13194	ENSMUSG00000086670	-1.323221832	0.000278803	0.029318365
Pvalb	ENSMUSG00000005716	-0.661637339	0.000282067	0.029467731
Map3k9	ENSMUSG00000042724	0.930922542	0.000287623	0.029660401
Uqcrq	ENSMUSG00000044894	-0.758887467	0.000287327	0.029660401
Gucy2e	ENSMUSG00000020890	0.612980812	0.00029035	0.029749724
Gm47572	ENSMUSG00000112922	1.066579287	0.000294465	0.029789385
Pspc1	ENSMUSG00000021938	0.394301005	0.000293753	0.029789385
Bcl9	ENSMUSG00000038256	0.679536182	0.000297024	0.029859301
Utp14b	ENSMUSG00000079470	0.538221429	0.000311966	0.030909486
Cops9	ENSMUSG00000073616	-0.742487588	0.000313272	0.030909486
Phf7	ENSMUSG00000021902	-0.742058749	0.000309941	0.030909486
Col20a1	ENSMUSG00000016356	0.999387182	0.000336083	0.031786686
Crlf2	ENSMUSG00000033467	-0.599422103	0.000328158	0.031786686
Entpd7	ENSMUSG00000025192	0.850237376	0.000326699	0.031786686
Zfp609	ENSMUSG00000040524	0.663705766	0.000325345	0.031786686
Ndufb9	ENSMUSG00000022354	-0.756345256	0.000332658	0.031786686
Chchd6	ENSMUSG00000030086	-0.569655664	0.000333102	0.031786686
C3	ENSMUSG00000024164	-0.631167711	0.000334851	0.031786686
Sac3d1	ENSMUSG00000024790	-0.582847263	0.00035863	0.033719623
Serpinf1	ENSMUSG00000000753	-0.507344693	0.000392671	0.034102983
Gstk1	ENSMUSG00000029864	-0.647211883	0.000389683	0.034102983

Cebpa	ENSMUSG00000034957	-0.535372452	0.000387946	0.034102983
St6gal2	ENSMUSG00000024172	0.711634376	0.000386981	0.034102983
Uqcr11	ENSMUSG00000020163	-0.796385753	0.000377472	0.034102983
Etfb	ENSMUSG00000004610	-1.063775027	0.0004028	0.034102983
Mrps21	ENSMUSG00000054312	-0.750500588	0.000401725	0.034102983
Mrpl28	ENSMUSG00000024181	-0.634543209	0.000376699	0.034102983
Adam19	ENSMUSG00000011256	0.454466651	0.000402383	0.034102983
Mrpl11	ENSMUSG00000024902	-0.667309613	0.000386134	0.034102983
Timm10b	ENSMUSG00000089847	-0.581240258	0.000381111	0.034102983
Slc6a6	ENSMUSG00000030096	0.421925494	0.000379585	0.034102983
Tnrc18	ENSMUSG00000039477	0.524102185	0.000392083	0.034102983
Mmp19	ENSMUSG00000025355	-1.074143659	0.000396056	0.034102983
Csnk1g1	ENSMUSG00000032384	0.495861802	0.000367789	0.034102983
Sdhaf1	ENSMUSG00000074211	-0.900556016	0.000403245	0.034102983
S100a6	ENSMUSG00000001025	-0.993008804	0.000402238	0.034102983
Pcsk1n	ENSMUSG00000039278	-0.659210254	0.000379048	0.034102983
Npy	ENSMUSG00000029819	-0.847768909	0.0003927	0.034102983
Zdhhc20	ENSMUSG00000021969	-0.372573875	0.000414008	0.034828938
Ctla2a	ENSMUSG00000044258	-0.717856911	0.000422138	0.035327011
Pcdhgc4	ENSMUSG00000023036	1.25754723	0.000429664	0.035592182
Ankub1	ENSMUSG00000074591	0.564952854	0.00042976	0.035592182
Lgals4	ENSMUSG00000053964	-1.441142832	0.000452405	0.036219154
Fam173a	ENSMUSG00000057411	-0.593624676	0.000447351	0.036219154
Zfp112	ENSMUSG00000052675	0.502369257	0.000446791	0.036219154
Isoc2a	ENSMUSG00000086784	-0.603213153	0.000457725	0.036219154
Ago1	ENSMUSG00000041530	0.46952662	0.000456027	0.036219154
Gjb6	ENSMUSG00000040055	-0.399247905	0.000451382	0.036219154
Klk6	ENSMUSG00000050063	-0.692848151	0.000449915	0.036219154
Senp1	ENSMUSG00000033075	0.422306497	0.000446468	0.036219154
Gm10736	ENSMUSG00000096842	-0.841268848	0.000457125	0.036219154
Nenf	ENSMUSG00000037499	-0.749282434	0.000463866	0.036441179
Calr4	ENSMUSG00000028558	0.706744044	0.00046509	0.036441179
2010315B03Rik	ENSMUSG00000074829	0.465425942	0.000473511	0.036459745
Pnck	ENSMUSG00000002012	-0.509432752	0.000473605	0.036459745
Gm7658	ENSMUSG00000082935	-1.200361663	0.000477564	0.036459745
Gabpb2	ENSMUSG00000038766	0.663786557	0.000476414	0.036459745

Ifitm1	ENSMUSG00000025491	-0.971168221	0.000481294	0.036459745
Nthl1	ENSMUSG00000041429	-0.767775134	0.000479401	0.036459745
Gm12709	ENSMUSG00000085181	-0.875405299	0.000480157	0.036459745
Kcnk2	ENSMUSG00000037624	-0.42974067	0.000493245	0.036841257
Hspb8	ENSMUSG00000041548	-0.593178187	0.00049214	0.036841257
Nnat	ENSMUSG00000067786	-0.527769881	0.000492852	0.036841257
Ndufb10	ENSMUSG00000040048	-0.60722284	0.000503261	0.03741454
Celf3	ENSMUSG00000028137	0.768872753	0.00051065	0.037613982
Gm12892	ENSMUSG00000083679	-0.89174802	0.000509008	0.037613982
Pmm2	ENSMUSG00000022711	0.46993925	0.000513011	0.037614539
Nyap2	ENSMUSG00000054976	0.595864596	0.000518794	0.037864832
Ndufc1	ENSMUSG00000037152	-0.839598214	0.000522905	0.037991408
Taf15	ENSMUSG00000020680	0.660189384	0.000532165	0.038315909
Timp4	ENSMUSG00000030317	-0.437230207	0.000531936	0.038315909
Poln	ENSMUSG00000045102	-1.432128029	0.000540204	0.038416528
AC161376.2	ENSMUSG00000116793	-0.812595963	0.000540773	0.038416528
Jakmip2	ENSMUSG00000024502	0.459610391	0.000536616	0.038416528
1110046J04Rik	ENSMUSG00000085457	-0.818049117	0.000546892	0.038523905
Zfp329	ENSMUSG00000057894	0.578449206	0.000547105	0.038523905
Nt5e	ENSMUSG00000032420	0.560795894	0.000552517	0.038734357
Lppos	ENSMUSG00000097867	-0.80340276	0.000557395	0.038905707
Crybb1	ENSMUSG00000029343	-0.768412998	0.000561586	0.039027768
Rps12	ENSMUSG00000061983	-0.806822844	0.000576526	0.039720622
Gm13205	ENSMUSG00000086606	-0.650774059	0.000574637	0.039720622
Gm45495	ENSMUSG00000106981	-0.452881568	0.000580808	0.039843958
Tmem267	ENSMUSG00000074634	-1.03886427	0.00058437	0.039916953
Zfp846	ENSMUSG00000058192	0.474607065	0.000602402	0.040016294
Epop	ENSMUSG00000043439	-0.605780361	0.000603212	0.040016294
H1fx	ENSMUSG00000044927	-0.708163708	0.000588532	0.040016294
Ndufab1	ENSMUSG00000030869	-0.548254075	0.000603349	0.040016294
Kcna6	ENSMUSG00000038077	-0.404630426	0.000595986	0.040016294
Dzip1	ENSMUSG00000042156	0.722192579	0.000596144	0.040016294
Rpl41	ENSMUSG00000093674	-0.781953674	0.000601252	0.040016294
Xlr3a	ENSMUSG00000057836	0.790145516	0.000613044	0.04030545
Hint2	ENSMUSG00000028470	-0.678768171	0.00061768	0.04030545
Spa17	ENSMUSG00000001948	-0.916310038	0.000617795	0.04030545

Particl	ENSMUSG00000108591	-0.599424732	0.000616146	0.04030545
Spef1	ENSMUSG00000027329	-0.644245761	0.000631816	0.041017307
Shroom3	ENSMUSG00000029381	0.418457039	0.000633839	0.041017307
Ephb2	ENSMUSG00000028664	0.496376774	0.000663344	0.042753584
Abcc12	ENSMUSG00000036872	-0.994489594	0.000667416	0.042843314
Gm37494	ENSMUSG00000108621	0.497517044	0.000679495	0.043444187
Gm17922	ENSMUSG00000115632	-1.893607564	0.000686502	0.043717296
Tmtc3	ENSMUSG00000036676	0.651728404	0.000693576	0.043992504
Ahnak2	ENSMUSG00000072812	-0.502296196	0.000698567	0.044133992
Ramp1	ENSMUSG00000034353	-0.529328253	0.000712052	0.044808808
Tesc	ENSMUSG00000029359	-0.608917503	0.000733795	0.045816319
Gm37459	ENSMUSG00000104283	-0.589964705	0.000733268	0.045816319
Gm49172	ENSMUSG00000115049	-0.822376187	0.000737827	0.045888842
Tmem37	ENSMUSG00000050777	-1.155341937	0.000744343	0.045938971
S100a13	ENSMUSG00000042312	-0.801435901	0.000744381	0.045938971
A730020M07Rik	ENSMUSG00000044522	0.586696135	0.000750588	0.046143828
Asnsd1	ENSMUSG00000026095	-0.741311835	0.000755395	0.046261434
Ralgapa2	ENSMUSG00000037110	0.533088481	0.000762972	0.046547138
Mxra7	ENSMUSG00000020814	-0.390177792	0.000781422	0.047311562
Psmc5	ENSMUSG00000020708	-0.498400437	0.000780948	0.047311562
Rab13	ENSMUSG00000027935	-0.678438066	0.000814272	0.047675199
Mga	ENSMUSG00000033943	0.475327512	0.000812482	0.047675199
Ppp1r1b	ENSMUSG00000061718	-0.351459649	0.000813838	0.047675199
Snrpd2	ENSMUSG00000040824	-0.691873164	0.00081414	0.047675199
Gm5905	ENSMUSG00000110275	-0.712224192	0.000796892	0.047675199
Chchd10	ENSMUSG00000049422	-0.60511958	0.000813071	0.047675199
Zfp526	ENSMUSG00000046541	0.983667299	0.000813317	0.047675199
Evpl	ENSMUSG00000034282	0.533380003	0.000802327	0.047675199
Alox8	ENSMUSG00000020891	0.527108537	0.000801494	0.047675199
Prelp	ENSMUSG00000041577	-0.507029665	0.000839593	0.048940219
Uchl1	ENSMUSG00000029223	-0.512234988	0.000842002	0.048940219
Gramd2	ENSMUSG00000074259	0.851586959	0.000848372	0.049131821
1600002K03Rik	ENSMUSG00000035595	-0.92410424	0.000861801	0.049729313

A1. Spinal Cord DEGs

Gene ID	EnsemblID	log2FoldChange	p-value	q-value
Gm19963	ENSMUSG00000109404	-3.397001222	8.00269E-43	1.41688E-38
Rps15a-ps7	ENSMUSG00000081087	-4.517793633	8.93403E-22	7.90885E-18
Hist1h1c	ENSMUSG00000036181	-1.609645343	1.4276E-16	8.42521E-13
Gm42047	ENSMUSG00000110631	1.724231291	1.12279E-15	4.96974E-12
Gm47163	ENSMUSG00000111977	-0.886079808	2.30983E-14	8.1791E-11
Hist1h2be	ENSMUSG00000047246	-1.45179137	3.48668E-13	1.02886E-09
Espn	ENSMUSG00000028943	-1.316104425	4.16231E-13	1.05277E-09
Fus	ENSMUSG00000030795	0.63059682	9.58979E-13	2.12234E-09
Cnot7	ENSMUSG00000031601	-0.590464226	1.27739E-12	2.5129E-09
Gjb6	ENSMUSG00000040055	-0.616367631	3.28741E-12	5.82035E-09
Gm765	ENSMUSG00000090667	-1.589189383	4.09646E-12	6.59344E-09
Gm42756	ENSMUSG00000104674	-1.90394965	6.44445E-12	9.50825E-09
Col6a2	ENSMUSG00000020241	1.469223519	1.19133E-11	1.62249E-08
Ackr1	ENSMUSG00000037872	-0.773577533	2.05028E-11	2.59287E-08
AC114585.1	ENSMUSG00000115099	0.803650324	3.23655E-11	3.82021E-08
Hist1h2bc	ENSMUSG00000018102	-1.171694864	1.02792E-10	1.10521E-07
Slc25a12	ENSMUSG00000027010	-0.596993146	1.06121E-10	1.10521E-07
Selenop	ENSMUSG00000064373	-0.826749078	1.22101E-10	1.201E-07
Gm38300	ENSMUSG00000104279	-1.620929602	1.55328E-10	1.37504E-07
Tmem116	ENSMUSG00000029452	1.221992972	1.52595E-10	1.37504E-07
Fam107a	ENSMUSG00000021750	-0.595773566	3.15709E-10	2.66173E-07
B930095G15Rik	ENSMUSG00000085133	0.642403164	7.58796E-10	6.10659E-07
Clgn	ENSMUSG00000002190	0.66976123	8.07033E-10	6.2124E-07
Nwd2	ENSMUSG00000090061	0.670954521	1.01529E-09	7.48986E-07
Ddc	ENSMUSG00000020182	-0.924968763	1.44918E-09	1.01101E-06
Etnppl	ENSMUSG00000019232	-0.983955342	1.48469E-09	1.01101E-06
Pbld2	ENSMUSG00000020072	1.458038986	1.86694E-09	1.22423E-06
Tmem201	ENSMUSG00000044700	0.449718157	2.35332E-09	1.48806E-06
Abhd3	ENSMUSG00000002475	-0.66680393	5.11997E-09	3.12583E-06
C1qb	ENSMUSG00000036905	-0.830452453	6.21879E-09	3.67012E-06
Atraid	ENSMUSG00000013622	-0.477420325	8.89484E-09	5.0801E-06
6330403L08Rik	ENSMUSG00000075585	-0.648707821	9.96271E-09	5.51218E-06
Mt1	ENSMUSG00000031765	-0.801635071	1.37831E-08	7.39483E-06
6430590A07Rik	ENSMUSG00000097583	1.852499857	2.40363E-08	1.25165E-05

Gm35339	ENSMUSG00000109179	1.583133731	3.8255E-08	1.93516E-05
Kcnj8	ENSMUSG00000030247	-1.0106887	4.55703E-08	2.24117E-05
Gstk1	ENSMUSG00000029864	-0.729052103	7.42224E-08	3.55164E-05
Ly6a	ENSMUSG00000075602	-0.831555751	7.72043E-08	3.59711E-05
Nuf2	ENSMUSG00000026683	-1.073247582	8.06569E-08	3.66162E-05
Rimklb	ENSMUSG00000040649	0.492333967	8.4078E-08	3.7215E-05
Gramd2	ENSMUSG00000074259	0.910082611	1.71906E-07	7.42339E-05
Gm47572	ENSMUSG00000112922	1.367471394	1.93939E-07	7.79055E-05
Gm45495	ENSMUSG00000106981	-0.683862439	1.98009E-07	7.79055E-05
Tyrobp	ENSMUSG00000030579	-0.80944009	1.97586E-07	7.79055E-05
Gm3519	ENSMUSG00000106380	2.881488065	1.9554E-07	7.79055E-05
Npc1l1	ENSMUSG00000020447	1.527381043	2.36611E-07	9.10694E-05
Pold4	ENSMUSG00000024854	-0.674465047	2.60257E-07	9.6581E-05
Thra	ENSMUSG00000058756	-0.504245194	2.6184E-07	9.6581E-05
Ccdc191	ENSMUSG00000022701	1.041803284	2.725E-07	9.84616E-05
Ly6c1	ENSMUSG00000079018	-0.729380143	2.86809E-07	0.00010021
Atxn2l	ENSMUSG00000032637	1.077141943	2.88658E-07	0.00010021
Hba-a2	ENSMUSG00000069917	-1.41701153	3.87751E-07	0.000132022
Gm44645	ENSMUSG00000108601	-1.172019002	3.9696E-07	0.000132607
Pcdha2	ENSMUSG00000104148	1.2043094	4.44623E-07	0.000145779
Hist2h3c2	ENSMUSG00000081058	-1.849204326	4.62608E-07	0.000148918
Col22a1	ENSMUSG00000079022	1.035796293	5.19503E-07	0.000164247
Gm42608	ENSMUSG00000106651	-1.441601092	5.30492E-07	0.000164778
Ccdc27	ENSMUSG00000039492	1.080492515	5.61142E-07	0.000171293
Ano2	ENSMUSG00000038115	-0.674918711	5.76825E-07	0.000173096
Gm26793	ENSMUSG00000096999	-2.730304195	5.93078E-07	0.000175007
Hspb8	ENSMUSG00000041548	-0.74267871	6.39389E-07	0.00018558
Crlf2	ENSMUSG00000033467	-0.652609018	6.66591E-07	0.000187193
Coasy	ENSMUSG00000001755	-0.553552857	6.76665E-07	0.000187193
Gm42829	ENSMUSG00000105895	-0.842966716	6.66774E-07	0.000187193
Prdx6	ENSMUSG00000026701	-0.622898495	6.88232E-07	0.000187464
Gm37345	ENSMUSG00000103947	1.195783621	7.29442E-07	0.000195678
Star	ENSMUSG00000031574	0.642053155	9.13505E-07	0.000241397
Taf15	ENSMUSG00000020680	0.832906346	1.00076E-06	0.000257124
Sorbs2os	ENSMUSG00000085440	1.725113738	1.00206E-06	0.000257124
Apod	ENSMUSG00000022548	-0.616148002	1.03383E-06	0.000261485

Akr1c14	ENSMUSG00000033715	-1.632741317	1.09041E-06	0.000271912
Efcab5	ENSMUSG00000050944	0.953099538	1.30595E-06	0.000321138
Med24	ENSMUSG00000017210	0.490628035	1.32811E-06	0.000322111
Col20a1	ENSMUSG00000016356	1.355292796	1.35425E-06	0.000324013
Slc25a34	ENSMUSG00000040740	-0.678068836	1.54884E-06	0.00036563
Spp1	ENSMUSG00000029304	-0.743526889	1.78202E-06	0.00041514
C1qa	ENSMUSG00000036887	-0.674495736	1.86039E-06	0.000416939
A730017L22Rik	ENSMUSG00000085566	0.702513996	1.81941E-06	0.000416939
Bcas1	ENSMUSG00000013523	-0.571477173	1.84164E-06	0.000416939
Rimbp2	ENSMUSG00000029420	0.716510546	1.95135E-06	0.000431858
Sdc4	ENSMUSG00000017009	-0.461389302	2.03948E-06	0.000445791
Olig1	ENSMUSG00000046160	-0.676009314	2.2909E-06	0.000492866
Camk2n1	ENSMUSG00000046447	-0.517204215	2.31053E-06	0.000492866
Acvrl1	ENSMUSG00000000530	-0.520665962	2.39271E-06	0.00050432
2410022M11Rik	ENSMUSG00000100017	-0.941913065	2.43915E-06	0.000508062
Ctss	ENSMUSG00000038642	-0.675470737	2.53316E-06	0.000521506
Ift172	ENSMUSG00000038564	0.727606063	2.78439E-06	0.00056664
Ndrg2	ENSMUSG00000004558	-0.488656026	2.90855E-06	0.000585181
CT010445.1	ENSMUSG00000117113	1.285646999	3.89723E-06	0.000775287
Samd11	ENSMUSG00000096351	1.296474496	4.28307E-06	0.000842574
Spi1	ENSMUSG00000002111	-0.864679967	4.60395E-06	0.000895746
H2-D1	ENSMUSG00000073411	-0.558492229	4.74491E-06	0.000913138
Aldh1a1	ENSMUSG00000053279	-0.497128889	5.06732E-06	0.000964698
Mipep	ENSMUSG00000021993	-0.543095141	5.13719E-06	0.000967594
3110053B16Rik	ENSMUSG00000085642	-1.185740257	5.21969E-06	0.000972785
Tkfc	ENSMUSG00000034371	-0.527980778	5.40632E-06	0.000986792
6430710M23Rik	ENSMUSG00000110127	3.16032328	5.39316E-06	0.000986792
Alas2	ENSMUSG00000025270	-0.993511192	5.54987E-06	0.001002658
Tprn	ENSMUSG00000048707	-0.488781787	5.66305E-06	0.00101277
Kazald1	ENSMUSG00000025213	-0.810319139	5.91603E-06	0.001047433
Wnt10a	ENSMUSG00000026167	-0.835838934	6.24939E-06	0.001095499
Tnni1	ENSMUSG00000026418	-1.084178218	6.62591E-06	0.001127997
Tenm4	ENSMUSG00000048078	0.487993413	6.59197E-06	0.001127997
Unc13c	ENSMUSG00000062151	-0.416471403	6.62289E-06	0.001127997
B330016D10Rik	ENSMUSG00000048406	-1.118454183	6.75784E-06	0.001139501
Gm42847	ENSMUSG00000106743	-0.71715111	7.86981E-06	0.001314482

Gpx3	ENSMUSG00000018339	-0.985416255	8.11504E-06	0.001330341
Mgp	ENSMUSG00000030218	-0.833956458	8.06913E-06	0.001330341
Bnip2	ENSMUSG00000011958	0.40138632	8.28703E-06	0.001346072
Pmm2	ENSMUSG00000022711	0.584825584	8.47945E-06	0.00135251
Heatr1	ENSMUSG00000050244	0.598669932	8.41952E-06	0.00135251
Gm48482	ENSMUSG00000113167	1.103373245	9.12751E-06	0.00144288
Efcab1	ENSMUSG00000068617	-0.643610378	9.42083E-06	0.00147607
Rhob	ENSMUSG00000054364	-0.378016117	1.0194E-05	0.001583196
Slc24a5	ENSMUSG00000035183	0.890467455	1.06714E-05	0.001642936
9230112E08Rik	ENSMUSG00000070461	0.593157225	1.07986E-05	0.001648189
Gm14295	ENSMUSG00000078877	-0.514463619	1.17802E-05	0.00178264
Ncapd3	ENSMUSG00000035024	0.705660878	1.20833E-05	0.001800423
Klhl3	ENSMUSG00000014164	0.522618222	1.21184E-05	0.001800423
Sh2d4b	ENSMUSG00000037833	1.905839792	1.22028E-05	0.001800423
Ralgps1	ENSMUSG00000038831	0.652846366	1.24573E-05	0.001822777
Yae1d1	ENSMUSG00000075054	0.366977942	1.28352E-05	0.001862684
Tmem88	ENSMUSG00000045377	0.945285444	1.4346E-05	0.002065004
Selplg	ENSMUSG00000048163	-0.612359643	1.45125E-05	0.002072122
Sytl4	ENSMUSG00000031255	-1.329610916	1.64898E-05	0.002335621
Jsrp1	ENSMUSG00000020216	-0.761577714	1.699E-05	0.002368562
Paqr8	ENSMUSG00000025931	-0.405555325	1.69686E-05	0.002368562
Hadhb	ENSMUSG00000059447	-0.431762642	1.72376E-05	0.002384313
Gm15631	ENSMUSG00000085067	0.516042654	1.7519E-05	0.002386179
Cntn6	ENSMUSG00000030092	0.472992561	1.75207E-05	0.002386179
4932442E05Rik	ENSMUSG00000104443	2.235583571	1.76556E-05	0.002386208
Tsc2	ENSMUSG00000002496	0.511012264	1.82785E-05	0.002451673
Bicd2	ENSMUSG00000037933	0.584483829	1.91756E-05	0.002552666
Havcr2	ENSMUSG00000020399	-0.789080668	1.97606E-05	0.0026109
Papln	ENSMUSG00000021223	0.863558377	2.02166E-05	0.002631872
Gm45353	ENSMUSG00000109957	-1.670452684	2.00773E-05	0.002631872
Smim1	ENSMUSG00000078350	-0.521161055	2.06496E-05	0.002668619
Tmprss7	ENSMUSG00000033177	0.881667792	2.09361E-05	0.00268604
Rapgef4	ENSMUSG00000049044	-0.556715225	2.18311E-05	0.002766705
Adam15	ENSMUSG00000028041	0.41346548	2.18774E-05	0.002766705
Sptan1	ENSMUSG00000057738	0.388690444	2.2584E-05	0.002835814
Wdr78	ENSMUSG00000035126	-0.558767374	2.33992E-05	0.002917487

Angptl4	ENSMUSG00000002289	-0.794540109	2.39046E-05	0.002959654
9830144P21Rik	ENSMUSG00000087528	1.390177551	2.43931E-05	0.002996434
Cttnbp2	ENSMUSG00000000416	0.723949339	2.46198E-05	0.002996434
Ash2l	ENSMUSG00000031575	0.349688575	2.47094E-05	0.002996434
Hipk4	ENSMUSG00000040424	-0.399833728	2.53484E-05	0.003047103
Gm47573	ENSMUSG00000112847	1.599244631	2.54714E-05	0.003047103
Lcat	ENSMUSG00000035237	-0.596414423	2.65355E-05	0.003153095
Gm11841	ENSMUSG00000081593	2.581545981	2.72443E-05	0.00321573
Gja1	ENSMUSG00000050953	-0.451239857	2.81972E-05	0.003265148
Chml	ENSMUSG00000078185	0.532208488	2.82162E-05	0.003265148
Hexdc	ENSMUSG00000039307	0.669921768	2.81881E-05	0.003265148
Fbxw15	ENSMUSG00000074060	-1.708444349	2.86993E-05	0.003299484
Tle2	ENSMUSG00000034771	0.925088554	3.03946E-05	0.00344959
Scrn3	ENSMUSG00000008226	-0.440848518	3.03648E-05	0.00344959
Lrrc10b	ENSMUSG00000090291	-0.64517014	3.1503E-05	0.00355261
Gm26724	ENSMUSG00000097090	1.778195868	3.18111E-05	0.003564656
Gm15834	ENSMUSG00000085054	1.603098351	3.2991E-05	0.003673622
Plec	ENSMUSG00000022565	0.8439733	3.40433E-05	0.003767105
Zfpm1	ENSMUSG00000049577	-0.43674719	3.60357E-05	0.00396281
Snrnp200	ENSMUSG00000003660	0.333403692	3.70232E-05	0.004046265
Cst3	ENSMUSG00000027447	-0.623039711	3.81039E-05	0.004138832
Cyp2j9	ENSMUSG00000015224	-0.515463472	3.87631E-05	0.004163889
Golga4	ENSMUSG00000038708	0.502014881	3.91817E-05	0.004163889
Glul	ENSMUSG00000026473	-0.414144334	3.92753E-05	0.004163889
Kcng4	ENSMUSG00000045246	-0.773113894	3.88497E-05	0.004163889
Pex7	ENSMUSG00000020003	-0.454775823	3.99355E-05	0.004208678
4930578M01Rik	ENSMUSG00000097587	1.085824978	4.05005E-05	0.004242968
Flna	ENSMUSG00000031328	1.224135161	4.13464E-05	0.004306108
Tmem119	ENSMUSG00000054675	-0.449297988	4.24074E-05	0.004390781
Rab13	ENSMUSG00000027935	-0.680127222	4.37379E-05	0.004502202
Tac2	ENSMUSG00000025400	-0.754397085	4.43179E-05	0.00450947
Gm5577	ENSMUSG00000084950	1.198639116	4.40813E-05	0.00450947
Xlr3a	ENSMUSG00000057836	1.273683401	4.60106E-05	0.004654958
Ccl25	ENSMUSG00000023235	0.785832612	4.71581E-05	0.004743939
Gatm	ENSMUSG00000027199	-0.412872715	4.766E-05	0.004767345
Gfap	ENSMUSG00000020932	-0.515275669	4.95699E-05	0.004930531

Cetn4	ENSMUSG00000045031	-0.571326663	5.00933E-05	0.004954759
Cartpt	ENSMUSG00000021647	-0.831704691	5.05492E-05	0.004972072
Lppos	ENSMUSG00000097867	-1.087968962	5.1266E-05	0.005014162
Gm45151	ENSMUSG00000108736	1.390524702	5.15435E-05	0.005014162
Upf1	ENSMUSG00000058301	0.349612082	5.20157E-05	0.005032448
C1qc	ENSMUSG00000036896	-0.611678142	5.365E-05	0.005162352
Col6a1	ENSMUSG00000001119	0.866743819	5.53049E-05	0.005288994
Gm8170	ENSMUSG00000112381	1.995302521	5.55636E-05	0.005288994
Dcst2	ENSMUSG00000109293	1.558380735	5.60665E-05	0.005308332
Igf2bp3	ENSMUSG00000029814	1.055465803	5.78149E-05	0.005444754
Tnrc6c	ENSMUSG00000025571	0.788328214	5.98271E-05	0.005604436
Zranb2	ENSMUSG00000028180	0.470288459	6.16863E-05	0.005718099
Ift88os	ENSMUSG00000086486	2.511543068	6.15268E-05	0.005718099
Pla2g7	ENSMUSG00000023913	-0.512581138	6.28976E-05	0.005800011
Ccng1	ENSMUSG00000020326	-0.480419507	6.39511E-05	0.005866607
G0s2	ENSMUSG00000009633	-0.752276146	6.59431E-05	0.006018162
Gpr137	ENSMUSG00000024958	-0.384631475	6.6316E-05	0.006021151
Gm37570	ENSMUSG00000102559	1.793288815	6.6681E-05	0.006023407
Aff2	ENSMUSG00000031189	0.887333082	6.87279E-05	0.006176788
Gm47976	ENSMUSG00000112300	1.284848016	7.01736E-05	0.006274869
Mpp6	ENSMUSG00000038388	-0.445264918	7.10362E-05	0.006320082
Plxna3	ENSMUSG00000031398	0.816209821	7.21386E-05	0.006362624
Tro	ENSMUSG00000025272	0.494673072	7.22331E-05	0.006362624
Nxn	ENSMUSG00000020844	-0.42847614	7.30541E-05	0.006403082
Uggt2	ENSMUSG00000042104	0.788954046	7.40063E-05	0.006454591
Zfp846	ENSMUSG00000058192	0.562759935	7.56051E-05	0.006561705
Slc39a11	ENSMUSG00000041654	-0.487700738	7.61893E-05	0.006580156
Gpr37l1	ENSMUSG00000026424	-0.547249375	7.71177E-05	0.006628005
4731419I09Rik	ENSMUSG00000097004	2.337254041	8.02724E-05	0.006865813
Cebpa	ENSMUSG00000034957	-0.574798629	8.14795E-05	0.00690566
Zc3h8	ENSMUSG00000027387	0.574283533	8.15184E-05	0.00690566
Gm11766	ENSMUSG00000086924	1.634541448	8.29352E-05	0.006992224
Csrp1	ENSMUSG00000026421	-0.455877613	8.36807E-05	0.007000092
Naa40	ENSMUSG00000024764	0.676123893	8.38192E-05	0.007000092
Crem	ENSMUSG00000063889	-0.522659448	8.51904E-05	0.007081201
Fxyd1	ENSMUSG00000036570	-0.491725716	8.83678E-05	0.007310991

Ankrd52	ENSMUSG00000014498	0.767610523	9.09422E-05	0.007488983
Eif2s3y	ENSMUSG00000069049	0.871660415	9.29269E-05	0.00761699
Afg3l1	ENSMUSG00000031967	0.333808459	9.41135E-05	0.007643508
D330050G23Rik	ENSMUSG00000085316	0.92824002	9.41138E-05	0.007643508
Hist1h4h	ENSMUSG00000060981	-1.398148561	9.48547E-05	0.00765869
1700126G02Rik	ENSMUSG00000107802	1.888724591	9.51659E-05	0.00765869
Cln3	ENSMUSG00000030720	0.532055439	9.64148E-05	0.007724094
Gng5	ENSMUSG00000068523	-0.591193488	9.72883E-05	0.007753628
Mthfsd	ENSMUSG00000031816	0.538714336	9.76594E-05	0.007753628
Prrc2c	ENSMUSG00000040225	0.635542328	9.93941E-05	0.007816539
Gigyf1	ENSMUSG00000029714	0.744647947	0.000100218	0.007816539
Serpine2	ENSMUSG00000026249	-0.515389621	0.000100161	0.007816539
Gm49492	ENSMUSG00000116180	-0.555390273	9.95498E-05	0.007816539
Htra1	ENSMUSG00000006205	-0.494660296	0.000102801	0.007913415
Prss23	ENSMUSG00000039405	-0.703280067	0.000102055	0.007913415
Unc13b	ENSMUSG00000028456	0.863124996	0.000102681	0.007913415
Wfs1	ENSMUSG00000039474	-0.451560084	0.000103429	0.007927319
Hist1h2ac	ENSMUSG00000069270	-1.751874734	0.000103978	0.007935082
Iqce	ENSMUSG00000036555	0.691378937	0.000104768	0.007961014
Lingo3	ENSMUSG00000051067	-0.427354625	0.000106008	0.008020849
Isoc2a	ENSMUSG00000086784	-0.474877604	0.000108068	0.008129712
Vwa5b2	ENSMUSG00000046613	0.846317248	0.000108366	0.008129712
Sema4a	ENSMUSG00000028064	0.58675874	0.000109636	0.008190304
Naa16	ENSMUSG00000022020	0.708027483	0.000110867	0.008247455
Klk6	ENSMUSG00000050063	-0.844612367	0.000114827	0.008435731
Atp1a2	ENSMUSG00000007097	-0.330086343	0.000114529	0.008435731
Ciita	ENSMUSG00000022504	1.311060125	0.000114611	0.008435731
Akap9	ENSMUSG00000040407	0.34804505	0.000115454	0.008446728
9530062K07Rik	ENSMUSG00000108030	1.136940275	0.000117062	0.008506938
Kifc2	ENSMUSG00000004187	-0.283447745	0.000117238	0.008506938
Ppp1r3c	ENSMUSG00000067279	-0.479375083	0.000121821	0.008803418
Phyh	ENSMUSG00000026664	-0.517613786	0.000124624	0.00893309
Gm43266	ENSMUSG00000107173	1.760494356	0.000124536	0.00893309
Nav1	ENSMUSG00000009418	0.648433719	0.000127107	0.009030991
Slc23a2	ENSMUSG00000027340	0.382467254	0.00012752	0.009030991
Eprs	ENSMUSG00000026615	0.292553575	0.00012684	0.009030991

Dlg4	ENSMUSG00000020886	-0.346670526	0.000129979	0.009168405
Gm20692	ENSMUSG00000093739	1.726968018	0.000132665	0.009320801
Nudt18	ENSMUSG00000045211	-0.514647729	0.000133441	0.009333404
Tsga10	ENSMUSG00000060771	0.550740529	0.000133899	0.009333404
Ptprk	ENSMUSG00000019889	0.383797215	0.00013499	0.009356249
1700020D05Rik	ENSMUSG00000100937	1.696704861	0.000135284	0.009356249
Ndrg1	ENSMUSG00000005125	-0.416019806	0.000138384	0.009524729
Pdlim7	ENSMUSG00000021493	0.587688241	0.000138796	0.009524729
Gm26645	ENSMUSG00000097684	-0.967631383	0.000142046	0.009672773
Dync1h1	ENSMUSG00000018707	0.386018489	0.000141612	0.009672773
Mast1	ENSMUSG00000053693	0.602497248	0.000142629	0.009675304
4931423N10Rik	ENSMUSG00000026774	2.629078801	0.000143837	0.009720007
Chd5	ENSMUSG00000005045	0.561092767	0.000146232	0.009823676
AC171205.1	ENSMUSG00000116766	1.07948766	0.000146481	0.009823676
Rtel1	ENSMUSG00000038685	0.794303303	0.000154316	0.010264291
Dnmt1	ENSMUSG00000004099	0.381362604	0.00015537	0.010264291
Lrrc56	ENSMUSG00000038637	-0.615134701	0.000155296	0.010264291
Gm26945	ENSMUSG00000098061	1.737042967	0.000154959	0.010264291
Sap130	ENSMUSG00000024260	0.381368407	0.000161136	0.010605633
Ankzf1	ENSMUSG00000026199	0.698330898	0.000161855	0.01061348
Plxna4	ENSMUSG00000029765	0.452904514	0.000164673	0.010758458
Bach2	ENSMUSG00000040270	0.724859349	0.000165767	0.010790096
Gm42656	ENSMUSG00000106841	2.051973703	0.000166558	0.010801879
Hnrnpa1	ENSMUSG00000046434	0.33249005	0.000171828	0.010912319
Hinfp	ENSMUSG00000032119	0.66208502	0.000170966	0.010912319
Fam208a	ENSMUSG00000040651	0.588619261	0.000172576	0.010912319
2810025M15Rik	ENSMUSG00000049881	-0.529725435	0.000172461	0.010912319
Kif1a	ENSMUSG00000014602	0.311299904	0.000170093	0.010912319
Vwa3a	ENSMUSG00000030889	0.84354628	0.000169077	0.010912319
Mal	ENSMUSG00000027375	-0.516143104	0.000171695	0.010912319
A830082N09Rik	ENSMUSG00000112280	0.407709566	0.0001732	0.010912844
Coro7	ENSMUSG00000039637	0.37850148	0.000174578	0.010960663
Trh	ENSMUSG00000005892	-0.865178741	0.000175234	0.010962985
Slc25a42	ENSMUSG00000002346	0.623442276	0.000176206	0.010984931
Tsc22d4	ENSMUSG00000029723	-0.462318258	0.00017691	0.010990158
C130023A14Rik	ENSMUSG00000102854	1.521943321	0.000178316	0.011038783

Trrap	ENSMUSG00000045482	0.582915639	0.000182186	0.011239028
Abcd4	ENSMUSG00000021240	0.70240624	0.000183112	0.011256948
B2m	ENSMUSG00000060802	-0.57798486	0.000183961	0.011270025
Atcayos	ENSMUSG00000085779	1.495180067	0.000184889	0.011273126
Calb1	ENSMUSG00000028222	-0.42995234	0.000185285	0.011273126
Map3k9	ENSMUSG00000042724	0.814361253	0.000187004	0.01133869
Gpx6	ENSMUSG00000004341	-1.709080466	0.000188325	0.011379866
Trio	ENSMUSG00000022263	0.481815748	0.000190567	0.011437229
Lamp5	ENSMUSG00000027270	-0.364027268	0.000190561	0.011437229
Numa1	ENSMUSG00000066306	0.546845844	0.0001934	0.011529125
Bfsp1	ENSMUSG00000027420	0.978849678	0.000192991	0.011529125
5430402O13Rik	ENSMUSG00000085776	1.324699978	0.000196257	0.011660157
mt-Te	ENSMUSG00000064369	-0.641179899	0.000197709	0.011707174
Tnrc6b	ENSMUSG00000047888	0.646056954	0.000200482	0.011831777
Tmem82	ENSMUSG00000043085	-1.755170531	0.000201291	0.011840048
Mir186	ENSMUSG00000065431	1.018682424	0.000203267	0.0119167
Ikbkap	ENSMUSG00000028431	0.331591	0.000205914	0.012032043
Rcn3	ENSMUSG00000019539	-0.740695761	0.000206798	0.012043961
Unc93b1	ENSMUSG00000036908	-0.440589515	0.000208317	0.012053102
Fyco1	ENSMUSG00000025241	0.664717007	0.000207806	0.012053102
Kif5b	ENSMUSG00000006740	-0.390343269	0.000210909	0.012156933
Btbd3	ENSMUSG00000062098	-0.334860452	0.000211485	0.012156933
Apln	ENSMUSG00000037010	-0.541521779	0.000214279	0.012277677
Zfp398	ENSMUSG00000062519	0.51346183	0.000217842	0.012441612
Kdm5c	ENSMUSG00000025332	0.461239085	0.000225198	0.012820342
Atp8a2	ENSMUSG00000021983	0.476290297	0.000228167	0.0129064
Sh3rf2	ENSMUSG00000057719	-0.448928741	0.00022805	0.0129064
AC098880.2	ENSMUSG00000117183	0.714762624	0.000229939	0.012965189
Chuk	ENSMUSG00000025199	0.782239114	0.000234325	0.013065653
Plxna1	ENSMUSG00000030084	0.416661886	0.000233676	0.013065653
Snhg4	ENSMUSG00000097769	0.735682442	0.000234673	0.013065653
Herc4	ENSMUSG00000020064	0.427365257	0.000233564	0.013065653
Elmo3	ENSMUSG00000014791	0.739033678	0.000235418	0.013066087
Ccdc159	ENSMUSG00000006241	0.731635492	0.000239296	0.013239785
Trem2	ENSMUSG00000023992	-0.565724874	0.000240339	0.013256105
Cpsf4l	ENSMUSG00000018727	1.614642116	0.000253806	0.013955384

Zfhx2	ENSMUSG00000040721	0.715160267	0.000256559	0.014029311
Ddx41	ENSMUSG00000021494	0.34856916	0.000256735	0.014029311
Cryzl2	ENSMUSG00000033488	-0.629776751	0.000259699	0.014147613
mt-Nd2	ENSMUSG00000064345	-0.487671281	0.000262129	0.014236184
Ryr1	ENSMUSG00000030592	0.812663049	0.000267856	0.014502748
Gm43759	ENSMUSG00000105368	1.33012236	0.000271333	0.014604067
mt-Cytb	ENSMUSG00000064370	-0.450383341	0.000271377	0.014604067
Ifitm3	ENSMUSG00000025492	-0.616312833	0.000272349	0.014611943
Rnf112	ENSMUSG00000010086	0.665745238	0.000274525	0.014684184
Hook1	ENSMUSG00000028572	0.747039899	0.00027541	0.014687136
Gm26982	ENSMUSG00000097994	0.713469741	0.000277997	0.014780595
Aoc2	ENSMUSG00000078651	0.998723251	0.000282593	0.014979987
Mvp	ENSMUSG00000030681	0.462371351	0.000284474	0.01503467
Sptbn4	ENSMUSG00000011751	0.633936793	0.000287028	0.015124471
Irs1	ENSMUSG00000055980	0.742906796	0.00028811	0.015136483
Ubb	ENSMUSG00000019505	-0.493826283	0.000291874	0.015262915
Pwwp2b	ENSMUSG00000060260	-0.413636595	0.000294827	0.015262915
Jakmip3	ENSMUSG00000056856	0.538186591	0.000294002	0.015262915
Gm44199	ENSMUSG00000107560	1.733436716	0.000294246	0.015262915
Dmrtb1	ENSMUSG00000028610	-1.266486629	0.000292436	0.015262915
Gm37111	ENSMUSG00000104494	-0.831862663	0.000297748	0.015369191
Abhd6	ENSMUSG00000025277	-0.342170486	0.000298987	0.015388261
Ndufaf5	ENSMUSG00000027384	-0.398249952	0.000299883	0.015389635
Polr2i	ENSMUSG00000019738	-0.546490404	0.000302005	0.015453733
Rpp40	ENSMUSG00000021418	-0.637190521	0.000303434	0.015482139
Spink10	ENSMUSG00000044176	1.166066695	0.000305246	0.015485306
Fam198b	ENSMUSG00000027955	-0.612920831	0.000304867	0.015485306
Lyz2	ENSMUSG00000069516	-0.724984319	0.000311908	0.015531591
D130017N08Rik	ENSMUSG00000097287	0.419533426	0.000316049	0.015531591
Cetn2	ENSMUSG00000031347	-0.476856489	0.00031396	0.015531591
Ifi30	ENSMUSG00000031838	-0.976014396	0.000311074	0.015531591
Fam173b	ENSMUSG00000039065	0.716071051	0.000318735	0.015531591
Col5a2	ENSMUSG00000026042	0.813207779	0.000308332	0.015531591
Gng7	ENSMUSG00000048240	-0.555250357	0.000313153	0.015531591
Arntl2	ENSMUSG00000040187	1.040957875	0.00030987	0.015531591
Sumf1	ENSMUSG00000030101	-0.356931164	0.000319317	0.015531591

Ifit3	ENSMUSG00000074896	-0.607241299	0.000319219	0.015531591
Stxbp2	ENSMUSG00000004626	0.807096058	0.000312748	0.015531591
Zbtb40	ENSMUSG00000060862	0.65809117	0.000319151	0.015531591
5430416N02Rik	ENSMUSG00000097772	1.059219613	0.000319145	0.015531591
S1pr1	ENSMUSG00000045092	-0.436844817	0.000310772	0.015531591
Rasal1	ENSMUSG00000029602	0.499243984	0.000317179	0.015531591
Commd10	ENSMUSG00000042705	-0.472424541	0.000328328	0.015926172
Gm12404	ENSMUSG00000087623	1.416322475	0.000330298	0.015977948
Cdo1	ENSMUSG00000033022	-0.41578033	0.000332451	0.016038281
Pstpip2	ENSMUSG00000025429	0.650983361	0.000335169	0.016038285
Atp2b4	ENSMUSG00000026463	0.361594547	0.000333685	0.016038285
Gm42692	ENSMUSG00000104901	1.808786212	0.000334304	0.016038285
Rnase4	ENSMUSG00000021876	-0.610379053	0.000342343	0.016337439
Slc4a11	ENSMUSG00000074796	-1.097675035	0.000349062	0.016568725
Mkx	ENSMUSG00000061013	0.615042184	0.000348853	0.016568725
Atg3	ENSMUSG00000022663	-0.419222669	0.000353926	0.016720901
Slit3	ENSMUSG00000056427	0.452833803	0.000354156	0.016720901
Clec2d	ENSMUSG00000030157	-0.853583476	0.000359292	0.016828761
Piezo1	ENSMUSG00000014444	0.741054558	0.000358901	0.016828761
Gm28192	ENSMUSG00000100629	1.195922002	0.000358164	0.016828761
Ptprt	ENSMUSG00000053141	0.409511858	0.000360838	0.016856563
Mobp	ENSMUSG00000032517	-0.367780386	0.00036194	0.016863524
Armcx4	ENSMUSG00000049804	0.526430413	0.000366215	0.017017923
Cnga3	ENSMUSG00000026114	-2.010334015	0.000371194	0.017204139
Ptgds	ENSMUSG00000015090	-0.696746663	0.00037718	0.017345365
Ubr4	ENSMUSG00000066036	0.483082858	0.000375497	0.017345365
Thap6	ENSMUSG00000102644	-0.784875945	0.000377142	0.017345365
Rcn1	ENSMUSG00000005973	-0.394876697	0.000378981	0.017383074
Tpr	ENSMUSG00000006005	0.36636314	0.000380899	0.017386922
Vps16	ENSMUSG00000027411	0.34129448	0.000381029	0.017386922
Ncf1	ENSMUSG00000015950	-0.59046526	0.000393382	0.017487266
Gm5124	ENSMUSG00000051537	0.424425192	0.000394093	0.017487266
B230216N24Rik	ENSMUSG00000089706	0.778678281	0.000390121	0.017487266
Fras1	ENSMUSG00000034687	0.526105294	0.00038709	0.017487266
Col4a1	ENSMUSG00000031502	0.716372155	0.00039122	0.017487266
Efs	ENSMUSG00000022203	-0.516357512	0.000391743	0.017487266

Incenp	ENSMUSG00000024660	0.476399016	0.00039238	0.017487266
Gm36936	ENSMUSG00000102411	1.277199996	0.000390636	0.017487266
Eps15	ENSMUSG00000028552	-0.34314162	0.000392804	0.017487266
G730003C15Rik	ENSMUSG00000097573	-1.311622135	0.000387696	0.017487266
Spata32	ENSMUSG00000044787	1.777536528	0.000389342	0.017487266
Cnot3	ENSMUSG00000035632	0.513642754	0.000399868	0.017575849
Hist1h2bq	ENSMUSG00000069307	-1.372487072	0.000402455	0.017575849
Hist1h1e	ENSMUSG00000051627	-1.941222728	0.000403038	0.017575849
Prr18	ENSMUSG00000055945	-0.459886131	0.0004024	0.017575849
Apol8	ENSMUSG00000056656	0.534586713	0.000402529	0.017575849
Htr1b	ENSMUSG00000049511	-0.42930893	0.00039816	0.017575849
Gm20394	ENSMUSG00000092509	1.968268693	0.000400086	0.017575849
8430429K09Rik	ENSMUSG00000034587	0.510139884	0.000413311	0.017732702
Eri2	ENSMUSG00000030929	0.639948006	0.000412283	0.017732702
Peg3	ENSMUSG00000002265	0.580401462	0.000413012	0.017732702
1700008J07Rik	ENSMUSG00000101225	-0.997715336	0.000413646	0.017732702
Pcdhb6	ENSMUSG00000051678	-0.762318248	0.000408838	0.017732702
Clec18a	ENSMUSG00000033633	0.991326856	0.000411151	0.017732702
1700109K24Rik	ENSMUSG00000097267	1.485907889	0.000409752	0.017732702
Hint2	ENSMUSG00000028470	-0.480536823	0.000417561	0.017771429
Nudt16	ENSMUSG00000032565	-0.553720707	0.000416397	0.017771429
Pkd1l3	ENSMUSG00000048827	0.813905205	0.000417196	0.017771429
Kctd8	ENSMUSG00000037653	-0.544107316	0.000419659	0.017775273
Tectb	ENSMUSG00000024979	1.288591468	0.000419138	0.017775273
Fgf7	ENSMUSG00000027208	1.529472389	0.000424205	0.017924954
Dmp1	ENSMUSG00000029307	-0.50388718	0.000429084	0.018087951
Cntrl	ENSMUSG00000057110	0.873327947	0.000435609	0.018287032
L3mbtl1	ENSMUSG00000035576	1.389135172	0.000435873	0.018287032
Ndufc1	ENSMUSG00000037152	-0.587079457	0.000447352	0.01838476
Tstd2	ENSMUSG00000035495	0.522850413	0.00044405	0.01838476
Gcfc2	ENSMUSG00000035125	0.695797211	0.000449045	0.01838476
Rap1gds1	ENSMUSG00000028149	-0.387580282	0.000449624	0.01838476
Nat8f1	ENSMUSG00000057103	-0.564035773	0.000444314	0.01838476
Eps15l1	ENSMUSG00000006276	0.507765367	0.000448003	0.01838476
Mecr	ENSMUSG00000028910	0.541599901	0.0004463	0.01838476
Mkl2	ENSMUSG00000009569	0.350454119	0.000444054	0.01838476

Pcnx2	ENSMUSG00000060212	0.404535112	0.000446116	0.01838476
Zcchc24	ENSMUSG00000055538	-0.337169595	0.000443525	0.01838476
Scd1	ENSMUSG00000037071	-0.409610374	0.000448233	0.01838476
Ralgapa2	ENSMUSG00000037110	0.62379723	0.000458344	0.018698097
Gcc2	ENSMUSG00000038039	0.360566561	0.000461907	0.018800163
Dcst1	ENSMUSG00000042672	0.596479787	0.000471848	0.019116874
Hcfc1	ENSMUSG00000031386	0.33286619	0.000471776	0.019116874
Parvg	ENSMUSG00000022439	-0.617892184	0.000473445	0.019137753
Rad54l2	ENSMUSG00000040661	0.54905545	0.000475019	0.019157661
Pcsk5	ENSMUSG00000024713	0.515570655	0.000479556	0.019296671
Kif21b	ENSMUSG00000041642	0.629004176	0.000485146	0.019389421
Dpy19l3	ENSMUSG00000043671	-0.282645971	0.000485024	0.019389421
Gm38413	ENSMUSG00000105218	1.047668072	0.000484679	0.019389421
Colgalt2	ENSMUSG00000032649	0.433349738	0.000490897	0.019531062
Plekhb1	ENSMUSG00000030701	-0.492512815	0.000490629	0.019531062
Prkn	ENSMUSG00000023826	0.554539217	0.000493139	0.019576284
Mpdz	ENSMUSG00000028402	0.392333077	0.000501906	0.019700103
Cers4	ENSMUSG00000008206	0.645695034	0.000498507	0.019700103
Fcer1g	ENSMUSG00000058715	-0.658999181	0.000501525	0.019700103
Cbln4	ENSMUSG00000067578	-0.547999329	0.000497512	0.019700103
Rxfp1	ENSMUSG00000034009	0.669413542	0.000502934	0.019700103
Gm42489	ENSMUSG00000104833	1.352783098	0.0005001	0.019700103
Ino80d	ENSMUSG00000040865	0.575356178	0.000504892	0.019733145
Gpc5	ENSMUSG00000022112	-0.471842511	0.000507085	0.019775196
4930488L21Rik	ENSMUSG00000097520	-0.930729989	0.000510016	0.019845784
Frzb	ENSMUSG00000027004	-0.491164531	0.000511257	0.019850462
Fam213a	ENSMUSG00000021792	-0.488176186	0.000513773	0.019904503
Gm49284	ENSMUSG00000114995	0.847310837	0.000515475	0.01992683
4930579G18Rik	ENSMUSG00000040840	1.150628944	0.000523375	0.020144263
Ankrd12	ENSMUSG00000034647	0.366816567	0.000523323	0.020144263
Dst	ENSMUSG00000026131	0.427573879	0.000529147	0.020322228
Strbp	ENSMUSG00000026915	0.570392767	0.000531554	0.020370471
Nefl	ENSMUSG00000022055	-0.360636204	0.000538486	0.020591555
Golgb1	ENSMUSG00000034243	0.61790493	0.000543527	0.020698263
Ube2o	ENSMUSG00000020802	0.324001502	0.000543614	0.020698263
Gstm5	ENSMUSG00000004032	-0.471855331	0.000547216	0.020746155

Cspp1	ENSMUSG00000056763	0.800614369	0.000546404	0.020746155
Ccdc77	ENSMUSG00000030177	0.715046389	0.000551161	0.020851073
Fancg	ENSMUSG00000028453	0.581758691	0.000552396	0.020853234
Eml6	ENSMUSG00000044072	0.644487229	0.000557303	0.020904776
P2ry12	ENSMUSG00000036353	-0.594323619	0.000557059	0.020904776
Gprc5b	ENSMUSG00000008734	-0.344029902	0.000555847	0.020904776
Cdon	ENSMUSG00000038119	0.512209027	0.00056208	0.020950775
Kmt2d	ENSMUSG00000048154	0.651775922	0.000561974	0.020950775
Nin	ENSMUSG00000021068	0.574238298	0.000561716	0.020950775
Kri1	ENSMUSG00000035047	0.568994822	0.000563593	0.020963064
Rngtt	ENSMUSG00000028274	-0.319966027	0.000564918	0.020968298
Unc79	ENSMUSG00000021198	0.447586675	0.000566497	0.020982898
Kcna5	ENSMUSG00000045534	-0.544897708	0.000570593	0.021090482
Ncapd2	ENSMUSG00000038252	0.664357348	0.000572235	0.021107133
Eln	ENSMUSG00000029675	0.676589041	0.000578985	0.021267472
Eif4g3	ENSMUSG00000028760	0.35166378	0.000578393	0.021267472
Ufsp1	ENSMUSG00000051502	-0.607652332	0.000589681	0.021570862
Abcg4	ENSMUSG00000032131	0.381485625	0.000588842	0.021570862
Ankhd1	ENSMUSG00000024483	0.516345761	0.000592487	0.021584308
Il33	ENSMUSG00000024810	-0.505345034	0.000591868	0.021584308
Ly86	ENSMUSG00000021423	-0.654643875	0.000594731	0.021593317
Bid	ENSMUSG00000004446	-0.495178958	0.000596642	0.021593317
Ostf1	ENSMUSG00000024725	-0.541444639	0.000599355	0.021593317
Gm12592	ENSMUSG00000053263	0.975944542	0.000600052	0.021593317
Dtnbos	ENSMUSG00000092286	1.342068927	0.00059712	0.021593317
Loxhd1	ENSMUSG00000032818	2.585644954	0.000598567	0.021593317
Adra2c	ENSMUSG00000045318	-0.63211422	0.000602206	0.02162688
Sbno2	ENSMUSG00000035673	0.577215504	0.000605191	0.02169011
Baalc	ENSMUSG00000022296	-0.450998803	0.00061072	0.021834579
Col5a1	ENSMUSG00000026837	1.275427141	0.000611689	0.021834579
Gm4134	ENSMUSG00000092571	1.585458419	0.000615293	0.021919042
Laptm4b	ENSMUSG00000022257	-0.437485441	0.000619211	0.02197021
Pecam1	ENSMUSG00000020717	-0.466863406	0.000618516	0.02197021
E330034L11Rik	ENSMUSG00000106383	0.562782679	0.000623651	0.022083495
Ints1	ENSMUSG00000029547	0.423924721	0.000625369	0.022100115
Mdm4	ENSMUSG00000054387	0.602695554	0.000626959	0.022112177

Riok1	ENSMUSG00000021428	0.443796718	0.000630817	0.022203994
Resp18	ENSMUSG00000033061	-0.53387384	0.000638523	0.022210301
Syne2	ENSMUSG00000063450	0.349535176	0.000636347	0.022210301
Ssh3	ENSMUSG00000034616	0.767107692	0.000638192	0.022210301
Col27a1	ENSMUSG00000045672	0.636524791	0.000638221	0.022210301
Gm26823	ENSMUSG00000096926	1.719486502	0.000638169	0.022210301
AC165271.1	ENSMUSG00000116641	1.30258878	0.000632757	0.022210301
Bdp1	ENSMUSG00000049658	0.430291321	0.000643709	0.022346815
B4galt4	ENSMUSG00000022793	-0.347763495	0.000650818	0.022520593
Flt3l	ENSMUSG00000110206	1.060599848	0.000651259	0.022520593
Gm46432	ENSMUSG00000114827	1.709619678	0.000654312	0.022582048
Tpm2	ENSMUSG00000028464	-0.557560091	0.000657103	0.022590293
Gm15777	ENSMUSG00000085269	1.279080695	0.000656559	0.022590293
Myo9b	ENSMUSG00000004677	0.72272467	0.000662197	0.022677378
Tmem150a	ENSMUSG00000055912	0.732478467	0.000661123	0.022677378
Zc3h13	ENSMUSG00000022000	0.495153499	0.000668385	0.022801059
Dennd3	ENSMUSG00000036661	0.533344601	0.000667854	0.022801059
Klf12	ENSMUSG00000072294	0.61630944	0.000670017	0.0228128
Gm44053	ENSMUSG00000108137	1.094264873	0.000682609	0.023152487
Mov10	ENSMUSG00000002227	0.852573656	0.000681321	0.023152487
Fam193b	ENSMUSG00000021495	1.024301583	0.000684726	0.023179868
Slco2b1	ENSMUSG00000030737	-0.421210949	0.000688759	0.023271902
Col23a1	ENSMUSG00000063564	0.709197939	0.000691518	0.02332061
Slc44a1	ENSMUSG00000028412	-0.389461989	0.000698596	0.02342545
Lmbr1l	ENSMUSG00000022999	0.754607759	0.000697742	0.02342545
Gm45632	ENSMUSG00000110077	1.967447631	0.000698505	0.02342545
Tmem219	ENSMUSG00000060538	-0.506624514	0.000708283	0.023691614
Trappc5	ENSMUSG00000040236	-0.423920401	0.00070921	0.023691614
Herc2	ENSMUSG00000030451	0.494416467	0.000714581	0.023781301
Catsperg2	ENSMUSG00000049123	1.432212522	0.000714023	0.023781301
Dnajc13	ENSMUSG00000032560	0.35835541	0.000723612	0.024036689
4833420G17Rik	ENSMUSG00000062822	0.570132643	0.000725567	0.024055435
Tgfb1	ENSMUSG00000002603	-0.514843564	0.000726894	0.024055435
Nars2	ENSMUSG00000018995	-0.43447802	0.000728675	0.024069384
Cep250	ENSMUSG00000038241	0.658469312	0.00073663	0.024241714
Efhd1	ENSMUSG00000026255	-0.491424206	0.000735914	0.024241714

H3f3b	ENSMUSG00000016559	-0.458964296	0.000742492	0.024382695
Zfp365	ENSMUSG00000037855	-0.40923401	0.000743669	0.024382695
St6gal2	ENSMUSG00000024172	0.384768714	0.000748218	0.024412702
Syngr2	ENSMUSG00000048277	-0.51253514	0.000746424	0.024412702
Rhoj	ENSMUSG00000046768	-0.716705126	0.000751478	0.024412702
Slc38a6	ENSMUSG00000044712	0.872429189	0.000749932	0.024412702
Dgat1	ENSMUSG00000022555	0.594784144	0.000750925	0.024412702
Them6	ENSMUSG00000056665	-0.472634047	0.000757623	0.024509339
Cacna1c	ENSMUSG00000051331	0.527858869	0.000758606	0.024509339
Raph1	ENSMUSG00000026014	0.442235864	0.000758016	0.024509339
Tmtc3	ENSMUSG00000036676	0.535193983	0.000770013	0.024810142
Mga	ENSMUSG00000033943	0.379336426	0.00077212	0.024810142
Setx	ENSMUSG00000043535	0.405206077	0.000771438	0.024810142
Gm26848	ENSMUSG00000097723	1.347518786	0.000773872	0.024821381
E130317F20Rik	ENSMUSG00000091994	-0.649082387	0.000782433	0.024972374
Gm10710	ENSMUSG00000074517	-1.032560823	0.000783576	0.024972374
Pygm	ENSMUSG00000032648	-0.387622088	0.000781827	0.024972374
5830462I19Rik	ENSMUSG00000091102	1.710837831	0.000784221	0.024972374
Atp11b	ENSMUSG00000037400	0.631175016	0.000786316	0.024976797
Zfp729a	ENSMUSG00000021510	0.590552888	0.000787182	0.024976797
Tbc1d19	ENSMUSG00000039178	0.395083061	0.000793378	0.025047946
Ift140	ENSMUSG00000024169	0.519205167	0.000791159	0.025047946
Fap	ENSMUSG00000000392	0.759567152	0.000793668	0.025047946
A930001A20Rik	ENSMUSG00000098008	-1.82124994	0.00079695	0.025106776
Epop	ENSMUSG00000043439	-0.427498526	0.000800593	0.025132085
AU041133	ENSMUSG00000078435	-0.542313733	0.000800394	0.025132085
Tpd52l1	ENSMUSG00000000296	-0.404808416	0.000802903	0.025139514
Gm37795	ENSMUSG00000102813	1.489662104	0.000804001	0.025139514
Gm36855	ENSMUSG00000111110	-0.9326524	0.000805089	0.025139514
Letm2	ENSMUSG00000037363	0.708896178	0.000807826	0.025180572
Bcl9	ENSMUSG00000038256	0.478171133	0.000810228	0.025211049
Tmem60	ENSMUSG00000045435	-0.437032313	0.000816894	0.025373863
Tpcn2	ENSMUSG00000048677	0.824216559	0.000825797	0.025605478
Mphosph9	ENSMUSG00000038126	0.688972705	0.000829861	0.025686532
Sdcbp	ENSMUSG00000028249	-0.427554329	0.000838437	0.02587507
Gm44210	ENSMUSG00000108079	-0.576264879	0.000838875	0.02587507

S100a13	ENSMUSG00000042312	-0.544633354	0.000855537	0.0263431
Qtrt2	ENSMUSG00000022704	0.60413769	0.000858416	0.026385867
Gm43300	ENSMUSG00000105572	0.987817763	0.000871076	0.026404679
Pkn1	ENSMUSG00000057672	0.546786593	0.000876386	0.026404679
Cntrob	ENSMUSG00000032782	0.619528636	0.000866417	0.026404679
C030006K11Rik	ENSMUSG00000116138	-0.505398124	0.000879907	0.026404679
Gm29237	ENSMUSG00000101872	1.1731392	0.000869608	0.026404679
Gm20632	ENSMUSG00000093577	-1.020274054	0.000873845	0.026404679
Pi4ka	ENSMUSG00000041720	0.341043746	0.000875342	0.026404679
Gk5	ENSMUSG00000041440	0.66669788	0.000861106	0.026404679
Mbp	ENSMUSG00000041607	-0.421860598	0.000876357	0.026404679
Dnajc12	ENSMUSG00000036764	-0.433070052	0.000865025	0.026404679
Zfp871	ENSMUSG00000024298	0.725095605	0.000878891	0.026404679
Ecm2	ENSMUSG00000043631	0.568246967	0.000862692	0.026404679
Slc25a21	ENSMUSG00000035472	-1.565312608	0.000879385	0.026404679
4930562C15Rik	ENSMUSG00000022518	1.801305477	0.000870739	0.026404679
Zfp609	ENSMUSG00000040524	0.552429625	0.000886004	0.026478431
Olfr287	ENSMUSG00000090129	-0.790165109	0.000884541	0.026478431
Tspan2	ENSMUSG00000027858	-0.486370909	0.000886852	0.026478431
Suclg2	ENSMUSG00000061838	-0.483755933	0.000897697	0.026712153
Rerg	ENSMUSG00000030222	-0.517517121	0.000897384	0.026712153
Nr6a1	ENSMUSG00000063972	0.682727377	0.000902037	0.026796249
Adgrl4	ENSMUSG00000039167	-0.446306521	0.000907643	0.026917632
Arhgef1	ENSMUSG00000040940	0.724994471	0.000912246	0.027008895
Slc35b2	ENSMUSG00000037089	-0.383070234	0.000914168	0.027020615
Kcnc3	ENSMUSG00000062785	0.625426468	0.000918253	0.027024919
Acin1	ENSMUSG00000022185	0.658988286	0.000920145	0.027024919
Zbtb34	ENSMUSG00000068966	0.645431599	0.000920419	0.027024919
Gm16287	ENSMUSG00000073739	1.79973482	0.000917083	0.027024919
Naa38	ENSMUSG00000059278	-0.493690143	0.000925212	0.027031312
Igfbp7	ENSMUSG00000036256	-0.491652866	0.000925217	0.027031312
Zfc3h1	ENSMUSG00000034163	0.626326067	0.000923124	0.027031312
Gm45768	ENSMUSG00000108434	-0.577360651	0.000929769	0.027119528
Tmem131	ENSMUSG00000026116	0.534778461	0.000937029	0.027178773
Btaf1	ENSMUSG00000040565	0.557019074	0.000945616	0.027178773
Rcan2	ENSMUSG00000039601	-0.343318909	0.000941165	0.027178773

Fasn	ENSMUSG00000025153	0.236377161	0.000939771	0.027178773
Acox3	ENSMUSG00000029098	0.269760566	0.000939586	0.027178773
Pigv	ENSMUSG00000043257	-0.478753604	0.000945604	0.027178773
Tpm4	ENSMUSG00000031799	-0.383712276	0.00094288	0.027178773
Myo5c	ENSMUSG00000033590	0.989087122	0.000936895	0.027178773
AC154486.3	ENSMUSG00000117333	1.345227703	0.000945002	0.027178773
Wfdc1	ENSMUSG00000023336	-0.578410237	0.000949497	0.027213245
Hdac7	ENSMUSG00000022475	0.735395244	0.000949889	0.027213245
4833413G10Rik	ENSMUSG00000104950	0.764870457	0.000955178	0.027320555
Ccl6	ENSMUSG00000018927	-0.928831677	0.000969908	0.027563758
Ppip5k1	ENSMUSG00000033526	0.405138361	0.000969465	0.027563758
Ddx55	ENSMUSG00000029389	0.601871541	0.000966092	0.027563758
Gm26773	ENSMUSG00000097358	1.716990972	0.000967419	0.027563758
Mt3	ENSMUSG00000031760	-0.393391803	0.000983001	0.027575422
Tac1	ENSMUSG00000061762	-0.530067327	0.000975814	0.027575422
Gm17732	ENSMUSG00000091744	0.952974793	0.00098468	0.027575422
Ciz1	ENSMUSG00000039205	0.678677169	0.000980878	0.027575422
Crtc2	ENSMUSG00000027936	0.601881809	0.000985893	0.027575422
Mbd6	ENSMUSG00000025409	0.660636118	0.000980477	0.027575422
Dpysl5	ENSMUSG00000029168	0.29713323	0.000972707	0.027575422
Scara3	ENSMUSG00000034463	-0.39454274	0.000981697	0.027575422
Gm43375	ENSMUSG00000106262	2.089221704	0.000982701	0.027575422
Gm48678	ENSMUSG00000111971	-1.657235081	0.000976579	0.027575422
Fam53c	ENSMUSG00000034300	0.28089324	0.000987527	0.027577562
Ccar1	ENSMUSG00000020074	0.416489267	0.000989192	0.027580545
Eva1a	ENSMUSG00000035104	-0.629410501	0.000992431	0.027627333
Gm42742	ENSMUSG00000107068	1.183718025	0.001000699	0.027813788
Gpatch8	ENSMUSG00000034621	0.694135602	0.001002849	0.02782985
Tm4sf1	ENSMUSG00000027800	-0.472532288	0.001008404	0.027940198
Ago1	ENSMUSG00000041530	0.380088712	0.001014311	0.027959505
Ank2	ENSMUSG00000032826	0.357849177	0.001022995	0.027959505
Acad10	ENSMUSG00000029456	0.840217945	0.001022656	0.027959505
Slc9a7	ENSMUSG00000037341	0.634548584	0.001023313	0.027959505
Tnfrsf18	ENSMUSG00000041954	1.399686929	0.00101879	0.027959505
Ppox	ENSMUSG00000062729	0.696454633	0.001022729	0.027959505
D630033A02Rik	ENSMUSG00000112237	0.9260724	0.001012265	0.027959505

Ptger1	ENSMUSG00000019464	1.162971608	0.001022812	0.027959505
Cmya5	ENSMUSG00000047419	0.48830489	0.001017404	0.027959505
Tcte2	ENSMUSG00000038347	0.561089459	0.001028469	0.027974013
Susd2	ENSMUSG00000006342	0.377324416	0.001028584	0.027974013
Cd82	ENSMUSG00000027215	-0.431733342	0.001028562	0.027974013
Kmt2b	ENSMUSG00000006307	0.617815118	0.001031926	0.027998299
Gm48604	ENSMUSG00000111291	0.705899301	0.00103264	0.027998299
Plcg1	ENSMUSG00000016933	0.439439965	0.001035771	0.028040248
Ryr2	ENSMUSG00000021313	0.540749105	0.001044708	0.028239028
Mcat	ENSMUSG00000048755	-0.418738058	0.001047814	0.028279784
Wdfy2	ENSMUSG00000014547	0.381396154	0.001052281	0.028314036
Scrt2	ENSMUSG00000060257	-0.409598994	0.001052044	0.028314036
Stoml3	ENSMUSG00000027744	-1.372343254	0.001057529	0.028412054
Msantd2	ENSMUSG00000042138	0.792389049	0.001059309	0.028416776
Dhtkd1	ENSMUSG00000025815	0.812744946	0.001073287	0.028748168
Clec4a3	ENSMUSG00000043832	-1.378001302	0.0010776	0.028820091
Csf1r	ENSMUSG00000024621	-0.309915456	0.001089052	0.029082439
2810049E08Rik	ENSMUSG00000100891	0.976307414	0.001095104	0.029200024
Ccl9	ENSMUSG00000019122	-0.850100142	0.001106204	0.029395254
Nde1	ENSMUSG00000022678	-0.418044888	0.001107746	0.029395254
Ighmbp2	ENSMUSG00000024831	0.365085861	0.001108781	0.029395254
Sidt2	ENSMUSG00000034908	0.358055589	0.001109067	0.029395254
Tpbgl	ENSMUSG00000096606	-0.775439115	0.001122997	0.029675627
Gm37776	ENSMUSG00000104037	1.623528459	0.001122904	0.029675627
Elk4	ENSMUSG00000026436	0.432129789	0.001129184	0.029750312
H2-Q2	ENSMUSG00000091705	-1.623466479	0.001127792	0.029750312
Tmem176b	ENSMUSG00000029810	-0.563813613	0.00113445	0.02980035
Gm34220	ENSMUSG00000114045	-0.498089059	0.001134249	0.02980035
Zfp362	ENSMUSG00000028799	0.347476719	0.001142967	0.029979603
B630019K06Rik	ENSMUSG00000052364	-0.49053032	0.0011492	0.030098506
Cd83	ENSMUSG00000015396	-0.508292422	0.001166226	0.030499304
Neu1	ENSMUSG00000007038	-0.282944684	0.001174447	0.030640212
Gba	ENSMUSG00000028048	0.352085999	0.001175075	0.030640212
Ccdc167	ENSMUSG00000024018	0.683941242	0.001183367	0.030811056
9030025P20Rik	ENSMUSG00000116953	0.633794852	0.001187064	0.030816677
Olfml1	ENSMUSG00000051041	-0.484252192	0.001186776	0.030816677

Penk	ENSMUSG00000045573	-0.495051383	0.001194001	0.030951366
Cpt1c	ENSMUSG00000007783	0.320867819	0.001198995	0.031035378
Scrg1	ENSMUSG00000031610	-0.480247933	0.001204605	0.031135083
Atg16l2	ENSMUSG00000047767	0.706929326	0.001207961	0.031176316
Tenm2	ENSMUSG00000049336	0.364577371	0.001213011	0.031204007
Brpf3	ENSMUSG00000063952	0.403201845	0.001214321	0.031204007
Olfr1420	ENSMUSG00000060878	2.267181942	0.001213427	0.031204007
Mgst1	ENSMUSG00000008540	-0.596746586	0.00121718	0.031232139
Kdm5d	ENSMUSG00000056673	0.464907129	0.001220315	0.031242351
Slc25a33	ENSMUSG00000028982	-0.396049366	0.001221107	0.031242351
Bmp1	ENSMUSG00000022098	0.697697677	0.001226636	0.031338522
Aldoc	ENSMUSG00000017390	-0.379190983	0.001233637	0.031381538
Mbip	ENSMUSG00000021028	0.574933159	0.001230441	0.031381538
Grid2ip	ENSMUSG00000010825	1.143615304	0.001232563	0.031381538
Jam2	ENSMUSG00000053062	-0.392580591	0.001240536	0.031511747
Tyk2	ENSMUSG00000032175	0.5880591	0.001242524	0.031517035
Tert	ENSMUSG00000021611	1.201584976	0.001248959	0.031548851
Ubap2l	ENSMUSG00000042520	0.30174074	0.00125447	0.031548851
Dock6	ENSMUSG00000032198	0.604411079	0.001253242	0.031548851
Col6a6	ENSMUSG00000043719	0.934218319	0.001249187	0.031548851
Col24a1	ENSMUSG00000028197	1.416948628	0.00125252	0.031548851
D430018E03Rik	ENSMUSG00000097559	1.812853239	0.001247993	0.031548851
Taf13	ENSMUSG00000048100	-0.385423585	0.001257197	0.031572582
Serpinf1	ENSMUSG00000000753	-0.528434547	0.001259306	0.031580757
Gal	ENSMUSG00000024907	-1.086344343	0.001264671	0.031670433
Plagl1	ENSMUSG00000019817	0.416762626	0.001266623	0.031674509
Fzd9	ENSMUSG00000049551	-0.744459622	0.001274837	0.031790119
Arhgap17	ENSMUSG00000030766	0.585167617	0.001274525	0.031790119
Grin2b	ENSMUSG00000030209	0.566142649	0.00128553	0.032003639
Csmd2	ENSMUSG00000028804	0.57325688	0.001287014	0.032003639
Csmd1	ENSMUSG00000060924	0.531846355	0.001294371	0.032051514
Gm42732	ENSMUSG00000107331	0.279811899	0.001294112	0.032051514
Gm38364	ENSMUSG00000103592	1.146183148	0.001293549	0.032051514
Mypopos	ENSMUSG00000086533	1.483825351	0.001304909	0.03226734
mt-Nd1	ENSMUSG00000064341	-0.464986791	0.001307681	0.032290788
Jund	ENSMUSG00000071076	-0.459063952	0.001314471	0.032368153

Itpkb	ENSMUSG00000038855	-0.3092369	0.001314037	0.032368153
Gm27030	ENSMUSG00000098221	-0.934183166	0.001318956	0.032433504
Arl16	ENSMUSG00000057594	-0.369094102	0.001324644	0.032449737
Creg1	ENSMUSG00000040713	-0.432772786	0.001325115	0.032449737
Rbm10	ENSMUSG00000031060	0.364428219	0.001322631	0.032449737
Ago2	ENSMUSG00000036698	0.389458461	0.001328466	0.032462506
Amer1	ENSMUSG00000050332	0.496867286	0.001329303	0.032462506
Drd5	ENSMUSG00000039358	-0.834204895	0.00133337	0.032516963
Cd302	ENSMUSG00000060703	-0.516585674	0.001336066	0.032520224
Pmp22	ENSMUSG00000018217	-0.423312679	0.001340985	0.032520224
Lims2	ENSMUSG00000024395	-0.386050223	0.001342688	0.032520224
Gm37127	ENSMUSG00000104358	1.481753253	0.001338235	0.032520224
B230208B08Rik	ENSMUSG00000092492	0.910349422	0.001342023	0.032520224
Gm13147	ENSMUSG00000087207	2.264145952	0.001345359	0.032540402
Gpd1	ENSMUSG00000023019	-0.276922902	0.001353183	0.032654709
Sowaha	ENSMUSG00000044352	-0.405054227	0.001353773	0.032654709
Ier3	ENSMUSG00000003541	-0.59675881	0.001368112	0.032742653
Trim66	ENSMUSG00000031026	0.4652541	0.001368515	0.032742653
Gm29093	ENSMUSG00000100201	1.05459423	0.001365326	0.032742653
Mrps33	ENSMUSG00000029918	-0.376881606	0.001365471	0.032742653
Gucy2g	ENSMUSG00000055523	0.504929173	0.001359632	0.032742653
Chmp1b	ENSMUSG00000109901	-0.388420668	0.001364737	0.032742653
Phlpp2	ENSMUSG00000031732	0.406822509	0.001373811	0.032781261
Gm25129	ENSMUSG00000064585	1.491096346	0.001373832	0.032781261
Pde1c	ENSMUSG00000004347	-0.350526529	0.0013823	0.032894659
1700013F07Rik	ENSMUSG00000027886	0.864862415	0.001380817	0.032894659
Arpc1b	ENSMUSG00000029622	-0.414076173	0.001388082	0.032987915
Tmbim1	ENSMUSG00000006301	-0.336008815	0.001394334	0.033092073
Ctsd	ENSMUSG00000007891	-0.410607409	0.001402614	0.033244014
Hjurp	ENSMUSG00000044783	0.506232086	0.001407892	0.033324511
Gpr146	ENSMUSG00000044197	-0.398784796	0.001414036	0.033425251
Gdf10	ENSMUSG00000021943	-0.569634626	0.001428525	0.033722702
Atxn7l2	ENSMUSG00000048997	0.672915029	0.001431792	0.033754839
Ccdc84	ENSMUSG00000043923	0.810334998	0.00144282	0.033969586
Gm3828	ENSMUSG00000083808	2.270365603	0.001445723	0.033992722
Snapc4	ENSMUSG00000036281	0.705116556	0.001448426	0.034011129

Hcn3	ENSMUSG00000028051	0.394292628	0.001460999	0.034260919
Dgkq	ENSMUSG00000004815	0.667321617	0.001466113	0.034335362
Scai	ENSMUSG00000035236	0.480991497	0.001470883	0.034401572
Dis3	ENSMUSG00000033166	0.418418985	0.001473872	0.034425998
Tcn2	ENSMUSG00000020432	-0.364114749	0.001476758	0.034441375
Aes	ENSMUSG00000054452	-0.415083179	0.001490243	0.034441375
Paxbp1	ENSMUSG00000022974	0.694416488	0.001494345	0.034441375
Kmt2c	ENSMUSG00000038056	0.427426889	0.001482377	0.034441375
Asxl1	ENSMUSG00000042548	0.410866126	0.001489216	0.034441375
Zkscan16	ENSMUSG00000038630	0.607100632	0.001490786	0.034441375
Arhgef2	ENSMUSG00000028059	0.322616493	0.001495929	0.034441375
Selenov	ENSMUSG00000046750	1.048243694	0.001479772	0.034441375
Hcls1	ENSMUSG00000022831	-0.553187759	0.001491793	0.034441375
Akirin1	ENSMUSG00000023075	-0.313413873	0.001492231	0.034441375
Gm42748	ENSMUSG00000105742	1.676347198	0.001482542	0.034441375
Pnma3	ENSMUSG00000046287	0.458263477	0.001500837	0.034464738
Sft2d2	ENSMUSG00000040848	-0.353503635	0.001500359	0.034464738
Mapkbp1	ENSMUSG00000033902	0.466112918	0.001504212	0.034494054
Frem2	ENSMUSG00000037016	0.513811757	0.00150601	0.034494054
Trmt1	ENSMUSG00000001909	0.436793546	0.001515923	0.034631501
Gm43140	ENSMUSG00000105286	1.416801041	0.001514162	0.034631501
Ntsr2	ENSMUSG00000020591	-0.320416424	0.00152415	0.03472983
AC125351.1	ENSMUSG00000113184	0.567055518	0.001524102	0.03472983
Pou3f1	ENSMUSG00000090125	-0.386133538	0.001528062	0.034757293
Ahr	ENSMUSG00000019256	0.423944831	0.001529282	0.034757293
Dad1	ENSMUSG00000022174	-0.485871614	0.001541659	0.034859605
Fgf3	ENSMUSG00000031074	-0.917107378	0.001539058	0.034859605
Hddc2	ENSMUSG00000000295	-0.415295814	0.001541325	0.034859605
Cenpt	ENSMUSG00000036672	0.446341431	0.001541045	0.034859605
Gm15721	ENSMUSG00000085565	-0.557769939	0.001543935	0.034866533
Larp1	ENSMUSG00000037331	0.345551577	0.001552345	0.034939329
Klhl5	ENSMUSG00000054920	-0.331395937	0.001552473	0.034939329
Pelp1	ENSMUSG00000018921	0.27214999	0.001553078	0.034939329
Atf7	ENSMUSG00000099083	0.486681187	0.001568152	0.03523367
Hepacam	ENSMUSG00000046240	-0.381988578	0.001572663	0.035290239
Rnf123	ENSMUSG00000041528	0.331216859	0.00157912	0.0353009

Atp2b3	ENSMUSG00000031376	0.556844928	0.001577946	0.0353009
H2-DMa	ENSMUSG00000037649	-0.515196347	0.001576974	0.0353009
Mmd	ENSMUSG00000003948	-0.456918275	0.001581734	0.03530421
Map4k2	ENSMUSG00000024948	0.482213713	0.001583256	0.03530421
Bcl9l	ENSMUSG00000063382	0.357083424	0.001589568	0.035311546
Colca2	ENSMUSG00000079559	-1.152360495	0.001588976	0.035311546
Acaa1a	ENSMUSG00000036138	0.338834035	0.001588517	0.035311546
Tspoap1	ENSMUSG00000034156	0.628626333	0.001596508	0.035421276
Supt16	ENSMUSG00000035726	0.309322852	0.001602201	0.03549661
Shisa4	ENSMUSG00000041889	-0.304557207	0.001605897	0.03549661
Cyp4v3	ENSMUSG00000079057	-0.498028254	0.001607658	0.03549661
Ntng2	ENSMUSG00000035513	0.289317023	0.001607923	0.03549661
Lrg1	ENSMUSG00000037095	-1.111257574	0.001617572	0.035620792
Pfkp	ENSMUSG00000021196	0.35233887	0.001615635	0.035620792
Zfp512b	ENSMUSG00000000823	0.532364346	0.001621937	0.035672546
Tnr	ENSMUSG00000015829	0.354034808	0.001630655	0.035731131
Epdr1	ENSMUSG00000002808	-0.369513546	0.001626933	0.035731131
Col16a1	ENSMUSG00000040690	0.741386727	0.001630647	0.035731131
Slc7a6	ENSMUSG00000031904	0.662958356	0.001632785	0.035733568
mt-Nd4	ENSMUSG00000064363	-0.430289345	0.001635936	0.035757228
Cpsf4	ENSMUSG00000029625	0.664974495	0.001637905	0.035757228
Tmed5	ENSMUSG00000063406	-0.455446275	0.001644523	0.035857496
Trub2	ENSMUSG00000039826	0.289070341	0.001648749	0.03590542
Ippk	ENSMUSG00000021385	-0.370200828	0.001654376	0.035983703
Arsk	ENSMUSG00000021592	-0.418894557	0.001659816	0.036057711
Fam208b	ENSMUSG00000033799	0.522203861	0.001664585	0.036117
Ifrd1	ENSMUSG00000001627	-0.309582491	0.001666842	0.036121709
Qdpr	ENSMUSG00000015806	-0.481044358	0.001671377	0.036170148
Herc1	ENSMUSG00000038664	0.392651784	0.001676565	0.036170148
Cherp	ENSMUSG00000052488	0.348104733	0.00168086	0.036170148
Ubp1	ENSMUSG00000009741	0.601579046	0.001683378	0.036170148
Ddhd2	ENSMUSG00000061313	0.38565852	0.001678559	0.036170148
Mdk	ENSMUSG00000027239	-0.411541407	0.001677961	0.036170148
Cdc25b	ENSMUSG00000027330	0.599985535	0.001681889	0.036170148
Nova2	ENSMUSG00000030411	0.413587971	0.001689343	0.036254325
Cr1l	ENSMUSG00000016481	0.330967485	0.001710609	0.03642263

Cryab	ENSMUSG00000032060	-0.457160762	0.001702172	0.03642263
Dennd6b	ENSMUSG00000015377	0.67412267	0.001711586	0.03642263
Rnf13	ENSMUSG00000036503	-0.436108416	0.001703992	0.03642263
Tcerg1l	ENSMUSG00000091002	-0.51792026	0.001709726	0.03642263
Lrp6	ENSMUSG00000030201	0.355095706	0.001705557	0.03642263
Slc26a6	ENSMUSG00000023259	0.461518645	0.001708684	0.03642263
Rpain	ENSMUSG00000018449	0.589003	0.001722643	0.036613922
Gm33869	ENSMUSG00000112358	0.917109295	0.001728322	0.036690574
Rps6kb2	ENSMUSG00000024830	0.661908224	0.001733833	0.036763483
Fhod1	ENSMUSG00000014778	0.738774247	0.001739759	0.036845016
Safb	ENSMUSG00000071054	0.517683879	0.001748259	0.036980791
Ppp1r14a	ENSMUSG00000037166	-0.459791198	0.001755661	0.036993359
Dock3	ENSMUSG00000039716	0.449794397	0.001757211	0.036993359
Glud1	ENSMUSG00000021794	-0.391344498	0.001753832	0.036993359
Gm5881	ENSMUSG00000107747	1.754316961	0.001753355	0.036993359
Serpina1b	ENSMUSG00000071178	-1.461747992	0.001760224	0.037012796
Gm43660	ENSMUSG00000107352	0.824736879	0.001766745	0.037105838
Mocs2	ENSMUSG00000015536	-0.31838362	0.001773276	0.037170294
Mms19	ENSMUSG00000025159	0.422837063	0.001774013	0.037170294
Tmem9b	ENSMUSG00000031021	-0.40357085	0.001778542	0.037221139
Pou2f1	ENSMUSG00000026565	0.672004144	0.00178294	0.037225175
Lrrc58	ENSMUSG00000034158	-0.305082815	0.001782814	0.037225175
Gm37459	ENSMUSG00000104283	-0.456510703	0.001800067	0.037239784
Brd9	ENSMUSG00000057649	0.522968281	0.001792721	0.037239784
Gm47113	ENSMUSG00000111465	0.805726251	0.001786239	0.037239784
Hdac6	ENSMUSG00000031161	0.386857733	0.001800466	0.037239784
Sugp2	ENSMUSG00000036054	0.491444814	0.001799069	0.037239784
A230001M10Rik	ENSMUSG00000105891	-0.67027116	0.001792629	0.037239784
Gm45606	ENSMUSG00000109715	-0.399856029	0.001791272	0.037239784
Smg7	ENSMUSG00000042772	0.335953589	0.001794555	0.037239784
Dynlt1a	ENSMUSG00000092074	0.841855292	0.00180732	0.037337926
Celf3	ENSMUSG00000028137	0.362546895	0.001817514	0.037461104
Gm2a	ENSMUSG00000000594	-0.408593884	0.001816008	0.037461104
Clasp1	ENSMUSG00000064302	0.326934393	0.001822609	0.037474348
Hmgcs2	ENSMUSG00000027875	-0.66050003	0.001825001	0.037474348

Cabp7	ENSMUSG00000009075	-0.437518108	0.001826533	0.037474348
Gm42664	ENSMUSG00000106099	1.100055019	0.001826623	0.037474348
2010315B03Rik	ENSMUSG00000074829	0.44296244	0.001829328	0.037486402
Entpd7	ENSMUSG00000025192	0.576403595	0.00185216	0.037546942
Dcx	ENSMUSG00000031285	0.659279708	0.001851318	0.037546942
Pik3c2b	ENSMUSG00000026447	0.507314509	0.001846311	0.037546942
Arid3a	ENSMUSG00000019564	0.641408698	0.001852497	0.037546942
Dbx2	ENSMUSG00000045608	-0.425388539	0.00183673	0.037546942
Zswim8	ENSMUSG00000021819	0.518788439	0.001843627	0.037546942
Plch2	ENSMUSG00000029055	0.536879323	0.00184141	0.037546942
Dmkn	ENSMUSG00000060962	-0.745258734	0.001853489	0.037546942
Maob	ENSMUSG00000040147	-0.370774392	0.00184706	0.037546942
Gm42672	ENSMUSG00000105395	1.924928592	0.001846856	0.037546942
Tmem41a	ENSMUSG00000022856	-0.412278199	0.001864689	0.037730652
Tmem123	ENSMUSG00000050912	-0.41402657	0.001867461	0.037743606
Ppp1r1b	ENSMUSG00000061718	-0.442814641	0.001876558	0.037830034
Gba2	ENSMUSG00000028467	0.365965681	0.001880329	0.037830034
Cacna1a	ENSMUSG00000034656	0.459054675	0.001875438	0.037830034
Rftn2	ENSMUSG00000025978	-0.456485161	0.001882421	0.037830034
Madd	ENSMUSG00000040687	0.320774253	0.00188149	0.037830034
Tmprss6	ENSMUSG00000016942	-1.201460624	0.001885928	0.037857539
Snx12	ENSMUSG00000046032	-0.309495572	0.00188986	0.03789351
Alms1	ENSMUSG00000063810	0.475503753	0.001893146	0.037916449
Ntmt1	ENSMUSG00000026857	-0.36652097	0.00190035	0.03797535
Gm26721	ENSMUSG00000096943	0.799992487	0.001902624	0.03797535
Ano8	ENSMUSG00000034863	0.41147153	0.001904666	0.03797535
Gm17022	ENSMUSG00000091784	1.510361105	0.001903417	0.03797535
Pdia5	ENSMUSG00000022844	0.735206183	0.001909961	0.038038095
Gm8213	ENSMUSG00000082474	1.662168093	0.001921085	0.038216639
Aldob	ENSMUSG00000028307	1.239938675	0.001929069	0.038332403
Mical3	ENSMUSG00000051586	0.527326087	0.001934083	0.038388946
D630045J12Rik	ENSMUSG00000063455	0.53312184	0.001951179	0.038512411
Sh3rf3	ENSMUSG00000037990	0.401796747	0.001946756	0.038512411
Ap4m1	ENSMUSG00000019518	0.415026072	0.001950067	0.038512411
Gm47372	ENSMUSG00000112990	1.332402315	0.001947987	0.038512411
Slc9b1	ENSMUSG00000050150	1.409683205	0.001948074	0.038512411

Dgat2	ENSMUSG00000030747	-0.348037066	0.0019534	0.038513295
Cacna1d	ENSMUSG00000015968	0.560274852	0.001962781	0.038655222
Smoc1	ENSMUSG00000021136	-0.405466568	0.001973556	0.03882423
Gm48249	ENSMUSG00000111447	1.300030635	0.001976757	0.038844039
Hist3h2a	ENSMUSG00000078851	-0.493240777	0.001983076	0.038881915
Tmem125	ENSMUSG00000050854	-0.610765273	0.001982805	0.038881915
Cc2d1b	ENSMUSG00000028582	0.529556014	0.001991781	0.039009392
Nfat5	ENSMUSG00000003847	0.488687142	0.001997766	0.039083371
Fth1	ENSMUSG00000024661	-0.465889701	0.002000595	0.039095522
Laptm5	ENSMUSG00000028581	-0.478738931	0.002006651	0.039170633
Cxcl14	ENSMUSG00000021508	-0.400989243	0.002012735	0.039246118
Gm43205	ENSMUSG00000105419	-1.055149475	0.00201842	0.039313664
Abca3	ENSMUSG00000024130	0.408192798	0.002021414	0.039328719
Srgn	ENSMUSG00000020077	-0.642023961	0.002027929	0.039368942
A930004J17Rik	ENSMUSG00000102602	1.130550927	0.002026769	0.039368942
Mrps35	ENSMUSG00000040112	-0.302154767	0.002035878	0.039479983
Cmtm8	ENSMUSG00000041012	-0.862430669	0.002040339	0.039523187
Ppp4r3a	ENSMUSG00000041846	0.349879122	0.002057813	0.039818119
Necab2	ENSMUSG00000031837	-0.410072441	0.002066707	0.039859537
Med12l	ENSMUSG00000056476	0.503878281	0.002065116	0.039859537
Gpr150	ENSMUSG00000045509	-0.5542268	0.002066582	0.039859537
Pde8a	ENSMUSG00000025584	-0.328197907	0.002078547	0.039877424
Srrm3	ENSMUSG00000039860	0.429514368	0.002077823	0.039877424
Hsdl2	ENSMUSG00000028383	-0.382168086	0.002078549	0.039877424
Gm6556	ENSMUSG00000097806	-0.89182492	0.002072916	0.039877424
Neurog2	ENSMUSG00000027967	-1.251837959	0.002078896	0.039877424
Cmtm5	ENSMUSG00000040759	-0.525376778	0.002088773	0.040023522
Gm44421	ENSMUSG00000107451	-0.97710711	0.002111645	0.040097992
Phc3	ENSMUSG00000037652	0.441921691	0.002111187	0.040097992
Psat1	ENSMUSG00000024640	-0.360375717	0.002099483	0.040097992
Bod1l	ENSMUSG00000061755	0.402546936	0.002101462	0.040097992
Zfp704	ENSMUSG00000040209	0.38404133	0.002113967	0.040097992
Dpysl3	ENSMUSG00000024501	0.27752836	0.002104865	0.040097992
Tmem145	ENSMUSG00000043843	0.598036956	0.002113263	0.040097992
Edc4	ENSMUSG00000036270	0.458520643	0.002103314	0.040097992
Satb2	ENSMUSG00000038331	0.355209297	0.002115308	0.040097992

Col6a5	ENSMUSG00000091345	0.775903948	0.002108671	0.040097992
Tesc	ENSMUSG00000029359	-0.428455463	0.002118128	0.040108505
Szt2	ENSMUSG00000033253	0.670230876	0.002124603	0.040188141
Cep131	ENSMUSG00000039781	0.562054132	0.002134187	0.040326331
Zc3h4	ENSMUSG00000059273	0.281229042	0.002137261	0.04034138
Gm14326	ENSMUSG00000078862	-0.350915273	0.002139821	0.040346684
Trnp1	ENSMUSG00000056596	-0.480138602	0.002149374	0.040375245
2610008E11Rik	ENSMUSG00000060301	0.383298923	0.002155019	0.040375245
Rfx1	ENSMUSG00000031706	0.636850164	0.002152733	0.040375245
Ntrk1	ENSMUSG00000028072	-0.743477222	0.002151297	0.040375245
Hps1	ENSMUSG00000025188	0.704964883	0.002153563	0.040375245
Trim72	ENSMUSG00000042828	1.240447651	0.002150964	0.040375245
Zfp661	ENSMUSG00000034800	0.494327289	0.002166497	0.040376658
Gm37928	ENSMUSG00000104362	1.017563607	0.002165048	0.040376658
C2cd5	ENSMUSG00000030279	0.480751926	0.002163166	0.040376658
Spop	ENSMUSG00000057522	-0.304648794	0.00216508	0.040376658
Gm16310	ENSMUSG00000086331	1.96462607	0.002164661	0.040376658
Ctps2	ENSMUSG00000031360	0.450489612	0.002178728	0.04056191
Mxra7	ENSMUSG00000020814	-0.412588999	0.002201597	0.040816001
Fbrs	ENSMUSG00000042423	0.418559145	0.002198353	0.040816001
Ccdc120	ENSMUSG00000031150	0.401932843	0.002200023	0.040816001
Metap1d	ENSMUSG00000041921	0.528375117	0.002194705	0.040816001
Gm26944	ENSMUSG00000098066	1.592995419	0.002208022	0.040892294
Zbtb42	ENSMUSG00000037638	-0.924192852	0.002211414	0.040912318
Ptprs	ENSMUSG00000013236	0.365960612	0.002223979	0.041101832
Kif3a	ENSMUSG00000018395	0.298376294	0.002234906	0.041174837
Atp7a	ENSMUSG00000033792	0.778848308	0.002234533	0.041174837
Lamb3	ENSMUSG00000026639	-0.558763572	0.002230266	0.041174837
D030055H07Rik	ENSMUSG00000086296	0.973075226	0.002240438	0.041197274
Gm47690	ENSMUSG00000112254	1.935040622	0.002240778	0.041197274
Gm43684	ENSMUSG00000105613	1.182731463	0.002244648	0.041225621
Phlda3	ENSMUSG00000041801	-0.432925114	0.002268616	0.04132533
Opalin	ENSMUSG00000050121	-0.549043894	0.002274048	0.04132533
Pnn	ENSMUSG00000020994	0.647895573	0.002271729	0.04132533
Rhog	ENSMUSG00000073982	-0.440770446	0.002275752	0.04132533
Cep290	ENSMUSG00000019971	0.433362676	0.002273354	0.04132533

Nemp2	ENSMUSG00000043015	0.62425141	0.002253772	0.04132533
Thap12	ENSMUSG00000030753	-0.349306232	0.002262129	0.04132533
Gpr37	ENSMUSG00000039904	-0.448122148	0.002272514	0.04132533
Abhd4	ENSMUSG00000040997	-0.39719948	0.002272724	0.04132533
Shcbp1l	ENSMUSG00000042708	0.974100802	0.002271302	0.04132533
AI839979	ENSMUSG00000107355	1.185409498	0.002256681	0.04132533
Kcnk1	ENSMUSG00000033998	-0.377381495	0.002280454	0.041368269
Huwe1	ENSMUSG00000025261	0.35598624	0.002285117	0.041410434
Ccpg1	ENSMUSG00000034563	1.107823271	0.00229138	0.04147015
Ubxn2b	ENSMUSG00000028243	-0.267741363	0.002293097	0.04147015
Cplane1	ENSMUSG00000039801	0.577278271	0.002297258	0.041503017
Dmrta2	ENSMUSG00000047143	0.645503393	0.002301009	0.041528396
Tmem181c-ps	ENSMUSG00000093880	0.709535663	0.002306913	0.041592566
C030029H02Rik	ENSMUSG00000110027	-0.54837437	0.002311048	0.041624729
Ubn2	ENSMUSG00000038538	0.65221889	0.002319058	0.041645247
Cit	ENSMUSG00000029516	0.512988827	0.002319244	0.041645247
Gm13844	ENSMUSG00000086855	1.629704758	0.002318889	0.041645247
Reln	ENSMUSG00000042453	0.328816685	0.002322017	0.041652806
Myoc	ENSMUSG00000026697	-0.914480072	0.002325307	0.041669599
Cacna1b	ENSMUSG00000004113	0.522128424	0.002331153	0.041689963
Eci2	ENSMUSG00000021417	-0.334059285	0.002331046	0.041689963
mt-Ty	ENSMUSG00000064350	-0.735428778	0.00233872	0.041783094
AC126457.1	ENSMUSG00000116632	0.457755871	0.00236035	0.042057274
Slc26a11	ENSMUSG00000039908	0.638263171	0.002361193	0.042057274
Fuk	ENSMUSG00000033703	0.448178245	0.00235898	0.042057274
Ccdc7b	ENSMUSG00000056018	1.436633083	0.002364131	0.042067271
Slc39a12	ENSMUSG00000036949	-0.317567757	0.002391506	0.042511663
Gm43692	ENSMUSG00000105429	1.551316425	0.002400925	0.042636293
Pttg1	ENSMUSG00000020415	-0.385339379	0.002404301	0.042653451
Ramp2	ENSMUSG00000001240	-0.443675	0.002426352	0.042657819
Cd63	ENSMUSG00000025351	-0.440590828	0.002451985	0.042657819
Tmem176a	ENSMUSG00000023367	-0.594998719	0.002448116	0.042657819
Cd59a	ENSMUSG00000032679	-0.402747685	0.002446028	0.042657819
Gm16638	ENSMUSG00000087088	0.707767712	0.002448195	0.042657819
Jarid2	ENSMUSG00000038518	0.321755347	0.002424747	0.042657819
Kcnma1	ENSMUSG00000063142	0.416243105	0.002462372	0.042657819

Rab10os	ENSMUSG00000079179	0.425156627	0.002440218	0.042657819
Fndc5	ENSMUSG00000001334	-0.324844968	0.002461104	0.042657819
Kmt2a	ENSMUSG00000002028	0.564174474	0.002458077	0.042657819
0610040F04Rik	ENSMUSG00000087341	1.141055191	0.002458442	0.042657819
5830417I10Rik	ENSMUSG00000078684	0.619502615	0.002431105	0.042657819
Ism1	ENSMUSG00000074766	-0.403502627	0.002435222	0.042657819
Ak3	ENSMUSG00000024782	-0.315962646	0.002423818	0.042657819
Coq5	ENSMUSG00000041733	-0.275962176	0.002409384	0.042657819
Cabin1	ENSMUSG00000020196	0.436739064	0.002444062	0.042657819
H6pd	ENSMUSG00000028980	0.4102104	0.002452103	0.042657819
Ccdc9	ENSMUSG00000041375	0.43147342	0.002410662	0.042657819
Gm11992	ENSMUSG00000040978	-0.821573602	0.002436286	0.042657819
Zc3h7a	ENSMUSG00000037965	0.510444524	0.0024195	0.042657819
A830082K12Rik	ENSMUSG00000087143	0.359959779	0.002461794	0.042657819
Gm37694	ENSMUSG00000102562	1.717200936	0.00245013	0.042657819
Sec14l3	ENSMUSG00000054986	-0.851033217	0.002428914	0.042657819
Gm38451	ENSMUSG00000108917	1.292869899	0.002443189	0.042657819
Sned1	ENSMUSG00000047793	0.615836619	0.002483864	0.042959636
Telo2	ENSMUSG00000024170	0.506080234	0.002484647	0.042959636
Catsperg1	ENSMUSG00000049676	1.311475676	0.002491392	0.043034235
B4galt3	ENSMUSG00000052423	0.314349763	0.002511425	0.043211635
Fnbp1l	ENSMUSG00000039735	0.457360053	0.002508993	0.043211635
Epha10	ENSMUSG00000028876	0.498931402	0.002509661	0.043211635
Adam1b	ENSMUSG00000062438	1.983117757	0.002510952	0.043211635
8430422M14Rik	ENSMUSG00000105095	0.975957396	0.002515843	0.043245636
Ndufa1	ENSMUSG00000016427	-0.41342757	0.002519082	0.043259306
Fcho1	ENSMUSG00000070000	0.430947466	0.002523337	0.043290385
BC024139	ENSMUSG00000044361	0.957583851	0.002541689	0.043563027
Fam183b	ENSMUSG00000049154	-0.694281943	0.002551666	0.043599439
Tmem2	ENSMUSG00000024754	0.445679618	0.00254815	0.043599439
Adi1	ENSMUSG00000020629	-0.415631167	0.002549226	0.043599439
Celsr3	ENSMUSG00000023473	1.105405093	0.002553664	0.043599439
Rnf11	ENSMUSG00000028557	-0.44248352	0.002556351	0.043603266
Zfp462	ENSMUSG00000060206	0.420788972	0.002565281	0.043713471
Tmem250-ps	ENSMUSG00000087679	-0.382262073	0.002569173	0.043737695
Dhx35	ENSMUSG00000027655	0.428878047	0.002582335	0.043919548

Rcl1	ENSMUSG00000024785	-0.33119735	0.00259737	0.04413286
Tln2	ENSMUSG00000052698	0.30224912	0.002611917	0.044295014
Gm37123	ENSMUSG00000103039	1.685238049	0.002609744	0.044295014
Zfp618	ENSMUSG00000028358	0.542815573	0.002623697	0.044409712
Bicra	ENSMUSG00000070808	0.433469995	0.002622859	0.044409712
Tmem215	ENSMUSG00000046593	-0.356248772	0.002631236	0.044494777
Cpxm1	ENSMUSG00000027408	-0.464422419	0.002638709	0.044578565
Kalrn	ENSMUSG00000061751	0.383873687	0.002643648	0.044619442
Smpd4	ENSMUSG00000005899	0.623269272	0.002648732	0.044620178
Col18a1	ENSMUSG00000001435	0.451755803	0.002646544	0.044620178
Kcnj10	ENSMUSG00000044708	-0.355572237	0.002653994	0.044666319
Zfp641	ENSMUSG00000022987	0.50427645	0.002659852	0.044679969
Cdh24	ENSMUSG00000059674	0.510419877	0.002657408	0.044679969
Nenf	ENSMUSG00000037499	-0.402539598	0.002681947	0.044822952
Atp6v1g1	ENSMUSG00000039105	-0.394603335	0.002683554	0.044822952
Sorbs2	ENSMUSG00000031626	0.40934264	0.002677845	0.044822952
S100b	ENSMUSG00000033208	-0.423854335	0.002673753	0.044822952
Polq	ENSMUSG00000034206	0.904783202	0.002681943	0.044822952
Nat8f5	ENSMUSG00000079494	-1.569508068	0.002682705	0.044822952
Hadh	ENSMUSG00000027984	-0.400070031	0.002690921	0.044861356
Ammecr1	ENSMUSG00000042225	0.693808029	0.002688907	0.044861356
Rmnd1	ENSMUSG00000019763	0.455189612	0.002699208	0.044957167
Utp20	ENSMUSG00000004356	0.440782692	0.00270437	0.045000821
Col4a2	ENSMUSG00000031503	0.92852314	0.002710411	0.045035255
Csf2ra	ENSMUSG00000059326	0.639700501	0.002714791	0.045035255
Gm13204	ENSMUSG00000082860	1.426895911	0.002719158	0.045035255
Gm43488	ENSMUSG00000105063	1.957761327	0.002717793	0.045035255
Gm28119	ENSMUSG00000100158	1.831754344	0.002715463	0.045035255
Gm42549	ENSMUSG00000107320	1.309682864	0.002723982	0.045072988
Usp19	ENSMUSG00000006676	0.448156394	0.002730832	0.045144146
Ly6e	ENSMUSG00000022587	-0.319583053	0.002736745	0.045157572
Morc2a	ENSMUSG00000034543	0.391545769	0.002736519	0.045157572
Ift81	ENSMUSG00000029469	0.258504972	0.002741035	0.045186238
Zfp169	ENSMUSG00000050954	0.534429492	0.002749469	0.045246542
Asrgl1	ENSMUSG00000024654	-0.348502555	0.002749804	0.045246542
Mthfr	ENSMUSG00000029009	0.482064894	0.002755766	0.04526311

Pan2	ENSMUSG00000005682	0.586044076	0.002758303	0.04526311
Fzd10	ENSMUSG00000081683	-0.809795833	0.00275848	0.04526311
Rcor3	ENSMUSG00000037395	0.492642599	0.002761323	0.045267804
Apcdd1	ENSMUSG00000071847	-0.297004195	0.002775844	0.045463759
Iars	ENSMUSG00000037851	0.280320345	0.002795637	0.045465687
Gon4l	ENSMUSG00000054199	0.517860294	0.002794022	0.045465687
Gm48239	ENSMUSG00000114230	1.7721586	0.002796506	0.045465687
Ulk3	ENSMUSG00000032308	0.570985809	0.002786959	0.045465687
Proser1	ENSMUSG00000049504	0.447030401	0.002787593	0.045465687
Robo3	ENSMUSG00000032128	1.394182061	0.002790375	0.045465687
Gcnt2	ENSMUSG00000021360	-0.363513046	0.002780181	0.045465687
Ackr4	ENSMUSG00000079355	0.93822034	0.002793075	0.045465687
Dido1	ENSMUSG00000038914	0.427427816	0.002812085	0.045512372
Slc5a5	ENSMUSG00000000792	0.446223143	0.002809937	0.045512372
Gltp	ENSMUSG00000011884	-0.371386133	0.002802399	0.045512372
Phf1	ENSMUSG00000024193	0.304103438	0.002814801	0.045512372
Gm36995	ENSMUSG00000103436	1.418578226	0.002814126	0.045512372
Gm45591	ENSMUSG00000109460	1.3790303	0.002810731	0.045512372
Gatb	ENSMUSG00000028085	-0.332842177	0.002822101	0.045588778
Copz2	ENSMUSG00000018672	-0.60260979	0.002844193	0.045604452
Zfp287	ENSMUSG00000005267	0.332205666	0.00284133	0.045604452
Pcmtd1	ENSMUSG00000051285	0.245241072	0.002836078	0.045604452
Ptpn23	ENSMUSG00000036057	0.47349322	0.002839836	0.045604452
Rock1	ENSMUSG00000024290	0.387508771	0.00283616	0.045604452
38596	ENSMUSG00000072214	-0.381742595	0.002837953	0.045604452
Simc1	ENSMUSG00000043183	0.409119785	0.002829699	0.045604452
Anks6	ENSMUSG00000066191	0.586514958	0.002846254	0.045604452
Gm31763	ENSMUSG00000112925	0.973046627	0.002838241	0.045604452
Ksr2	ENSMUSG00000061578	0.497332843	0.002849751	0.045619212
Apoe	ENSMUSG00000002985	-0.411325841	0.002858625	0.045719919
Gm44168	ENSMUSG00000108049	1.368922595	0.002875998	0.045832176
Atxn1	ENSMUSG00000046876	0.293823574	0.00286874	0.045832176
Cyp4f14	ENSMUSG00000024292	-0.524545769	0.002875567	0.045832176
Car7	ENSMUSG00000031883	0.558310573	0.002874058	0.045832176
Ccdc82	ENSMUSG00000079084	0.494449633	0.002884467	0.045904471
Gm13111	ENSMUSG00000085069	-0.341182501	0.00288572	0.045904471

Gstm1	ENSMUSG00000058135	-0.426750945	0.002905365	0.045928114
Eef2k	ENSMUSG00000035064	0.384167669	0.002897948	0.045928114
Aqp4	ENSMUSG00000024411	-0.325525266	0.002901123	0.045928114
Clic4	ENSMUSG00000037242	-0.412023238	0.002903831	0.045928114
Chac2	ENSMUSG00000020309	-0.494566906	0.00289172	0.045928114
Adk	ENSMUSG00000039197	-0.35403378	0.002898314	0.045928114
Gm15494	ENSMUSG00000091177	1.315408447	0.002899212	0.045928114
Itfg1	ENSMUSG00000031703	-0.397246941	0.002908084	0.045930093
Sema5b	ENSMUSG00000052133	0.321016397	0.002920048	0.046045261
Fuca2	ENSMUSG00000019810	-0.311781049	0.002920578	0.046045261
Abat	ENSMUSG00000057880	-0.299648195	0.00292465	0.046068447
Dnmbp	ENSMUSG00000025195	0.456806478	0.002930016	0.046111947
Erich6	ENSMUSG00000070471	0.730655973	0.002942874	0.046273162
Ncstn	ENSMUSG00000003458	0.232564256	0.002946454	0.046288349
BC022960	ENSMUSG00000081137	0.852979124	0.002953057	0.046309902
Gm43413	ENSMUSG00000104951	1.544890695	0.002952792	0.046309902
Itgb1bp1	ENSMUSG00000062352	-0.364661843	0.002960385	0.046351965
Pcp4l1	ENSMUSG00000038370	-0.455973578	0.002960976	0.046351965
Tut4	ENSMUSG00000034610	0.386303464	0.00296924	0.046404027
Bbof1	ENSMUSG00000057265	0.810244762	0.002969543	0.046404027
Cdc42ep4	ENSMUSG00000041598	-0.36879695	0.0029734	0.046423323
S100a10	ENSMUSG00000041959	-0.421756115	0.002979379	0.046475687
S100a1	ENSMUSG00000044080	-0.407763277	0.00298568	0.046532986
Ylpm1	ENSMUSG00000021244	0.401592979	0.002990634	0.04656919
Cep295	ENSMUSG00000046111	0.430368844	0.003005823	0.046723525
Dysf	ENSMUSG00000033788	0.447035005	0.003004765	0.046723525
Gm42853	ENSMUSG00000107021	1.330140361	0.003012571	0.046787345
Krba1	ENSMUSG00000042810	0.570800884	0.003020633	0.046830395
Gm42527	ENSMUSG00000105592	1.666062747	0.003020386	0.046830395
Fam227a	ENSMUSG00000042564	0.742964019	0.00302372	0.046837245
Ndufb11	ENSMUSG00000031059	-0.455069819	0.003035013	0.046930045
Gpr83	ENSMUSG00000031932	-0.342389027	0.003034194	0.046930045
Pcnx3	ENSMUSG00000054874	0.470418647	0.003038932	0.046949645
Cfap54	ENSMUSG00000020014	0.630805446	0.003064817	0.047308267
Lsm11	ENSMUSG00000044847	0.361516591	0.003085248	0.047582153
Nrsn2	ENSMUSG00000059361	-0.568271233	0.003097607	0.047610199

Fndc8	ENSMUSG00000018844	1.007985444	0.003092684	0.047610199
Fchsd1	ENSMUSG00000038524	0.570472049	0.003097823	0.047610199
CT025671.1	ENSMUSG00000117220	1.029587947	0.003097301	0.047610199
Kcnk2	ENSMUSG00000037624	-0.436063517	0.003104411	0.04767008
Gm26811	ENSMUSG00000097816	1.765360722	0.003112652	0.047755196
Slc16a7	ENSMUSG00000020102	0.34066346	0.003116547	0.047773556
Gabra4	ENSMUSG00000029211	-0.358586468	0.003121682	0.047810882
Col11a1	ENSMUSG00000027966	1.215448412	0.003127652	0.04786092
Rom1	ENSMUSG00000071648	-0.549524142	0.003154402	0.048198639
Stat6	ENSMUSG00000002147	0.357644349	0.003155167	0.048198639
Lrp1	ENSMUSG00000040249	0.388638907	0.003165491	0.048314677
Gm43668	ENSMUSG00000105176	0.53254236	0.003174058	0.048403704
Zfp280c	ENSMUSG00000036916	0.51474921	0.003194096	0.04866736
Atp8b2	ENSMUSG00000060671	0.481887267	0.003205201	0.048716719
Lgals9	ENSMUSG00000001123	-0.486973353	0.00320559	0.048716719
AC110534.2	ENSMUSG00000116779	1.251727033	0.003200835	0.048716719
Ist1	ENSMUSG00000031729	0.397783774	0.003213307	0.048792103
Hba-a1	ENSMUSG00000069919	-1.063743912	0.003244532	0.049097804
Neurl3	ENSMUSG00000047180	-1.143371879	0.003242991	0.049097804
Scrib	ENSMUSG00000022568	0.404646155	0.003240632	0.049097804
Trpm3	ENSMUSG00000052387	0.572045272	0.003236521	0.049097804
Usf3	ENSMUSG00000068284	0.382704873	0.003250769	0.049125013
Isca1	ENSMUSG00000044792	-0.334516407	0.003258426	0.049125013
Zbtb7b	ENSMUSG00000028042	-0.345289	0.003262977	0.049125013
Fdps	ENSMUSG00000059743	0.940727747	0.003253321	0.049125013
Oxt	ENSMUSG00000027301	-1.817479068	0.003257537	0.049125013
Prok2	ENSMUSG00000030069	-1.213113817	0.00326025	0.049125013
Nhlrc3	ENSMUSG00000042997	0.327030904	0.003284818	0.049411805
Gm11611	ENSMUSG00000087042	1.239556619	0.003299163	0.049585471
Celf1	ENSMUSG00000005506	0.328550338	0.003320362	0.049861752

A2. Frontal brain DEGs

Gene ID	EnsemblID	log2FoldChange	p-value	q-value
Pank1	ENSMUSG00000033610	-1.110998262	2.98633E-20	4.51145E-16
Sbk2	ENSMUSG00000030433	-1.418144965	6.86392E-20	5.18466E-16
Hist1h2be	ENSMUSG00000047246	-1.57966715	1.16888E-19	5.88609E-16
Hist1h1e	ENSMUSG00000051627	-1.715776091	2.04022E-17	7.70541E-14
Gm47708	ENSMUSG00000112188	2.170821752	2.72302E-16	8.22734E-13
6330403L08Rik	ENSMUSG00000075585	-0.971533486	6.53666E-16	1.64582E-12
Fus	ENSMUSG00000030795	0.852839653	3.14177E-15	6.78038E-12
Gstm2	ENSMUSG00000040562	0.867975289	5.33877E-15	1.00244E-11
Myhas	ENSMUSG00000085348	0.765229003	5.97203E-15	1.00244E-11
Rps15a-ps7	ENSMUSG00000081087	-3.064115533	3.72048E-14	5.62053E-11
Tm6sf1	ENSMUSG00000038623	-1.283054978	4.82639E-13	6.62839E-10
Car3	ENSMUSG00000027559	0.969344537	1.75724E-12	2.21221E-09
Pbld2	ENSMUSG00000020072	1.997509044	2.98365E-12	3.46723E-09
Tmem116	ENSMUSG00000029452	1.689769208	9.96969E-12	1.0758E-08
Lrtm2	ENSMUSG00000055003	-1.567872001	2.43272E-11	2.45007E-08
Tmem37	ENSMUSG00000050777	-1.229459508	3.60742E-11	3.40608E-08
2310039H08Rik	ENSMUSG00000062619	0.76986858	4.51581E-11	4.01296E-08
Xlr3b	ENSMUSG00000073125	2.364309976	4.88595E-11	4.10067E-08
Nceh1	ENSMUSG00000027698	-0.878006859	1.79318E-10	1.35448E-07
Anxa11	ENSMUSG00000021866	-0.648185083	1.71361E-10	1.35448E-07
B230312C02Rik	ENSMUSG00000084843	1.474073053	2.55109E-10	1.83521E-07
Kif26b	ENSMUSG00000026494	-1.326165712	3.34038E-10	2.29378E-07
Trp53inp2	ENSMUSG00000038375	-0.575715488	6.53794E-10	4.29429E-07
P2rx6	ENSMUSG00000022758	0.87523574	2.62066E-09	1.6496E-06
Kcnq4	ENSMUSG00000028631	-0.818611931	3.02689E-09	1.82909E-06
Fbl	ENSMUSG00000046865	0.611483366	4.29104E-09	2.49326E-06
2010001A14Rik	ENSMUSG00000087165	1.725417095	6.15635E-09	3.44459E-06
Cntnap2	ENSMUSG00000039419	1.531260917	8.11763E-09	4.37975E-06
Pdlim7	ENSMUSG00000021493	0.647214154	1.07175E-08	5.5831E-06
Tfrc	ENSMUSG00000022797	-0.857247455	1.62201E-08	8.16788E-06
Slc30a2	ENSMUSG00000028836	-0.942167603	1.99217E-08	9.49133E-06
C1qtnf12	ENSMUSG00000023571	0.770977976	2.01048E-08	9.49133E-06
Ldlr	ENSMUSG00000032193	-1.387688805	2.86868E-08	1.31325E-05
B4galt1	ENSMUSG00000028413	-0.711504874	3.17442E-08	1.41047E-05

Npr1	ENSMUSG00000027931	0.735439578	3.9045E-08	1.63848E-05
Yjefn3	ENSMUSG00000048967	-1.032250317	3.81898E-08	1.63848E-05
Lgals4	ENSMUSG00000053964	-1.360452975	4.02378E-08	1.6429E-05
Pon2	ENSMUSG00000032667	-0.566263203	4.59726E-08	1.82765E-05
Fam57b	ENSMUSG00000058966	0.624111794	5.04953E-08	1.95598E-05
Zfp385b	ENSMUSG00000027016	-1.346751585	7.61492E-08	2.87597E-05
Knop1	ENSMUSG00000030980	-0.612228072	8.45316E-08	3.11468E-05
Ptpn3	ENSMUSG00000038764	-1.060420098	1.14959E-07	4.13496E-05
Hist2h3c2	ENSMUSG00000081058	-1.873020685	1.57625E-07	5.20119E-05
Emid1	ENSMUSG00000034164	0.81128907	1.56101E-07	5.20119E-05
Ahdc1	ENSMUSG00000037692	-0.615346935	1.58373E-07	5.20119E-05
Capn1	ENSMUSG00000024942	-0.372456059	1.52197E-07	5.20119E-05
Otog	ENSMUSG00000009487	-1.487256527	1.7992E-07	5.78309E-05
Ndn	ENSMUSG00000033585	0.765886831	2.00283E-07	6.30349E-05
Fam193b	ENSMUSG00000021495	0.69761137	2.14691E-07	6.61905E-05
Htra4	ENSMUSG00000037406	1.62613234	2.73962E-07	8.2775E-05
Best3	ENSMUSG00000020169	-0.828446495	3.03852E-07	9.00057E-05
Adam8	ENSMUSG00000025473	-3.202957618	3.20441E-07	9.30944E-05
Hspa4l	ENSMUSG00000025757	-0.884194575	5.11264E-07	0.00014573
Xlr3a	ENSMUSG00000057836	2.088482566	6.14208E-07	0.00017183
Rhou	ENSMUSG00000039960	-1.211170297	6.33714E-07	0.000174064
Hist1h1c	ENSMUSG00000036181	-0.621250458	7.0753E-07	0.000190869
38231	ENSMUSG00000020486	0.542594384	7.44243E-07	0.000197251
Skil	ENSMUSG00000027660	-0.629505526	7.96077E-07	0.000207351
Nsun4	ENSMUSG00000028706	-0.482483642	8.80209E-07	0.000214473
Amotl1	ENSMUSG00000013076	-0.565140849	8.44402E-07	0.000214473
Slc38a2	ENSMUSG00000022462	-0.501569339	8.61797E-07	0.000214473
Irx3os	ENSMUSG00000046413	-0.975089756	8.72872E-07	0.000214473
Napb	ENSMUSG00000027438	0.799796066	9.34219E-07	0.00022402
Rap1gds1	ENSMUSG00000028149	-0.594230897	1.01984E-06	0.000233435
1600020E01Rik	ENSMUSG00000097048	-1.006255777	1.01835E-06	0.000233435
Xlr4a	ENSMUSG00000079845	4.395380535	9.94317E-07	0.000233435
Parp3	ENSMUSG00000023249	-0.582224765	1.03731E-06	0.000233891
Ecm2	ENSMUSG00000043631	0.607055629	1.15704E-06	0.000257051
Sema4d	ENSMUSG00000021451	-0.468475874	1.24126E-06	0.000271765
Kcnq5	ENSMUSG00000028033	-1.20503472	1.26296E-06	0.000272565

Myh7	ENSMUSG00000053093	3.658698085	1.40008E-06	0.000297902
Nacc2	ENSMUSG00000026932	-0.464810423	1.64162E-06	0.000339725
BC049352	ENSMUSG00000091996	1.819287492	1.6352E-06	0.000339725
Trip6	ENSMUSG00000023348	0.6553295	1.85516E-06	0.000378729
Tmem82	ENSMUSG00000043085	-2.59139869	1.89587E-06	0.000381879
Osbpl1a	ENSMUSG00000044252	-0.580242164	2.16032E-06	0.00042942
Ccny	ENSMUSG00000024286	-0.383310742	2.22193E-06	0.000434121
Pbld1	ENSMUSG00000112129	1.53479274	2.24144E-06	0.000434121
Parvb	ENSMUSG00000022438	-0.450075266	2.43081E-06	0.000464838
Nt5dc3	ENSMUSG00000054027	-0.532848907	2.5757E-06	0.000486389
A930016O22Rik	ENSMUSG00000040705	1.027326959	2.79244E-06	0.000520808
Tead1	ENSMUSG00000055320	-0.464931013	2.96998E-06	0.000547164
Aldh1a7	ENSMUSG00000024747	1.690509136	3.17259E-06	0.000577449
Bola1	ENSMUSG00000015943	0.470382976	3.36143E-06	0.000604537
Mars2	ENSMUSG00000046994	-0.635200306	3.43148E-06	0.000609875
Klk1b26	ENSMUSG00000053719	-4.785062103	3.76448E-06	0.000661278
Gramd1b	ENSMUSG00000040111	-0.708068975	3.97152E-06	0.000683049
Slc25a16	ENSMUSG00000071253	-0.518622727	3.97884E-06	0.000683049
Flywch2	ENSMUSG00000023911	1.571226837	4.02812E-06	0.00068374
AW549877	ENSMUSG00000041935	0.561289771	4.19169E-06	0.000695866
Abcd1	ENSMUSG00000031378	-0.533022189	4.18681E-06	0.000695866
Thbs4	ENSMUSG00000021702	-1.133354198	5.0704E-06	0.000832593
Igdcc4	ENSMUSG00000032816	-0.746232928	5.14775E-06	0.000836206
Apol10b	ENSMUSG00000050014	1.269864739	6.3096E-06	0.001014034
Fitm2	ENSMUSG00000048486	-0.472168891	6.43852E-06	0.00102386
Ankrd33b	ENSMUSG00000022237	-0.590559111	6.7285E-06	0.001058828
Rnf130	ENSMUSG00000020376	0.414240934	6.8327E-06	0.00106414
Gpd1l	ENSMUSG00000050627	-0.441387069	7.11366E-06	0.001096592
Gdap1	ENSMUSG00000025777	-1.196639492	7.27188E-06	0.001109659
Adamtsl5	ENSMUSG00000043822	-0.555420368	7.52337E-06	0.001136555
Pptc7	ENSMUSG00000038582	-0.694859107	8.16816E-06	0.001221747
Trmu	ENSMUSG00000022386	-0.569163178	8.31234E-06	0.001231122
Hccs	ENSMUSG00000031352	-0.475268026	9.06399E-06	0.001329414
Stard7	ENSMUSG00000027367	-0.383295299	9.20383E-06	0.001336944
Mapk8ip1	ENSMUSG00000027223	0.817123432	9.63919E-06	0.001347494
Neo1	ENSMUSG00000032340	-0.440443476	9.72244E-06	0.001347494

Actr3b	ENSMUSG00000056367	-1.202664361	9.47133E-06	0.001347494
Plbd1	ENSMUSG00000030214	-1.249870784	9.64002E-06	0.001347494
Asb15	ENSMUSG00000029685	-0.699618698	9.60563E-06	0.001347494
Park7	ENSMUSG00000028964	0.305592348	1.26044E-05	0.001715449
C3ar1	ENSMUSG00000040552	-3.491815701	1.25859E-05	0.001715449
Gprc5b	ENSMUSG00000008734	-0.782470839	1.2833E-05	0.00172382
Fscn2	ENSMUSG00000025380	-1.539650251	1.28941E-05	0.00172382
Tmem232	ENSMUSG00000045036	0.983103493	1.30376E-05	0.001727708
Hist1h1d	ENSMUSG00000052565	-2.16053227	1.35939E-05	0.001785768
Gm47863	ENSMUSG00000113165	-1.193289628	1.38422E-05	0.001802712
Gm42047	ENSMUSG00000110631	1.428161678	1.43848E-05	0.001857367
Taco1	ENSMUSG00000001983	-0.740462512	1.5102E-05	0.001929617
Gm11752	ENSMUSG00000087404	1.775520017	1.51999E-05	0.001929617
Pik3cd	ENSMUSG00000039936	0.650162323	1.63717E-05	0.002021017
Otub2	ENSMUSG00000021203	0.921936591	1.61257E-05	0.002021017
Slc17a7	ENSMUSG00000070570	1.778048282	1.6455E-05	0.002021017
Pitx3	ENSMUSG00000025229	-1.00238683	1.64292E-05	0.002021017
Lingo3	ENSMUSG00000051067	-0.8076005	1.66919E-05	0.002033589
Zfp629	ENSMUSG00000045639	-0.51045283	1.77928E-05	0.002150368
Exoc7	ENSMUSG00000020792	0.524447325	1.82156E-05	0.002183992
Zfp97	ENSMUSG00000095990	-1.016115745	1.97212E-05	0.00234589
Pja2	ENSMUSG00000024083	-0.401081819	1.99534E-05	0.002354968
Mybpc2	ENSMUSG00000038670	0.429985644	2.07406E-05	0.002428898
Ccdc82	ENSMUSG00000079084	0.57945339	2.09127E-05	0.002430221
Naprt	ENSMUSG00000022574	0.823365297	2.23665E-05	0.002579324
Arl3	ENSMUSG00000025035	0.380879223	2.27419E-05	0.002602745
Stom	ENSMUSG00000026880	-0.67528598	2.294E-05	0.002605457
Tpm1	ENSMUSG00000032366	0.419226835	2.31106E-05	0.002605457
Rcan2	ENSMUSG00000039601	-0.707051436	2.34212E-05	0.002620924
Diaph1	ENSMUSG00000024456	-0.767109127	2.39993E-05	0.002665867
5830454E08Rik	ENSMUSG00000052658	1.186229373	2.43683E-05	0.002687096
Abra	ENSMUSG00000042895	0.450793993	2.48423E-05	0.002719511
Thpo	ENSMUSG00000022847	-0.745184892	2.5136E-05	0.002731863
Mindy2	ENSMUSG00000042444	-0.405391488	2.62611E-05	0.002813659
Bcl2l13	ENSMUSG00000009112	-0.44050767	2.609E-05	0.002813659
Cdc37l1	ENSMUSG00000024780	-0.289478943	2.67325E-05	0.002844

Trmt2b	ENSMUSG00000067369	-0.493617873	2.73649E-05	0.002890915
Sin3b	ENSMUSG00000031622	0.372059858	2.86814E-05	0.003008962
Npnt	ENSMUSG00000040998	-1.410889408	2.91852E-05	0.003040694
Wipi1	ENSMUSG00000041895	-0.416689576	2.96955E-05	0.003059112
Ldb1	ENSMUSG00000025223	0.376800352	2.9767E-05	0.003059112
Slc11a2	ENSMUSG00000023030	-0.497977217	3.07577E-05	0.003139574
Fnbp1l	ENSMUSG00000039735	0.656300321	3.17133E-05	0.003209755
Ifi203-ps	ENSMUSG00000090222	0.733217821	3.18702E-05	0.003209755
Irx3	ENSMUSG00000031734	-0.89145674	3.34494E-05	0.003346494
Clip4	ENSMUSG00000024059	-0.605909118	3.47977E-05	0.003458483
Hsdl2	ENSMUSG00000028383	-0.750669136	3.58978E-05	0.003498762
Cd24a	ENSMUSG00000047139	-0.877583499	3.57215E-05	0.003498762
Adam33	ENSMUSG00000027318	0.720401987	3.54527E-05	0.003498762
Cc2d1b	ENSMUSG00000028582	0.418650236	3.71401E-05	0.003572083
Ano5	ENSMUSG00000055489	-0.540306328	3.73594E-05	0.003572083
Ces2c	ENSMUSG00000061825	-2.7905041	3.69229E-05	0.003572083
Trim16	ENSMUSG00000047821	-0.472783291	3.76802E-05	0.003580097
Fbxl17	ENSMUSG00000023965	-0.4826481	3.79187E-05	0.003580236
Sema5b	ENSMUSG00000052133	1.639606632	3.96884E-05	0.003716033
Lrrn1	ENSMUSG00000034648	-1.543621903	3.98489E-05	0.003716033
Fam160a1	ENSMUSG00000051000	-0.468528699	4.24108E-05	0.003930672
Cstad	ENSMUSG00000047363	1.542656357	4.52871E-05	0.0041214
Vwa7	ENSMUSG00000007030	0.504793384	4.52869E-05	0.0041214
Tnfrsf25	ENSMUSG00000024793	-2.125319753	4.50644E-05	0.0041214
Sipa1	ENSMUSG00000056917	0.481409026	4.89679E-05	0.004429692
Dag1	ENSMUSG00000039952	-0.35600536	5.35206E-05	0.004812711
Palld	ENSMUSG00000058056	-0.459347589	5.55492E-05	0.004965573
Tmie	ENSMUSG00000049555	-1.785281519	5.61203E-05	0.004987114
Synj2	ENSMUSG00000023805	-0.647485441	5.90948E-05	0.005160375
Masp1	ENSMUSG00000022887	-0.729779244	5.86676E-05	0.005160375
Fam19a3	ENSMUSG00000055865	-0.686190731	5.90266E-05	0.005160375
Ccl25	ENSMUSG00000023235	0.744743892	5.98209E-05	0.005164086
Asb18	ENSMUSG00000067081	-0.684152446	5.97869E-05	0.005164086
Sbk1	ENSMUSG00000042978	-0.461949133	6.42687E-05	0.005485348
Fads6	ENSMUSG00000044788	-0.649798371	6.39645E-05	0.005485348
Xlr4b	ENSMUSG00000067768	3.529117843	6.68815E-05	0.005644575

Tek	ENSMUSG00000006386	0.515532551	6.67139E-05	0.005644575
Gzmm	ENSMUSG00000054206	-0.972528833	6.74952E-05	0.005664725
Lipo3	ENSMUSG00000024766	0.602537667	7.01446E-05	0.005854553
Phyhd1	ENSMUSG00000079484	-1.879502393	7.25347E-05	0.006020778
Sncaip	ENSMUSG00000024534	0.860620955	7.58632E-05	0.006228617
Inppl1	ENSMUSG00000032737	-0.298858023	7.55443E-05	0.006228617
Cluh	ENSMUSG00000020741	-0.420817104	7.67992E-05	0.006271379
Irgq	ENSMUSG00000041037	-0.503862512	7.84336E-05	0.00637041
Dlat	ENSMUSG00000000168	-0.459881053	7.92795E-05	0.006404682
Sh3tc2	ENSMUSG00000045629	0.706936964	8.06696E-05	0.006482317
Dusp22	ENSMUSG00000069255	-0.405272867	8.43609E-05	0.006743067
Gm20632	ENSMUSG00000093577	-1.65842845	8.51309E-05	0.006768802
Cdh4	ENSMUSG00000000305	1.483320704	8.62159E-05	0.006819178
Stim1	ENSMUSG00000030987	-0.442995002	8.77591E-05	0.006869311
Snora34	ENSMUSG00000065336	2.506834941	8.7411E-05	0.006869311
Efr3a	ENSMUSG00000015002	-0.375569778	8.91413E-05	0.006941536
Tbc1d17	ENSMUSG00000038520	0.47266036	9.19753E-05	0.007056609
Slc20a2	ENSMUSG00000037656	-0.408572908	9.20204E-05	0.007056609
Acsl4	ENSMUSG00000031278	-0.526763752	9.10989E-05	0.007056609
Cox15	ENSMUSG00000040018	-0.406316494	9.53197E-05	0.007236152
Tbx15	ENSMUSG00000027868	-0.356384245	9.48733E-05	0.007236152
B3gnt3	ENSMUSG00000031803	0.61742367	9.73176E-05	0.007350882
Bphl	ENSMUSG00000038286	0.359389388	9.92986E-05	0.007463204
Coq5	ENSMUSG00000041733	-0.411407713	0.000101422	0.007585025
Trim35	ENSMUSG00000022043	-0.641579686	0.000102281	0.007611594
Atxn2l	ENSMUSG00000032637	0.425991024	0.000105395	0.007766821
Ip6k2	ENSMUSG00000032599	0.530199575	0.000105136	0.007766821
Ccdc191	ENSMUSG00000022701	0.762394488	0.000110214	0.00800446
Tmem135	ENSMUSG00000039428	-0.413450864	0.000109648	0.00800446
Pla2g4e	ENSMUSG00000050211	-0.507212375	0.000110739	0.00800446
Tnfaip2	ENSMUSG00000021281	-0.771168755	0.00011063	0.00800446
4430402I18Rik	ENSMUSG00000064202	1.430557253	0.000111519	0.008022468
Nipsnap2	ENSMUSG00000029432	-0.367153276	0.000113004	0.008090769
Kif13b	ENSMUSG00000060012	0.393563425	0.000113593	0.008094537
Hexim1	ENSMUSG00000048878	-0.413387689	0.000117115	0.008306334
Zfp677	ENSMUSG00000062743	1.097249589	0.000119828	0.008448696

Hoxb4	ENSMUSG00000038692	0.884347497	0.00012024	0.008448696
Ccdc84	ENSMUSG00000043923	0.708802531	0.000121074	0.008467894
Ucp3	ENSMUSG00000032942	-0.788320009	0.000123751	0.008486877
Ppargc1a	ENSMUSG00000029167	-0.907628643	0.000124154	0.008486877
Mgmt	ENSMUSG00000054612	0.789365046	0.000123124	0.008486877
Impdh2	ENSMUSG00000062867	0.361058387	0.000123715	0.008486877
Adig	ENSMUSG00000044405	-1.671781921	0.000123482	0.008486877
Hspb11	ENSMUSG00000063172	0.976941844	0.000125992	0.008573691
Colgalt2	ENSMUSG00000032649	0.661080502	0.000126867	0.008594519
Ccdc162	ENSMUSG00000075225	-1.36507298	0.000131295	0.008854763
Acyp1	ENSMUSG00000008822	0.724005401	0.000132105	0.008869829
Abcb1b	ENSMUSG00000028970	0.516761333	0.000134643	0.008993291
Gm45512	ENSMUSG00000110071	-2.378819806	0.000135135	0.008993291
Col20a1	ENSMUSG00000016356	1.023021114	0.000137055	0.009081107
Pdss2	ENSMUSG00000038240	-0.393808338	0.000138513	0.009137623
Odf2l	ENSMUSG00000028256	0.53810272	0.000139691	0.009175237
Lman2	ENSMUSG00000021484	-0.363949397	0.000140756	0.009205226
BB123696	ENSMUSG00000113737	-2.281769799	0.000142887	0.009304266
Tle2	ENSMUSG00000034771	0.7083045	0.000146639	0.009374373
Armcx4	ENSMUSG00000049804	-0.726269882	0.000148204	0.009374373
Gm8407	ENSMUSG00000103964	-1.622561401	0.000148203	0.009374373
Cx3cl1	ENSMUSG00000031778	-1.191200022	0.000145499	0.009374373
Prkcd	ENSMUSG00000021948	-0.725858594	0.000147944	0.009374373
Hrh2	ENSMUSG00000034987	-2.037591548	0.000148307	0.009374373
Zbtb7a	ENSMUSG00000035011	-0.316078433	0.000148005	0.009374373
Myh1	ENSMUSG00000056328	-0.656804464	0.000149335	0.009400043
Tmem246	ENSMUSG00000039611	-0.416036224	0.000154301	0.009672285
Dapp1	ENSMUSG00000028159	-1.29154579	0.000164037	0.010197973
Cadm3	ENSMUSG00000005338	0.774228263	0.000163439	0.010197973
Slc9a2	ENSMUSG00000026062	-0.479173636	0.000165267	0.010232315
Slc25a23	ENSMUSG00000046329	0.486787568	0.000165987	0.010234974
Fam173a	ENSMUSG00000057411	0.334676749	0.000167629	0.010294213
Lpgat1	ENSMUSG00000026623	-0.390833979	0.000178981	0.010946847
Gm45769	ENSMUSG00000107838	0.612655541	0.000181443	0.011052681
Relt	ENSMUSG00000008318	-0.540512042	0.000182775	0.011089062
Nkain1	ENSMUSG00000078532	-0.723473599	0.000185482	0.011208327

Emb	ENSMUSG00000021728	-2.679971151	0.000186515	0.011225807
Plcl1	ENSMUSG00000038349	-0.623608096	0.000187716	0.011253273
Ephb6	ENSMUSG00000029869	1.297649874	0.000189428	0.011266508
Ripor2	ENSMUSG00000036006	-1.159775735	0.000189128	0.011266508
2310039L15Rik	ENSMUSG00000100550	-1.685447249	0.000190247	0.011270843
Msi2	ENSMUSG00000069769	-0.395518696	0.000191539	0.011303061
Mill2	ENSMUSG00000040987	0.616340938	0.000193571	0.011371586
Wnt5b	ENSMUSG00000030170	-1.056834847	0.000194206	0.011371586
Tppp3	ENSMUSG00000014846	0.533592144	0.000196313	0.011450562
Malat1	ENSMUSG00000092341	-0.362417814	0.000198178	0.011514906
Rnaseh2c	ENSMUSG00000024925	0.458796299	0.000207381	0.012003439
Mpeg1	ENSMUSG00000046805	-3.62752432	0.00021103	0.012086982
Mrpl45	ENSMUSG00000018882	-0.342238861	0.000210077	0.012086982
AB124611	ENSMUSG00000057191	-3.02519222	0.000211224	0.012086982
Osbpl11	ENSMUSG00000022807	-0.377158466	0.000213387	0.012164689
Gja5	ENSMUSG00000057123	0.649987745	0.000214747	0.012196204
Gpr146	ENSMUSG00000044197	-0.447392398	0.000219156	0.01228875
D730003I15Rik	ENSMUSG00000073478	1.034677059	0.000219939	0.01228875
Txnrd2	ENSMUSG00000075704	0.429085437	0.000220444	0.01228875
Prrg1	ENSMUSG00000047996	0.890634673	0.000218327	0.01228875
BC048679	ENSMUSG00000061877	-1.458139533	0.000219168	0.01228875
Psmd4	ENSMUSG00000005625	0.335917996	0.000222369	0.012334749
Ush1g	ENSMUSG00000045288	-2.290925262	0.000222902	0.012334749
Nxn	ENSMUSG00000020844	-0.404690116	0.00022588	0.012453927
Tle1	ENSMUSG00000008305	0.519316866	0.000227679	0.01250742
Gm1840	ENSMUSG00000043192	0.394853314	0.000231061	0.012622699
Dusp4	ENSMUSG00000031530	-1.005016945	0.000231448	0.012622699
1110019D14Rik	ENSMUSG00000097616	-0.99373176	0.00023426	0.012730115
Amhr2	ENSMUSG00000023047	-0.653843646	0.000237001	0.012832871
Phyh	ENSMUSG00000026664	-0.4017927	0.000241986	0.013055983
Ntn4	ENSMUSG00000020019	-0.695909591	0.000243253	0.013077659
P4ha1	ENSMUSG00000019916	-0.375495187	0.000247599	0.013249282
Khk	ENSMUSG00000029162	0.436813393	0.000248199	0.013249282
Azin1	ENSMUSG00000037458	-0.753676766	0.000249801	0.013287841
Zdhhc23	ENSMUSG00000036304	-0.726808588	0.000258642	0.013709849
Dis3	ENSMUSG00000033166	0.443217236	0.000260837	0.013777858

Selplg	ENSMUSG00000048163	-2.754619992	0.000265089	0.013953681
Acot4	ENSMUSG00000052392	-2.243746689	0.000266732	0.013991374
Leng8	ENSMUSG00000035545	0.33658659	0.000269065	0.014064942
Tmem159	ENSMUSG00000030917	0.536021052	0.000270203	0.014075701
Gm11613	ENSMUSG00000085586	0.716126614	0.000272571	0.014150295
Nme1	ENSMUSG00000037601	-0.478977172	0.000274826	0.014185949
Gabbr1	ENSMUSG00000024462	0.441275351	0.000275136	0.014185949
Scd1	ENSMUSG00000037071	-1.234351181	0.000289921	0.014897392
Hsp90aa1	ENSMUSG00000021270	-0.570671396	0.000294488	0.015080763
Rtp3	ENSMUSG00000066319	1.261314458	0.000299832	0.015302567
Thbs1	ENSMUSG00000040152	-0.932536738	0.000301465	0.015334137
Zfand2a	ENSMUSG00000053581	-0.488230891	0.000306832	0.015554716
D530033B14Rik	ENSMUSG00000108332	-1.228670928	0.000308297	0.015576717
Plekha2	ENSMUSG00000031557	-0.654044051	0.000316169	0.015868332
Metap1	ENSMUSG00000005813	-0.359548788	0.000315191	0.015868332
Acsl1	ENSMUSG00000018796	-0.721375461	0.000322462	0.016077321
Hp	ENSMUSG00000031722	-2.982098863	0.000322422	0.016077321
Sgpp1	ENSMUSG00000021054	-0.438103248	0.00032698	0.016248948
Nos1	ENSMUSG00000029361	-0.637890911	0.000332542	0.016465305
Zdhhc4	ENSMUSG00000001844	0.396312703	0.000334603	0.016465305
Tbc1d4	ENSMUSG00000033083	-0.608194194	0.00033435	0.016465305
Pik3r1	ENSMUSG00000041417	-0.426033412	0.00033603	0.016481849
39692	ENSMUSG00000018398	0.350163736	0.000339312	0.016588965
Dgcr6	ENSMUSG00000003531	0.298770918	0.000353397	0.01722181
2810004N23Rik	ENSMUSG00000031984	-0.448490154	0.000356829	0.01733319
Arhgap1	ENSMUSG00000027247	0.477590616	0.000358445	0.017355884
Tmem8b	ENSMUSG00000078716	-0.546157245	0.000360228	0.017386471
Lrpprc	ENSMUSG00000024120	-0.437370867	0.000367876	0.01769904
Matk	ENSMUSG00000004933	-1.761169845	0.000372959	0.017886653
Kazald1	ENSMUSG00000025213	0.610266314	0.000380149	0.018025749
Wfs1	ENSMUSG00000039474	-0.720551818	0.000380632	0.018025749
Pdk4	ENSMUSG00000019577	-0.686094875	0.00037927	0.018025749
2310014F06Rik	ENSMUSG00000085945	-0.981672091	0.000377719	0.018025749
Itfg1	ENSMUSG00000031703	-0.411710306	0.000382894	0.018053327
Irak1bp1	ENSMUSG00000032251	0.643162829	0.000383605	0.018053327
H2-T22	ENSMUSG00000056116	0.537650257	0.000391138	0.018350708

Zyg11b	ENSMUSG00000034636	-0.369011362	0.000393688	0.018356321
Gadl1	ENSMUSG00000056880	-0.629876625	0.000392608	0.018356321
Pdp2	ENSMUSG00000048371	-0.821243338	0.000401949	0.018683824
1110051M20Rik	ENSMUSG00000040591	0.419536938	0.000404121	0.018727172
Lynx1	ENSMUSG00000022594	-0.40429852	0.000406083	0.018760553
Mrpl19	ENSMUSG00000030045	-0.417833049	0.000407531	0.018770031
Nqo1	ENSMUSG00000003849	0.681397973	0.000417311	0.019162051
Kcnc1	ENSMUSG00000058975	-0.475005269	0.000427338	0.019503935
Esrrg	ENSMUSG00000026610	-0.791800607	0.000426816	0.019503935
Ift172	ENSMUSG00000038564	0.427505358	0.000430907	0.019607564
Ostn	ENSMUSG00000052276	0.970384885	0.000432737	0.0196317
Plec	ENSMUSG00000022565	-0.501238596	0.000436829	0.019758025
Usp15	ENSMUSG00000020124	-0.373984449	0.000442022	0.019933199
Ncoa1	ENSMUSG00000020647	-0.430770716	0.000446452	0.02007307
Gtf3a	ENSMUSG00000016503	0.462780993	0.000456839	0.020479119
Kbtbd13	ENSMUSG00000054978	-0.42168685	0.000460623	0.020587681
Hist1h2bc	ENSMUSG00000018102	-0.426233561	0.000462474	0.020609419
Mir133a-1hg	ENSMUSG00000095438	0.586267666	0.000468083	0.020798033
Afg1l	ENSMUSG00000038302	-0.58207832	0.000469521	0.020798696
Vegfa	ENSMUSG00000023951	-0.391011233	0.000470852	0.020798696
Rft1	ENSMUSG00000052395	-0.529759443	0.000482609	0.021194132
Gm40634	ENSMUSG00000111377	-1.437166728	0.000481311	0.021194132
Trmt112	ENSMUSG00000038812	0.368139105	0.000486834	0.021317681
Vtn	ENSMUSG00000017344	0.534157449	0.000493762	0.021558561
Sgf29	ENSMUSG00000030714	0.423319716	0.000498956	0.021722562
Filip1	ENSMUSG00000034898	-0.564035536	0.000503435	0.02180653
Katnal2	ENSMUSG00000025420	-2.062113079	0.000503881	0.02180653
H2afj	ENSMUSG00000060032	0.682093029	0.000505215	0.02180653
Ypel3	ENSMUSG00000042675	0.36105853	0.000507561	0.021808634
Bmp8a	ENSMUSG00000032726	-2.109100335	0.000508151	0.021808634
Fcgrt	ENSMUSG00000003420	0.344096874	0.000527276	0.02256533
Acot6	ENSMUSG00000043487	-0.805651687	0.000533275	0.022757596
Gm32219	ENSMUSG00000113302	0.755281474	0.000550911	0.023443974
E2f3	ENSMUSG00000016477	-0.341925563	0.00055318	0.023474426
Tgfb3	ENSMUSG00000021253	-0.309423867	0.000554954	0.023483744
Il16	ENSMUSG00000001741	0.759457133	0.000559386	0.023605169

Tmem136	ENSMUSG00000048503	-0.760472624	0.000562632	0.023610218
Trpt1	ENSMUSG00000047656	0.337679438	0.000561215	0.023610218
Slco5a1	ENSMUSG00000025938	-0.359445297	0.000566035	0.023621805
Shisa2	ENSMUSG00000044461	-0.441160622	0.000565578	0.023621805
Mag	ENSMUSG00000036634	1.552083373	0.000575674	0.023849711
Srebf1	ENSMUSG00000020538	-0.445306334	0.000576233	0.023849711
Ccr2	ENSMUSG00000049103	-1.992647586	0.000574776	0.023849711
Flna	ENSMUSG00000031328	0.393850064	0.000583075	0.024066985
Sh3pxd2a	ENSMUSG00000053617	-0.324240828	0.000589443	0.024263545
Bcap29	ENSMUSG00000020650	0.428773557	0.000596171	0.024341487
Gpc1	ENSMUSG00000034220	-0.288988831	0.000594454	0.024341487
Gm826	ENSMUSG00000074623	-1.359879547	0.000596079	0.024341487
Slc43a2	ENSMUSG00000038178	-0.543551117	0.000600218	0.024440696
Camk1	ENSMUSG00000030272	0.317733496	0.000606268	0.02462069
Abca8b	ENSMUSG00000020620	0.322652292	0.00061859	0.025053713
Cers4	ENSMUSG00000008206	0.600937053	0.000621044	0.025085872
5730419F03Rik	ENSMUSG00000099364	-3.30653493	0.000623537	0.025119386
Obsl1	ENSMUSG00000026211	-0.44164849	0.000629351	0.025211797
4632428C04Rik	ENSMUSG00000097184	-0.734506759	0.000630837	0.025211797
Hmgb3	ENSMUSG00000015217	-0.995872971	0.000627942	0.025211797
Meox2	ENSMUSG00000036144	0.533804208	0.000646961	0.025787975
Rpl7a	ENSMUSG00000062647	0.249940032	0.00065307	0.02588383
Gm15860	ENSMUSG00000087336	1.393731022	0.000654506	0.02588383
Ushbp1	ENSMUSG00000034911	0.496261953	0.000653659	0.02588383
9430015G10Rik	ENSMUSG00000059939	0.603735144	0.000661745	0.026101773
Gimap1	ENSMUSG00000090019	0.693525917	0.000678492	0.026692667
Ufsp1	ENSMUSG00000051502	-0.553808778	0.000706611	0.027726692
Itga1	ENSMUSG00000042284	0.456857895	0.000708962	0.027746852
Xpot	ENSMUSG00000034667	-0.386413992	0.000712856	0.027755443
Lhb	ENSMUSG00000100916	-1.721447817	0.00071237	0.027755443
Aldh1a1	ENSMUSG00000053279	-0.365413905	0.000723453	0.028086457
Abtb2	ENSMUSG00000032724	-0.556754676	0.000725076	0.028086457
Cntfr	ENSMUSG00000028444	-0.830112376	0.000733263	0.02833096
Epb41l2	ENSMUSG00000019978	0.378133595	0.000743843	0.028666407
Cryl1	ENSMUSG00000021947	0.701925136	0.000758836	0.029169809
Cd99l2	ENSMUSG00000035776	-0.297401643	0.000762663	0.029178867

Cidec	ENSMUSG00000030278	-2.32207507	0.000762935	0.029178867
Gstm1	ENSMUSG00000058135	0.527200938	0.000767154	0.029266164
Gm11839	ENSMUSG00000083246	1.508254204	0.000769829	0.029294225
Pik3ap1	ENSMUSG00000025017	-3.419841471	0.000778174	0.02953736
Aga	ENSMUSG00000031521	0.360860327	0.000783731	0.029599753
Tmem53	ENSMUSG00000048772	0.739781559	0.000783736	0.029599753
Rreb1	ENSMUSG00000039087	-0.340914884	0.000791788	0.029829262
Tox4	ENSMUSG00000016831	-0.350325834	0.000796047	0.029915137
Ptprq	ENSMUSG00000035916	1.23163069	0.00080298	0.030100786
Lmo7	ENSMUSG00000033060	-0.421729967	0.000805586	0.030123746
Eml6	ENSMUSG00000044072	0.737649474	0.000808705	0.030165704
Riox2	ENSMUSG00000022724	-0.420301224	0.000811628	0.030200167
Atp13a5	ENSMUSG00000048939	-0.703728544	0.000820832	0.030432039
Cidea	ENSMUSG00000024526	-1.594092636	0.000821889	0.030432039
Rtca	ENSMUSG00000000339	0.36685521	0.000835936	0.030577442
Alas1	ENSMUSG00000032786	-0.411684952	0.000833176	0.030577442
Mrps9	ENSMUSG00000060679	-0.413692786	0.000828662	0.030577442
Tmem25	ENSMUSG00000002032	-0.511471616	0.000835438	0.030577442
Cbr2	ENSMUSG00000025150	-0.606367911	0.000835702	0.030577442
Tmem154	ENSMUSG00000056498	0.991134368	0.000840727	0.030678395
Slc38a10	ENSMUSG00000061306	-0.543153857	0.000845955	0.030723448
Npepps	ENSMUSG00000001441	-0.370848991	0.000846029	0.030723448
Ctss	ENSMUSG00000038642	-3.616992652	0.000852542	0.030885735
Sspn	ENSMUSG00000030255	-0.423393712	0.00085465	0.030888048
Ppip5k1	ENSMUSG00000033526	-0.558228375	0.000861539	0.031040342
Mapt	ENSMUSG00000018411	-0.562261127	0.000862974	0.031040342
Slc28a2	ENSMUSG00000027219	0.63203163	0.00087008	0.031221629
Gramd3	ENSMUSG00000001700	-0.505287175	0.000874235	0.031296382
Tmem65	ENSMUSG00000062373	-0.559307345	0.000883108	0.031539282
Hmcn2	ENSMUSG00000055632	0.435045401	0.000888757	0.03166616
Hdac8	ENSMUSG00000067567	0.609931985	0.000894821	0.031807186
Kank2	ENSMUSG00000032194	-0.362653465	0.000898789	0.031873249
mt-Te	ENSMUSG00000064369	-0.85881664	0.000909571	0.032104893
Fbf1	ENSMUSG00000020776	0.348066539	0.000908292	0.032104893
Npc1l1	ENSMUSG00000020447	1.084105183	0.000917239	0.032224963
Nufip2	ENSMUSG00000037857	-0.433600211	0.000917205	0.032224963

Rab39	ENSMUSG00000055069	1.491801976	0.000922623	0.032338888
Trem2	ENSMUSG00000023992	-3.372907896	0.000926534	0.032400798
Rfx2	ENSMUSG00000024206	0.751521514	0.000940207	0.032803021
Car1	ENSMUSG00000027556	1.970207078	0.000946581	0.032949316
St13	ENSMUSG00000022403	-0.320682293	0.000958706	0.033294643
P2ry6	ENSMUSG00000048779	-1.109254716	0.000961027	0.033298705
Foxk1	ENSMUSG00000056493	-0.328799678	0.000970937	0.033565087
Eif3h	ENSMUSG00000022312	0.215853276	0.000977305	0.03370809
mt-Ts2	ENSMUSG00000064365	-0.840817276	0.000985954	0.033928947
Cd2ap	ENSMUSG00000061665	0.415445582	0.001003154	0.03436428
Msln	ENSMUSG00000063011	-3.274250116	0.00100248	0.03436428
Ermp1	ENSMUSG00000046324	-0.417793827	0.001010041	0.034443992
Gm10390	ENSMUSG00000097368	-0.661833961	0.00100826	0.034443992
Fth1	ENSMUSG00000024661	0.287364809	0.001014921	0.034532466
Hdac7	ENSMUSG00000022475	0.428101027	0.001030006	0.03476742
Iba57	ENSMUSG00000049287	-0.526127283	0.001033334	0.03476742
Adcy2	ENSMUSG00000021536	-0.431341169	0.001031118	0.03476742
Zfp61	ENSMUSG00000050605	0.688855936	0.001031091	0.03476742
Upf3a	ENSMUSG00000038398	0.375120744	0.001031941	0.03476742
Cav2	ENSMUSG00000000058	0.393916195	0.001055287	0.035427153
Meg3	ENSMUSG00000021268	1.50121206	0.001077324	0.036006936
Tspan3	ENSMUSG00000032324	-0.373260229	0.001077268	0.036006936
Pltp	ENSMUSG00000017754	0.442315017	0.001080908	0.036046983
Bfsp1	ENSMUSG00000027420	2.209163503	0.001083336	0.036048372
Dock6	ENSMUSG00000032198	0.456189238	0.001087367	0.03609438
Tfap4	ENSMUSG00000005718	0.717203863	0.001089497	0.03609438
Smad3	ENSMUSG00000032402	-0.387462413	0.001094406	0.036177666
Srl	ENSMUSG00000022519	-0.351841004	0.001104904	0.036444957
Dock9	ENSMUSG00000025558	0.404899263	0.001113364	0.036643979
Brd3	ENSMUSG00000026918	-0.323824296	0.001121498	0.036831469
Tyrobp	ENSMUSG00000030579	-2.059364929	0.001131722	0.037006326
Ndst1	ENSMUSG00000054008	-0.494494363	0.001130007	0.037006326
Snta1	ENSMUSG00000027488	-0.366625824	0.001140449	0.037099553
Akt1	ENSMUSG00000001729	-0.26835042	0.00114194	0.037099553
Larp6	ENSMUSG00000034839	-0.722756521	0.001141036	0.037099553
As3mt	ENSMUSG00000003559	-0.322004102	0.001151761	0.037338311

Rpain	ENSMUSG00000018449	0.436672181	0.001170265	0.037780856
Slc25a22	ENSMUSG00000019082	-0.767002466	0.001170414	0.037780856
Usf3	ENSMUSG00000068284	0.413262151	0.001184871	0.038165981
Timm29	ENSMUSG00000048429	-0.2635641	0.001194211	0.038384992
Zfp827	ENSMUSG00000071064	-0.554630458	0.001198043	0.038426398
Srrt	ENSMUSG00000037364	0.326028299	0.001207614	0.03862799
Galnt17	ENSMUSG00000034040	-0.700593948	0.001209442	0.03862799
Txnl4a	ENSMUSG00000057130	-0.50166868	0.001218512	0.038835584
Got1	ENSMUSG00000025190	-0.510257586	0.001224074	0.0389307
Asb7	ENSMUSG00000030509	-0.52431858	0.0012505	0.039687628
Pde9a	ENSMUSG00000041119	0.842630443	0.0012643	0.039874295
Hist1h3d	ENSMUSG00000099583	-1.120736342	0.001262167	0.039874295
2310016D03Rik	ENSMUSG00000102098	-1.294831959	0.001264032	0.039874295
Tspan6	ENSMUSG00000067377	0.591825116	0.001278811	0.040247914
Clec4a3	ENSMUSG00000043832	-2.42600168	0.001291515	0.04039527
Cab39	ENSMUSG00000036707	-0.470930662	0.001290703	0.04039527
Hist1h3i	ENSMUSG00000101972	-1.810279948	0.001290425	0.04039527
Ppp2ca	ENSMUSG00000020349	-0.341086176	0.001299662	0.040482459
4930553P18Rik	ENSMUSG00000106791	-2.138605115	0.001298932	0.040482459
Ankrd52	ENSMUSG00000014498	-0.487614407	0.001306677	0.040560491
Ino80b	ENSMUSG00000030034	0.409338038	0.001307537	0.040560491
Stxbp6	ENSMUSG00000046314	0.53734994	0.001311338	0.040595059
Trim3	ENSMUSG00000036989	0.282845352	0.001319231	0.040755867
Cd164	ENSMUSG00000019818	-0.296782782	0.001337917	0.041248797
Pgpep1	ENSMUSG00000056204	-0.434334939	0.0013469	0.041441186
Lrp8	ENSMUSG00000028613	-3.829577285	0.001352587	0.041531554
Npr3	ENSMUSG00000022206	-0.797760518	0.001363097	0.041767217
Mymk	ENSMUSG00000009214	-4.134522782	0.001365791	0.041767217
Hsph1	ENSMUSG00000029657	-0.522267996	0.001373288	0.04185086
Fmod	ENSMUSG00000041559	-0.895747514	0.001374067	0.04185086
Haghl	ENSMUSG00000061046	0.555779909	0.001380108	0.041893493
Myh3	ENSMUSG00000020908	-3.340650116	0.001381013	0.041893493
Cd53	ENSMUSG00000040747	-2.225250279	0.001393465	0.042113874
Snrpf	ENSMUSG00000020018	0.499235733	0.001393853	0.042113874
Snx13	ENSMUSG00000020590	-0.324842851	0.001404158	0.042340535
Snx12	ENSMUSG00000046032	-0.363241875	0.001413831	0.042378454

Arhgef5	ENSMUSG00000033542	0.51551951	0.001408826	0.042378454
Vamp5	ENSMUSG00000073002	0.366300796	0.001413528	0.042378454
Ak3	ENSMUSG00000024782	-0.298122255	0.001418983	0.042398698
Vcpkmt	ENSMUSG00000049882	0.578627711	0.001420119	0.042398698
Mgea5	ENSMUSG00000025220	-0.304792579	0.001433348	0.042709235
Rpl18a	ENSMUSG00000045128	0.255714641	0.0014446	0.042888766
Tmco6	ENSMUSG00000006850	0.544989787	0.001445051	0.042888766
Gm45819	ENSMUSG00000109904	-0.964129935	0.001457611	0.043176731
Rack1	ENSMUSG00000020372	0.213399712	0.001473967	0.04357578
Opa3	ENSMUSG00000052214	-0.308430593	0.001500397	0.044270499
Hnmt	ENSMUSG00000026986	1.032829578	0.001510601	0.044311931
Gm49477	ENSMUSG00000116066	0.87977543	0.001509899	0.044311931
Sh2d4a	ENSMUSG00000053886	-1.207432549	0.001506014	0.044311931
Lin7c	ENSMUSG00000027162	-0.36612846	0.001518588	0.04445989
Rab31	ENSMUSG00000056515	-0.66298452	0.001524498	0.044471407
Irak2	ENSMUSG00000060477	-0.543869417	0.001524869	0.044471407
Smim8	ENSMUSG00000028295	0.42706838	0.001536394	0.044720227
Wipf3	ENSMUSG00000086040	-0.48647889	0.001539321	0.044720227
Fat4	ENSMUSG00000046743	0.594451829	0.001564535	0.045003807
Plscr2	ENSMUSG00000032372	1.011049735	0.001554887	0.045003807
Tecr	ENSMUSG00000031708	0.3694749	0.001566956	0.045003807
Pstpip1	ENSMUSG00000032322	-2.010938848	0.001563207	0.045003807
Midn	ENSMUSG00000035621	-0.519785101	0.00155974	0.045003807
Gm48616	ENSMUSG00000114052	2.569665207	0.001555113	0.045003807
Hnrnpa2b1	ENSMUSG00000004980	-0.238467155	0.001580462	0.045305571
Kdm7a	ENSMUSG00000042599	-0.330275784	0.001613546	0.045992138
Ipo4	ENSMUSG00000002319	0.366774196	0.001612465	0.045992138
Drap1	ENSMUSG00000024914	0.315539481	0.001607641	0.045992138
Prg4	ENSMUSG00000006014	-0.684100161	0.001619269	0.046068366
Prex2	ENSMUSG00000048960	0.507230339	0.001628897	0.046255175
Rai14	ENSMUSG00000022246	-0.778022531	0.001639092	0.046385449
Psmb10	ENSMUSG00000031897	0.362055425	0.001639626	0.046385449
Grk6	ENSMUSG00000074886	0.34281367	0.001650358	0.046422028
Filip1l	ENSMUSG00000043336	0.385537071	0.00165321	0.046422028
Hars	ENSMUSG00000001380	0.292718676	0.001645719	0.046422028
H2-Ea-ps	ENSMUSG00000036322	-1.57639946	0.001647326	0.046422028

Il1r1	ENSMUSG00000026072	-0.759563196	0.00165912	0.046501528
Rnf128	ENSMUSG00000031438	-0.421749593	0.001662582	0.046512262
Gm10167	ENSMUSG00000066554	2.02127588	0.001667833	0.046572914
Heg1	ENSMUSG00000075254	0.323222957	0.001676934	0.046734102
Eif2s3x	ENSMUSG00000035150	-0.324317573	0.001679792	0.046734102
2900052L18Rik	ENSMUSG00000043993	0.681464068	0.001692621	0.047004459
Plscr4	ENSMUSG00000032377	0.574564377	0.001699357	0.047104916
Krba1	ENSMUSG00000042810	0.407580407	0.001708344	0.0472673
B330016D10Rik	ENSMUSG00000048406	-0.626706822	0.001714089	0.047339577
Plxdc1	ENSMUSG00000017417	0.561609466	0.001717923	0.047358875
Slc22a23	ENSMUSG00000038267	-0.52817178	0.001729303	0.047585748
Zfp112	ENSMUSG00000052675	0.525953835	0.001738955	0.047764357
Aig1	ENSMUSG00000019806	-0.956771522	0.00174588	0.04786754
Zfp672	ENSMUSG00000049755	-0.371619177	0.001770838	0.04834335
Kif5c	ENSMUSG00000026764	-1.827112296	0.001772835	0.04834335
Ssc5d	ENSMUSG00000035279	-1.034580316	0.001768896	0.04834335
Gipc3	ENSMUSG00000034872	0.759843913	0.001799741	0.048988621
Dock2	ENSMUSG00000020143	-2.427818139	0.001805997	0.049070501
Vcl	ENSMUSG00000021823	-0.505837133	0.001814506	0.049184793
Arhgdig	ENSMUSG00000073433	-1.813670159	0.001816715	0.049184793
Insig2	ENSMUSG00000003721	-0.344808794	0.001831623	0.049499684
Pcnx	ENSMUSG00000021140	-0.499744039	0.001840781	0.04960014
Abtb1	ENSMUSG00000030083	0.293664646	0.001841906	0.04960014
Sdhaf2	ENSMUSG00000024668	-0.327441211	0.001857783	0.049849949
Pik3r5	ENSMUSG00000020901	-1.694739873	0.001856595	0.049849949
Amy1	ENSMUSG00000074264	-0.383976023	0.00186139	0.04985818
C030034I22Rik	ENSMUSG00000073374	0.973662505	0.001866137	0.049896863
Ppm1j	ENSMUSG00000002228	-0.315923492	0.001870192	0.049916943
Dnmt3a	ENSMUSG00000020661	-0.355076458	0.001875545	0.049965686
Myo6	ENSMUSG00000033577	0.420788934	0.001878633	0.049965686

A3. Muscle DEGs

Gene ID	EnsemblID	log2FoldChange	p-value	q-value
Rps15a-ps7	ENSMUSG00000081087	-4.447831991	1.78272E-18	3.14597E-14
Mup11	ENSMUSG00000073834	-2.173442132	3.93E-18	3.46764E-14
Fmo3	ENSMUSG00000026691	7.687187648	3.29436E-17	1.93785E-13
Moxd1	ENSMUSG00000020000	-8.860656489	1.06673E-14	4.70615E-11
Cd36	ENSMUSG00000002944	2.021443763	5.47367E-14	1.6099E-10
A530083I20Rik	ENSMUSG00000097322	-2.368746669	4.93044E-14	1.6099E-10
Mup20	ENSMUSG00000078672	-1.312017355	1.28814E-13	3.24739E-10
Tmc5	ENSMUSG00000030650	-8.250735298	2.13541E-13	4.71045E-10
Mup15	ENSMUSG00000096674	-1.648363204	7.62744E-13	1.49557E-09
Kcnk1	ENSMUSG00000033998	-4.29905856	8.91204E-13	1.57271E-09
Cyp2a4	ENSMUSG00000074254	3.42824091	6.68161E-12	1.07191E-08
Prlr	ENSMUSG00000005268	1.181145565	2.12173E-11	3.12018E-08
Hspb1	ENSMUSG00000004951	-1.922056778	2.81078E-11	3.81553E-08
Abcd2	ENSMUSG00000055782	2.353023952	4.55969E-11	5.74749E-08
Gm35696	ENSMUSG00000112527	-1.157243144	7.18378E-11	8.45147E-08
Crym	ENSMUSG00000030905	-1.617376568	3.13074E-10	3.45301E-07
Dpy19l3	ENSMUSG00000043671	-1.108980715	5.47277E-10	5.68105E-07
Gtpbp4-ps1	ENSMUSG00000098330	-2.269591011	1.03585E-09	1.01554E-06
Pdilt	ENSMUSG00000030968	-0.967834305	3.06145E-09	2.84344E-06
Tcf24	ENSMUSG00000099032	1.863889728	3.54204E-09	3.12531E-06
Cyp2b9	ENSMUSG00000040660	4.792608242	3.78205E-09	3.17818E-06
Gstp1	ENSMUSG00000060803	-0.948324179	5.28296E-09	4.23765E-06
Cyp2c38	ENSMUSG00000032808	1.736012446	6.8319E-09	5.24185E-06
Aqp4	ENSMUSG00000024411	1.731743375	2.33125E-08	1.64558E-05
Lrtm1	ENSMUSG00000045776	1.560771822	2.24744E-08	1.64558E-05
Slc22a26	ENSMUSG00000053303	4.18528796	3.72594E-08	2.52891E-05
Ugt2b38	ENSMUSG00000061906	-1.083513489	8.8873E-08	5.80867E-05
Cyp2c39	ENSMUSG00000025003	1.421867558	1.41227E-07	8.90083E-05
Cyp2a22	ENSMUSG00000091867	2.272289491	2.00811E-07	0.000122197
Ocstamp	ENSMUSG00000027670	-1.929789118	2.2283E-07	0.000131076
Nr1i3	ENSMUSG00000005677	0.900243754	2.31595E-07	0.000131837
C4a	ENSMUSG00000015451	-1.015366547	3.22585E-07	0.000177896
C6	ENSMUSG00000022181	-0.762835074	4.01683E-07	0.000214803
Capn8	ENSMUSG00000038599	-1.850343685	4.89716E-07	0.000254177

Cyp2d41-ps	ENSMUSG00000058613	-2.044625465	5.52454E-07	0.000278547
Csad	ENSMUSG00000023044	-1.301500448	9.33549E-07	0.000443945
Cyp7b1	ENSMUSG00000039519	-1.127779402	9.55965E-07	0.000443945
Cyp2c69	ENSMUSG00000092008	3.242985786	9.22348E-07	0.000443945
Mup17	ENSMUSG00000096688	-1.343333606	1.06026E-06	0.000479753
Nipal1	ENSMUSG00000067219	1.67657356	1.65392E-06	0.00072967
Lrg1	ENSMUSG00000037095	-1.276710491	1.74195E-06	0.000749759
Nenf	ENSMUSG00000037499	-0.89292711	2.82872E-06	0.001188533
Susd4	ENSMUSG00000038576	-0.702228622	3.23525E-06	0.00132773
Leap2	ENSMUSG00000036216	-0.747498679	3.53172E-06	0.00141646
Rarres1	ENSMUSG00000049404	-0.860295372	3.85403E-06	0.001511378
Gm1600	ENSMUSG00000116270	1.762290655	4.01248E-06	0.001539308
Snhg11	ENSMUSG00000044349	1.040611501	4.95369E-06	0.001859952
Naaladl2	ENSMUSG00000102758	1.060905208	7.21576E-06	0.002652845
Fkbp11	ENSMUSG00000003355	-1.022558423	7.9619E-06	0.002867421
Meg3	ENSMUSG00000021268	1.111626409	9.3353E-06	0.003273534
Col11a2	ENSMUSG00000024330	-1.72344699	9.46452E-06	0.003273534
Irf7	ENSMUSG00000025498	-0.729378935	9.64605E-06	0.003273534
Selenbp2	ENSMUSG00000068877	-0.641954228	1.11704E-05	0.00371933
Mrap	ENSMUSG00000039956	-0.600545832	1.20438E-05	0.003935872
Tceal8	ENSMUSG00000051579	0.679070922	1.38368E-05	0.0044396
Elovl3	ENSMUSG00000038754	-0.952037541	1.55905E-05	0.004863248
A930004J17Rik	ENSMUSG00000102602	1.290263959	1.62595E-05	0.004863248
Slc3a1	ENSMUSG00000024131	-1.327556042	1.61356E-05	0.004863248
Spink6	ENSMUSG00000055095	-5.492856778	1.58763E-05	0.004863248
Adamts13	ENSMUSG00000014852	0.770134537	1.93639E-05	0.005695252
Slc16a5	ENSMUSG00000045775	1.388516403	1.98122E-05	0.005731567
Tpm2	ENSMUSG00000028464	1.211909503	2.12826E-05	0.005993345
Ildr2	ENSMUSG00000040612	0.756207531	2.14356E-05	0.005993345
4732463B04Rik	ENSMUSG00000097762	1.698387266	2.17359E-05	0.005993345
Gstp-ps	ENSMUSG00000103653	-1.373337034	2.2606E-05	0.006137362
Ntrk2	ENSMUSG00000055254	-1.390994481	2.30277E-05	0.006157119
Fnip2	ENSMUSG00000061175	0.613806279	2.59196E-05	0.006641663
Vldlr	ENSMUSG00000024924	1.65675951	2.52891E-05	0.006641663
C9	ENSMUSG00000022149	-0.538550758	2.5969E-05	0.006641663
Mup-ps19	ENSMUSG00000082644	-1.374462896	2.77508E-05	0.00699598

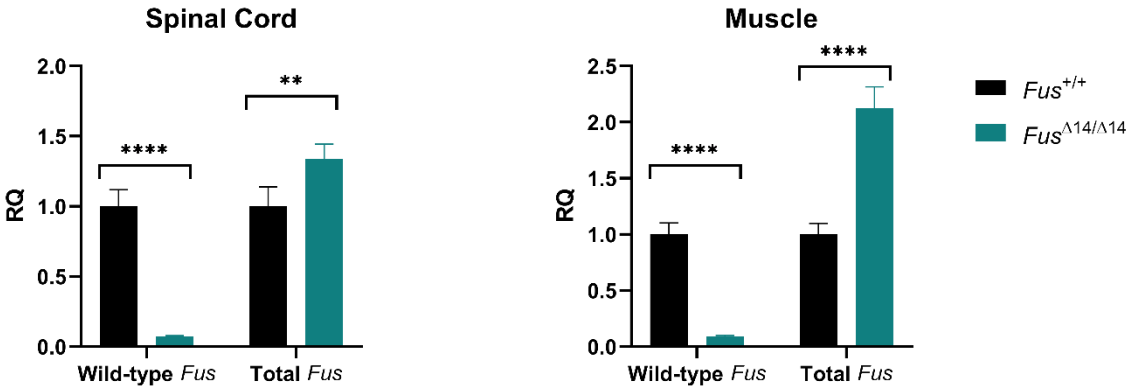
Rassf4	ENSMUSG00000042129	1.180153146	3.20542E-05	0.007967054
Arhgef9	ENSMUSG00000025656	1.332571295	3.41175E-05	0.008362093
Slc13a5	ENSMUSG00000020805	-1.658598334	3.52677E-05	0.008525601
Fam13a	ENSMUSG00000037709	0.872091291	3.69116E-05	0.008802429
Lrp2	ENSMUSG00000027070	-2.459823516	3.82459E-05	0.008999003
Stap1	ENSMUSG00000029254	1.277718957	4.21126E-05	0.00977844
Fus	ENSMUSG00000030795	0.722337093	4.78937E-05	0.01095087
Fam19a2	ENSMUSG00000044071	5.064142485	4.8403E-05	0.01095087
Sox9	ENSMUSG00000000567	-1.403870876	5.11393E-05	0.011418627
Fabp5	ENSMUSG00000027533	-1.393962281	5.24117E-05	0.011418627
Cyp21a2-ps	ENSMUSG00000092471	-1.381272671	5.2355E-05	0.011418627
Serpina12	ENSMUSG00000041567	-0.819670682	5.59457E-05	0.012039925
mt-Tn	ENSMUSG00000064348	-1.21120185	5.94163E-05	0.012632756
Ogt	ENSMUSG00000034160	0.765110841	6.3042E-05	0.013244076
Gpx3	ENSMUSG00000018339	-1.096219348	6.5294E-05	0.0135558
Per2	ENSMUSG00000055866	0.886680183	7.20131E-05	0.014776913
Ttn	ENSMUSG00000051747	3.256403729	8.46114E-05	0.017162508
Acot3	ENSMUSG00000021228	2.623178517	9.59968E-05	0.019250632
Fam131c	ENSMUSG00000006218	-0.955305219	0.000102374	0.019273532
Insc	ENSMUSG00000048782	-1.09149482	0.000101487	0.019273532
Slc25a30	ENSMUSG00000022003	-1.109405113	0.00010343	0.019273532
Gm15408	ENSMUSG00000086610	1.031287493	0.00010655	0.019273532
Bst2	ENSMUSG00000046718	-0.603584422	9.98857E-05	0.019273532
Arhgap6	ENSMUSG00000031355	0.859670901	0.000105628	0.019273532
Cyp46a1	ENSMUSG00000021259	0.796906216	0.000100264	0.019273532
Ces2b	ENSMUSG00000050097	-1.752505477	0.000106537	0.019273532
2310034O05Rik	ENSMUSG00000100157	1.609196844	9.89097E-05	0.019273532
Themis	ENSMUSG00000049109	2.688175903	0.000107033	0.019273532
Upp1	ENSMUSG00000020407	1.408123426	0.000115595	0.020605112
Cystm1	ENSMUSG00000046727	-0.744594679	0.00012914	0.022789381
Abcc5	ENSMUSG00000022822	0.936930876	0.000138665	0.02422786
Cfd	ENSMUSG00000061780	5.274929343	0.000142419	0.024525801
Smim1	ENSMUSG00000078350	-1.086687026	0.000143926	0.024525801
Crybb3	ENSMUSG00000029352	-2.281785237	0.000145929	0.024525801
S100a8	ENSMUSG00000056054	-3.830735916	0.000145798	0.024525801
Nrep	ENSMUSG00000042834	1.144112421	0.000152244	0.025219523

Cyp7a1	ENSMUSG00000028240	0.822268682	0.000152915	0.025219523
Scara5	ENSMUSG00000022032	-2.044847373	0.000159975	0.025981224
1700028E10Rik	ENSMUSG00000097321	0.923282542	0.000160478	0.025981224
Pik3r3	ENSMUSG00000028698	-1.320068147	0.000162975	0.026145697
Cers6	ENSMUSG00000027035	0.704689554	0.000171827	0.027075814
Mup16	ENSMUSG00000078675	-1.852960498	0.000171842	0.027075814
A1cf	ENSMUSG00000052595	0.591436064	0.000182213	0.028455835
Wfdc17	ENSMUSG00000069792	-1.077068725	0.000184763	0.028600983
Serpina6	ENSMUSG00000060807	0.660314966	0.000191198	0.029339731
AC169509.1	ENSMUSG00000115852	0.74945645	0.000195919	0.029805032
Saa1	ENSMUSG00000074115	-2.54677794	0.000206231	0.03110569
Dynll1	ENSMUSG00000009013	-0.962411624	0.000213497	0.031660285
Gm11844	ENSMUSG00000087241	0.775067052	0.000212655	0.031660285
Ppp1r14a	ENSMUSG00000037166	-0.836010799	0.000229264	0.033711273
Gm43743	ENSMUSG00000105506	-2.118519454	0.000231148	0.033711273
Xlr3b	ENSMUSG00000073125	1.937099136	0.000234446	0.033912058
Hist1h1c	ENSMUSG00000036181	-0.744853929	0.000239923	0.034422089
Ppm1m	ENSMUSG00000020253	-0.476783278	0.00024357	0.034578147
Ifi27	ENSMUSG00000064215	-0.877856635	0.000244929	0.034578147
Serpinb8	ENSMUSG00000026315	1.117527226	0.000251803	0.035266405
Slc20a1	ENSMUSG00000027397	0.521425585	0.000269344	0.037426057
H1fx	ENSMUSG00000044927	-2.606204436	0.000273726	0.03773784
Lad1	ENSMUSG00000041782	-1.177718606	0.000289488	0.039079861
Cdhr5	ENSMUSG00000025497	-0.509134654	0.000289709	0.039079861
Adgrf1	ENSMUSG00000041293	-0.859760659	0.000290104	0.039079861
Pnp	ENSMUSG00000115338	-0.557098993	0.000324141	0.04300843
Crlf2	ENSMUSG00000033467	-0.935346006	0.000321839	0.04300843
Rorc	ENSMUSG00000028150	0.725183169	0.000330171	0.043481573
Rpl13a	ENSMUSG00000074129	-0.575158869	0.000338377	0.044232111
Agap2	ENSMUSG00000025422	-1.19931953	0.000355496	0.045622928
Atp11a	ENSMUSG00000031441	-1.279295316	0.000351664	0.045622928
Mtcp1	ENSMUSG00000031200	0.960243014	0.000356772	0.045622928
Gm16505	ENSMUSG00000096107	-3.688062147	0.000361769	0.045928994

A4. Liver DEGs

Gene ID	EnsemblID	log2FoldChange	p-value	q-value
Xlr4b	ENSMUSG00000067768	4.294419195	7.47597E-16	1.24363E-11
Rps15a-ps7	ENSMUSG00000081087	-3.426755062	2.22035E-15	1.84678E-11
Vil1	ENSMUSG00000026175	1.725937354	2.5831E-13	1.43233E-09
Pdzd7	ENSMUSG00000074818	-2.168691659	1.73595E-11	7.2194E-08
Tfr2	ENSMUSG00000029716	1.434533988	5.01265E-11	1.66771E-07
Lyz1	ENSMUSG00000069515	-2.466156667	1.26833E-07	0.000351644
Ccnd1	ENSMUSG00000070348	1.305372847	2.40598E-07	0.000500294
Fgl2	ENSMUSG00000039899	-1.195068293	2.36653E-07	0.000500294
Rufy4	ENSMUSG00000061815	-0.907935795	3.61401E-07	0.000667989
Retnla	ENSMUSG00000061100	1.469390163	5.81404E-07	0.000967165
Fbp2	ENSMUSG00000021456	0.998397197	3.79126E-06	0.005733419
Klhdc7a	ENSMUSG00000078234	-0.776535676	4.6989E-06	0.006513851
Pla2g2e	ENSMUSG00000028751	1.674226747	5.35827E-06	0.006856519
Kcp	ENSMUSG00000059022	1.108324078	5.94228E-06	0.007060704
Ndn	ENSMUSG00000033585	1.06551055	6.88919E-06	0.007640113
Dchs1	ENSMUSG00000036862	0.95660676	9.78937E-06	0.010177883
Fam131c	ENSMUSG00000006218	1.05101329	1.74318E-05	0.017057558
Fn1	ENSMUSG00000026193	0.761820544	1.86315E-05	0.017218596
Colgalt2	ENSMUSG00000032649	0.842248456	2.42024E-05	0.02118986
2010001A14Rik	ENSMUSG00000087165	1.139053007	3.52938E-05	0.02935559
Acot1	ENSMUSG00000072949	0.822271699	4.22924E-05	0.033501588
Lrtm2	ENSMUSG00000055003	-3.69702469	4.83506E-05	0.03351298
AI413582	ENSMUSG00000062753	1.12125554	4.72009E-05	0.03351298
Gm15241	ENSMUSG00000087505	1.601274658	4.54494E-05	0.03351298
Gprc5b	ENSMUSG00000008734	-0.763073459	5.61305E-05	0.037349246
Plscr2	ENSMUSG00000032372	1.356464084	6.07134E-05	0.037410091
D330023K18Rik	ENSMUSG00000087269	1.10383719	6.07197E-05	0.037410091
Rps4l	ENSMUSG00000063171	0.956323949	7.20703E-05	0.042817463
Gck	ENSMUSG00000041798	-2.256752681	8.12697E-05	0.046306462
Clu	ENSMUSG00000022037	-1.342573822	8.60231E-05	0.046306462
Plekhg6	ENSMUSG00000038167	-1.44495562	8.6294E-05	0.046306462

A5. BAT DEGs



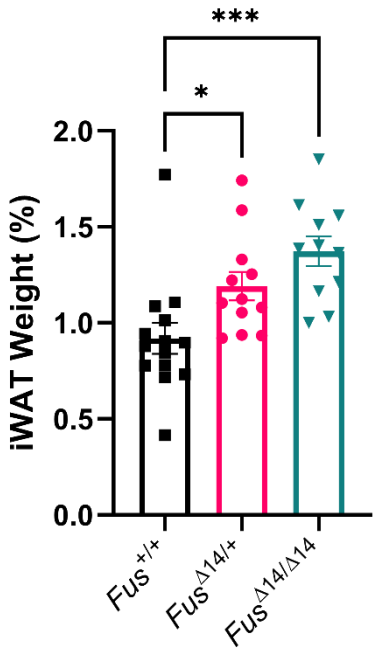
A6. *Fus* gene expression in $Fus^{\Delta 14}$ mice. Graphs show QRT-PCR data from the spinal cords and TA muscles of 9-week old male mice. Data shown as mean relative quantification (RQ). Error bars denote upper and lower limits. Data analysed using unpaired t-test to compare between genotypes. s16 was used as the reference gene. Spinal cord: n= 5 $Fus^{+/+}$ and n=4 $Fus^{\Delta 14/\Delta 14}$. Muscle: n= 5 $Fus^{+/+}$ and n=5 $Fus^{\Delta 14/\Delta 14}$. **p<0.01. ****p<0.0001.

Mouse ID	Tissue	Genotype	RIN
48.2g	BAT	HOM	6.4
48.2g	Frontal brain	HOM	7.8
48.2g	iWAT	HOM	6.8
48.2g	Liver	HOM	7.2
48.2g	Spinal cord	HOM	8.9
48.2g	TA muscle	HOM	8
48.2i	BAT	HOM	6.7
48.2i	Frontal brain	HOM	8.5
48.2i	iWAT	HOM	6.1
48.2i	Liver	HOM	7.1
48.2i	Spinal cord	HOM	8.7
48.2i	TA muscle	HOM	7.9
50.1e	BAT	HOM	7.6
50.1e	Frontal brain	HOM	8.2
50.1e	iWAT	HOM	6.8
50.1e	Liver	HOM	7.2
50.1e	Spinal cord	HOM	9
50.1e	TA muscle	HOM	8
54.2i	BAT	HOM	7
54.2i	Frontal brain	HOM	8.1
54.2i	iWAT	HOM	6.9
54.2i	Liver	HOM	7.2
54.2i	Spinal cord	HOM	9
54.2i	TA muscle	HOM	8.4
48.1d	BAT	WT	6.6
48.1d	Frontal brain	WT	8.6
48.1d	iWAT	WT	5.9
48.1d	Liver	WT	7
48.1d	Spinal cord	WT	7
48.1d	TA muscle	WT	7
48.1f	BAT	WT	7.6
48.1f	Frontal brain	WT	7.2
48.1f	iWAT	WT	7.1
48.1f	Liver	WT	6.3
48.1f	Spinal cord	WT	6.6
48.1f	TA muscle	WT	8
50.1g	BAT	WT	7.6
50.1g	Frontal brain	WT	8.6
50.1g	iWAT	WT	6.6
50.1g	Liver	WT	6.3
50.1g	Spinal cord	WT	9
50.1g	TA muscle	WT	7.9
54.2c	BAT	WT	7.9
54.2c	Frontal brain	WT	8.1
54.2c	iWAT	WT	6
54.2c	Liver	WT	7.9

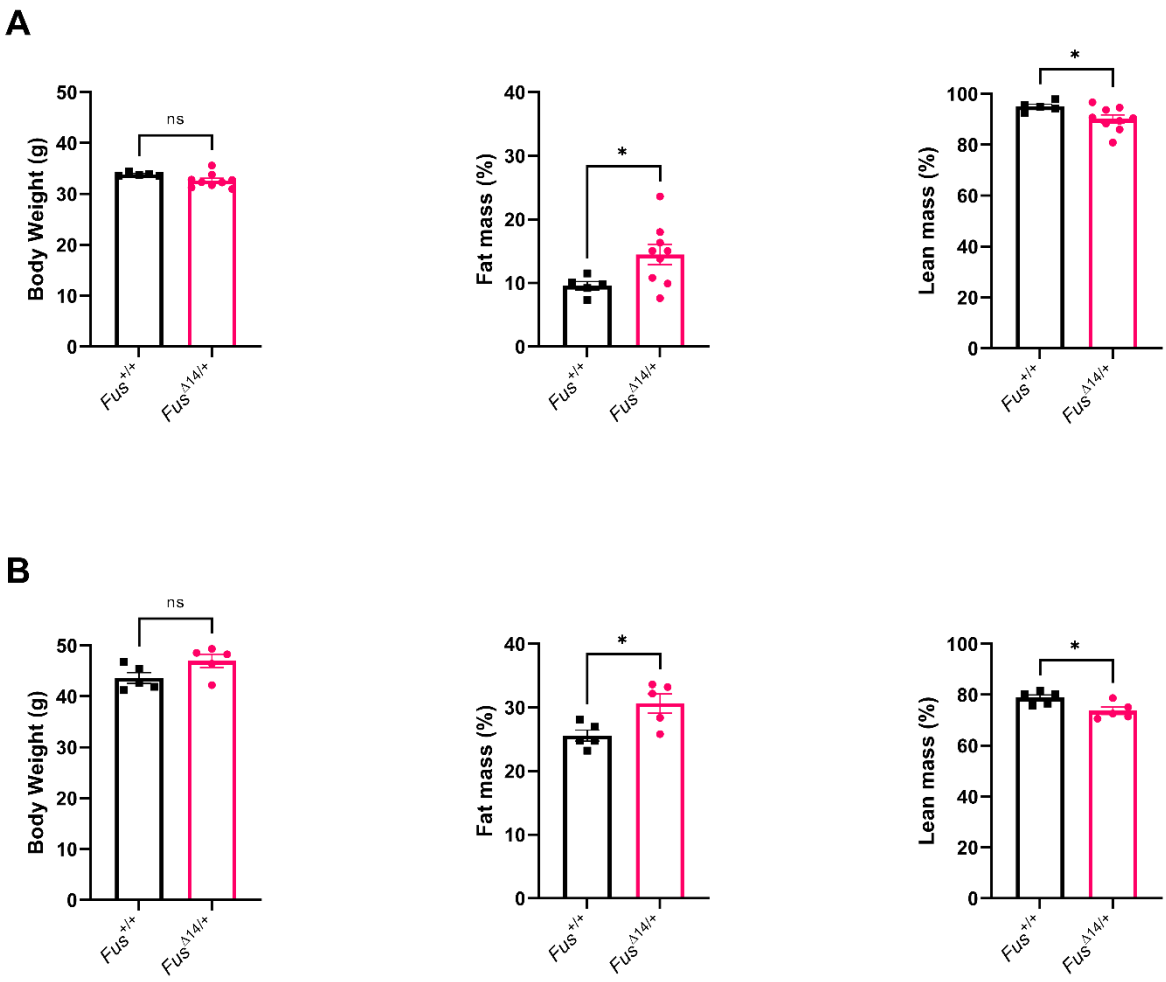
54.2c	Spinal cord	WT	5.9
54.2c	TA muscle	WT	8

A7. *Fus*$^{\Delta 14}$ tissues used for RNA-sequencing. Graph shows mouse IDs, genotypes and RIN of tissues used in RNA-seq. WT= wild-type. HOM= homozygous. RIN= RNA integrity number.

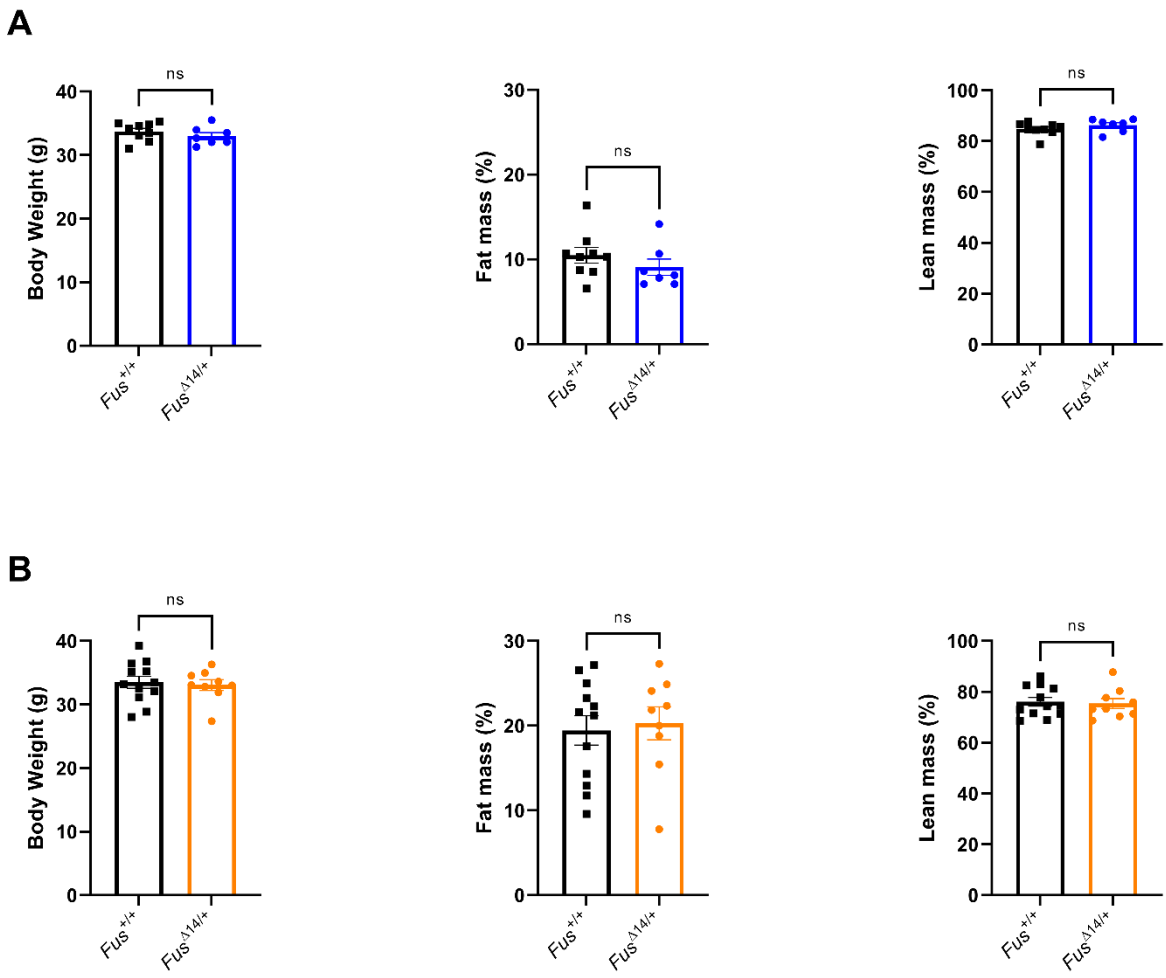
Appendix B: Additional metabolic data from the *Fus*$^{\Delta 14}$ mouse.



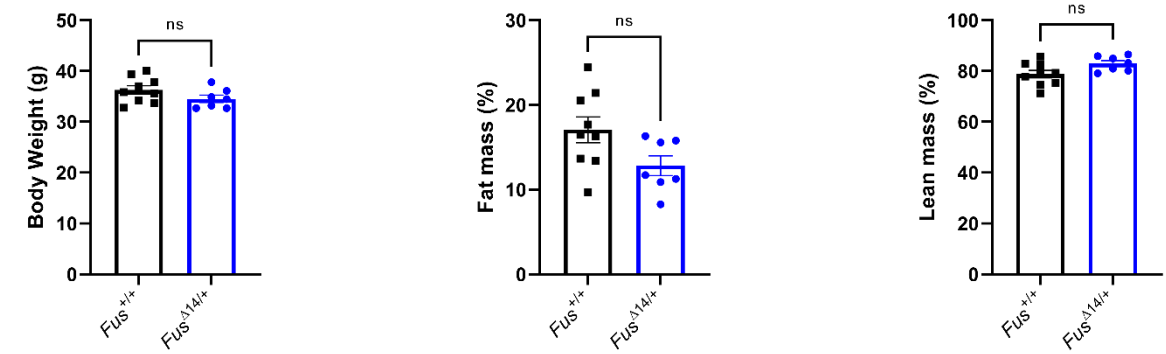
B1. Proportionate dissected iWAT weights of male *Fus*$^{\Delta 14}$ mice at 9 weeks of age. Data shown as mean. Error bars denote SEM of data. Data analysed using one-way ANOVA followed by Dunnett's multiple comparisons test to compare between genotypes. n=14 *Fus*$^{+/+}$, n=12 *Fus*$^{\Delta 14/+}$ and n=11 *Fus*$^{\Delta 14/\Delta 14}$. *p<0.05. ***p<0.001.



B2. Body composition of male *Fus*$^{\Delta 14}$ mice at 3 (A) and 8-months (B) of age. Data shown as mean. Error bars denote SEM of data. Data analysed using unpaired t-test to compare between genotypes. 3-months: n=5 *Fus*$^{+/+}$ and n=9 *Fus*$^{\Delta 14/+}$. 8-months: n=5 *Fus*$^{+/+}$ and n=5 *Fus*$^{\Delta 14/+}$. ns= not significant. *p<0.05.



B3. Body composition of male *Fus*$^{\Delta 14}$ mice on the C57BL/6J (A) and DBA/2J (B) backgrounds at 6 months of age. Data shown as mean. Error bars denote SEM of data. Data analysed using unpaired t-test to compare between genotypes. C57BL/6J: n=9 *Fus*$^{+/+}$ and n=7 *Fus*$^{\Delta 14/+}$. 8-months: n=12 *Fus*$^{+/+}$ and n=9 *Fus*$^{\Delta 14/+}$. ns= not significant.



B4. Body composition of male *Fus*$^{\Delta 14}$ mice on the C57BL/6J background at 12 months of age. Data shown as mean. Error bars denote SEM of data. Data analysed using unpaired t-test to compare between genotypes. n=9 *Fus*$^{+/+}$ and n=7 *Fus*$^{\Delta 14/+}$. ns= not significant.

Appendix C: Significantly altered brain structural volumes in *Tardbp*$^{M323K/M323K}$ mice.

Brain Region	Difference in mean volume (mm^3)	q-value
amygdala	1.243	0.000096
anterior commissure pars anterior	0.1854	0.000096
anterior commissure pars posterior	0.1286	0.000096
basal forebrain	1.004	0.000096
bed nucleus of stria terminalis	0.2153	0.000096
cerebellar peduncle inferior	0.2216	0.000096
cerebellar peduncle middle	0.3242	0.000096
cerebellar peduncle superior	0.1902	0.000096
cerebral aqueduct	0.07842	0.000096
cerebral peduncle	0.4622	0.000096
colliculus inferior	1.038	0.000096
colliculus superior	1.61	0.000096
corpus callosum	2.603	0.000096
corticospinal tract pyramids	0.3638	0.000096
cuneate nucleus	0.06897	0.000096
facial nerve cranial nerve 7	0.03616	0.000096
fasciculus retroflexus	0.05207	0.000096
fimbria	0.5769	0.000096

fornix	0.1001	0.000096
fundus of striatum	0.03769	0.000096
globus pallidus	0.8393	0.000096
hypothalamus	1.501	0.000096
internal capsule	0.6615	0.000096
interpedunclar nucleus	0.04346	0.000096
lateral olfactory tract	0.2613	0.000096
lateral septum	0.3165	0.000096
lateral ventricle	0.4172	0.000096
mammilothalamic tract	0.06017	0.000096
medial lemniscus medial longitudinal fasciculus	0.4232	0.000096
medial septum	0.2108	0.000096
medulla	5.203	0.000096
midbrain	2.024	0.000096
nucleus accumbens	0.4329	0.000096
olfactory peduncle	0.3368	0.000096
optic tract	0.2755	0.000096
periaqueductal grey	0.8301	0.000096
pons	2.967	0.000096
pontine nucleus	0.2425	0.000096
posterior commissure	0.02705	0.000096
pre para subiculum	0.2425	0.000096

stria medullaris	0.1005	0.000096
stria terminalis	0.1971	0.000096
striatum	4.07	0.000096
superior olivary complex	0.1301	0.000096
thalamus	3.4	0.000096
ventral tegmental decussation	0.02795	0.000096
lobules 1 2 lingula and central lobule ventral	0.5073	0.000096
lobule 3 central lobule dorsal	0.5552	0.000096
lobules 4 5 culmen ventral and dorsal	1.26	0.000096
lobule 6 declive	0.4269	0.000096
lobule 8 pyramis	0.3284	0.000096
lobule 9 uvula	0.8423	0.000096
lobule 10 nodulus	0.2418	0.000096
anterior lobule lobules 4 5	0.5592	0.000096
simple lobule lobule 6	1.589	0.000096
crus 1 ansiform lobule lobule 6	1.097	0.000096
crus 2 ansiform lobule lobule 7	0.7642	0.000096
flocculus FL	0.3526	0.000096
paraflocculus PFL	1.182	0.000096
trunk of arbor vita	1.013	0.000096
lobule 1 2 white matter	0.02814	0.000096

lobule 3 white matter	0.04683	0.000096
trunk of lobules 1 3 white matter	0.03796	0.000096
lobules 4 5 white matter	0.1771	0.000096
lobules 6 7 white matter	0.1529	0.000096
lobule 8 white matter	0.04012	0.000096
trunk of lobules 6 8 white matter	0.03559	0.000096
lobule 9 white matter	0.0785	0.000096
lobule 10 white matter	0.03312	0.000096
anterior lobule white matter	0.035	0.000096
simple lobule white matter	0.1596	0.000096
crus 1 white matter	0.1155	0.000096
trunk of simple and crus 1 white matter	0.02575	0.000096
crus 2 white matter	0.06677	0.000096
paramedian lobule	0.03878	0.000096
trunk of crus 2 and paramedian white matter	0.0486	0.000096
copula white matter	0.01774	0.000096
paraflocculus white matter	0.08869	0.000096
flocculus white matter	0.02244	0.000096
dentate nucleus	0.09016	0.000096
nucleus interpositus	0.1228	0.000096
fastigial nucleus	0.113	0.000096

Cingulate cortex area 25	0.09479	0.000096
Cingulate cortex area 29a	0.1818	0.000096
Cingulate cortex area 29b	0.08633	0.000096
Cingulate cortex area 29c	0.3514	0.000096
Cingulate cortex area 30	0.4696	0.000096
Cingulate cortex area 32	0.5787	0.000096
Caudomedial entorhinal cortex	0.7138	0.000096
Cingulum	0.2498	0.000096
Dorsal nucleus of the endopiriform	0.2398	0.000096
Dorsolateral entorhinal cortex	0.257	0.000096
Dorsal tenia tecta	0.1147	0.000096
Ectorhinal cortex	0.3553	0.000096
Frontal cortex area 3	0.1226	0.000096
Intermediate nucleus of the endopiriform claustrum	0.1144	0.000096
Insular region not subdivided	0.6223	0.000096
Lateral orbital cortex	0.8708	0.000096
Primary motor cortex	1.251	0.000096
Secondary motor cortex	0.8731	0.000096
Medial entorhinal cortex	0.08158	0.000096
Medial parietal association cortex	0.06964	0.000096

Piriform cortex	1.643	0.000096
Posteromedial cortical amygdaloid area	0.1714	0.000096
Perirhinal cortex	0.3359	0.000096
Primary somatosensory cortex	0.559	0.000096
Primary somatosensory cortex barrel field	1.172	0.000096
Primary somatosensory cortex dysgranular zone	0.06912	0.000096
Primary somatosensory cortex forelimb region	0.6666	0.000096
Primary somatosensory cortex hindlimb region	0.5011	0.000096
Primary somatosensory cortex jaw region	0.07651	0.000096
Primary somatosensory cortex shoulder region	0.03222	0.000096
Primary somatosensory cortex trunk region	0.08706	0.000096
Primary somatosensory cortex upper lip region	0.9824	0.000096
Secondary somatosensory cortex	0.9759	0.000096
Temporal association area	0.3529	0.000096
Primary visual cortex monocular area	0.4171	0.000096
Secondary visual cortex lateral area	0.3333	0.000096
Secondary visual cortex mediolateral area	0.2028	0.000096
Secondary visual cortex mediomedial area	0.2184	0.000096
Ventral nucleus of the endopiriform claustrum	0.121	0.000096

Ventral orbital cortex	0.4324	0.000096
CA3Py Outer	0.1621	0.000096
CA30r	0.4246	0.000096
CA3Rad	0.2844	0.000096
SLu	0.1255	0.000096
MoDG	0.4626	0.000096
GrDG	0.1464	0.000096
PoDG	0.08165	0.000096
Olfactory bulb glomerular layer	0.6627	0.000096
Olfactory bulb external plexiform layer	1.295	0.000096
Olfactory bulb mitral cell layer	0.256	0.000096
Olfactory bulb internal plexiform layer	0.2191	0.000096
Olfactory bulb granule cell layer	0.9491	0.000096
Accessory olfactory bulb glomerular external plexiform and mitral cell layer	0.1233	0.000096
Accessory olfactory bulb granule cell layer	0.07233	0.000096
Anterior olfactory nucleus	0.2864	0.000096
subiculum	0.3851	0.000096
Medial amygdala	0.1575	0.000096
Medial preoptic nucleus	0.02802	0.000096

subependymale zone rhinocele	0.007845	0.000183
Secondary auditory cortex ventral area	0.1705	0.000183
Lateral parietal association cortex	0.04158	0.000183
Medial orbital cortex	0.4414	0.000183
Primary visual cortex binocular area	0.2538	0.000183
CA10r	0.2833	0.000183
CA20r	0.06937	0.000183
fourth ventricle	0.1198	0.000347
third ventricle	0.112	0.000347
copula pyramis lobule 8	0.3107	0.000347
Cingulate cortex area 24a.1	0.1112	0.000347
Cingulate cortex area 24b.1	0.06759	0.000347
Dorsal intermediate entorhinal cortex	0.166	0.000347
Frontal association cortex	0.7508	0.000347
Posterolateral cortical amygdaloid area	0.1149	0.000347
olfactory tubercle	0.6002	0.000578
paramedian lobule lobule 7	0.4881	0.000578
Amygdalopiriform transition area	0.118	0.000578
Parietal cortex posterior area rostral part	0.01378	0.000578
LMol	0.1586	0.000578

CA2Py	0.01996	0.000578
CA2Rad	0.03517	0.000578
CA1Py	0.1274	0.000578
Cingulate cortex area 24a	0.3246	0.000985
Cingulate cortex area 24b	0.1739	0.001513
Dorsolateral orbital cortex	0.1133	0.001513
Rostral amygdalopiriform area	0.0331	0.001513
Primary visual cortex	0.1827	0.001513
Ventral intermediate entorhinal cortex	0.08092	0.001513
Primary auditory cortex	0.1044	0.002362
CA1Rad	0.1424	0.002362
Cortex amygdala transition zones	0.09441	0.003424
CA3Py Inner	0.008792	0.003424
habenular commissure	0.003042	0.006189
Secondary auditory cortex dorsal area	0.08425	0.006692
inferior olivary complex	0.03568	0.008974
Ventral tenia tecta	0.01605	0.008974
Claustrum dorsal part	-0.01639	0.019134
Claustrum	0.01675	0.020155
Claustrum ventral part	-0.01129	0.034252
mammillary bodies	0.02014	0.040087

lobule 7 tuber or folium	0.04937	0.053033

C1. Absolute brain structure volumes (mm^3). Difference in mean volume between *Tardbp*$^{+/+}$ and *Tardbp*$^{M323K/M323K}$ mice. Statistical significance at $p<0.05$ after false discovery rate correction. Man Whitney U test. n=7 *Tardbp*$^{+/+}$ and n=6 *Tardbp*$^{M323K/M323K}$.

Brain Region	Difference in mean volume (mm^3)	q-value
Insular region	-0.001572	0.003671
CA1Rad	-0.0008943	0.003671
nucleus accumbens	-0.0007876	0.003671
LMol	-0.000735	0.003671
MoDG	-0.0006419	0.003671
subiculum	-0.0005128	0.003671
Primary auditory cortex	-0.0004128	0.003671
Claustrum ventral part	-0.0002795	0.003671
CA2Rad	-0.0001476	0.003671
CA3Py Inner	-0.00004161	0.003671
Secondary auditory cortex dorsal area	-0.0004632	0.004942
Secondary visual cortex lateral area	-0.0004493	0.004942
lateral septum	-0.0004404	0.004942
Dorsal intermediate entorhinal cortex	-0.0003731	0.004942
Secondary auditory cortex ventral area	-0.0003579	0.004942
Ventral intermediate entorhinal cortex	-0.0003005	0.004942
Dorsal tenia tecta	-0.0001825	0.004942

GrDG	-0.0001812	0.004942
Claustrum dorsal part	-0.0001442	0.004942
Medial entorhinal cortex	-0.0001194	0.004942
amygdala	-0.0008771	0.008712
midbrain	-0.0008496	0.008712
Dorsolateral entorhinal cortex	-0.0004277	0.008712
Claustrum	-0.00009335	0.008712
CA2Py	-0.0000434	0.008712
Primary visual cortex	-0.0006851	0.013628
Frontal association cortex	-0.001131	0.020025
pre para subiculum	-0.0004009	0.020025
Temporal association area	-0.0003709	0.020025
Primary visual cortex binocular area	-0.0003283	0.020025
mammillary bodies	-0.0001944	0.020025
third ventricle	-0.0001405	0.020025
Perirhinal cortex	-0.000255	0.029774
Primary somatosensory cortex barrel field	-0.001113	0.043313
Secondary visual cortex mediomedial area	-0.0003013	0.043313
Amygdalopiriform transition area	-0.0001864	0.043313
CA1Py	-0.0001753	0.043313
Rostral amygdalopiriform area	-0.0001068	0.043313

lobule 10 white matter	0.00004275	0.003671
trunk of lobules 6 8 white matter	0.00004774	0.003671
anterior lobule white matter	0.00004841	0.003671
paraflocculus white matter	0.00008481	0.003671
dentate nucleus	0.00008947	0.003671
crus 1 white matter	0.0001217	0.003671
nucleus interpositus	0.000123	0.003671
stria terminalis	0.0001535	0.003671
anterior commissure pars posterior	0.000154	0.003671
cerebellar peduncle inferior	0.0001802	0.003671
lobules 4 5 white matter	0.0001909	0.003671
simple lobule white matter	0.0002284	0.003671
pontine nucleus	0.0002626	0.003671
cerebellar peduncle middle	0.0002629	0.003671
Cingulum	0.0003043	0.003671
flocculus FL	0.0004048	0.003671
internal capsule	0.0005162	0.003671
anterior lobule lobules 4 5	0.0006707	0.003671
globus pallidus	0.0008064	0.003671
trunk of arbor vita	0.0008164	0.003671
lobule 9 uvula	0.0008241	0.003671

paraflocculus PFL	0.001128	0.003671
lobules 4 5 culmen ventral and dorsal	0.001151	0.003671
simple lobule lobule 6	0.001742	0.003671
corpus callosum	0.001916	0.003671
lobule 8 white matter	0.0000404	0.004942
lobule 9 white matter	0.0000799	0.004942
fastigial nucleus	0.0000932	0.004942
Cingulate cortex area 29a	0.000135	0.004942
cerebral peduncle	0.0002463	0.004942
fimbria	0.0002986	0.004942
Ventral orbital cortex	0.0004046	0.004942
crus 2 white matter	0.00005123	0.008712
cuneate nucleus	0.00005912	0.008712
trunk of lobules 1 3 white matter	0.00002294	0.013628
lobule 1 2 white matter	0.0000305	0.013628
lobule 3 central lobule dorsal	0.0004309	0.013628
Lateral orbital cortex	0.0006833	0.013628
crus 1 ansiform lobule lobule 6	0.0007274	0.013628
thalamus	0.001295	0.013628
flocculus white matter	0.00002618	0.020025
mammilothalamic tract	0.00004813	0.020025

Accessory olfactory bulb granule cell layer	0.0000781	0.020025
lobules 1 2 lingula and central lobule ventral	0.0004392	0.020025
periaqueductal grey	0.000481	0.020025
ventral tegmental decussation	0.00001351	0.029774
posterior commissure	0.00001601	0.029774
lobule 3 white matter	0.00002764	0.029774
paramedian lobule	0.00003027	0.029774
fasciculus retroflexus	0.00003023	0.043313
fundus of striatum	0.00003298	0.043313

C2. Relative brain structure volumes (mm^3). Difference in mean volume between *Tardbp*$^{+/+}$ and *Tardbp*$^{M323K/M323K}$ mice. Statistical significance at $p<0.05$ after false discovery rate correction. Man Whitney U test. n=7 *Tardbp*$^{+/+}$ and n=6 *Tardbp*$^{M323K/M323K}$.

Appendix D: Mouse cohort information.

Sex	Female	Male	
Expected ratio	1:1		
Outcome	85	59	
Females			
Genotype	WT	HET	HOM
Expected ratio		1:2:1	
Outcome	19	52	14
Males			
Genotype	WT	HET	HOM
Expected ratio		1:2:1	
Outcome	18	26	15

D1. Sex and genotype outcomes in a *Fus*$^{\Delta 14}$ cohort. WT= wild-type. HET= heterozygous. HOM=homozygous.

Sex	Female	Male	
Expected ratio	1:1		
Outcome	61	72	
Females			
Genotype	WT	HET	HOM
Expected ratio		1:2:1	
Outcome	10	38	13
Males			
Genotype	WT	HET	HOM
Expected ratio		1:2:1	
Outcome	15	33	24

D2. Sex and genotype outcomes in a *Tardbp*^{M323K} cohort. WT= wild-type. HET= heterozygous. HOM=homozygous.